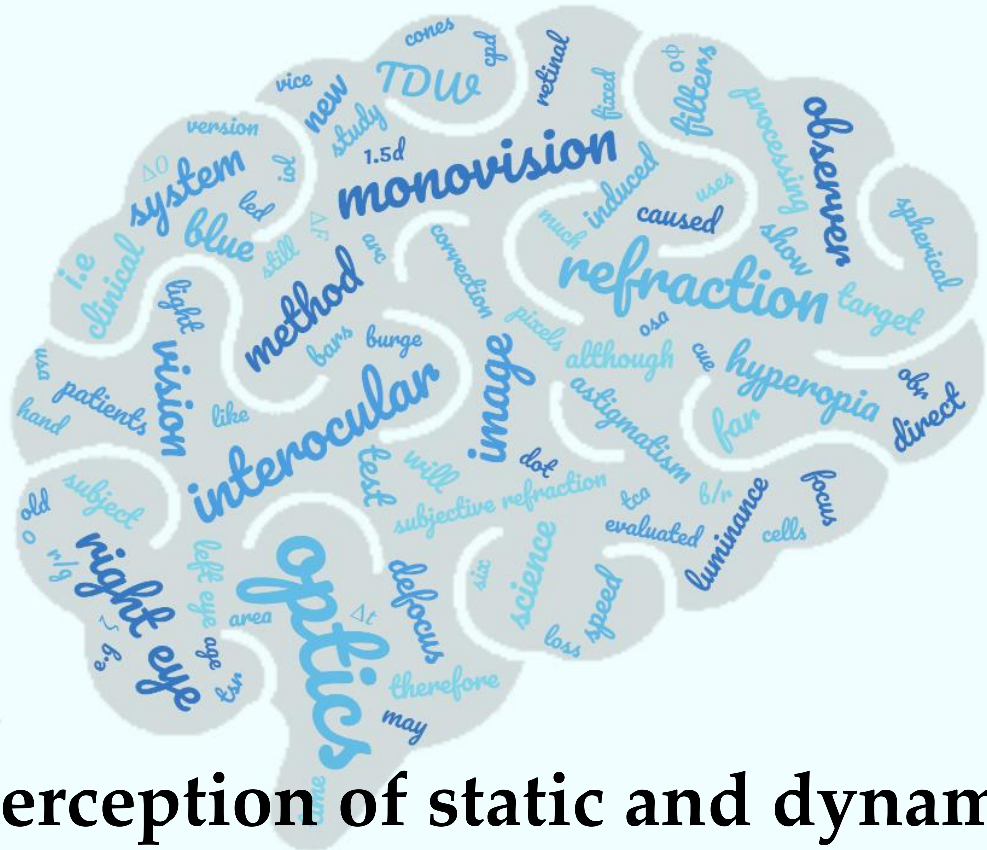

Perception of static and dynamic blur for developing clinical instrumentation in optometry and ophthalmology

Víctor Rodríguez López

Doctoral Thesis

Madrid 2022

Perception of static and dynamic blur for developing clinical instrumentation in optometry and ophthalmology

by

Víctor Rodríguez López

A dissertation submitted by in partial fulfillment of the requirements for the degree of Doctor of Philosophy in

Biomedical Science and Technology

Universidad Carlos III de Madrid

Advisor:

Carlos Dorronsoro Díaz

Tutor:

Jorge Ripoll Lorenzo

November 2022

A mis abuelos y abuelas, Remigio, Valentín, Cristina y Felipa

“El ojo que ves no es
ojo porque tú lo veas;
es ojo porque te ve”.
Antonio Machado, 1912

“Keep on paddling!”
Anonymous, 2019

Acknowledgments

Igual que empezó, ya acaba. La tesis por fin ha llegado a su final. Cuánto tiempo ha pasado y, a la vez, qué rápido que ha pasado. Durante estos años, han sido muchas las personas que me han ayudado, directa o indirectamente, en mayor o menor medida, a llegar de la mejor manera posible al final de este proceso. Y es por ello que se merecen un espacio en esta tesis.

La primera persona a la quiero agradecerle es a **Carlos**. No solo has sido mi director de tesis si no que has sido (y eres) un grandísimo mentor, guiándome en muchos de los pasos que he ido dando tanto en el mundo científico como en otros caminos que he querido emprender. Tu consejo y tu tiempo siempre han sido fundamentales. Muchas gracias por confiar en mí aquel primer día de visita al laboratorio para hacer un TFM. No sé muy bien lo que verías en mí, pero mira ahora…doctor. Tampoco sabía entonces que iba a encontrar a una referencia profesional tan importante para mí. Muchas gracias por seguir confiando en mí todos los días, por bajarme a la tierra cuando me voy por las nubes, y por pasar tardes en el laboratorio haciendo experimentos, pensando nuevos experimentos, nuevas ideas. Que sigan habiendo más de esas.

Of course, I want to thank you, **Johannes**, for welcoming me to your research group. I remember my first day in Upenn crystal clear. I did not even know how to speak fluently in English and I was kind of scared, but very enthusiastic. You were extremely patient, especially when I tried to explain myself, and you taught me a lot (many English expressions, how to write code, write papers, etc.). You have been like a second advisor to me, always willing to give me some advice when I asked for it. Thanks to this research collaboration I was lucky enough to live in the city of Philadelphia, my second favorite city in the world. Many thanks for giving me the opportunity.

Volviendo a mi primer día en el laboratorio, lo recuerdo perfectamente por cómo me marcó. Aquella visita exprés que me hicisteis Susana y Carlos, y cómo me quedé maravillado por un modelo 3D del ojo. Luego por una lente intraocular acomodativa. Y después por un sistema de óptica adaptativa. Y por las mil cosas que hacíais, y que ni sabía que existían. Y desde ese momento supe que VioBio era un sitio donde me iba a gustar estar. Gracias **Susana** por confiar en mí y acogerme en VioBio, eres una inspiración.

En general, en las tesis (y esta no es diferente), aunque el título de doctor/a lo consiga solo una persona, el mérito depende de muchas otras. En concreto, una parte importante es la gente de **VioBio** (y no solo por participar “voluntariamente” en los experimentos). Gracias a **Xoana** por haber formado parte del camino, con todas sus subidas y bajadas, has sido un apoyo muy importante, a pesar de no haber cumplido con el horario de trabajo, aunque se haya intentado (solo nos engañamos a nosotros mismos). Ah, y por mantener el carné de la uni en el despacho. A **Clara**, por el apoyo moral, por ser compi de boxeo y por permitirme ser testigo de la mejor técnica de hacer rebotar piedras en el agua. A **Elena**, por todos los consejos no científicos, por esa perspectiva desde fuera que siempre me ha ayudado a ver las cosas más claras, y por tu paciencia con las mil cosas referidas a los pedidos. Porque hay que tener paciencia.

A **Merche**, por, entre otras cosas, obligarme a ir a VioBio a buscar un TFM, que ha acabado en una tesis. A **Edu**, por ser una referencia vital, de mayor quiero ser como tú. A **Sara**, por estar siempre dispuesta a ayudar de manera desinteresada. A **Carmen**, por saberse bien los nombres de las personas. A **Dani**, por todos los '*Dani, una cosa que querría hacer*...', y no mandarme a paseo, porque oportunidades has tenido. A **Alberto**, por tener siempre un rato para comentar cualquier tontería (que son muchas) que se me ocurriera. A **Rocío**, por sacar un rato siempre para discutir cosas, de divulgación, de ciencia, de emprendimiento. A **Edu**, que viniste en medio de la pandemia, pero tu apoyo y ayuda en los experimentos ha sido muy importante. A **Enrique** por ayudarme a alinear focímetros y sistemas 4f y por tener siempre 10 minutos para comentar cualquier duda. Y al resto de gente que sigue o que ha pasado por el lab, **Nohelia**, **Judith**, **James**, **Carlos**, **Yassine**, **Andrea**, **Pilar**, **Andrés**, **Lupe**, **Ana**, **Amal**, **Lucie**, **Miriam**, **Iván**, **Lekha**, y un largo etcétera. Y también a **Brian**, **Nuria**, **Alfons**, **Elena**, y otras muchas personas que no son del laboratorio pero que me han dedicado su tiempo para guiarme en buena parte del camino.

Years ago, when I first when to Uppen, people from **Burge's Lab** welcomed me and helped me adapt to my new life in Philadelphia during my research stays. Many thanks to **Ben**, **Taka**, **Linq-qi**, **Arvind**, **Seha**, **Michael**, **Yuni**. You have been an important support for the completion of this thesis. And, as once Ben said: '*any day Victor will come across the door to spend some days in the lab, but you never know when will be the next time*…'. We'll see when.

Otro grupo de personas muy importante para mí han sido los amigos de siempre, **Dani**, **Mendo**, **Guille**, **Diego**, **Sabas**, por vuestro apoyo moral, psicológico, deportivo, ocioso, desinteresado, verdadero. Gracias por estar ahí siempre, por haber estado (prácticamente) siempre, y por saber que en el futuro también estaréis. Por más conversaciones de nostálgicos recuerdos de la infancia, findes de *Shingeki*, brindis aleatorios, ppts con propuestas vacacionales, 5 cervezas y 1 cocacola, y un larguísimo etcétera. Gracias por contar conmigo, aunque yo a veces no estuviera.

Uno de los grupos de amigos que se hacen a lo largo de la vida son los de la uni. A **Nacho**, **Z**, **Fuerte**, **Massó**, **Chus**, **Pitu**, **Guille**, **Andrés**, **Nachete**, **Terri**, **Arturo**, **Alejandro**, gracias por las incontables risas, comunios, muffins, historias, motes, frases. Sabiendo que el 5 tiene que funcionar, porque si no funciona...

Iluminando por donde pasaba, apareció un rayo de luz rubio durante el desarrollo de esta tesis. Y que vino acompañada de otros 3 rayitos más pequeños, tan pequeños como unos caracoles, pero que iluminan igual. Gracias **I** por aparecer en mi vida, y darle luz al camino de un óptico. Por haber comenzado una novela juntos, que no tendrá final.

Finalmente, mi familia. **Mamá**, **Papá**, **Juancar**. Muchas gracias por estar ahí siempre, sin hacer ruido, dejando hacer, siempre confiando en que haría las cosas bien. Aunque algunas no salieran bien. Quién os iba a decir que acabaría siendo doctor. Sé que muchas veces no habéis tenido muy claro lo qué hacía, y que los intentos de explicarlo han ido bien, pero que son cosas algo complejas. Muchas gracias por vuestro apoyo, incondicional. No me quiero olvidar de mis abuelos, **Remigio**, **Valentín**, **Cristina** y **Felipa**, a quienes va dedicada esta tesis. Nunca olvidaré lo último que me dijo mi abuelo Valentín antes de que, por desgracia, tuviera que irse. "*Víctor, aprovecha y vete a estudiar inglés, que seguro que te va muy bien*". Pues al final me fui, abuelo. Y mira cómo he acabado.

Published and submitted content

Published Journal Articles

The inclusion in the thesis of material from the articles presented below is specified in each chapter where an inclusion occurs.

1. Victor Rodriguez-Lopez, Carlos Dorronsoro. *Beyond traditional subjective refraction*. Current Opinion in Ophthalmology. 3(3), 228-234 (2022). DOI: 10.1097/ICU.0000000000000834

   Contribution completely included in Chapter 1. The specific author contributions are described in the chapter.

2. Victor Rodriguez -Lopez, Alfonso Hernandez-Poyatos, Carlos Dorronsoro. *The Direct Subjective Refraction: Unsupervised measurements of the subjective refraction using defocus waves*. bioRxiv 2021.12.04.471123. DOI: https://doi.org/10.1101/2021.12.04.4711232020

   Contribution completely included in Chapter 4. The specific author contributions are described in the chapter.

3. Victor Rodriguez-Lopez, Carlos Dorronsoro, Johannes Burge. *Contact lenses, the Reverse Pulfrich effect, and anti-Pulfrich monovision corrections*. Scientific Reports, 10, 16086 (2020). DOI: https://doi.org/10.1038/s41598-020-71395-y

   Contribution completely included in Chapter 9. The specific author contributions are described in the chapter.

4. Johannes Burge, Victor Rodriguez-Lopez, Carlos Dorronsoro. *Monovision and the misperception of Motion*. Current Biology, 29(15), 2586 - 2592 (2019). DOI: https://doi.org/10.1016/j.cub.2019.06.070

   Contribution completely included in Chapter 8. The specific author contributions are described in the chapter.

Submitted Journal Articles

1. Victor Rodriguez-Lopez and Carlos Dorronsoro. *Evidence of a Spontaneous Reverse Pulfrich Effect in Monovision after cataract surgery*. Submitted to PLOS One.

   Contribution completely included in Chapter 10. The specific author contributions are described in the chapter.

2. Victor Rodriguez-Lopez, Wilson Geisler, Carlos Dorronsoro. *The Spatiotemporal defocus sensitivity function*. Submitted to Journal of Vision.

Contribution completely included in Chapter 3. The specific author contributions are described in the chapter.

3. Victor Rodriguez-Lopez, Xoana Barcala, Amal Zaytouny, Carlos Dorronsoro, Eli Peli, Susana Marcos. *Ocular dominance measurements and monovision correction preference*. Submitted to Translational Vision Science and Technology.

   Contribution completely included in Chapter 7. The specific author contributions are described in the chapter.

4. Victor Rodriguez-Lopez, Carlos Dorronsoro, Johannes Burge. *The effect of overall light-level on the Classic and Reverse Pulfrich effects*. Submitted to Journal of Vision.

   Contribution completely included in Chapter 11. The specific author contributions are described in the chapter.

Patents

1. Enrique Gambra, Carlos Dorronsoro, Xoana Barcala, Irene Sisó, Jose Ramon Alonso, Pilar Urizar, Eduardo Esteban-Ibanez, Victor Rodriguez-Lopez, Susana Marcos. *Binocular see-through vision device for far and near distances*. Application number: M2201P006EP. Filling date: 8th June 2022.
2. Carlos Dorronsoro, Victor Rodriguez-Lopez. *Aparato y sistema para realizar medidas optométricas y método para ajustar la potencia óptica de una lente ajustable*. Application number: P201930198. Reference number: P190451ES. Filling date: 4th March 2019. PCT extension: 20th October 2021.
3. Johannes Burge, Victor Rodriguez-Lopez, Carlos Dorronsoro. *Anti-Pulfrich monovision ophthalmic corrections*. U.S. Provisional Application No. 62/799,468. Filing date: 31st January 2019. European extension: 16th March 2022.
4. Carlos Dorronsoro, Xoana Barcala, Enrique Gambra, Victor Rodriguez-Lopez, Susana Marcos. *Aparato para medir a alta velocidad la potencia óptica de una lente y método de medida*. Application number: P201730854. Reference number: P171471ES. Filling date: 28th June 2017.

Conferences

All the conference contributions (talk or poster, indicated by *t* or *p*, respectively, at the end of the contribution between brackets) listed below where the author of the thesis is placed as the first author, was delivered by him. Otherwise, the first author listed was who delivered the talk or poster.

1. Victor Rodriguez-Lopez, Johannes Burge and Carlos Dorronsoro. *Changes of the Reverse Pulfrich Effect at various levels of illumination*. Vision Science Society (VSS) Meeting, Online, 2022 [p].
2. Victor Rodriguez-Lopez, Eduardo Esteban-Ibañez, Carlos Dorronsoro. *Fast subjective estimation of astigmatism with the Direct Subjective Refraction*. Association for Research in Vision and Ophthalmology Conference (ARVO) Online, 2021 [t].

3. Xoana Barcala, Victor Rodriguez-Lopez, Amal Zaytouny, Carlos Dorronsoro, Eli Peli and Susana Marcos. *Ocular dominance measurements and monovision correction*. Association for Research in Vision and Ophthalmology Conference (ARVO) Online, 2021 [t].
4. Victor Rodriguez-Lopez, Ignacio Serrano-Pedraza, Johannes Burge and Carlos Dorronsoro. *Measuring the Reverse Pulfrich Effect in the General Population*. Vision Science Society (VSS) Meeting, Online, 2020 [p].
5. Victor Rodriguez-Lopez, Johannes Burge and Carlos Dorronsoro. *The Reverse Pulfrich effect: depth misperceptions with contact-lens-induced monovision corrections*. Association for Research in Vision and Ophthalmology Conference (ARVO) Online, 2020 [t].
6. Victor Rodriguez-Lopez, Xoana Barcala, Enrique Gambra, Lucie Sawides, Susana Marcos, Carlos Dorronsoro. Can tunable lenses provide accurate multifocal simulations? International OSA Network for Students (IONS) Conference Barcelona (Spain), 2019 [p].
7. Xoana Barcala, Ivan Martinez-Ibarburu, Victor Rodriguez-Lopez, Enrique Gambra and Carlos Dorronsoro. Image quality of tunable-lens based visual simulators. International OSA Network for Students (IONS) Conference Barcelona (Spain), 2019 [p].
8. Victor Rodriguez-Lopez, Johannes Burge and Carlos Dorronsoro. The Reverse Pulfrich Effect: Misperception of Motion in Depth. 8th Iberian Conference of Perception. San Lorenzo de El Escorial, Spain, 2019 [t].
9. Johannes Burge, Victor Rodriguez-Lopez, Carlos Dorronsoro. Monovision and the Reverse Pulfrich Effect, Vision Science Society (VSS) Meeting, Florida, US, 2019 [t].
10. Carlos Dorronsoro, Victor Rodriguez-Lopez, Xoana Barcala, Enrique Gambra, Vyas Akondi, Lucie Sawides, Yassine Marrakchi, Eduardo Lage, Wilson S. Geisler, Susana Marcos. Perceptual and physical limits to temporal multiplexing simulations of multifocal corrections. Association for Research in Vision and Ophthalmology Conference (ARVO), Vancouver, Canada, 2019 [t].
11. Victor Rodriguez-Lopez, Carlos Dorronsoro. Direct subjective refraction with temporal defocus waves. Association for Research in Vision and Ophthalmology Conference (ARVO), Vancouver, Canada, 2019 [t].
12. Johannes Burge, Victor Rodriguez-Lopez, Carlos Dorronsoro. The Reverse Pulfrich Effect. 43 Annual Interdisciplinary Conference (AIC), Wyoming, US, 2019 [t].
13. Victor Rodriguez-Lopez, Xoana Barcala, Enrique Gambra, Susana Marcos and Carlos Dorronsoro. High Speed Focimeter to measure the dynamic optical power of tunable lenses. International OSA Network for Students (IONS) Conference Scandinavia, Copenhague (Denmark) y Lund (Sweden), 2018 [t].

Other research merits

Other scientific publications not included in this thesis

1. Angel G. Lopez-de-Haro, Xoana Barcala, Ivan Martinez-Ibarburu, Yassine Marrakchi, Enrique Gambra, Victor Rodriguez-Lopez, Lucie Sawides, Carlos Dorronsoro. *Closed-loop experimental optimization of tunable lenses*. Applied Optics, *in press*, (2022). DOI: 10.1364/AO.467848

2. Carlos Dorronsoro, Xoana Barcala, Enrique Gambra, Vyas Akondi, Lucie Sawides, Yassine Marrakchi, Victor Rodriguez-Lopez, Clara Benedi-Garcia, Maria Vinas, Eduardo Lage and Susana Marcos. *Tunable lenses: dynamic characterization and fine-tuned control for high-speed applications*. Optics Express, 27, 2085-2100 (2019). DOI: https://doi.org/10.1364/OE.27.002085

Other scientific publications in preparation

1. Victor Rodriguez-Lopez, Eduardo Esteba-Ibanez, Nerea Arejita, Daniel Pascual, and Carlos Dorronsoro. The Direct subjective refraction method: fast and accurate subjective measurements of the refractive error".
2. Victor Rodriguez-Lopez, Callista Dyer, Carlos Dorronsoro, Johannes Burge. *The prevalence of the Pulfrich effect*.
3. Victor Rodriguez-Lopez, Xoana Barcala, Irene Siso, Nora El Harchaoui, Alberto de Castro, Carlos Dorronsoro. *Evaluation of stereoacuity for different distances using SimVis Gekko*.

Other proceedings not included in this thesis

1. Xoana Barcala, Enrique Gambra, Lucie Sawides, Ivan Martinez-Ibarburu, Victor Rodriguez-Lopez, Carlos Dorronsoro. *Optical quality evaluation for active afocal systems*. Proceedings of the Society of Photo-Optical Instrumentation Engineers (SPIE), 11871, Optical Design and Engineering VIII, 118710Q (12 September 2021); DOI: https://doi.org/10.1117/12.2596921

Grants

1. Caixa Research Validate program. Granted by "La Caixa" Foundation. Code: CI22-00018. The author of the thesis is the Project Leader. Research project carried out at the Institute of Optics (IO) of CSIC with 50.000€ of funding with the title: Direct Subjective Refraction. 2022.
2. Healthstart acceleration program granted by Madrid+d Foundation. The author of the thesis is the Project Leader. June 2022-April 2023.
3. CRAASH Barcelona acceleration program granted by Biocat. The author of the thesis was the Project Leader. September-December 2021.

4. ARVO Science Communication Training Fellowship. Granted by Association for Research in Vision and Opthalmology (ARVO). 2021
5. ARVO Mentorship Global Program. Granted by Association for Research in Vision and Opthalmology (ARVO). 2020.
6. Doctorate Fellowship ‘Inphinit – Retaining’. Granted by “La Caixa” Foundation. ID 100010434; LCF/BQ/DR19/11740032. Doctoral thesis carried out at the Institute of Optics (IO) of CSIC with the title: Binocular simultaneous vision: development of optical technology and visual applications. 2019.
7. ARVO International Travel Grant for ARVO VANCOUVER 2019, at Vancouver, Canada. Granted by an evaluation panel of experts amongst all the contributions to the conference. 2019.
8. Travel grant for international conference IONS SCANDINAVIA 2018, at Copenhagen, Denmark. 2018.
9. Doctorate Fellowship ‘Formacion de Profesorado Universitario – FPU’. Granted by the Spanish government. FPU17/02760. Doctoral thesis carried out at the Institute of Optics (IO) of CSIC with the title: Binocular simultaneous vision: development of optical technology and visual applications. 2018
10. Youth Guarantee program of the Community of Madrid for predoctoral research. 2018.

Education and courses during this thesis

1. Master in Business and Administration (MBA): The Power MBA. 2021-2022.
2. Animate Your Science course. Expertise in Blender 3D for Modelling, Shading and texturing, Rendering, Lightning, and simple animations for scientific research. 2021
3. Expert in 3D Printing and Modelling. AIRobots. 3D printing, FDM fabrication, 3D modelling (FreeCAD, TinkerCAD, Blender3D). 2020-present
4. Expert in Robotics and Programming. AIRobots. Electronics, components, and Arduino and apps programming and developing. 2020-present
5. Basics of statistics applied to research. Sampling, experimental design, and inference. CSIC. April 2021.
6. Entrepreneurship and company creation. UC3M. May 2021.
7. Degree in Physics. Science Faculty of Universidad Nacional de Educacion a Distancia (UNED). Completed 1st year of classes. 2017-present.

Research stays

Burge’s Lab. Department of Psychology of the University of Pennsylvania (Upenn). Philadelphia, PA, USA. The main goal of these research stays was to study the perceptual impact of interocular blur differences on binocular motion and depth perception. A total of 6 months, divided into four different visits.

- March 2018 - April 2018. Discovery of the Reverse Pulfrich effect. Chapter 7 of the thesis.
- February 2019. Final measurements for the discovery of the Reverse Pulfrich effect. Chapter 7.
- July 2019. The impact of overall light level on the Pulfrich effect. Chapter 11.
- September 2021 -December 2021. Final measurements of the impact of overall light level on the Pulfrich effect (Chapter 11) and development of a portable autostereoscopic device for fast measurements of the Pulfrich effect (Chapter 12).

Invited talks

1. 2022. *A new method for obtaining the spherical refraction of an eye: the Direct Subjective Refraction*. Optica Vision & Color Summer Data Blast Session organized by Optica. Held August 10th, 2022. Online.
2. 2021. *Outreach in microscopy*. Part of the course *Microscopía y Aplicaciones* organized by the Institute of Optics (IO-CSIC) and the University of Castilla La Mancha. Held March 11th, 2021. In-person.

Other merits

1. Participation in Demo Day CSIC 2022 as speaker.
2. Finalist in I Hackaton CSIC among 29 projects presented. 2022
3. Director of the Master's thesis of Nerea Arejita Abaitua, '*Evaluación de la Refracción Subjetiva Directa, nuevo método de refracción subjetiva, en entorno clínico*'. Master's in Hospital Optometry by Complutense University of Madrid.
4. Member of the IO-CSIC Student Chapter of the Optical Society of America (IOPTICA, formerly IOSA, https://sites.google.com/view/iosa-student-chapter-csic/)
   Member since 2017.
   Treasurer from January 2019 to December 2019.
   President from January 2020 to December 2021.
   We organize outreach activities to disseminate scientific knowledge to our local community, in many aspects of optics, from photonics to lasers, vision, and color, among others. We perform workshops in schools and suburbs of Spain (collaborating with *Ciudad Ciencia* and *Ciencia en el Barrio*), organizing conferences, invited talks, and teaching courses. We also participate in key events such as the *Week of Science* (held in November), the *International Day of Women and Girls in Science* (11th of February), and the *Night of the Researchers* (usually held in September). All the activities are funded by OPTICA (formerly OSA).
5. The organizer of the 6th and 7th editions of the IOSA scientific seminars. Organized by IOPTICA (formerly IOSA) and held Institute of Optics of the Spanish National Research Council (CSIC) Madrid (Spain).
6. Interviewed by Revista Haz.
7. Interviewed as an example of Intellectual Property transfer in young researchers as part of the activities of the International Day of the Intellectual Property: *IP and Youth: Innovating for a Better Future*. 26th April 2022. Link to the interview: https://youtu.be/sVu0596-4YI. Link to the interview with other young researchers: https://youtu.be/Tk1jQTlAkHg.
8. Interviewed by Medscape Medical News 2020 regarding our work presented in ARVO 2020 (*The Reverse Pulfrich effect: depth misperceptions with contact-lens-induced monovision corrections*) https://www.medscape.com/viewarticle/931032
9. Design and development of *Women in STEM Challenge* card game. 2021. In collaboration with Colette DeHarpporte, Francesca Gallazi, Marcia Leski, Danuta Sampson, Gavrielle Untracht, Maria Vinas. https://www.optica.org/en-us/get_involved/education_outreach/educational_games/
10. Committee member of *Premios Fotón* awards to recognize, motivate, and promote Scientific Communication (*Fotón Emitido* award) and Teaching (*Fotón Absorbido* award) in optics and photonics. Organized by the Institute of Optics of the Spanish National Research Council (CSIC) Madrid (Spain). Jury of the 2021 edition.

11. Reviewer for Indexed journals *Heliyon*, *Journal of Experimental Psychology,* and *Annals of Eye Science*.
12. Certified OSA Reviewer.

Keywords


vision
DSR
eye
binocular
science
sensitivity
Pulfrich effect
perception
blur
depth
subjective refraction
eye dominance
optical corrections
astigmatism
technology
image
method
near
far
focus
features
portable
spatial
clinical
metric
knowledge
subjects
temporal
delay
presbyopia
patients
accommodation
defocus
luminance
level
fast
monovision
overall
implications
hyperopia
illusion
lenses
spatiotemporal
chromatic
processing speed
objects
aberration
myopia
pulfrich
anti-pulfrich
refractive error
measurements
limits
brain
correction
setup

Abstract

Blur degrades our retinal images and affects our vision, more and more as we old. Understanding blur is key in the study of many processes in visual perception, from the development of the visual system to the diagnosis and compensation of refractive errors (myopia, hyperopia, astigmatism, and presbyopia). Blur also provides cues for accommodation (focusing near objects) or depth estimation.

Besides refractive errors, other sources of visual blur are high-order geometrical aberrations, chromatic aberrations, and some presbyopia corrections such as multifocality or monovision. In monovision, one eye is corrected for far vision and the other one for near. By design, monovision corrections produce interocular differences in blur, affecting binocular vision.

Optotunable lenses, programmable lenses able to change their optical power very quickly (in the order of milliseconds), provide new opportunities for the study of blur perception, both static and dynamic, and the development of new technologies in optometry and ophthalmology. In fact, recent developments like SimVis technology make use of optotunable lenses driven at high speed to simulate multifocal corrections.

In this thesis, we have used optotunable lenses to find the spatiotemporal limits of defocus perception. Besides, we have proposed and measured for the first time the spatiotemporal defocus sensitivity function, which provides a complete description of defocus perception. We have also developed a model to characterize defocus sensitivity, based on well-established models for contrast sensitivity. We found that the maximum spatiotemporal sensitivity to defocus is around 14 cycles per degree (cpd) and 10 Hertz (Hz), and the upper limits to sensitivity are around 50 cpd and 40 Hz. We found similar results with functional or paralyzed accommodation, suggesting that in this defocus flicker-detection task the presence of varying blur deactivates the accommodation response. These scientific discoveries provide a powerful framework for technologies that make use of temporal changes in defocus.

We have also developed a new subjective refraction method for obtaining the refractive error of an eye, called Direct Subjective Refraction (DSR). This method is based on the use of fast temporal changes in defocus in combination with the longitudinal chromatic aberration of the eye and a bichromatic stimulus made of two monochromatic (red and blue) circles to create flicker and chromatic distortion cues. These cues can guide the patient, without the supervision of the clinician, to obtain their spherical refractive error. We compared it with an unsupervised version of the traditional subjective refraction and also performed the same experiment with paralyzed accommodation, and we found out that accommodation barely influences the results of the DSR. We have demonstrated that the DSR method provides a highly repeatable spherical equivalent (±0.17 D) in less than 1 minute (39 seconds), with barely any supervision of the clinician, and minimizing the impact of accommodation.

Moreover, we have extended the DSR method for estimating the astigmatic component of the refraction using a similar stimulus but with oriented features instead of circles to capture the refractive error in different axes. Several experiments confirmed that the DSR

method can capture the amount of astigmatism very precisely and with similar outcomes to the ones obtained with the traditional subjective refraction method.

Finally, we improved the psychophysical procedure of the DSR to estimate the full refractive error (spherical equivalent and astigmatism) and we evolved the on-bench optical setup to a clinical portable device (made of custom highly monochromatic LEDs) to allow measurements in clinical environments. We measured 33 real patients from two clinical sites, demonstrating the viability of the new clinical prototype. Comparing the DSR method with the traditional subjective refraction, we found similar results between methods (-0.34±0.53 D of difference in the spherical equivalent). Although the technology needs more improvements and adaptations to the clinical environment, the initial results are promising and already reveal the potential of the DSR technology.

In monovision, the dominant eye is compensated for far vision, and the non-dominant eye for near vision. The selection of the dominant eye is probably the main issue. In this thesis, we have developed the Eye Dominance Strength (EDS), a new metric based on the perceptual preference of the patient to randomized monovision in one eye or the other, while observing natural images. The EDS metric not only provides a binary result (left eye or right) as conventional tests do but also a quantification of the strength of eye dominance, with high repeatability. The EDS metric might help to prescribe monovision corrections more confidently and reduce the discomfort and the neuroadaptation times.

We have also studied the influence of monovision corrections in dynamic visual scenarios. We have discovered a new version of a 100-year-old optical illusion, called the Pulfrich effect, which produces misperceptions of the depth of moving objects due to interocular differences in the processing speed between eyes. This speed difference is interpreted by the brain as binocular disparity which arises a depth illusion. Classically, the Pulfrich effect was described with interocular differences in luminance: the dimmer image is processed slower than the brighter image. We discovered that interocular blur differences, like those produced in monovision corrections, produce the opposite effect: the blurrier image is processed faster than the sharper image. We report that blurring an eye with 1.50 D while keeping the other focused can cause delays in the processing speed as high as 3.7 milliseconds, with a remarkable impact on the depth illusion size. For that reason, we called the illusion the Reverse Pulfrich effect. The Reverse Pulfrich effect can affect public safety as the depth illusions, for example, while driving, can entail severe problems for monovision wearers.

In this thesis, we have also developed the anti-Pulfrich monovision corrections, which take advantage of the opposite sign of the Classic and Reverse Pulfrich effects, to null the effect caused by monovision by reducing the light of the blurring lens with a tint. We have demonstrated the efficacy of anti-Pulfrich monovision corrections delivered by contact lenses in young volunteers. Additionally, we demonstrated that interocular differences in retinal magnifications do not cause any difference in the processing speed and therefore do not produce the Pulfrich effect.

The classic version of the Pulfrich effect has been reported to occur in some pathologies, such as cataracts, or optic neuritis, producing a spontaneous Pufrich effect. In this thesis, we have reported for the first time a case of spontaneous Reverse Pulfrich effect in a patient adapted to surgical monovision after cataract surgery. The spontaneous Pulfrich effect measured was as high as 4.82 ms and caused severe binocular symptoms in the patient. After removal of the surgical monovision correction due to strong visual impairment, we measured a readaptation process with a timeframe of weeks.

We have also evaluated the effect of overall luminance level (from 0.4 to 12.8 cd/m^2) for different pupil sizes (2, 4, and 6 mm) in the different versions of the Pulfrich effect. We found that reducing the overall light level increases the delay caused by interocular luminance differences (Classic Pulfrich effect, confirming results from the literature) and increases the delay with interocular blur differences (Reverse Pulfrich effect, first time reported). The similarity of the results in the Reverse Pulfrich effect for 4 and 6 mm pupil sizes suggests that high-order aberrations play a role in the delay caused by differential blur. The different increasing ratio of both the Classic and Pulfrich effects has implications for the development of potential anti-Pulfrich monovision corrections, which may need to modify their characteristics depending on the overall light level.

Finally, we have developed a portable setup based on an autostereoscopic technology using lenticular lenses to measure the prevalence of the Classic and Reverse Pulfrich effects on a young population. Although both effects are present in this sample (93% of them showed both effects), the effect sizes only elicit a considerable Pulfrich effect in half of the subjects measured. The framework developed opens the possibility for fast measurements of the Pulfrich effect in clinical environments. Furthermore, we also developed another portable setup for measuring stereoacuity based on a parallax barrier tablet. We have shown that stereoacuity can be precisely measured through SimVis Gekko, allowing fast and accurate predictions for different optical corrections.

In summary, this thesis has covered different aspects of vision related to blur perception, covering from their theoretical description to their direct clinical application. First, a new subjective refraction method for measuring the refractive error of an eye based on quick blur changes was developed and validated, providing fast and accurate measurements with high potential for clinical implementation. Second, a new metric for selecting the best eye for monovision corrections was designed and tested providing a measurement of the strength of eye dominance. Third, a new optical illusion caused by differential ocular blur, with important clinical implications, was discovered. Fourth, a new optical correction to compensate for the optical illusion previously discovered, the anti-Pulfrich monovision correction, was developed. Finally, two new portable devices based on autostereoscopic techniques were developed with the potential to measure different aspects of binocular vision, stereoacuity and the Pulfrich effect, in clinical environments. The outcomes of this thesis have advanced the understanding of blur perception and the application of that knowledge to the development of clinical instrumentation in optometry and ophthalmology.

Table of contents

List of figures

List of tables

List of abbreviations and acronyms

Acronym	Meaning
‘’	Arc seconds
3D	Three Dimensional
cd/m^2	Candela/square meters
CFF	Critical Fusion Frequency
CL	Contact Lens
cm	Centimeters
cpd	Cycles Per Degree
CSF	Contrast Sensitivity Function
D	Diopters
DCFF	Defocus Critical Fusion Frequency
DSR	Direct Subjective Refraction
EDOF	Extended Depth Of Focus
EDS	Eye Dominance Strength
FT	Fourier Transform
HOAs	High Order Aberrations
Hz	Hertz
IOL	Intraocular Lens
J_0	Horizontal astigmatism
J_{45}	Oblique Astigmatism
JND	Just Noticeable Difference
LCA	Longitudinal Chromatic Aberration
LE	Left eye
LGN	Lateral Geniculate Nucleus
lm	Lumen
LOAs	Low Order Aberrations/Limits of Agreement
LSF	Line Spread Function
M	Spherical equivalent
m	Meters
MAS-2EV	Multifocal Acceptance Score to Evaluate Vision
min	Minute
ms	Milliseconds
MTF	Modulation Transfer Function
NCSF	Neural Contrast Sensitivity Function
nm	Nanometers
OBR	Objective Refraction
OD	Optical Density

OTF	Optical Transfer Function
PCB	Printed Circuit Board
PSE	Point of Subjective Equality
PSF	Point Spread Function
QUEST	QUick Estimation by Sequential Testing
RE	Right eye
RMS	Root Mean Square
s	Seconds
SCSF	Spatial Contrast Sensitivity Function
SDSF	Spatial Defocus Sensitivity Function
SR	Strehl Ratio
STCSF	Spatiotemporal Contrast Sensitivity Function
STDSF	Spatiotemporal Defocus Sensitivity Function
TCA	Transverse Chromatic Aberration
TCSF	Temporal Contrast Sensitivity Function
TDSF	Temporal Defocus Sensitivity Function
TDW	Temporal Defocus Wave
tro	Trolands
TSR	Traditional subjective Refraction
TVR	Threshold Versus Reference
VA	Visual Acuity
VAS	Visual Analogue Scale
VSOTF	Visual Strehl Ratio

Chapter 1. Introduction

Vision is the sense that provides the most information from the real world. The optical system of the eye focuses the visible light onto the retina, which transforms said light into electric pulses. After that, neurons bring those pulses to the visual cortex in the brain, what we ultimately conceive as visual perception.

However, the optical visual system, like any other optical system, is not perfect. Defocus and optical aberrations degrade the optical quality and are translated into different degrees of blur. Although the effect of blur on the retinal image is frequently experienced and therefore intuitively assumed and understood, blur itself is a complex concept with many implications in visual perception. Blur affects many aspects of vision, from the prescription of optical corrections to motion and depth perception.

The impact of blur on vision has been studied for decades. However, the development of tunable lenses, programmable optical elements able to change their optical power, enables new methods for static and dynamic manipulation of blur, new scientific approaches in the study of blur perception, and new development and technologies to compensate for blur or to take advantage of its presence.

In this chapter, a revision of the state-of-the-art, motivation, goals of the thesis, open questions, and hypothesis are presented. Particularly, this chapter addresses the structure of the human visual system, the imperfections of the optical system of the eye, visual perception, the static and dynamic perception of blur (both for dynamic changes in blur and for moving blurred objects), refractive errors, optical corrections, eye dominance, and other aspects of binocular perception.

This chapter is partially based on the review article by Victor Rodriguez-Lopez and Carlos Dorronsoro '*Beyond traditional Subjective Refraction*' published in *Current Opinion in Ophthalmology (2022)*.

1.1. The human eye and the human visual system

1.1.1. The optical system of the eye

The optical system of the eye is composed of three **main components**: cornea, crystalline lens, and retina. The first two components focus the incoming light onto the third one, like the objective of a camera focuses the luminous energy of the scene on the image sensor. Each of them has its structure optimized to fulfill its function. In total, the visual optical system has a total power of 60D.

The cornea is the first optical surface of the eye. It is a convex-concave lens that provides the main optical power to the optical system (2/3, 40D) and therefore is the most important element from an optical point of view[1,2].

The crystalline lens is a biconvex lens located between the iris and the vitreous humor. It provides the remaining optical power to the optical system (1/3), and it is attached to the ciliary muscles by elastic fibers of the zonula that allows the accommodation process. This process permits the shape change of the crystalline lens and therefore the change in optical power to focus near objects. The main theory for accommodation was proposed by Helmholtz in 1855[3]. During the process, the ciliary muscles contract and the fibers of the zonula reduce the force applied, increasing the curvature of the crystalline lens and thus the optical power of the system. When the ciliary muscles relax, the fibers of the zonula increase the force applied, reducing the curvature of the crystalline lens and thus the optical power of the system, recovering the original state. The accommodation process also elicits the convergence of the eyes and the miosis (contraction) of the pupils, the so-called near-triad or accommodation reflex[4].

The amplitude of accommodation is the total dioptric amount that the accommodation process can elicit. Its maximum occurs when we are born, and it decreases since then, as can be seen in Figure 1.1[5–8]. At teenage age, we can accommodate as much as 10-14D, which progressively decreases close to 0 at about 50 years old. The lack of enough amplitude of accommodation produces the loss of ability to focus near objects (in absence of refractive error or when fully compensated for far vision), in a process called presbyopia. Presbyopia is caused by the progressive stiffness of the proteins that constitute the crystalline lens, which avoids the movement and therefore prevents the accommodation process from happening[9].

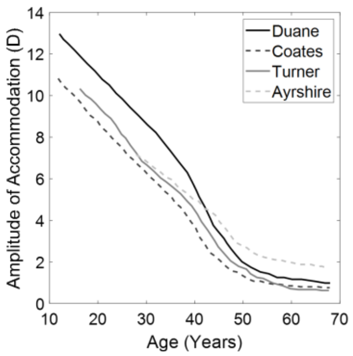

Figure 1.1. Amplitude of accommodation measured in different studies. Adapted from Charman 2008[9].

Another important process that may happen together with presbyopia is the opacification of the crystalline lens, physiological and non-pathological with age[10] but more pronounced and pathological in a process called cataracts. The reason behind this process lies in the denaturation of the proteins inside the crystalline lens that produces an opacification of the lens that scatters the light going through. The prevalence of cataracts increases with age, from 3% at age 55 years to 93% at age 80 years and older[11]. The main symptoms are related to the loss of visual acuity and glares caused by the scattered light[12].

Once the light has passed through the optical system, it focuses on the retina, which acts as a light detector. It contains different types of neurons, with a wide variety of functions. The most important ones are the photoreceptors, which transform the incoming light (photons) into electrical impulses via the phototransduction process. After that, the electrical impulses are transmitted to the ganglion cells, located at the end of the retina. The axons (the arms) of the ganglion cells form the optic nerve.

The retina is divided into different regions, with different types of photoreceptors and functions associated. Briefly, the center of the vision is called the fovea, aligned with the visual axis of the eye. The maximum density of cones is in the fovea, although only represents 4% of the total amount, which are also distributed along the rest of the retina. Cones are classified mainly into three types depending on their spectral sensitivity and the main wavelengths that they process: large (L-cone, red wavelength), medium (M-cone, green wavelength), and small (S-cone, blue wavelength). These photoreceptors are used to see in color and objects with high detail and to perceive the world in daylight conditions. The area of the retina outside the fovea is called the peripheral retina. In this part, cones proportion decreases dramatically, and the number of rod photoreceptors increases, with a maximum density of rods at 20º of retinal eccentricity. Within the peripheral retina, rods are used to perceive moving objects and other functions that do not require high-definition processing. Rods are also used to perceive the world in nightlight conditions and do not provide color vision. At 15º of eccentricity in the nasal region is located the optic nerve, where there are no photoreceptors. Figure 1.2A shows the spectral absorption of the photoreceptors[13], Figure 1.2B their spectral sensitivity[14], and Figure 1.2C their distribution along the retina[15].

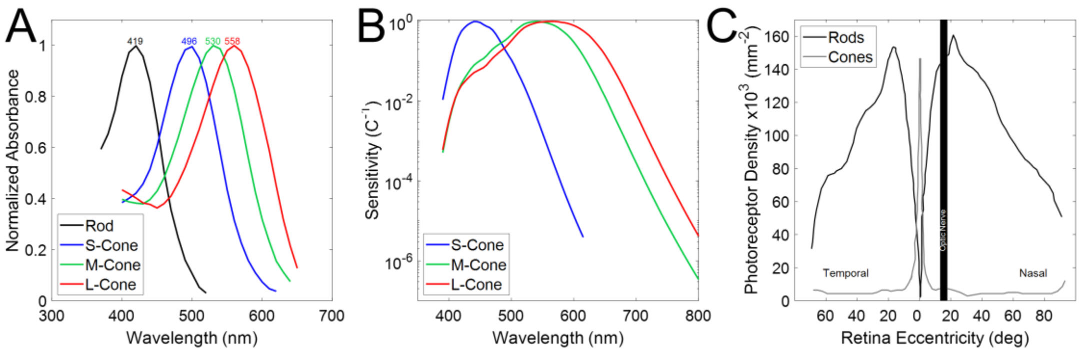

Figure 1.2. Photoreceptors in the retina. **A.** Normalized absorption as a function of the wavelength, showing the peak of absorption in nanometers, for rods and cones. Adapted from Dartnall et al. 1983[13]. **B.** Sensitivity as a function of the wavelength for cones. Adapted from Stockman at al. 2000[14]. **C.** Distribution of the photoreceptors at both sides of the fovea (temporal and nasal). Black shaded region indicates the blind spot (optic nerve). Adapted from Osterberg 1935[15].

1.1.2. Imperfections of the optical system: aberrations

A perfect optical system forms a point image from a point object. However, perfect optical systems are far from reality, and the visual system is not different. Retinal images are affected by diffraction, scattering, and optical aberrations, influencing the optical quality, monochromatically and polychromatically.

Optical aberrations refer to the difference in the phase of the wavefront of the optical system with respect to an ideal sphere[16]. In an aberrated optical system, all the parallel rays entering the pupil do not converge to the same focus point. The image of a point through an aberrated optical system is deformed and represents a unique pattern of the ocular optical system, like a fingerprint. Optical aberrations are divided into monochromatic (caused by the geometrical structure of the optical system) and polychromatic (caused by the variation of the refractive index with wavelength). Both are described hereinafter.

1.1.2.1. Monochromatic aberrations

Monochromatic aberrations only consider one wavelength and arise from the geometry of the optical system[1,17]. The optical quality of the visual system can be assessed mainly by two metrics, the Modulation Transfer Function (MTF) and the Point Spread Function (PSF). The MTF describes the loss of contrast across spatial frequencies and the PSF describes the image of a point through the optical system. Convolving the PSF with the ideal image provides a simulation of the retinal image of the system[18]. For large pupil diameters, optical aberrations dominate the optical quality and for small pupil sizes diffraction does. The PSF limited by diffraction is the Airy disk[19].

Usually, Zernike polynomials are used to mathematically describe the wavefront, represented as the weighted sum of the Zernike polynomials

$$W(\rho,\theta) = \sum_{n=1}^{K} \sum_{m=-n}^{n} c_n^m Z_n^m(\rho,\theta) \tag{1.1}$$

where $W(\rho,\theta)$ is the wave aberration phase in polar coordinates, c_n^m is the Zernike coefficient of radial order n and the angular frequency m, and Z_n^m is the Zernike polynomial term. Zernike coefficients are usually reported in microns (µm).

The conventions recommended by the Optical Society of America regarding ordering, normalization, and sign are followed in the thesis[20]. A two-dimensional representation of the Zernike polynomials is displayed in Figure 1.3 up to 6th order. Above the 7th order, human aberrations are considered negligible[21–23].

The first polynomial (Z_0^0) is called Piston and refers to the average of the wavefront and is not represented in Figure 1.3, as it does not have impact on vision. The second and third polynomials (Z_1^1 and Z_1^{-1}) refer to tilt in horizontal and vertical directions, and only affect the position of the retinal image. These first three are usually not considered true optical aberrations as they do not provide information about the optical system or the optical quality. The fourth (Z_2^{-2}), fifth (Z_2^0), and sixth (Z_2^2) polynomials represent oblique astigmatism, defocus, and vertical astigmatism, respectively. These first 6 polynomials are called Low Order Aberrations (LOAs). Aberrations represented by higher order polynomials (in Figure 1.3 all wavefronts below LOAs) are considered High Order Aberrations (HOAs).

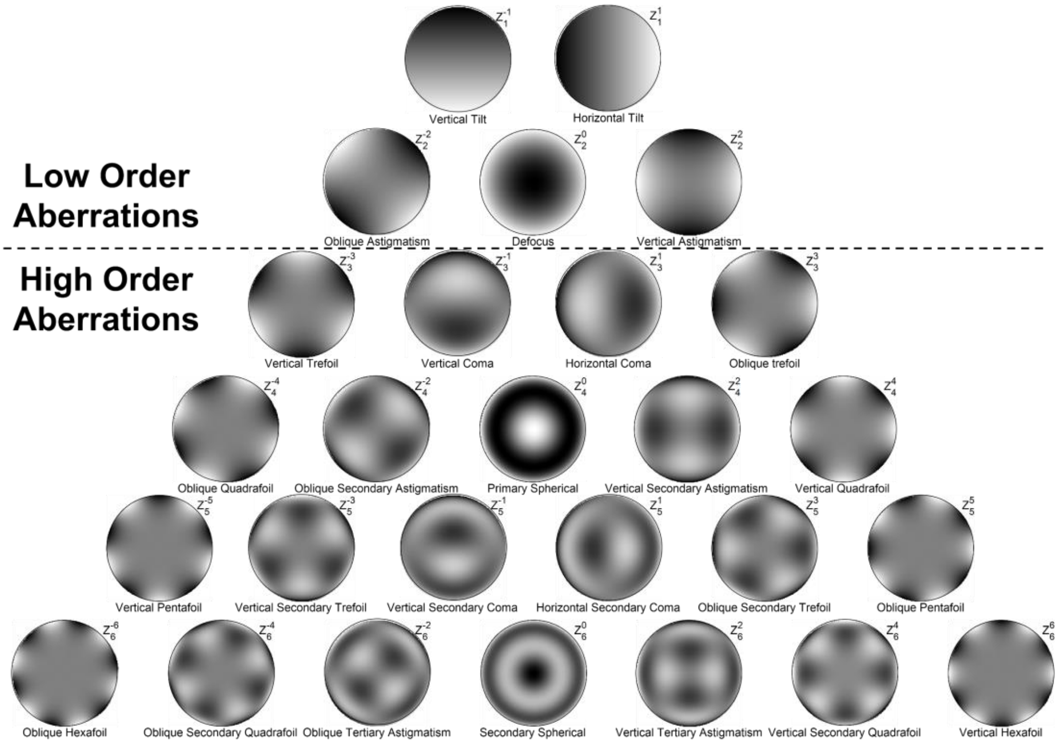

Figure 1.3. Wavefront representation of the Zernike polynomials from the 2nd to the 6th order. Zernike coefficient for each Zernike polynomial displayed is 0.05 µm.

LOAs can be compensated with ophthalmic corrections (spectacles, contact lenses, or surgery) and refers to the refractive error, which is the amount of myopia, hyperopia, and astigmatism in the eyes. An approximation of the refractive error can be obtained by transforming the second-order Zernike coefficients to spherocylindrical power vector notation (M, J_0, J_{45})[24,25], shown in Equation 1.2. The 4th term can be used to approximately determine the spherical equivalent component of the refractive error and the 5th and 6th terms are the astigmatic components of the refractive error

$$M = \frac{-c_2^0 4\sqrt{3}}{r^2}$$
$$J_0 = \frac{-c_2^2 2\sqrt{6}}{r^2} \qquad 1.2$$
$$J_{45} = \frac{-c_2^2 2\sqrt{6}}{r^2}$$

where r is the radius of the pupil of the eye in millimeters and the Zernike coefficients (c_n^m) are in microns. This objective approximation of the optical corrections will be discussed in more detail in section 1.3.1.

It has been reported that LOAs, discarding piston and tilts, represent more than 90% of the wavefront aberration[22]. Although HOAs cannot be compensated using ophthalmic corrections, they have a certain impact on the subjective prescription to compensate for the refractive error of the eye, especially spherical aberration (Z_4^0)[26–28].

Optical aberrations are measured using aberrometers, based on the emerging wavefront from the eye or in the ray deviations that the light suffers as it passes through the visual optical system. Aberrometers are increasingly approaching clinical environments, as they have proven to be very useful in monitoring changes in the optical quality of the eye, especially after surgical procedures[29], pathologies[18], aging[30,31], or accommodation[32].

1.1.2.2. Chromatic aberrations

In chromatic aberrations, different wavelengths are focused on different distances, causing two types of chromatic aberrations: Transverse Chromatic Aberration (TCA) and Longitudinal Chromatic Aberration (LCA). TCA is produced when oblique light reaches the retina, focusing wavelengths on different lateral planes of the retina. LCA is produced by the different axial focusing positions of the rays for different wavelengths. Figure 1.4 shows both chromatic aberrations.

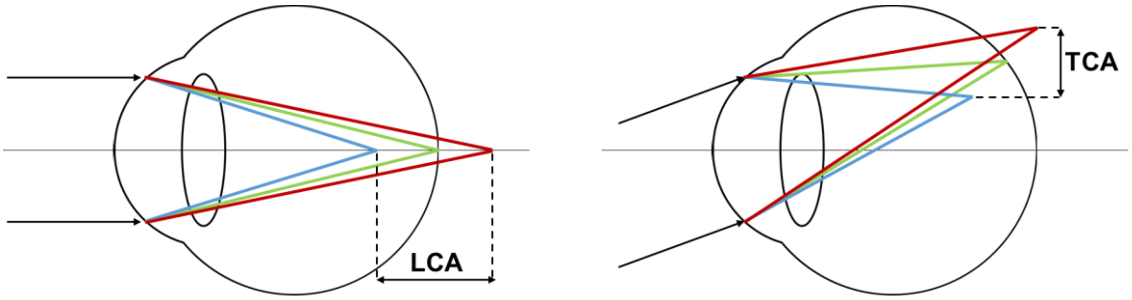

Figure 1.4. Schematic representation of the types of chromatic aberration. On the left, the Longitudinal Chromatic Aberration (LCA). On the right, the Transverse Chromatic Aberration (TCA).

TCA produces a lateral shift on the image for different wavelengths[33,34]. TCA has been reported to depend on the subject[35], the pupil size[36], and the location of the fovea[37] with respect to the optical axis, and it is affected by the Styles-Crawford effect[38]. TCA is usually measured using psychophysical subjective methods. However, the comparison of the results between the optical (objective) TCA and the perceived (subjective) TCA[38,39] slightly differ.

LCA focuses short wavelengths (blue) in front of long wavelengths (red). LCA value depends on the method used, the wavelength range measured, and the sample of the study, ranging from 3.20D (365-750 nm)[40] to 1.00D (458-632 nm)[41]. Different studies have reported different values, distinguishing between a subjective LCA based on psychophysical experiments (1.33D[39], 1.84D (450-700 nm)[42]) or an objective LCA, based on reflectometry techniques or wavefront sensing (1.40D (460-700 nm)[43], 0.72D (532-787nm)[44]). A chromatic eye model developed by Thibos et al.[45] is usually used as the reference for the estimation of the LCA, with an accepted value of 1.75D (range 400-700). This definition of the LCA will be used throughout this thesis. The expression of the model is shown in Equation 1.3.

$$LCA(\lambda) = \frac{n_{555} - n(\lambda)}{r_c - n_D} \qquad 1.3$$

where n_{555} is the refractive index at 555nm wavelength, $n(\lambda)$ is the refractive index as a function of the wavelength of Le Grand's index of refraction model, r_c is the radius of curvature of the eye model and n_D is the refractive index at the model's emmetropic wavelength ($n_D = 1.33,\ \lambda = 589$ nm, coincident with the sodium D line). Figure 1.5 shows the LCA (i.e., the refractive error as a function of the wavelength) computed with Equation 1.3.

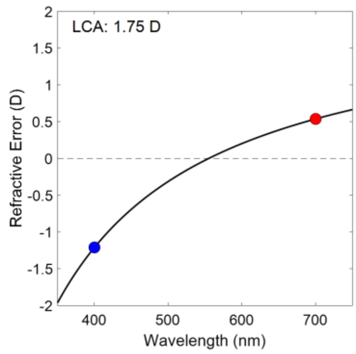

Figure 1.5. Longitudinal chromatic aberration (LCA). Based on the chromatic eye model developed by Thibos et al.[45]. Blue dot represents the axial refractive error at 400 nm and the red dot at 700 nm.

1.2. Visual perception

1.2.1. Visual pathway

The visual pathway begins with the optic nerve, which is the aggrupation of the axons of the ganglion cells, right after the retina. Then, in the optic chiasma, approximately 50% of the information of both eyes, corresponding to the nasal portion of the retina, is crossed to be processed by the contralateral part of the brain. The information from the temporal portion remains in the same stream. Most of the information carried by the ganglion cells is directed to the lateral geniculate nucleus (LGN) and the rest to the superior cuniculus. The LGN is divided into 6 layers where information from only one eye, crossed in the chiasma, reaches each layer. After the LGN, the optic track can be divided into magnocellular and parvocellular pathway[46]. Table 1.1 shows the main characteristics of each of them.

Table 1.1. **Characteristics of the magnocellular and parvocellular pathways.** Main characteristics are color, temporal response, spatial response, and processing of movement.

Characteristic	Magnocellular pathway	Parvocellular pathway
Color	Achromatic	Process color stimulus
Temporal response	Higher resolution to low temporal frequencies and fast transmission speed	Higher resolution to high temporal frequencies and slow transmission speed
Spatial response	Low spatial frequencies	High spatial frequencies
Movement	Process moving stimulus	Mainly static stimulus

1.2.1.1. Perception in the visual cortex

The area of the brain that processes visual information is in the occipital region. More than half of the visual cortex is dedicated to only 10% of the total visual field, mainly associated with the processing of the fovea. The visual cortex is divided into 5 regions (V1-V5), where V1 is also called the primary visual cortex. In the visual cortex, there are different types of cells, distinguishing between simple, complex, and hypercomplex cells. In brief, simple cells respond to stimulus orientated in a certain direction, complex cells respond to a specific movement of direction, and hypercomplex cells respond to edged moving objects in specific directions and/or orientations. Cells with specific functions are said to be tuned to that specific function, such as color-tuned, disparity-tuned, and orientation-tuned, among others.

The visual cortex fulfills a wide variety of functions carried out by cells in different parts of the retina[47]. The information initially travels to the V1, or primary visual cortex, which later sends the information to V2. From these two regions, the information is segregated and processed in specialized regions. Based on this differentiation according to the function, four independent systems have been established. Table 1.2 summarizes the neuronal pathway, the specialized region, and the function of these systems.

Table 1.2. **Functions of the independent systems for processing specific functions in the retina.** The independent systems are movement, color, color shapes, and dynamic shapes.

System	Neuronal pathway	Specialized region	Function
Movement	Magnocellular	V5	Movement, localization, and spatial organization
Chromatic	Parvocellular	V4	Color in low resolution
Color shapes	Parvocellular	V4	Color in high resolution
Dynamic shapes	Magnocellular	V3	Shape of moving objects

In this thesis, processes that imply the information from both eyes are relevant. In the visual cortex, binocular cells receive input from the two eyes and corresponding points on the retina. However, if only exists binocular cells which receive input from the corresponding points of both retinas, such cells will not be able to discriminate depth[48]. Therefore, binocular cells that incorporate information from slightly different points of each eye, called disparity detectors, allow for the creation of a 3D representation of the outer world, what is called stereoscopic vision. In the primate cortex, disparity-tuned cells are present in several parts of the visual cortex and have been found in V1, V2, and some parts of V3. This thesis explores the clinical impact of binocular information, described in detail in section 1.5 of the Introduction.

The magnocellular pathway ends in the V5 region, and the parvocellular pathway ends in both V2 and V4. The main functions of each visual cortex region are V1 processes shape, color, and movement; V2 receives information from V1; V3 processes form as it receives information from the fovea; V4 also processes color, and V5 is specialized in movement.

1.2.2. Visual quality metrics

As stated in the previous section, due to the presence of monochromatic and polychromatic aberrations, the optical visual system is far from being a perfect system and, consequently, the retinal image is distorted. Many metrics have been developed to evaluate the degradation of the perceived image. While some of them consider optical parameters only, others also consider perceptual aspects of vision.

From the point of view of the processing of visual information, the visual system can be considered a Fourier analyzer, which decomposes an image in its spatial frequencies. The PSF describes the image of a point through the optical system. The Fourier transform of the PSF defines the Optical Transfer Function (OTF), which measures both the shift of the phase and the loss of contrast of the image[25]. The module of the OTF defines the MTF. The MTF describes the contrast passing through the optical system across spatial frequencies, which is, essentially, the relationship between the final and the initial contrast once the image has passed through the optical system.

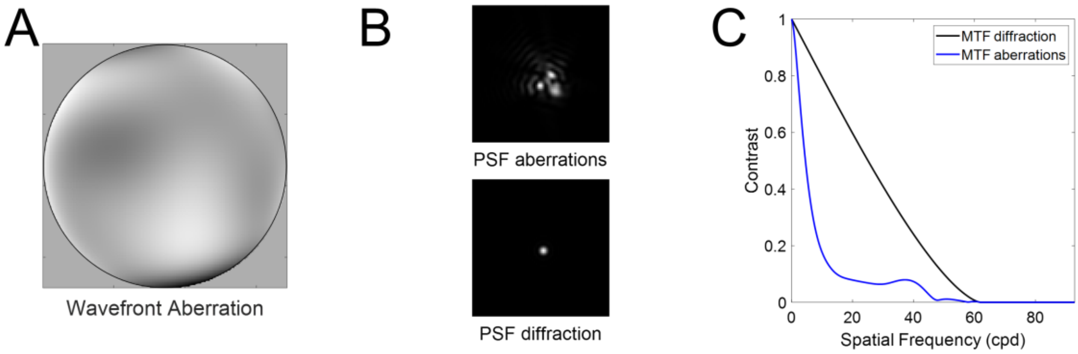

Figure 1.6. Optical aberrations of the eye of one subject (left eye of the author of the thesis) and typical metrics for estimating the optical quality. A. Wavefront aberration. **B.** Point Spread Function (PSF). Above, the PSF of the visual optical system of the subject. Below, the PSF of the optical system limited by diffraction and without aberrations. **C.** Modulation Transfer Function (MTF). Contrast as a function of the spatial frequency for the aberrated optical system (in blue) and limited by diffraction and no aberrations (in black).

Different metrics derived from the wavefront aberration can be used to estimate the optical quality of an optical system. Apart from the PSF and the MTF, the most common metric is the Root Mean Square (RMS) wavefront error, calculated using Zernike coefficients (c_n^m)

$$RMS = \sqrt{\sum_{n,m} c_n^{m\,2}} \qquad 1.4$$

The metrics described, PSF, MTF, and RMS, refer to the optical quality of the eye and describe the objective quality of the retinal image. Other metrics consider perceptual aspects of vision and provide a more complete description of the subjectively perceived quality. Thibos et al.[25] analyzed 33 metrics (optical and perceptual) to estimate objectively the visual performance of the visual system, with some of them arising as suitable candidates for predicting visual performance. For the purposes of this thesis, the Strehl Ratio (SR) and the Visual Strehl, also called Visual OTF (VSOTF) are the most important[49]. The SR (Equation 1.5) is defined as the ratio of the maximum of the PSF aberrated through the optical system (PSF) and the maximum of the PSF limited by diffraction (PSF_{DL}), and therefore estimated in the spatial domain.

$$SR = \frac{max\ (PSF)}{max\ (PSF_{DL})} \qquad 1.5$$

The VSOTF approximates the SR but in the frequency domain and has been reported to have a high correlation with the visual acuity[49,50]. This metric also considers the neural contrast sensitivity function, which describes the spatial frequencies that the neural visual system, removing the effect of the optics system. It is estimated using Equation 1.6

$$VSOTF = \frac{sum(CSF_N \cdot OTF)}{sum(CSF_N \cdot OTF_{DL})} \qquad 1.6$$

where OTF is the optical transfer function and, OTF_{DL} is the optical transfer function limited by diffraction, and CSF_N is the neural contrast sensitivity function. The next section will discuss in detail the contrast sensitivity.

1.2.2.1. Spatial Contrast Sensitivity Function (SCSF or CSF)

Contrast is the difference in luminance that makes a stimulus distinguishable from the background[51]. It can be defined in different ways, such as Weber contrast, preferred for letter stimuli, Michelson contrast, preferred for gratings stimuli, or RMS contrast, preferred in natural stimuli[52]. The mathematical description for each of them is shown in Equation 1.7.

$$C_{Weber} = \frac{L_{max} - L_{min}}{L_{bkg}}$$
$$C_{Michelson} = \frac{L_{max} - L_{min}}{L_{max} + L_{min}} \qquad 1.7$$
$$C_{RMS} = \frac{L_{\sigma}}{L_{\mu}}$$

where L_{max}, L_{min}, L_{bkg}, L_{σ}, and L_{μ} are maximum luminance, minimum luminance, background luminance, mean luminance, and standard deviation luminance, respectively.

Also, stimuli can be defined by their spatial frequency spectrum, measured in cycles per degree (cpd). Low-frequency components define the overall shape and form of an object and high-frequency components its fine details. Figure 1.7 shows the effect of filtering an image with a low-pass filter (only coarse details pass) and with a high-pass filter (only fine details pass) using a Gaussian-shaped filter with a cutoff frequency at half-height. Furthermore, it has been widely reported studied that natural images spectrum is made of low and high frequencies, with $1/f^2$ spatial frequency behavior[53]. Another important feature of the stimuli is their orientation, as our cells are programmed for processing oriented features.

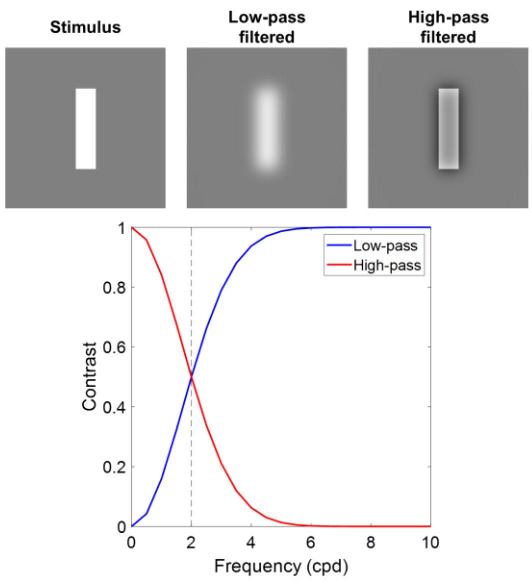

Figure 1.7. Low-pass and high-pass spatial filtering of a visual stimulus of 1x0.25 visual degrees with a Gaussian-shape filter. Above, from left to right, the original stimulus, filtered with a low-pass filter of a cutoff frequency of 2cpd and filtered with a high-pass filter of a cutoff frequency of 2cpd. Below, a graphical representation of the filters in one direction (horizontal or vertical), blue for low-pass and red for high-pass filters.

The minimum detectable contrast is the contrast threshold, which determines the sensitivity (the inverse of the contrast). The Spatial Contrast Sensitivity Function (SCSF), usually referred to only as Contrast Sensitivity Function (CSF), describes the sensitivity to different spatial frequencies and can be summarized as a band-pass filter where low and high spatial frequencies are stronger filtered than medium frequencies[52,54]. It has a maximum sensitivity at around 4 cpd and decreases at similar rates for low and for high frequencies. Beyond 40-60 cpd is considered the cutoff frequency, i.e., the minimum contrast spatial frequency visible when contrast is 1.

CSF is an important feature of vision tested in the clinic[54], mainly because it can reveal visual dysfunctions that are otherwise missed in the clinical practice routine, playing a role in pathologies such as cataracts[55,56], multiple sclerosis[57], post-refractive surgery[58], age-related macular degeneration[59]. Measuring contrast sensitivity is also useful for monitoring the changes after clinical interventions, such as age-related macular degeneration, cataracts, or optic neuritis[54].

Another variation of the CSF is the Neural Contrast Sensitivity Function (NCSF), which subtracts from the measurement of the CSF the impact of the visual optical system, i.e., the wavefront aberration. By doing so, the influence of the optics is eliminated and only the perceptual part remains. Equation 1.8 shows how to estimate the NCSF[60].

$$NCSF = \frac{CSF}{MTF} \tag{1.8}$$

1.2.2.2. Temporal Contrast Sensitivity Function (TCSF)

On the other hand, the perception of temporally modulated contrast is defined in the Temporal Contrast Sensitivity Function (TCSF)[61,62]. When observing an object changing over time, the visual system might perceive said temporal change (flicker) or not (fusion). The TCSF is a similar curve to SCSF, although the maximum is found at around 10 Hertz (Hz), falling more rapidly for high than for low temporal frequencies with a higher ratio than the SCSF. The cutoff temporal frequency, which defines the boundary between flicker and fusion perception, is known as contrast Critical Fusion Frequency (CFF). The CFF is well known to be around 50-70Hz, depending on the features of the stimulus[62]. Another interesting example is that the visual system is not able to capture the movement of the minute and hour hands of a watch, because the frequency rate is remarkably low.

The effect of the TCSF on clinical environments has not been so widely studied. However, it has been reported to be affected by age[63–65] and by some pathologies, such as retinal degeneration[66], age-related macular degeneration[67], and age-related maculopathy[68]. The neural TCSF has also been studied before[69].

1.2.2.3. Spatiotemporal contrast sensitivity function

Combining the SCSF and the TCSF, the spatiotemporal contrast sensitivity function (STCSF) defines what is visible in space and time domains. Robson[70] measured STCSF for the first time, studying the contrast thresholds of a stimulus for different spatial and temporal frequencies. The limits of spatiotemporal perception define the 'window of visibility'[71], a region of the spatiotemporal domain that defines the boundaries for the perception of visible and fused images. For the STCSF, the model developed by Burbeck et al.[72] and later refined by Lambretch et al.[73] has been used in this thesis.

1.2.2.4. Measuring spatial and temporal sensitivity functions

Traditionally, psychophysical tests take a long measurement time and use cumbersome stimuli and procedures, which might prevent the implementation of straightforward tests in the clinic. Pelli et al.[52] suggested practical advice about the psychophysical parameters to evaluate the CSF, which can also be extrapolated to the TCSF. In summary, they suggested using forced-choice tasks, many alternatives in the choice (at least 4), and an adaptive algorithm for estimating the threshold. Within the same lines, there have been attempts to simplify traditional psychophysical procedures to fast and reliable measurements. For the CSF, the qCSF (quick CSF) algorithm uses the information of the CSF knowledge to estimate the threshold successfully[74], significantly reducing measurement time. For the TCSF, Wooten et al.[75] developed an easier test for measuring the TCSF, although it has not significantly reduced measurement time, but has improved the task.

1.2.3. Optical blur

The main perceptual consequence of an imperfect optical system is blur. Blur is inherent to every optical system and, although we usually take it for granted, it may be difficult to define. From the visual point of view, it can be defined as a smearing of the image[76]. From the theoretical point of view, blur is considered like a low-pass filter that eliminates high-frequency components of the image and maintains low- and medium-frequency components.

Traditionally, blur has been defined as a Gaussian-shape filter[76]. For instance, for an edge stimulus, i.e., an abrupt change in luminance, the transition across the orthogonal direction is a step function. For a blurred edge with a Gaussian filter, the transition is not a step function anymore and the standard deviation of the Gaussian determines the amount of blur. Several studies have reported the sensitivity blur in these terms for different types of stimuli[77–80]. However, optical blur is more complex than a Gaussian filter. With the wavefront aberration measurement of the optical system, the optical blur can be defined by its PSF[23], and the transition takes the form of the Line Spread Function (LSF), which provides a complete characterization of the optical system and a more accurate mathematical definition of blur. Other studies have also measured the sensitivity to optical blur[41,81–83].

Two main components regulate blur perception[84]. On one hand, blur detection refers to the ability to detect the presence of blur, i.e., the absolute threshold. On the other hand, blur discrimination refers to the amount of blur to discriminate changes in blur in an already blurred stimulus. To estimate blur discrimination, an additional blur is added over an amount of blur base (reference). Repeating the estimation for different reference blurs, the threshold vs. reference (TVR) curve reports the threshold blur increment as a function of the reference blur.

Interestingly, the TVR curve shows a higher lower threshold (maximum sensitivity) to changes in blur when the image had already a particular amount of blur. Watson and Ahumada[76] reviewed the studies that investigated the TVR curve to find a model that can describe better blur discrimination. Classically, Weber's model was used to describe the TVR curve

$$a = -r + \sqrt{\omega^2(\beta^2 - r^2)^\rho - \beta^2} \qquad 1.9$$

where a represents the threshold blur and r the reference blur in arcmin and ω, β and ρ are factors that represent the gain, the intrinsic blur, and the power, respectively.

Watson and Ahumada[76] developed a model called Visible Contrast Energy (ViCE), that accounts for the differences between two Gaussians with a different standard deviation (i.e., different amount of blur). The model was in high agreement with the data from those studies. They concluded that the main limitation of their model, for small amounts of blur, is that optical blur cannot be removed from the equation.

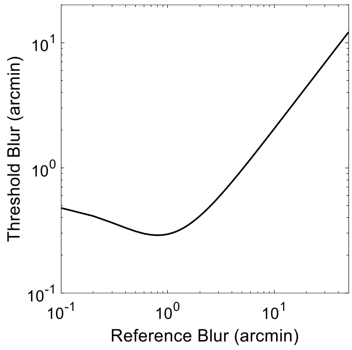

Figure 1.8. Blur discrimination curve (threshold vs. reference, TVR). Based on Weber's model.

Optical blur is used for several visual tasks. The most intuitive is for resolving the details of images, but blur is also used as a cue for depth perception[84–87] and accommodation[88]. The interest in blur not only resides in its impact on perception itself but also in its clinical application. Blurry images are likely the most common and easily identified symptom to attend to for testing the state of vision. Although blur, as said before, can be represented by the aberrations, only the LOAs can be compensated using ophthalmic corrections. The next section of Chapter 1 will cover it in detail.

1.3. Clinical evaluation of the visual function

The assessment of visual function consists of performing different tests that evaluate different aspects of vision, from visual acuity to the perception of color. Typically, the most performed tests in the clinic include the evaluation of the refractive error, the visual acuity achieved with said refractive error compensated, color perception and the presence of color abnormalities, proper binocular fusion and depth perception, and eye dominance. In this section, a description of these tests will be provided, with special emphasis on the evaluation of refractive error.

1.3.1. Refractive error

The LOAs, that can be compensated with ophthalmic lenses such as spectacles glasses, contact lenses, intraocular lenses, or laser refractive surgery, are commonly known in clinical practice as refractive error. Refractive error is the condition where the optics of the eye does not focus the light on the retina, resulting in blurred images and reduced visual performance. It is estimated that 1 billion people worldwide suffer from near or far vision impairment due to non-corrected refractive error, resulting in the second most important cause of avoidable blindness[89].

Refractive error is one of the most important pieces of information required in eyecare practice, and its evaluation is likely the most frequent procedure performed. It is not only used for the prescription of ophthalmic corrections, but also as a method to obtain basic information about the state of the patient's eyes (i.e., emmetropia, moderate or high myopia or hyperopia, etc.), before many other ophthalmology procedures.

<u>1.3.1.1. Types of refractive error and their compensation</u>

The condition where the eye can perfectly focus the incoming light is called emmetropia. On the other hand, ametropia, commonly known as refractive error, can be classified into four categories: myopia, hyperopia, presbyopia, and astigmatism. Myopia refers to the condition where the rays focus before the retina, i.e., the optical system has an excess of optical power. Hyperopia refers to the condition where the rays focus behind the retina, i.e., the optical system has an insufficiency of optical power.

The visual optical system is a spheroid, with two main principal axes. Astigmatism refers to the different refractive errors for different axes, and the optical difference between them provides the amount of astigmatism. Astigmatism can be classified into different classes. According to the principal axis, which is the most powerful (more optical power), astigmatism is classified as with-the-rule (principal axis is horizontal, 180±20º), oblique ([45±20º, 135±20º), or against-the-rule (principal axis is vertical, 90±20º). According to the refractive error in each axis, astigmatism can be simple myopic or simple hyperopic if only one axis is myopic or hyperopic and the perpendicular is emmetropic; compound myopic and compound hyperopic when both axes are hyperopic; mixed when one axis and the perpendicular is either hyperopic or myopic. Finally, presbyopia is a refractive error in which the eye loses its ability to focus near objects, as defined in section 1.1.

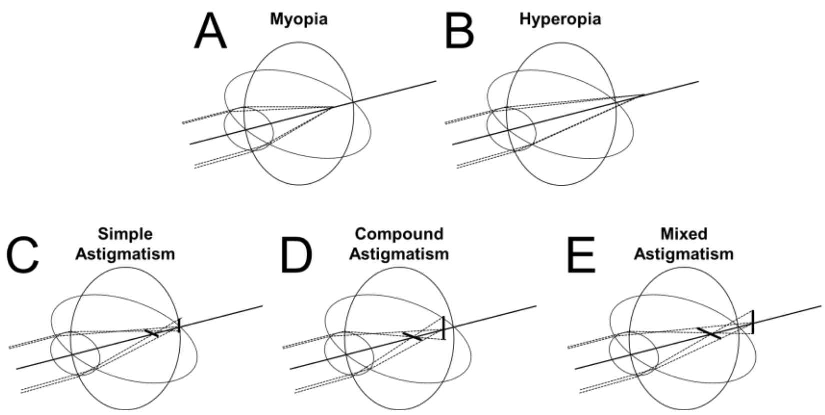

Figure 1.9. Types of refractive errors. **A.** Myopia. Rays focus before the retina. **B.** Hyperopia. Rays focus behind the retina. **C.** Simple astigmatism. Only one axis does not focus on the retina. In this case, is simple myopic astigmatism. **D.** Compound astigmatism. Both axes do not focus on the retina. In this case, is compound myopic astigmatism. **E.** Mixed astigmatism. Both axes do not focus on the retina, but one axis focus behind the retina (myopic) and the other beyond the retina (hyperopic).

The compensation for refractive error varies depending on its type. Myopes need a divergent lens (negative) to reduce the extra optical power of the optical system of the eye. Hyperopes need a convergent lens (positive) to increase the lack of optical power in the optical system of the eye. However, due to the ability of the crystalline lens to increase the optical power of the visual optical system, some small amount of hyperopia may be naturally compensated with the accommodation[90]. Unfortunately, when the accommodation begins to malfunction with age, small hyperopias arise as early presbyopes. Astigmatism requires a toric lens, with different optical powers for each axis, depending on the type of astigmatism. The compensation for these refractive errors can be delivered by spectacles (the most frequent), contact lenses, refractive surgery, or intraocular lenses, mainly depending on the lifestyle of the patient.

The compensation for presbyopia requires a lens that focuses near objects again, therefore requiring an additional (positive) lens. Depending on the age, a tentative addition could be +1.00D for 45 years old, +1.50 for 50, +2.00D for 55 and +2.25D for 60[91]. Above that age, the addition depends on the activities that the patient most demands to focus on objects. However, the types of corrections for presbyopia are more diverse, with different solutions depending on the patient’s lifestyle.

In clinical practice, the prescription to compensate for the refractive error is provided in a spherocylindrical approach, which refers to the combination of spherical and cylindrical lenses, usually selecting the axis of the cylindrical lens to make negative the astigmatism amount. However, the comparison between different corrections to perform statistical analysis or to evaluate repeatability is difficult using this approach. Many computational tools have been developed to tackle this problem. The most popular and used approach is the power vectors[24], which uses Fourier analysis to transform a spherocylindrical prescription (sphere, cylinder, axis) into a three-dimensional vector of spherical equivalent (M), vertical astigmatism (J_0) and oblique astigmatism (J_{45}).

$$
\begin{gathered}
M = S + C/2 \\
J_0 = -\,C/2\,(cos2\theta) \\
J_{45} = -\,C/2\,(sin2\theta) \\
B = \sqrt{M^2 + J_0^2 + J_{45}^2}
\end{gathered}
\tag{1.10}
$$

where S is the sphere, C is the cylinder, and θ is the principal axis of the more myopic foci. Figure 1.10 shows the refractive error as a three-dimensional vector. Besides, the length of the power vector, B, can be used as a measure of the blurring strength[92]. In this thesis, power vectors are usually used to compare different refraction methods.

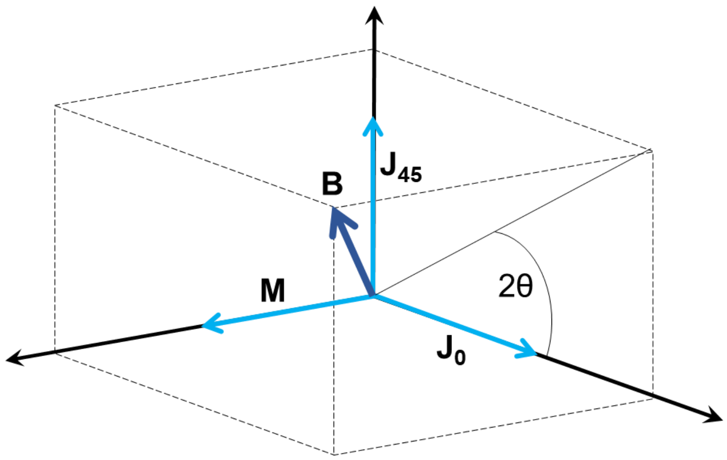

Figure 1.10. Power vector notation representation.

1.3.1.2. Optical corrections for presbyopia

Apart from a pair of glasses with the addition needed for focusing near objects, alternating vision is the most spread compensation for presbyopia. The correcting lens has different powers throughout its structure, and the patient must move their gaze (moving the head or the eye) to see through the desired power to focus at different distances. The first type of lens fabricated with this approach was the bifocal lens, with two differentiated zones, the upper region for distance vision and the lower region for near vision, with an abrupt change in the transition between them. An evolution of the bifocal lens is the progressive lens, which provides a smooth transition between the distance and the near regions, with many intermediate distances in between. The drawback of progressive lenses is that the smooth transition produces peripheral regions with severe optical quality decrease and, because of that, the fitting process may require time for neuroadaptation to the change[93]. Alternating vision strategies are usually delivered in spectacles.

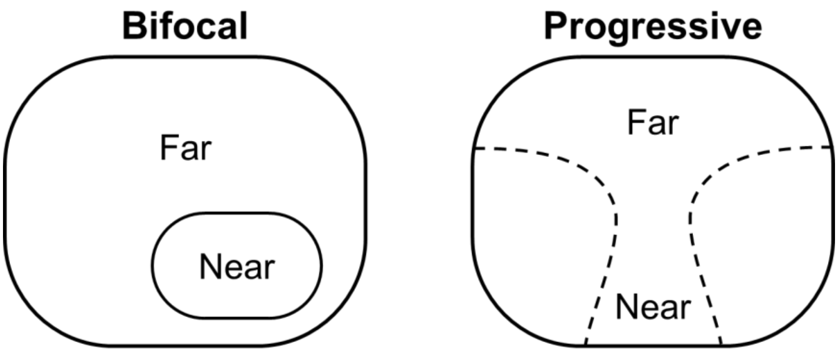

Figure 1.11. Presbyopia corrections using alternating vision approaches.

Another type of correction is monovision. With monovision, each eye is fitted with a lens that sharply focuses light from different distances, providing near vision to one eye and far vision to the other. For patients in which the correction is successful, it has been suggested that the visual system suppresses the lower quality image and preferentially processes the higher quality image[94–96]. However, the adaptation or not to monovision corrections has not been fully demonstrated[97]. The selection of the eye to compensate for far or near distance is based on the dominant eye, which can be obtained with different tests, although the process is not standardized. Section 1.3.6 will tackle more detailed eye dominance tests. Unfortunately, although monovision has a high acceptance ratio, it has drawbacks: degrades stereoacuity[98,99] and contrast sensitivity[96], hampering fine-scale depth discrimination and reading in low light. Monovision is also thought to cause difficulties in driving[100] and has been implicated in an aviation accident[101]. Despite these drawbacks, many people prefer monovision corrections to other corrections or no corrections at all[102], being the most popular prescription for presbyopia spectacles-free[103].

The usual amount of addition for monovision corrections ranges from 1.50D to 2.50D, depending on the degree of the presbyopia. Lenses for monovision have the drawback of not only inducing the difference in optical power but also a difference in retinal image magnification between the eyes due to the distance of the lens to the pupil of the eye, clinically called anisocoria. A typical monovision correction of 1.50D could cause an anisocoria of 2%, which may produce discomfort and clinical issues[104]. Therefore, the most common method for delivering monovision corrections is contact lenses, and then surgery[97]. It also exists mini-monovision corrections, with a smaller addition than 1.50D[105,106].

Unlike monovision corrections or bifocals, which only provide two foci, simultaneous vision corrections provide foci for many different locations, similar to progressive lenses, but independent of the gaze position. Simultaneous vision creates a unique image on the retina conformed of superimposed images corresponding to different visual distances. Thus, the perception is a sharp image coexisting with a background of defocused images, reducing the overall contrast of the perceived image. There are different types of simultaneous vision corrections, bifocals (two main foci), trifocals (three main foci), and extended depth of focus (EDOF, providing close to perfect vision for far and intermediate distance[107]). Currently, more than 70 multifocal designs exist in the ophthalmology market[108]. As in progressive spectacles, a neural adaptation process is key for a successful simultaneous vision prescription[109,110].

Simultaneous vision is usually delivered in contact lenses (CLs) or intraocular lenses (IOLs). Simultaneous vision is achieved by modifying the spatial structure of the lens, and the design is classified based on the optical principle. Refractive designs use the principle of refraction, and a different curvature in different regions of the lens creates different foci[111]. Diffractive designs use the principle of diffraction to create different steps in the lens that produces different foci[112].

Instead of spatial modifications, new technologies use temporal changes in optical power to create simultaneous vision corrections. SimVis technology was developed in the Visual Optics and Biophotonics Laboratory, Institute of Optics (IO-CSIC), representing an evolution from an on-bench monocular optical system to a miniaturized, portable, and binocular system[113]. Briefly, SimVis uses the principle of temporal multiplexing to create simultaneous vision images, using an optotunable lens to produce fast temporal changes in the optical power, faster than the integration time of the visual system, producing the perception of a static multifocal retinal image. Liquid optotunable lenses usually are liquid lenses with a deformable surface and an actuator that allows programmable changes in the optical power. In the case of SimVis, the optotunable lens is a liquid-filled lens with an elastic membrane and a magnetic actuator that pushes the liquid and deforms the membrane, allowing changes in optical power in timeframes of milliseconds. SimVis Gekko is now commercially available to show patients different presbyopia corrections before surgical implantation or fitting, allowing them to try the visual experience of different corrections in a short period of time. Chapter 2 describes in detail this technology and its use in this thesis.

Other presbyopia corrections include the combination of monovision and simultaneous vision, such as modified monovision, with one eye corrected with monofocal and the other with multifocal[114], and different types of multifocal corrections between both eyes, varying the type (bifocal, trifocal, EDOF) and the amount of the additions (from 0.75D to 1.75D)[114–119].

Finally, the ultimate goal in presbyopia corrections is the restoration of the misfunctioning of the aged crystalline and recovering the accommodation function typical of young eyes. This type of correction relies on the maintenance of the muscle contraction of the ciliary muscle, which drives the accommodation process, remaining in presbyopic subjects[120] and can only be delivered in IOLs. The zonules of the crystalline lens, attached to the capsule bag, are still able to apply force. The main working principles of these accommodative lenses are pushing and pulling a lens changing the axial position and therefore changing the optical power; or modifying the curvature of a lens attached to the capsule bag, aiming at mimicking the functioning of the healthy crystalline lens[121]. Several attempts to develop Accommodating IOLs have been carried out, using different working principles, although only one of them has reached the market[122].

Before considering the most appropriate prescription for each patient, clinicians must find out the refractive error. The following sections will cover the different techniques for that purpose.

1.3.2. Objective refraction

In an attempt to reduce the measurement time and facilitate both the task of the patient and the complexity of the procedure followed by the practitioner, many objective refraction technologies, without the need for subjective responses from the patient, have been improved throughout the years.

Autorefractors provide a direct measurement of the refractive error of the patient. Classic autorefractors project optical objects (typically dots or rings) onto the eye and obtain the refractive state of the eye from the analysis of the retinal image (typically the size or the blur of the image), using different technologies such as infrared lasers, LEDs, superluminescent diodes, Badal systems, CCD or CMOS cameras[123]. Many of them also incorporate fogging algorithms. Moreover, new technologies based on wavefront analysis have emerged over the years[25]. Several studies have reported very high repeatability of autorefractometers, with a standard deviation of repeated measurements ranging from ±0.12 to ±0.37D[124–127].

Other studies have reported significant differences in spherical equivalent between autorefractometers and subjective refraction. Thibos et al.[25] studied the precision of 33 different metrics derived from the wavefront aberration map of the eye, to predict the spherical equivalent of the refractive error. They found mean absolute differences on the spherical equivalent, compared with the subjective refraction, ranging from ±0.25 to ±0.48D, giving birth, in 2004, to wavefront autorefractometry, a discipline that has provided several autorefraction technologies over the years[125,127–133]. Modern autorefractometers provide mean absolute differences ranging from ±0.55 to ±0.24D, depending on the autorefractometer[129,134]. A recent review[135] analyzed four portable autorefractors and reported that QuickSee provides the lowest mean absolute difference (±0.21D)[136]. Many other studies have compared subjective refraction with different types of autorefractors, reporting similar differences[126,128,130–133]. To summarize, both classic autorefraction and wavefront-based autorefraction provide high repeatability, with wavefront autorefractors providing better predictions of the spherical component of the subjective refraction (mean absolute deviations between ±0.25 and ±0.50D). Other objective tools, such as deep-learning algorithms[137], have been used to predict the spherical refractive error from retinal fundus images, but their outcomes are still far from other objective techniques (±0.91D with respect to the subjective refraction).

Over many years, aiming at increasing efficiency by eliminating the subjective and iterative approach of traditional refraction, different objective techniques have been developed. Except for traditional retinoscopy, a technique that requires years of expertise to master and additional time with each patient, all other objective techniques, even modern autorefractometers using sophisticated technologies such as aberrometry, are fast and easy to use. Because of that, the use of modern objective refraction instruments -many of them open-field, wavefront based, portable, or combined with keratometry- has been extended to almost every clinic. However, except for remarkable exceptions[138], objective autorefractors are not considered to provide a result interchangeable with subjective refraction but are a valuable starting point for the subjective refraction procedure.

1.3.3. Subjective Refraction

Objective refraction techniques are normally fast measurements and do not require the input of the patient. Subjective refraction techniques generally require repeated responses of the patient during letter identification, blur comparison, or blur minimization, which are often cumbersome. Although objective refraction techniques are improving, clinicians still rely on traditional subjective refraction as the gold standard method to evaluate refractive error[91]. This method consists in testing different lenses until maximum visual acuity (the minimum size of recognizable letters on a chart) is achieved. Traditional subjective refraction is often performed with a trial frame and a set of trial lenses, but also with a phoropter. The stimuli have evolved from static eyecharts to dynamic optotype projections and digital displays fully programmable and controlled by software.

Accommodation is the main issue while evaluating the refractive error, particularly in children and young adults where the accommodation process is elicited very easily, producing overcorrection of myopes and undercorrection of hyperopes (that are often not detected and therefore left uncorrected). To minimize its impact, cycloplegic agents are widely used, although this approach is not always possible because it entails some medical risks and, in most countries, requires the presence of an ophthalmologist. The most used approach is the fogging technique, carried out by adding positive lenses to induce myopic blur in the retinal image and then reducing the addition step by step. Because this process increases the duration of the procedure, it tends to be tedious and can cause fatigue in the patient. Furthermore, other refinement techniques, such as the duochrome or cross-cylinders tests, are often included in the final adjustments of subjective refraction. Most importantly, despite its status as the gold standard, traditional subjective refraction delivers measurements of refractive error that are marred by long measurements with low repeatability.

Subjective refraction is time-consuming. It entails, for each patient's eye, the full dedication of a well-trained eye care professional for more than 6 minutes on average[123,139–142] and can be much more in some patients. Subjective refraction represents, for many eye care practitioners, a considerable portion of every workday. The scarce availability of optometrists represents one of the main causes of non-corrected refractive errors in developing countries, representing a bottleneck in many vision care services. The time constraints in optometry practice reduce the number of more thorough eye examinations and visual tests.

In practice, variability is tightly related to the restrictions in measurement time. The intraoptometrist repeatability, which is the standard deviation across repetitions performed by the same optometrist evaluating the same eye, has been reported to range in the spherical component from ±0.20 to ±0.32D[124,127,143–145]. The interoptometrist variability, which is the standard deviation across repetitions performed by different optometrists evaluating the same eye, is slightly higher than the intraoptometrist variability, ranging from ±0.20 to ±0.38D[127,128,143,145,146].

One might think that this error is small, subclinical, and thus non-significant. Atchison et al.[147] found that differences of just ±0.25D away from the best refraction can produce visual problems like headaches or distortions. Also, Freeman et al.[148] reported that most intolerances to prescriptions could be corrected by modifying the prescription by less than 0.50D. In addition, Bist et al.[149] have recently reported in a meta-analysis a significant non-tolerance to spectacles (between 1.6% and 2.7%), and that almost 50% of them are due to errors in the estimation of refractive error. Ravikumar et al.[150] reported significant perceptual preferences between different corrections, all of them producing the same maximum visual acuity, highlighting the perceptual importance of the residual refraction caused by the variability of the subjective responses of the patients, present in all subjective refraction procedures.

1.3.4. Beyond traditional subjective refraction

The combination of autorefractometers and traditional subjective refraction has been the standard clinical practice workflow for decades, reducing time compared to subjective refraction alone, but maintaining the outcomes. There is still strong demand to reduce the variability and time involved in subjective refraction.

This section reports recent progress in technologies and methodologies to subjectively evaluate refractive error and provides an overview of the advances and trends in this old field dominated by a universal gold standard, the traditional subjective refraction, that conceptually has not evolved much over decades, if not centuries. A summary of the new technologies can be found in Table 1.3.

1.3.4.1. Programmable phoropters

Otero et al.[141] transformed an existing manual phoropter into an automatic phoropter, using 8 motors and custom software. Automatic phoropters have been available for years, but the authors automatized the whole process to drive the phoropter in combination with a psychophysical procedure to perform subjective refraction. Their results, in terms of repeatability and time (see Figure 1.12 and Table 1.3 for a comparison with other approaches), were similar to traditional subjective refraction but with a higher degree of automation and standardization.

Digital Infinite Refraction is a new concept implemented in a recent commercial automatic phoropter (Vision-R 800, Essilor, Charenton-le-Pont, France) that incorporates tunable lenses and allows changes in sphere and cylinder as precise as 0.01D. This instrument also includes an algorithm that evaluates spherical and cylindrical power at the same time and at each step, instead of separating both tasks in consecutive phases as in traditional subjective refraction. Venkataram et al.[142] compared this instrument with two different algorithms (one used fogging, the other did not) with the traditional subjective refraction. They found no statistical differences in spherical equivalent and the mean deviation was 0.0D (Limits of agreement (LOAs): [-0.80, +0.80]D) with fogging, and -0.20D (LOAs: [-1.00, +0.60]D) without fogging. The measurement time was significantly lower (5.4±1.0min with fogging; 3.1±0.6min without fogging) than with traditional subjective refraction (9.5±1.6min in that study). The combination of a very precise technology with a methodology unifying all the components of refraction within the same commercial instrument, providing measurement time reductions, makes this instrument a powerful clinical option.

Nidek TS-610 (Nidek, Gamagori, Japan) is a compact tabletop refraction system that provides subjective refraction using a programmable phoropter and a digital eye chart embedded within the same instrument. The clinical studies of this commercial instrument, which can be remotely controlled and aims at substituting a full refraction unit, are still ongoing.

VisionFit (Adaptica, Padova, Italy) is a head-mounted automatic phoropter that can be remotely controlled. In a recent study, Curtis et al.[151] showed that VisionFit was also able to provide a remotely controlled subjective refraction, with a high agreement in the spherical equivalent with the traditional subjective refraction (LOAs: 0.12±1.53D). However, the sample was comprised of elder and low vision patients. This feature of the sample population may contribute to the increased variability.

1.3.4.2. Self-refraction instruments

Leube et al.[152] proposed a quick subjective self-refraction procedure based on adjusting the shift of pair of Alvarez lenses until the refractive error is compensated. As in other self-refraction techniques (see later), the results show poor agreement compared to traditional subjective refraction (LOAs: ±1.20D).

A more sophisticated self-refraction tool is Netra (EyeNetra, Cambridge, USA), a portable device based on a smartphone that can perform subjective refractions without supervision[153]. Their method projects onto the eye a stimulus presented on a smartphone that retrieves the subjective response of the patient. Compared with traditional subjective refraction, Netra shows a lack of control of accommodation that results in statistically significant differences (more myopic by -0.53D), and high variabilities (spherical equivalent LOAs: ±1.40D).

Easee eye test (Easee, Amsterdam, Netherlands) is a web-based online tool to evaluate refractive error with only a smartphone and a computer screen, that was designed to facilitate access to visual care and does not require phoropters, trial lenses, or other devices[154]. The results were different from traditional subjective refraction, (LOAs: ±1.35D in spherical equivalent), especially for hyperopes (mean difference of -0.50D in spherical equivalent). The measurements took much more time (22±10 minutes on average). Similarly to the Netra, this tool could be useful in environments where the lack of clinicians prevents appropriate measurements of refractive error, but it still needs much more development.

Delegating blur-detection tasks to patients seems to result in inaccuracies that are higher even than those obtained with objective refraction, and with longer measurement times.

1.3.4.3. Hybrid technologies combining objective and subjective refraction

As mentioned, combining objective and subjective measurements is probably the most common workflow in the clinic. Doing it within the same instrument represents an efficient approach that optimizes chair time.

The first instrument that included objective and subjective refraction within the same instrument, and also an automatic method to obtain subjective refraction, was the Topcon BV1000 (Topcon, Tokyo, Japan) in 2004[155]. It was able to provide high agreement with traditional subjective refraction (LOAs in spherical equivalent: 0.05±0.69D) although with a high measurement time (9.75±0.18min). The company is now commercializing an evolution, Chronos (Topcon, Japan), a compact instrument combining autorefraction and subjective refraction with an automatic phoropter and an integrated display.

The i.Scription (Zeiss, Oberkochen, Germany), combines the information of wavefront aberrometry with the result of a conventional subjective refraction procedure performed by a practitioner. By considering the information on enlarged pupil sizes, it could provide more accurate prescriptions for night-time conditions, reducing night vision complaints[156].

The Voice-Assisted Subjective Refraction system (VARS, Vmax Vision, Maitland, USA) also uses a wavefront aberrometer, this time in combination with an unsupervised voice-guided procedure controlled by an artificial intelligence algorithm to provide both objective and subjective refractions. The patient answers the questions of the algorithm using a remote controller while visualizing a letter chart embedded within the instrument[123]. This automatic refraction system has been demonstrated to provide (in a mostly young population) acceptable prescriptions (spherical equivalent LOAs: ±0.84D), but it takes one minute longer than the traditional subjective refraction (6.78min vs 5.38min of the traditional subjective refraction in that study).

The Eye Refract (Visionix, Pont-de-l'Arche, France), is an open-field aberrometer and phoropter, with the ability to measure both objective and subjective refraction, using an algorithm fed with the subjective responses of the patients. Carracedo et al.[140] studied its performance versus the traditional subjective refraction and demonstrated in a heterogeneous population (including teenagers, adults, and presbyopes) that Eye Refract (EYER in their study) also produces acceptable results in spherical equivalent (LOAs: ±0.90D), although statistical differences in astigmatism. Remarkably, EYER reduced by several minutes the time needed for the evaluation to 3.42±0.63 min on average.

The Visual Adaptive Optics instrument (VAO, Voptica, Murcia, Spain) is an adaptive optics visual simulator incorporating an aberrometer, that can be used to perform subjective refraction[128]. The authors report similar results to traditional subjective refraction and claim that it requires 60% less time (data not published). The system can use a fixed pupil size to evaluate the refractive error. As opposed to other hybrid methods described, the system is not binocular, nor open-view.

1.3.4.4. Subjective refraction beyond blur

Lastly, other subjective techniques do not use the blur perceptual cue directly and avoid the traditional tasks used in subjective refraction (letter identification, blur detection, or blur minimization). They propose new visual tasks are based on the response of the patient to other physical attributes of the retinal image, caused by blur on specific stimuli, but not perceived as blur.

The first precedent, the speckle refraction[157], was described more than 50 years ago and related the refractive state of the eye to the apparent movement of laser speckle patterns.

A more recent method within this category is the Optokinetic Nystagmus Refraction (ONR). This method exploits the fact that the speed and precision of the optokinetic nystagmus, the involuntary movement of the eye when tracking a drifting stimulus, is directly related to the amount of spherical refraction[158]. This method is particularly interesting in children that have not developed communication skills.

This thesis (Chapters 4, 5, and 6) proposes a new method of subjective refraction called Direct Subjective Refraction (DSR), describes its development and evaluates its performance. As described later in this thesis, DSR does not use the blur as a main perceptual task, but flicker and chromatic effects in a stimulus observed through a temporal defocus wave that interacts with the chromatic aberration (LCA) of the eye[159,160].

Table 1.3. Comparison of important features of new subjective refraction technologies. Working principle means the task that the patients must perform to obtain the refractive error. Self-refraction means that the subject does not need clinician supervision and automatic means that the optical power changes are not induced manually. We compared Limits of Agreement (LOAs) with Traditional Subjective Refraction (TSR) for the spherical equivalent. *We selected the experiment without fogging (faster). **Compared with objective refraction. ***In these studies, time is reported for monocular measurements; we multiplied by two for a fair comparison with the rest of the technologies. Adapted from Rodriguez-Lopez et al.[161].

Characteristic	Otero et al. [141]	Vision R800 [142]	Vision Fit [151]	EyeNetra [153]	Easee [154]	BV-1000 [155]	VARS [123]	EYER [140]	VAO [128]	OKN [158]	DSR [159,160]
Working principle	Letter identification	Letter identification	Letter identification	Letter identification	Letter identification	Letter identification	Letter identification	Letter identification	Letter identification	Optokinetic nystagmus	Defocus flicker and chromatic effects
Repeatability (D)	M: ±0.26 J0: ±0.06 J45: ±0.11	-	-	-	-	M: ±0.19 J0: ±0.08 J45: ±0.07	M: ±0.10 S: ±0.07 C: ±0.03	-	-	-	M: ±0.17 J0: ±0.13 J45: ±0.13
Comparison with TSR: LOAs (D)	-0.05±0.57	-0.20±0.80*	0.12±1.53	-0.53±1.40	0.00±1.35	0.05±0.69	-0.10±0.84	0.05±0.90	-0.02±0.67	0.05±0.96**	-0.28±0.42
Time (min)	4.27±0.73	3.14±0.60	-	-	22±10	9.75±0.18	6.78	3.42±0.63	-	7x2 = 14***	0.78x2 = 1.56***
Self-refraction	✓	×	×	✓	✓	✓	×	✓	×	×	✓
Automatic	✓	Semi	✓	✓	✓	✓	✓	✓	×	✓	✓
Own stimulus	×	×	✓	✓	✓	✓	✓	×	✓	✓	✓
Mono/ binocular	Bino	Bino	Bino	Bino	Bino	Bino	Bino	Bino	Mono	Mono	Mono
Objective + subjective	×	×	×	×	×	✓	✓	✓	✓	×	×

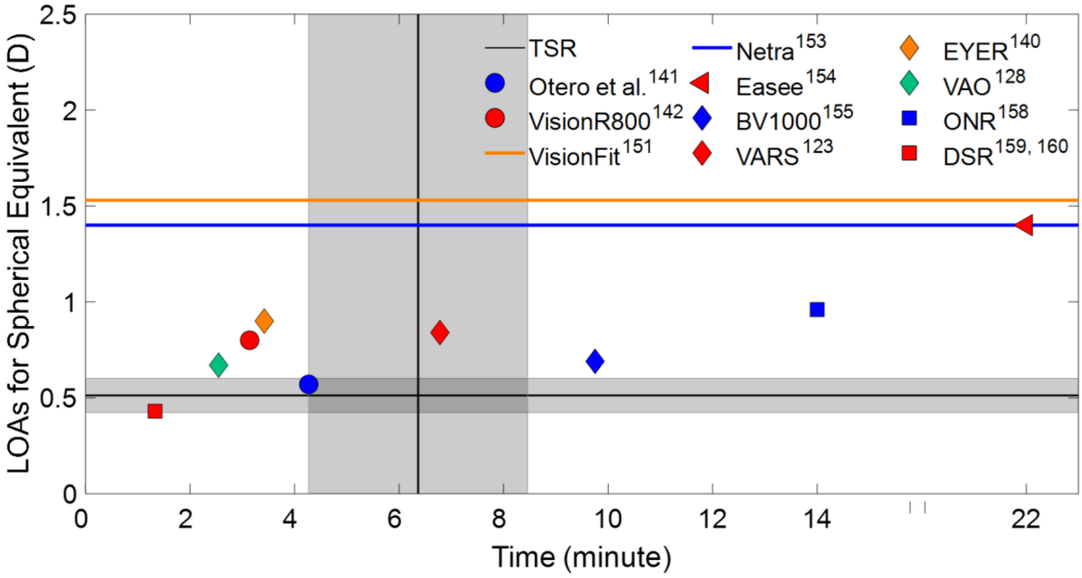

Figure 1.12. Comparison of subjective refraction methods. Gray bars represent the traditional subjective refraction method. Adapted from Rodriguez-Lopez et al. 2022[161].

1.3.5. Visual acuity

Ideally, a complete eye examination should include more tests to provide a whole description of the visual function. However, it is not realistic in clinical practice, and only a couple of them are performed, depending on the patient and the available time. Although is usually evaluated while performing subjective refraction, visual acuity is key for confirming the result of the prescription. In fact, the traditional subjective refraction procedure ends when a maximum of visual acuity is achieved. Visual acuity (VA) measures the minimum resolvable detail, called Minimum Angle Resoluble (MAR), usually in letters. Figure 1.13 shows a graphical estimation of the VA. Traditionally, Snellen eye charts were used for more than 100 years, although they provide poor repeatability due to using a decimal scale, irregular spacing between letters, and varying the number of letters in each row[162]. Current trends position the LogMAR Bailey-Love[163] as more frequently used, especially with the increase of digital eye charts, because it provides more repeatable results than other scales[164]. Other modern optotypes use a dynamic measurement of the VA, providing highly repeatable results[165], also in a pediatric population[166].

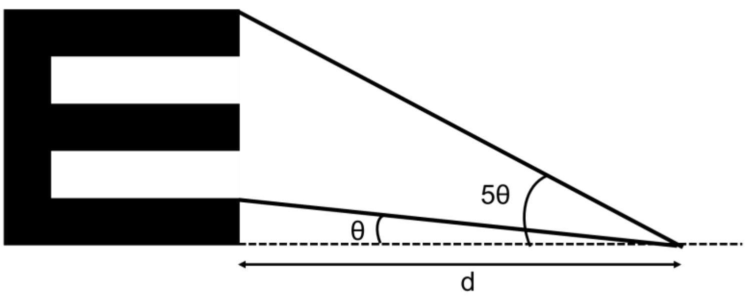

Figure 1.13. Estimation of visual acuity in a letter chart. Visual acuity is estimated as the angle between each feature of the letter (θ) and the distance of observation (d).

1.3.6. Eye dominance

Eye dominance (or ocular dominance) is the preference for the information of one eye over the other. Eye dominance has high implications in clinical practice. Traditionally, eye dominance tests are sighting ocular dominance and sensory ocular dominance tests, which are controversial because their outcomes do usually not agree.

As already described in this thesis, monovision is a widespread treatment strategy for presbyopia, the age-related loss of dynamic focusing of the eye from distance to near vision. Conventional monovision clinical practice involves correcting the dominant eye for distance[167–169] and the non-dominant eye for near.

Numerous tests for ocular dominance have been proposed in the literature and a few are performed clinically, yet it is not clear whether the dominance that they capture is relevant to the prescription of monovision. The tests used can be grouped into three categories[170]: 1) binocular rivalry tests; 2) sensory dominance, determining the eye with better visual acuity, contrast sensitivity, or other measures of visual functioning; and 3) sighting dominance, which identifies the eye that is selected to look at a (distant) target (such as the 'hole in the card' test[171]). While results of tests within each category are generally matching, provided that the conditions of the tests are comparable, there is a high degree of disagreement across categories[172–175].

A typical assessment of sensory dominance test in the clinic is the introduction of monocular blur (normally +1.50D). The patient subjectively compares the comfort during right-eye vs. left-eye blurring while binocularly viewing an optotype at distance. The dominant eye is the one where the patient feels less comfortable with blur, or conversely, the non-dominant eye is the one where blur will be more easily suppressed. The extent to which this sensory eye dominance test matches, for example, the one based on binocular rivalry has not been established. In any case, this approach appears to be more directly related to monovision, as, ultimately, the comfortable left/right eye combination of plano/positive lens is sought in a monovision treatment.

The clinical implementation of this sensory dominance test is either done using trial lenses (repeated three or four times) or using contact lenses. Trial lenses are held in front of the patient's eyes, and (although blur is the main effect) are subject to bilateral differences in magnification and prismatic effects. Also, the lenses need to be changed manually. Contact lenses allow a more faithful representation of monovision, although a direct comparison of vision with blur imposed in one eye or the contralateral is not straightforward.

This thesis tackles those issues and proposes different methods for estimating eye dominance in monovision corrections, compared with current methods. Therefore, Chapter 7 will cover the state of the art in ocular dominance measurements.

1.3.7. Other tests

Other supplementary tests performed in clinical practice are stereopsis, color perception, accommodation, cover test, or fusion tests. Stereopsis is a very important test in clinical practice which measures the minimum discrimination of depth and has implications for presbyopia corrections. It will be thoroughly covered in the following section. The other tests mentioned are also important and, depending on the pathology or optical condition of the patient, they can provide key insights for determining the treatment. However, these tests have not been covered in this thesis.

1.4. Depth perception

The visual system integrates information from the two slightly retinal images captured by the right and left eye to reconstruct a single three-dimensional (3D) visual representation of the world.

There are 3 hierarchical levels of binocular vision[176]: 1) simultaneous perception, which involves the motor system and includes the activities for aligning the eye with the object of interest; 2) fusion, which includes activities for the fusion of the images from both eyes; and 3) stereopsis, which includes the activities related to collect and transmit the visual information to the cortex. The last level depends on the healthy state of the others, although some anomalies may include problems at different levels at the same time.

For depth perception, there are monocular cues, which only need the information from one eye, and binocular cues, which require the integration of the images from both eyes[48]. Monocular cues are size (known or unknown), relative distance, motion parallax, perspective, shading, overlapping, accommodation, or blur, among others[177]. Stereopsis (or binocular disparity) relates to the integration of the information from the two slightly retinal images captured by the right and left eye to reconstruct a single three-dimensional (3D) visual representation of the world. Binocular disparity is the strongest cue for depth perception. This thesis has focused on understanding binocular disparity as a depth cue and the impact of blur in both static and moving objects to understand its implication in ophthalmological clinical practice.

1.4.1. Binocular disparity

Stereoscopic acuity is the stereopsis threshold for depth discrimination. This threshold is the minimum depth that can be perceived when only binocular disparity is the cue. Normal values of stereoacuity range between 40 and 60 arc seconds[176], although in optimal conditions it can be as small as 2 arc seconds[48]. Depth from binocular disparity can only happen if the images from both eyes lie within the horopter. The horopter is the region of the visual field where rays reach corresponding retinal points in the retina. In this region and its surroundings, images are fused. The maximum difference between the images of both eyes that can still be fused but reach non-corresponding retinal points is called the Panum's area[178,179]. Figure 1.14 shows the geometrical estimation of the horopter and the Panum's area. Depending on the difference between the eyes, images can be perceived with crossed disparity (the object is perceived closer) or uncrossed disparity (the object is perceived further).

Another important cue for depth is blur. In the absence of any other cue for depth, a sharp image is perceived closer than the same blurry image, only because of blur[85]. Binocular disparity is the dominant cue when occurs close to the fixation point, and blur dominates at further distances when binocular integration fails. It has been reported that, when binocular disparity coexists with blur, the influence of blur at distances near the fixation point is negligible, mainly considering the information from binocular disparity to perceive depth[180].

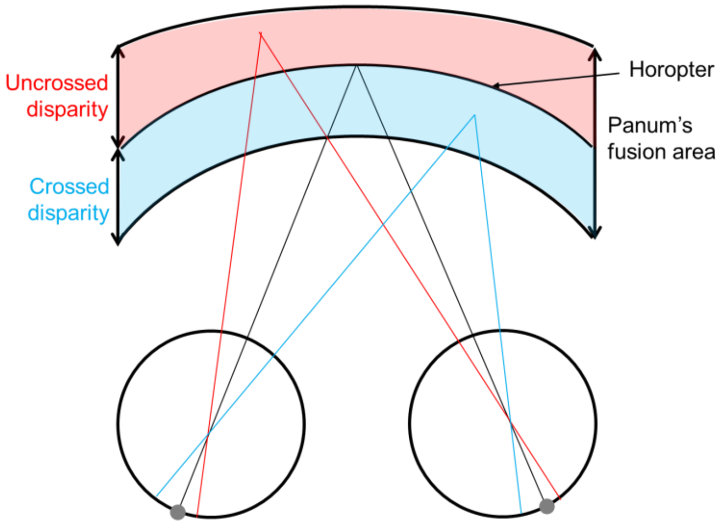

Figure 1.14. Horopter and Panum's area. Crossed disparity region is displayed in blue and uncrossed disparity region in red.

1.4.2. Stereoacuity tests

Stereoacuity measures the threshold of the visual system to discriminate objects in depth. Stereoacuity tests are usually used to identify problems in binocular vision, such as amblyopia[48]. Also, with some optical corrections, stereoacuity is affected[98]. During the development, stereoacuity appears in the initial stages, is maximum in adulthood, and degrades when we age[181].

Clinical stereoacuity tests are based on presenting a slightly different image to each eye using anaglyph filters, polarization filters, physical depth, or autostereoscopic methods (such as lenticular lenses or parallax barrier). Stereoacuity is usually measured at near distance, existing a smaller number of tests developed for far than for near distance. However, it has been reported that the distance of the test does not influence the measurement of stereoacuity in healthy patients[182–184] (with no binocular vision dysfunctionalities).

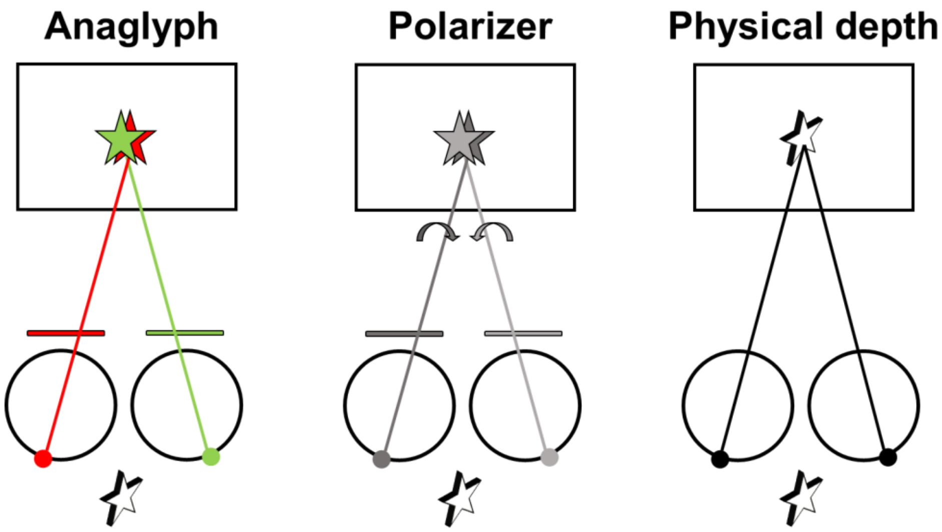

Figure 1.15. Conventional methods to create 3D images. Anaglyph (red/green) filter in the left, polarizer filters in the middle (arrows represent circular polarization), and physical depth in the right.

1.4.2.1. Conventional stereoacuity tests

Many commercial tests that use different working principles are available in clinical practice. For physical depth, the most extended is Frisby and FD2 (Frisby-Davis 2) tests, which do not require filters as the depth is physical. The tests consist of a plate with four portions, each of them with a different depth. One might think that physical depth tests are more reliable instead of the image disassociation produced by filters. However, it has been demonstrated that dissociating filters do not influence the measurement of stereoacuity[185,186].

Among the tests that use anaglyph (red/green) filters, the TNO, developed in 1975[187], is the most extended. The test consists of red/green printed random dot stereograms. Although it has been reported its usefulness compared to other tests, some studies have shown poor reliability[188] and it has been reported that the red/green filters affect the stereoacuity measured because the red filter effectively reduces contrast more than the green filter[189]. Red/green filters reduce contrast in both chromatic and luminance[190], and even recent versions of the TNO test show differences due to slight differences in the transmittance of the filters[191]. The use of anaglyph filters has huge potential because current monitors have red, green, and blue (RGB) LEDs that can easily allow the creation of custom stereo tests. However, the emission and filtering characteristics of the glasses must be considered. An extreme version of anaglyph filters is Infitec, a new stereoscopic tool that uses very narrow emission spectra for the red, green, and blue wavelengths[192].

The Titmus/Fly test uses polarizer glasses to present different images to each eye and measure stereoacuity. This test is commonly used in clinics and laboratories worldwide[177]. The main reason refers to the initial test, which consists of a fly with 3000'' of disparity, a large level that can be used as a screening tool. Failing in the fly test may probably indicate stereo blindness. It also contains circles and shapes with different levels of disparity for measuring the stereoacuity. The Randot Test also uses polarizer filters to present random-dot stereograms with different disparities. A pediatric version was developed in 1998[193].

1.4.2.2. Autostereoscopic techniques

Autostereoscopic techniques show different images to each eye but do not require filters. Autostereoscopic techniques slice the resolution of the display into different views, each of them reaching only one eye. Recent advances in 3D displays report the development of novel types of technologies for creating autostereoscopic displays[194,195]. Among them, the most important for this thesis are lenticular and parallax barrier displays.

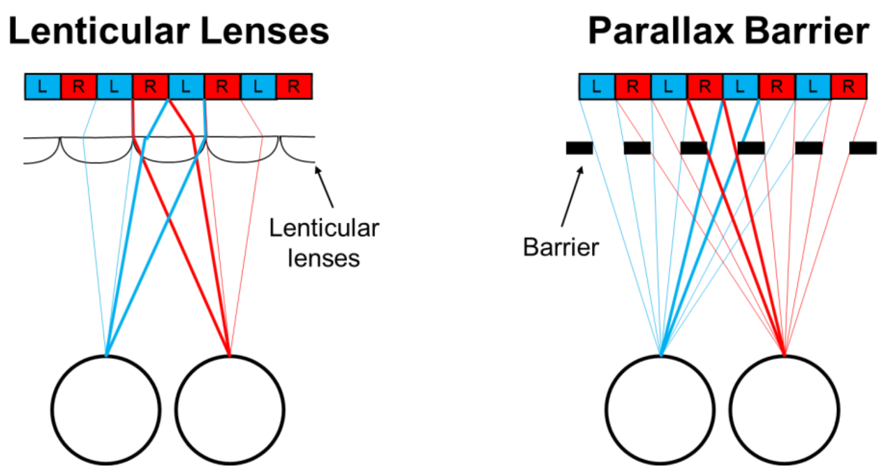

Figure 1.16. Working principle of autostereoscopic displays. Adapted from Dogson 2005[194]. Parallax barrier approach on the left and lenticular lenses approach on the right.

Lenticular lenses approach is the most common type of autostereoscopic display. It uses vertical cylindrical lenses to show columns of pixels to each eye. Figure 1.17A illustrates the process. The main drawback is that only allows a limited number of views. Recent advances have proposed slanted lenses (instead of purely vertical or horizontal) to increase the number of views[195]. The Lang Stereo test developed in 1983[196] uses a lenticular sheet to show random-dot stereograms with hidden figures, although it can only be used for screening[48,197]. A new clinical test called BEST was developed using lenticular lenses[198], reporting results similar results to the Randot test.

Parallax barrier technique uses vertical opaque regions to enable the view of only columns of pixels. The main drawback compared to lenticular displays is that, by design, parallax barrier is less bright as the barriers block some portion of the emitting light (Figure 1.17B). Slanting the barriers also allows the creation of more views[195]. There have been attempts to develop clinical tests using parallax barrier displays. ASTEROID (developed at Newcastle University, Newcastle, Great Britain) is a gamified stereo test that estimates the stereoacuity with an adaptive staircase procedure[199,200] which has been also tested in a pediatric population with satisfactory results[201].

<u>1.4.2.3. Agreement between stereoacuity tests</u>

There have been several studies investigating the agreement between different stereoacuity tests. In general, there is a low correlation among them[48]. The reasons behind this may be due to several factors, including the features of the stimuli (size, shape, figure familiarization), the presence of monocular cues, and the static nature of the tests, among others. In this thesis, Chapter 13 explores the stereoacuity measured using different methods to create depth.

1.4.3. The Pulfrich effect

Binocular vision is usually tested in the clinical environment for static stimuli. However, depth perception is more complex when moving stimuli are involved, as the signal that reaches each eye is constantly changing. Some authors compared static versus dynamic stereopsis, finding results not correlated at all, reporting that dynamic stimulus is more easily recognizable than static stimuli[48,183]. The most widely known stereoscopic effect involving moving objects is the Pulfrich effect.

The Pulfrich effect is a well-known stereo illusion that occurs due to imbalances in the retinal images reaching each eye. Classically, the Pulfrich effect was described for interocular differences in the retinal illuminance, where the image with lower illuminance is processed slower than the image with higher illuminance. These differences are not problematic for static objects but are important for moving objects. The slower processing speed of the image of the dimmer eye with respect to the image of the brighter eye produces an effective binocular disparity, provoking the illusion of depth. Figure 1.17 illustrates the effect.

For example, if the left eye is dimmer and the object is moving from left to right, the left eye image is processed slower, and the object will be perceived further from its real position (Figure 1.17A). For the same object, but the right eye is dimmer and therefore its image is processed slower, the object will be perceived closer to its real position (Figure 1.17B). The depth illusion can be easily estimated using geometry[202].

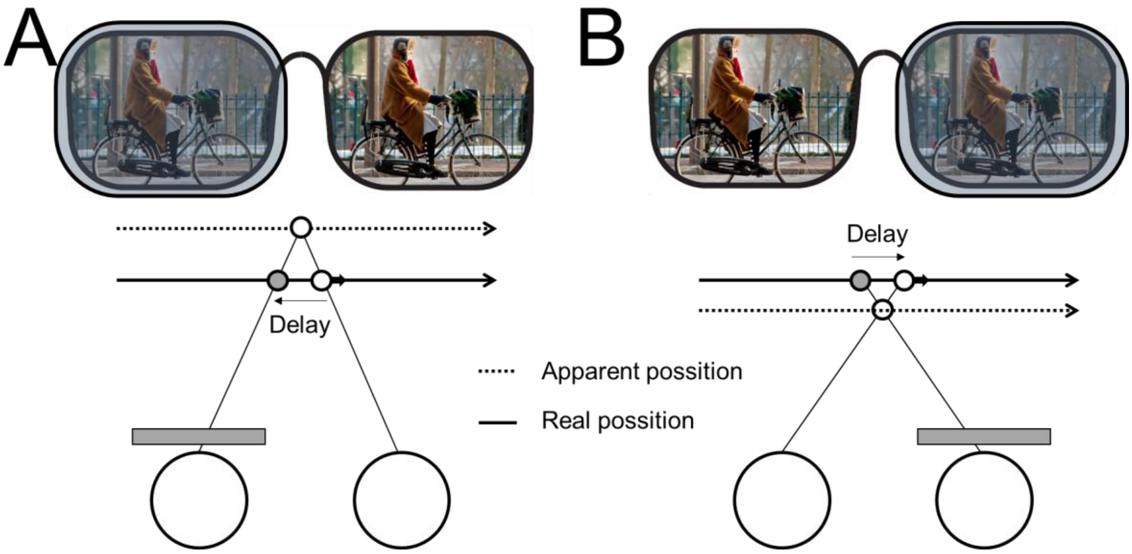

Figure 1.17. Pulfrich effect illusion. Object moving in front of the observer to the right (perspective from above). **A.** Reducing the incoming light of the left eye (using a filter) delays its processing speed and the object appears further than its real position. **B.** Reducing the incoming light of the right eye delays its processing speed and the object appears closer than its real position.

The Pulfrich effect in its classical version has been extensively studied, from the factors that influence the effect, such as the overall light level[203,204], the speed[205], the prior light adaptation[206–208] or the eye movements[209–211], to its clinical relevance in pathologies such as optic neuritis, cataracts, retinal diseases, or anisocoria [212–217].

Other psychophysical studies of the Pulfrich effect have shown that can also happen with interocular differences in contrast, where the image with lower contrast is processed slower than the image with higher contrast (similar to illuminance differences)[218]. However, the impact of interocular differences in blur, like those occurring in some presbyopia corrections such as monovision, where one eye is corrected for far vision and the other for near vision, has not been addressed and may influence the perceived depth.

In this thesis, Chapter 8 describes the discovery of a new Pulfrich-related phenomenon, named the Reverse Pulfrich effect. It occurs when interocular blur differences occur, like those induced in monovision corrections, instead of the classical description with differences in luminance. Chapters 9, 10, 11, and 12 cover the progress on the scientific and clinical implication and applicability of the Reverse Pulfrich effect.

1.5. Motivation of this thesis

Blurry vision is the main visual symptom perceived by patients and the most intuitive sign of malfunction of the visual system. The importance of blurry vision in clinical practice is crucial. For that reason, blur has been extensively studied, from the purely theoretical and optical point of view to its perceptual impact on human vision. This thesis further studies the applicability of blur to clinical instrumentation in ophthalmology and optometry.

At the beginning of this thesis, the use of optotunable lenses had spread across several fields of optics, from microscopy to smartphone cameras. However, the implementation of tunable lenses in the vision field was still small, mainly due to limitations on the aperture size of most tunable lenses available in the market, with diameters below 2 mm. The release of tunable lenses with larger apertures, and therefore permitting the implementation of new applications in vision science, was very recent. Besides, some of the new lenses also had the capability of changing their optical power very quickly, allowing not only studying vision with static blur but also with dynamic blur.

Furthermore, the use of tunable lenses for evaluating refractive errors had been already explored, but most conventionally: instead of manually changing trial lenses in a trial frame or a phoropter, tunable lenses were used to automatize and speed up the process. However, the full potential of the tunable lenses for the estimation of refractive errors had not been explored before.

Finally, monovision, a presbyopia correction in which one eye is corrected for far vision and the other one for near vision, is a very common ophthalmic correction inducing important blur differences between the eyes. The implications of that interocular blur on vision, as well as the clinical performance of the patients, had been widely studied. However, the influence of monovision on moving-in-depth illusions had not been addressed before. In addition, the measurement of ocular dominance to select the laterality in monovision correction (which eye is corrected for near vision, and which eye is corrected for far vision) is not well standardized, and it is key for the success of these corrections. These gaps in the prescription and evaluation of monovision corrections are addressed in this thesis, also taking advantage of the new opportunities of using optotunable lenses to define new methods in visual optics research and, potentially, in eye care clinical practice.

1.6. Open questions

Blur, both static and dynamic, is present in the daily life of most of the population in developed countries, who are affected by refractive errors and presbyopia. Blurry vision, with refractive errors, presbyopia, or ophthalmic corrections, alters perception differently at different distances.

In this thesis we have designed, developed, and validated new setups and methodologies to tackle the following scientific and clinical questions:

1. What are the spatial and temporal limits of the perception of defocus? Which are the clinical implications of those limits? How does the spatiotemporal defocus sensitivity function differ from the spatiotemporal contrast sensitivity function?
2. Is it possible to use temporal changes in defocus to evaluate the refractive error, one of the most important and standardized methods in clinical optometry and ophthalmology? Is it possible to overpass the conventional methods of measuring refractive errors?
3. Is it possible to develop a more precise test to establish the preferred laterality in the prescription of monovision correction?
4. Does the interocular blur difference between the left and the right eye induced by monovision introduce interocular differences in processing speed?
5. What are the implications of monovision in the perception of depth, and in the perception of moving objects? Does it introduce relevant perceptual illusions? How are they affected by the overall ambient luminance level, or by interocular differences in luminance?
6. Is it possible to compensate for those perceptual illusions in depth induced by monovision?

1.7. Goals of this thesis

The main goal of this thesis is to study blur perception and its potential application to the development of clinical instrumentation for eye care in clinical practice.

Specific goals include:

1. To evaluate the spatial and temporal fusion limits for defocus perception of the human visual system.
2. To develop a model of the spatiotemporal defocus sensitivity function.
3. To develop a new method, based on blur manipulation, for estimating the refractive error of an eye.
4. To develop a portable prototype for exploring the clinical applicability of the new method for estimating the refractive error of the eye.
5. To develop a metric for estimating the eye laterality and its strength for selecting the best eye in monovision corrections.
6. To study the impact of differential blur caused by monovision corrections in the perception of depth in moving objects in different scenarios.

1.8. Hypothesis

The hypotheses of the thesis are:

1. Optotunable lenses are suitable for studying the limits of blur perception.
2. The spatiotemporal limits of defocus and contrast perception follow similar trends and can be described with parallel models.
3. Fast changes in defocus, programmed in optotunable lenses, allow the development of a new subjective refraction method, based on the definition of new visual tasks.
4. Tunable lenses can also enable the development of new tests to prescribe monovision corrections, and in particular to determine the best eye for far vision and the best eye for near vision.
5. Monovision corrections, interocular differences in blur, also produce interocular differences in processing speed, provoking depth misperceptions.
6. Differences in processing speed caused by interocular blur differences can be nulled with those induced by interocular luminance differences.
7. Differences in processing speed with monovision should be attributed to interocular blur differences and not to interocular magnification differences.
8. Differences in processing speed affect patients after undergoing cataract surgery.
9. Differences in processing speed are influenced by the ambient luminance light level.

1.9. Structure of this thesis

The content is organized into 15 chapters, briefly described below.

Chapter 1 covers major concepts regarding blur, optical aberrations, contrast, blur perception, evaluation of the visual function and, in particular, refractive error (evaluation and correction), ocular dominance, and 3D perception. In addition, the motivation, open questions, goals, and hypotheses of this thesis are detailed.

Chapter 2 describes the experimental setups used in this thesis: commercial instrumentation, displays, psychophysical paradigms, perceptual models, and new developments including setups and protocols.

Chapter 3 presents a study on the spatial and temporal limits of perception of defocus changes, obtaining the thresholds using an adaptive psychophysical procedure and different stimuli (Gabor patches of different spatial frequencies, natural images, and edges). Finally, this chapter also presents the development of a model for describing the spatiotemporal defocus sensitivity function of the human visual system.

Chapter 4 presents the Direct Subjective Refraction, a new method developed in this thesis for estimating the refractive error of an eye using temporal defocus waves and a bichromatic stimulus made of blue and red components and taking advantage of the longitudinal chromatic aberration of the eye. This chapter reports, in volunteer subjects, the repeatability and measurement time of the new method for estimating the spherical equivalent, as well as a comparison with the traditional subjective refraction method and an unsupervised version of it.

Chapter 5 describes the extension of the Direct Subjective Refraction method for estimating the astigmatic component of the refractive error. This chapter shows the psychophysical procedure to estimate astigmatism, including the evolution of the stimulus, and the measurement of astigmatism using the new refraction method. Results are also compared with the traditional subjective refraction method, in volunteer subjects.

Chapter 6 reports the evolution of the Direct Subjective Refraction method for providing a full prescription to compensate for the refractive error. This chapter shows the evolution from the on-bench setup described in previous chapters (Chapters 4 and 5) to a portable clinical device. Pilot experiments refining the procedure, selecting the optimal parameters of the experiment, and the most suitable stimulus are also described. In addition, this chapter reports the measurements performed on real patients in different clinical sites compared with the traditional subjective refraction method, to explore the possibility of clinical measurements and to obtain feedback from their experience.

Chapter 7 describes the eye dominance strength**,** a new method for estimating eye dominance, alternating the laterality of induced monovision corrections. The new metric does not only select the dominant eye but also provides a new numerical magnitude, dominance strength, describing how important is that dominance for each subject. The new method is relevant in monovision corrections, where the selection of the eye to be corrected for far vision is critical for the success of the correction.

Chapter 8 reports the discovery of the Reverse Pulfrich effect, an optical illusion caused by interocular differences in blur, like those present in monovision corrections. This chapter shows the paradigm used for estimating differences in the processing speed; the first measurements of the Reverse Pulfrich effect; the description of the anti-Pulfrich monovision corrections and an estimation of the size of the misperception in depth caused by the illusion.

Chapter 9 presents a study on the Reverse Pulfrich effect and the anti-Pulfrich monovision corrections in contact lenses, the most common method for prescribing monovision corrections, comparing the results with those obtained with trial lenses, which induces induce interocular magnification differences besides blur differences. The suitability of anti-Pulfrich monovision corrections with contact lenses is also reported.

Chapter 10 reports a unique case of a 45-years-old patient corrected with monovision after a unilateral cataract surgery that reveals a spontaneous Pulfrich effect mainly caused by the Reverse Pulfrich effect. The study also reveals an adaptation process to the Reverse Pulfrich effect, never reported before, and describes its timeframe.

Chapter 11 describes the influence of the overall light level in the Classic Pulfrich effect (comparing with the literature) and in the Reverse Pulfrich effect (novel result). The influence of the high order aberrations and their implication on both versions of the Pulfrich effect is discussed.

Chapter 12 presents a study on the estimation of the prevalence of the Classic and Reverse Pulfrich effects in a population of 15 young subjects and provides a technological and methodological framework for performing massive measurements in clinical environments.

Chapter 13 reports the use of a new autostereoscopic display to measure stereoacuity, compared with conventional methods of producing 3D stimuli (commercial Titmus, anaglyph filters, and polarizers filters in a stereo 3D). In addition, this chapter reports the suitability of SimVis Gekko for measuring stereoacuity.

Chapter 14 shows a set of 7 pilot experiments performed during this thesis that open new research lines for future investigation. For each experiment, besides a brief description, the chapter provides preliminary results, graphs, and a description of the possibilities and implications of the research line.

Chapter 15 summarizes the main findings of this thesis and presents its main conclusions.

Chapter 2. Methods

This chapter describes the experimental setups, commercial instrumentation, experimental and clinical procedures, psychophysical paradigms, perceptual models, and new developments including setups and protocols. The specific implementations and developments for each particular experiment and/or study are included in the corresponding chapter.

The first section of this chapter describes the optical systems developed to measure blur perception, and in particular, the spatiotemporal defocus sensitivity function and the refractive error of the eye using a new refraction method. Both optical systems include an optotunable lens to allow fast changes in defocus. The second section describes the optical systems used and developed to measure the binocular function of the visual system, using haploscope systems, polarized filters, anaglyph filters, and autostereoscopic techniques (lenticular lenses and parallax barrier). Particularly, these setups were used to measure the Pulfrich effect and the stereoacuity. The third section describes the measurement of the optical quality using adaptive optics systems. The fourth section describes the protocol of the traditional subjective refraction method used in this thesis to measure the refractive error of the eye. The fifth section describes the psychophysical methods used in this thesis. The sixth section provides a technical description of the displays used in this thesis. The seventh section presents a summary of the setups used in the different chapters of the thesis. Finally, a detailed description of the perceptual models of contrast sensitivity used for this thesis is provided in the last section.

The author of the thesis has developed, aligned, and calibrated the optical system to measure the perception of spatiotemporal changes in defocus and to estimate the refractive error of the eye using temporal defocus waves in collaboration with Carlos Dorronsoro. In the final stage, he developed a portable prototype in collaboration with Daniel Pascual, who assembled the electronics needed. Other specific contributions of the author of the thesis to the same project are the 3D modeling and 3D printing of the housing for the portable prototype, a servomotor system to allow the rotation of the stimulus, and the software to control the whole system. The author of the thesis has also developed and aligned two optical systems to allow measurements of the binocular vision function of the human visual system. One of them, a haploscope system, in collaboration with Johannes Burge and Benjamin Chin, and the other one, is a 3D display optical system, in collaboration with Carlos Dorronsoro. Moreover, the author of the thesis has developed a setup for measuring the stereoacuity using autostereoscopic devices, as well as alignment protocols. In addition, the author of the thesis has developed a complete toolbox in MATLAB to carry out the psychophysical experiments described in this thesis, as well as other functions to allow the storing and analysis of psychophysical data, plotting routines, stimuli creation, video creation, control of external devices, among others.

2.1. Measuring blur perception

To measure different features of blur perception in Chapters 3, 4, 5, and 6, three laboratory setups were developed for different experiments. All those experiments and setups shared the same optical system, with small modifications for each particular experiment in terms of its combination with different stimuli, displays, visual tasks, and procedures.

2.1.1. Optical system

The optical system used to measure blur perception is conformed of two achromatic doublets of 50mm of focal length forming a 4f optical system, that creates conjugated pupil planes. Figure 2.1A shows a schematic representation of the optical system. Conjugated pupil planes have the particularity of being optically identical: with the same magnification and vergence of the rays. In this optical system, the use of conjugated pupil planes allowed the projection of an optotunable lens (Pupil Plane 2) onto the pupil of an observer's eye (Pupil Plane 1), allowing changes of optical power without changing the magnification or position. The total length of the optical system is around 190 mm.

Figure 2.1B shows a lateral view of the representation of the optical system in Optics Studio (ANSYS Inc., Canonsburg, USA), specialized software for designing and simulating optical systems. Figure 2.1D shows a 3D view of the optical system. This optical system requires a bite bar to align the pupil of the eye with the optical system and is monocular (Figure 2.1F).

SimVis Gekko represents the evolution of the optical system to a compact and binocular system. To create a miniaturized version of the optical system, six flat mirrors were introduced in the optical path, measuring only 110 mm and therefore reducing the length by 42%. Further versions also replaced the achromatic doublets with aplanatic lenses which improved the optical quality both in the center and at the periphery, remarkably reducing the field of curvature and distortion. A custom housing was developed to allow the insertion of the optical modules both in a laboratory setup and in a wearable and commercial instrument. The alignment of the optical module only required a chinrest with the possibility of adjusting the horizontal and vertical positions of the head. The wearable system included a custom screw system to allow adjusting the position in horizontal and vertical directions of the optical axis with respect to the visual axis. Figure 2.1C shows the optical system and the location of the mirrors, Figure 2.1E is a 3D view of the optical system, and Figure 2.1G is a subject wearing SimVis Gekko.

2.1.2. Spatiotemporal defocus sensitivity function

To measure sensitivity to spatial and temporal changes to defocus, we used the linear optical system described above with an optotunable lens model EL-10-30-TC (Optotune, Dietikon, Switzerland) with 10 mm of effective aperture and a dioptric range between -1.0D to +5.00D. The monitor used was HP EliteDisplay E240 23.8''. The monitor was located 1 m away from the optotunable lens. In Chapter 3 there is a more detailed description.

2.1.3. Direct Subjective Refraction

To measure the refractive error of the eye using the Direct Subjective Refraction method, we used the linear optical system with an optotunable lens model EL-10-30-TC with 10 mm of effective aperture and a dioptric range between -1.0D to +5.00D. The display was a combination of a projector with a white screen, described in more detail in Chapter 4.

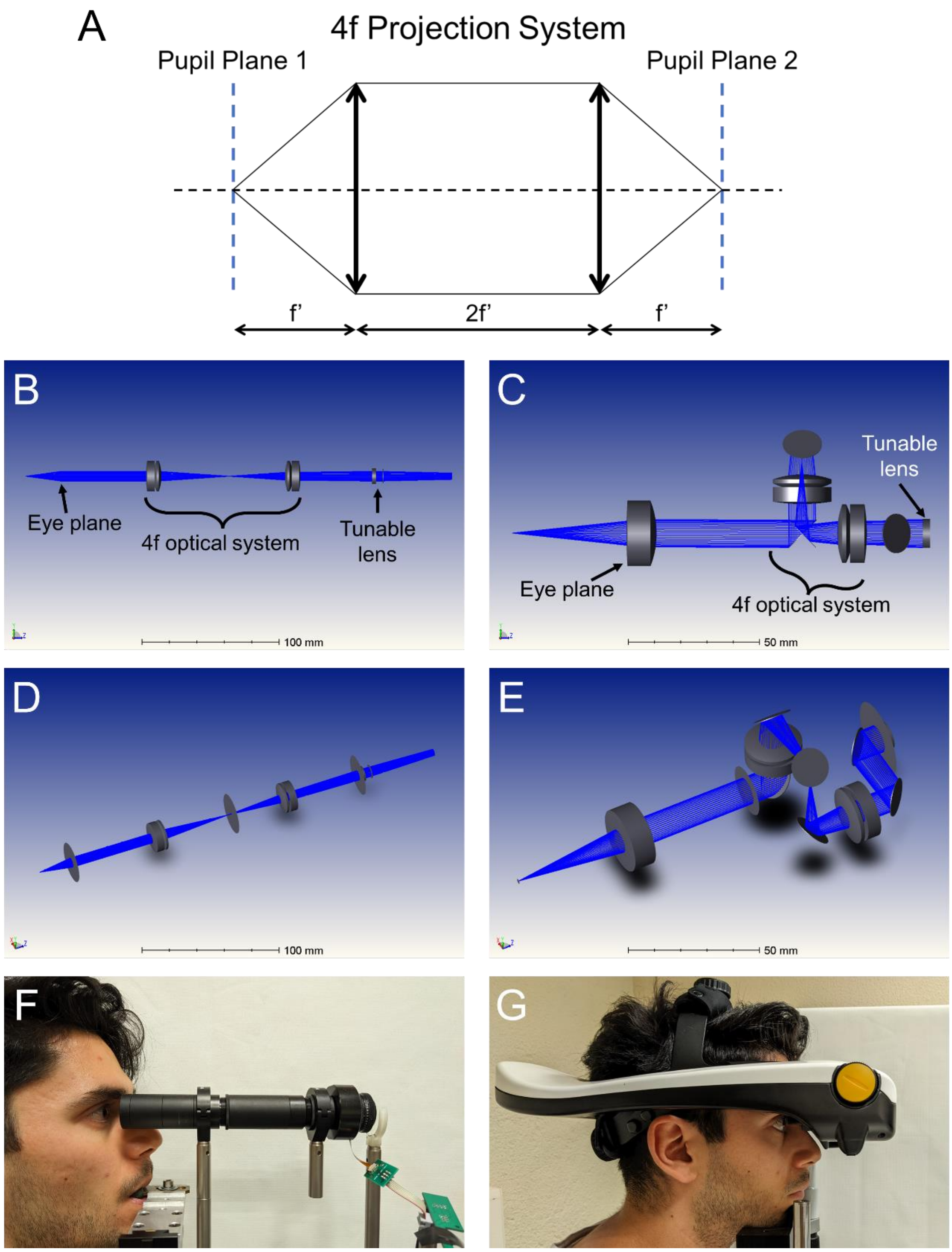

Figure 2.1. Optical systems used in this thesis to measure blur perception. **A.** Schematic representation of the 4f projection optical system. In blue, the conjugated pupil planes created by the optical system. **B.** Linear optical system in a lateral view. **C.** Miniaturized optical system (SimVis Gekko) in a lateral view. **D.** Linear optical system in a 3D view. E. Miniaturized optical system in a 3D view. **F.** Observer looking through the linear optical system using a bite bar and a micrometric system for alignment. **G.** Observer looking through SimVis Gekko.

In further developments, the Direct Subjective Refraction method was implemented to perform measurements in a clinical environment. For that purpose, the optical system used was the wearable SimVis Gekko, a commercial system implementing an optical system similar to that described in section 2.1.1. A custom display based on monochromatic LEDs was also developed. The complete system is described more in detail in Chapter 6.

2.2. Measuring binocular visual function

To measure binocular vision function, in particular stereoacuity and the Pulfrich effect, 6 laboratory setups were developed. They are described in the following subsections.

2.2.1. Haploscope system

A haploscope system is an optical system that shows independent images to each eye with a set of mirrors. The system, a variation of the Wheatstone stereoscope, allows the creation of 3D stimuli presenting slightly different images to each eye, which elicits binocular disparity. Two different versions of the haploscope system were used in this thesis to study the Pulfrich effect: Haploscope system I (HI) and Haploscope system II (HII). Both share the same optical system and display but differ in the optical distances, luminances, and extra channels. A schematic representation of both systems is shown in Figure 2.2.

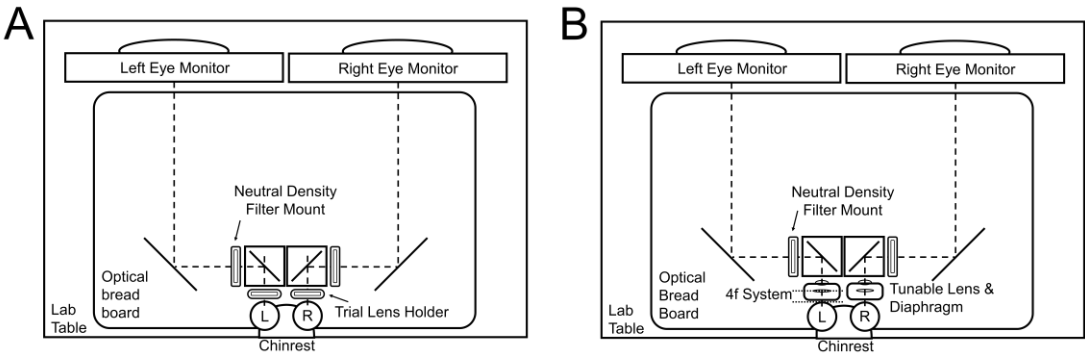

Figure 2.2. Haploscope system. **A**. Schematic representation of the Haploscope system I (HI). **B**. Schematic representation of the Haploscope system II (HII).

<u>2.2.1.1. Haploscope system I (HI)</u>

This system was already developed, and the contribution of the author of the thesis was the addition of a channel for defocus induction with trial lenses and luminance reduction with neutral density filters. Figure 2.2A shows a schematic representation of the optical system. This system was used in Chapter 8 to measure the Pulfrich effect with interocular blur difference.

Stimuli were displayed on a custom-built four-mirror haploscope. Left- and right-eye images were presented on two identical VPixx VIEWPixx LED monitors. Monitors were calibrated (i.e., the gamma functions were linearized) using custom software routines. The monitors were daisy-chained together and controlled by the same graphics card to ensure that the left and right eye images were presented synchronously. The maximum luminance after light loss due to mirror reflections was 93.9cd/m^2. Simultaneous measurements with two optical fibers connected to an oscilloscope confirmed that the left and right eye monitor refreshes occurred within ~5 microseconds of one another. Custom firmware was written so that each monitor was driven by a single-color channel; the red channel drove the left monitor and the green channel drove the right monitor. The single-channel drive to each monitor was then split into all three channels to enable grayscale presentation.

Observers viewed the monitors through mirror cubes with 2.5cm circular openings positioned one inter-ocular distance apart. Heads were stabilized with a chin and forehead rest. The haploscope mirrors were adjusted such that the vergence distance matched the distance of the monitors. The light path from the monitor to the eye was 100cm, as confirmed both by a laser ruler measurement and by visual comparison with a real target at 100cm. At this distance, each pixel subtended 1.09arcmin.

To manipulate the amount of defocus blur in each eye, we positioned trial lenses at about 12mm from each eye in two trial lens holders, centered on each optical axis, between each eye and the front of the mirror cubes of the haploscope. To manipulate the amount of luminance reaching the eye, mounts for 15x15mm squared neutral density filters were placed, centered on each optical axis, after the mirror cubes.

2.2.1.2. Haploscope system II (HII)

This system was a replication of HI but w extra channels. It was built by the author of the thesis in collaboration with Johannes Burge, including a channel for automatic defocus induction with a tunable lens, a channel for pupil diameter control, and a channel for luminance reduction with neutral density filters. functionalities. Figure 2.2B shows a schematic representation of the system. This system was used in Chapter 11 to measure the impact of overall light levels on the Classic and Reverse Pulfrich effects.

We used a two-monitor, four-mirror haploscope system, and a custom 4-f optical system to present the experimental stimuli. The monitors were two identical VPixx VIEWPixx LED displays. To ensure the synchronous presentation of the left- and right-eye images, the monitors were daisy-chained together and controlled by the graphics card. The light from the monitors reached the eyes by first reflecting off a pair of large mirrors and then off a pair of small mirrors. The mirrors were adjusted such that the vergence distance matched the distance of the light path between the monitors and the eyes. The small mirrors were housed in mirror cubes having 2.5cm diameter circular ports that were positioned one inter-pupillary distance apart. Given the distance along the light path between the monitors and the eyes, each pixel subtended 1.36 arcmin of visual angle. The 4f optical system projected two optotunable lenses and precision-printed diaphragms of fixed sizes into the pupil planes of the eyes. This system provided a means to programmatically change the interocular focus difference on each trial, and to control the effective pupil size. Through the entire optical system, the maximum luminance was 12.8cd/m^2. The optical distance from the eyes of the observer to the screen was 80 cm.

2.2.2. Stereoscopic monitor (SM)

The main disadvantage of a haploscope system is the use of several mirrors and two monitors to present 3D stimuli. This section describes the use of passive polarizers in combination with a 3D display to present 3D stimuli using only one monitor. The setups were built by the author of the thesis in collaboration with Carlos Dorronsoro. Figure 2.3 shows a schematic representation of the optical system. It was used in Chapters 9 and 10 to measure the Reverse Pulfrich effect and anti-Pulfrich monovision corrections with contact lenses and to monitor the process of readaptation to the Reverse Pulfrich effect in a patient after a cataract surgery procedure, respectively. In other scenarios, the screen was also used as a 3D display with anaglyph (red/green) filters, presenting the left image in red and the right image in cyan. This was carried out in Chapter 13 to measure the stereoacuity. Finally, the TV can be also used as a 2D screen, as it was performed in Chapter 7 to measure ocular dominance with monovision corrections. All these setups could be used in combination with trial lenses (Figure 2.3A) or in combination with the optical system for measuring blur perception, as described in section 2.1.1 (Figure 1B).

The stimulus was displayed on a stereoscopic UK UHD 49” monitor (LG49UH850V, LG). The monitor uses row-by-row spatial interlacing (e.g., pixels in even rows to the left eye and pixels in odd rows to the right eye) to present different temporally coincident images to the left and right eyes. Passive circular polarization glasses selectively passed the appropriate image to each eye. The observer viewed the monitor from 2m, with his/her head stabilized by a chin and forehead rest. At this viewing distance, each pixel subtended 0.46 arcmin of visual angle. When observers viewed the display through custom-built mounts for trial lenses, mounts were horizontally and vertically adjusted so that the optical element was centered along the line of sight of each eye. When observers viewed the monitor through tunable lenses, the optical system was adjusted horizontally and vertically with screws, so the optical elements were centered along the line of sight of each eye.

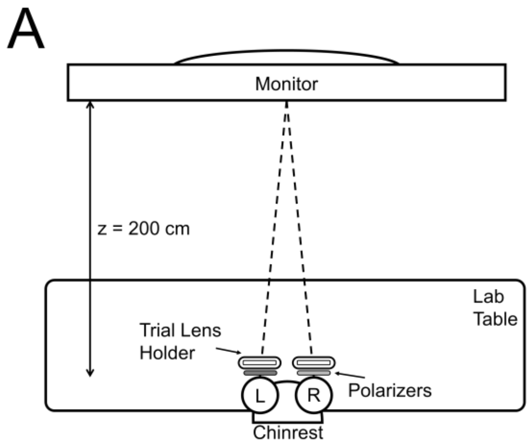

Figure 2.3. Stereoscopic monitor (SM). **A**. Combination with trial lens holder to induce blur differences with trial lenses. **B**. Combination with 4f optical system and tunable lenses for automatic changes in defocus.

2.2.3. Tablets and portable displays

Using the previous 3D displays in a clinical environment entails issues in terms of size, space, and portability. To miniaturize and approach the evaluation of binocular vision in clinical environments, several optical setups involving portable displays were developed by the author of the thesis. Alignment was easier with the autostereoscopic tablets described below.

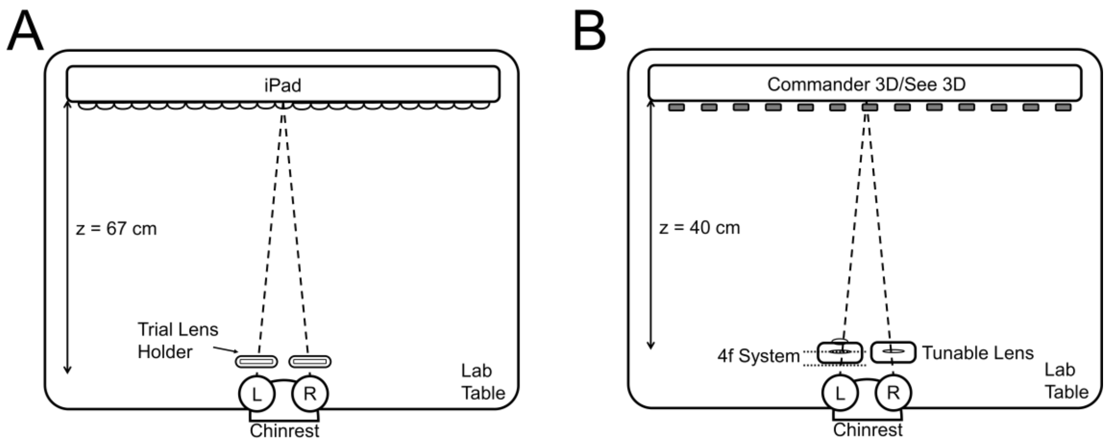

Figure 2.4. Schematic representation of tablets and portable devices optical setups. **A**. Lenticular Lenses tablet (LLT). **B**. Parallax Barrier tablet I (PBI) and II (PBII).

2.2.3.1. Lenticular Lenses tablet (LLT)

This system was built by the author of the thesis. Figure 2.4A shows a schematic representation of the optical system. This system was used in Chapter 12 to measure the prevalence of the Classic and Reverse Pulfrich effect in a young population.

The stimulus was displayed on an iPad Pro 12.9'' (iPad 3rd gen, Apple). The monitor was used in combination with a lenticular lenses sheet manufactured by MOPIC (Suwon, South Korea) that uses the lenticular approach to create an autostereoscopic display with row-by-row spatial interlacing (e.g., pixels in even rows to the left eye and pixels in odd rows to the right eye). The cylindrical lenses of the sheet are slanted 10 degrees to reduce crosstalk and increase the quality of the stereoscopic image. The display was held in a custom-built (3D designed and 3D printed) mount for optimum alignment purposes. According to the specifications of the manufacturer, 3D could be perceived between 30 and 80 cm, with an optimum distance of around 50-70 cm. The observer viewed the monitor from 67cm, with his/her head stabilized by a chin and forehead rest. Observers viewed the display through custom-built mounts for trial lenses. The mounts were horizontally and vertically adjusted so that the optical element was centered along the line of sight of each eye.

2.2.3.2. Parallax Barrier tablet I (PBTI)

This system was built by the author of the thesis. Figure 2.4B also shows a schematic representation of the optical system. This system was used in Chapter 7 to measure ocular dominance and in Chapter 13 to measure stereoacuity in pilot experiments.

The stimulus was displayed on a Commander 3D 10.1'' (Commander 3D, Toronto, Canada) driven by a PowerVR SGX544 Graphics card. The monitor used the parallax barrier approach to create an autostereoscopic display with row-by-row spatial interlacing (e.g., pixels in even rows to the left eye and pixels in odd rows to the right eye). The display was held in a custom-built (3D designed and 3D printed) mount for optimum alignment purposes. According to the specifications of the manufacturer, 3D could be perceived between 30 and 50 cm, with an optimum distance of around 40cm. The observer viewed the monitor from 40cm, with his/her head stabilized by a chinrest. Observers viewed the display through custom-built mounts for trial lenses which were horizontally and vertically adjusted so that the optical element was centered along the line of sight of each eye. In addition, observers viewed the display through SimVis Gekko, with its own alignment strategy.

2.2.3.3. Parallax Barrier tablet II (PBTII)

This system was built by the author of the thesis. Figure 2.4B shows a schematic representation of the optical system. This system was used in Chapter 13 to measure stereoacuity.

See3D tablet (See3D Tablet Corporation, Toronto, Canada), was an evolution of the previous version, Commander3D. The display was loaned to the laboratory as a Proof of Concept by the company. The tablet is driven by an Adreno GPU 650 Graphics card. The display used the parallax barrier approach to create an autostereoscopic display with row-by-row spatial interlacing (e.g., pixels in even rows to the left eye and pixels in odd rows to the right eye). The display was held in a custom-built (3D designed and 3D printed) mount for optimum alignment purposes. The observer viewed the monitor from 40cm, with his/her head stabilized by a chinrest. According to the specifications of the manufacturer, 3D could be perceived between 30 and 50 cm, with an optimum distance of around 40cm. Observers viewed the display through custom-built mounts for trial lenses which were horizontally and vertically adjusted so that the optical element was centered along the line of sight of each eye. In addition, observers viewed the display through SimVis Gekko, with its own alignment strategy.

The main improvement compared to the previous version was that the display could be used as a secondary screen, overcoming the limitations of creating ad-hoc fixed stimuli (e.g., images or videos) to be played in a specific application.

2.2.3.4. Anaglyph filters

Modern screens are based on three types of LEDs -red, green, and blue- to allow a polychromatic representation of images. Therefore, those screens have 3 color channels available, that can be used in combination with glasses with color filters, to show different images to each eye and generate the perception of a 3D image from a stimulus of 2 different colors. To present different images to each eye, anaglyph (red/green) filters were used in this thesis, so that the left eye received the red image, and the right eye received the green image. Anaglyph filters approach was carried out in the SM display.

2.3. Objective measurements of optical blur

The optical quality of the visual optical system can be assessed objectively and subjectively. The objective measurement of the optical quality was evaluated using a commercial autorefractometer that provides an estimation of the spherocylindrical refractive error in Chapters 4, 5, 6, 7, and 13. Moreover, the measurement of the wavefront aberration was accomplished using a laboratory setup already developed in the Viobio Lab. Subjectively, the optical quality was measured using the traditional subjective refraction method that provides an estimation of the spherocylindrical refractive error in Chapters 3, 4, 5, 6, 7, 9, 10, and 13.

2.3.1. Autorefractor

The autorefractor used in this thesis was ARK1 (Nidek, Gamagori, Japan), which uses an approach of keratometry to measure the corneal curvature at several axes to estimate the refractive error of an eye. The stimulus shown is a hot-air balloon to prevent accommodation. The information from the autorefractometer was used as a first approximation of the refractive error of the subjects' eyes in Chapters 4, 5, 6, 7, and 13.

2.3.2. Optical aberration measurement

The wavefront aberration was measured using a laboratory setup already developed in the lab. The system uses adaptive optics to measure and compensate within the same loop for the wavefront aberration of the observer's eye. In the lab, there were two generations of a similar adaptive optics system, the Adaptive Optics 1st generation (AOI) which is described in detail in several manuscripts[219–221], and the Adaptive Optics 2nd generation (AOII), also described in detail in other manuscripts[222,223]. The author of the thesis did not contribute to the development of the system and only used the AOII system as a user for measuring the wavefront aberration.

2.4. Traditional Subjective Refraction

As mentioned in section 1.3.3, traditional subjective refraction is the gold standard method to estimate the refractive error of an eye, especially due to the subjective input from the patient. The method followed for performing the subjective refraction is described below and is based on standard optometric techniques[91].

First, traditional subjective refraction estimates the refraction monocularly, examining one eye and then the other. The starting point is usually the previous prescription of the subject, or the result obtained from the objective refraction. The process follows these steps:

1. Occlusion of the eye not measured.
2. Fogging technique: addition of +1.50D to the starting point refraction (Visual Acuity (VA) should be approximately 0.52 logMAR). Reduce the value of the added sphere progressively (in steps of 0.25D) until achieving 0.15 logMAR.
3. Switch to Jackson's Cylinder test. Refine the magnitude and axis of astigmatism using the Jackson Cross Cylinders (JCC) method.
4. Once the amount of astigmatism has been adjusted, reduce the sphere value previously added at the beginning until reaching the highest visual acuity. The reduction must stop when the subject has reached a maximum visual acuity of -0.2logMAR.
5. Refinement of the value of the sphere employing the duochrome test.
6. Record the maximum VA achieved.

Finally, binocular refinement should be addressed to reduce the possible impact of accommodation.

1. Biocular balance
    a. Starting from the subjective refraction found monocularly, defocus the image in both eyes with +0.75D. Isolation of a line of letters corresponding to 2 lines larger than the best VA achieved.
    b. Dissociation of the image using a 4-diopter prism (upper base) in the right eye and a 4-diopter prism (lower base) in the left eye. The patient will see vertically double *"an image above perceived by the right eye, and the other below perceived by the left eye."* One of them might be better perceived than the other. If not, increase the value of the sphere added in step 1.
    c. The goal is to worsen the one that sees better (since it is the eye in which a residual accommodation might be happening). Addition of a positive lens to that eye in steps of +0.25D until the same blur perception is achieved in both eyes (the positive spherical value that has been added should not exceed 0.75D. If so, the monocular refraction of that eye must be double-checked).
    d. When the same blur in both eyes is achieved, prisms must be removed.
2. Binocular balance
    a. Progressively reduction, in both eyes at the same time, of the spherical value that was added during the biocular balance, until the maximum positive value that provides the best VA is achieved.

2.5. Psychophysical methods

In this thesis, different psychophysical experiments were developed to measure the relationship between the psychical properties of the stimulus and the perceptual experience to describe the visual function and visual quality[224]. A psychometric function describes the probability of a response as a function of the physical property of a stimulus[225]. Considering that the maximum probability is 1 and the minimum is 0, the thresholds can be found at 0.5, 0.625, or 0.75, depending on the particular task.

2.5.1. Classical methods

There are three classical psychophysical methods classified into the method of limits, the method of constant stimuli, and the method of adjustment.

The method of limits has two variants: the ascending and the descending. The ascending consists of showing a property of a stimulus so low that is undetectable, and gradually increasing that property until the observer perceives it. In the descending method of limits, the process is the opposite, the property of the stimulus is visible and decreases until the observer does not perceive it. Usually, the average across the ascending and descending results is considered the threshold. This method has some disadvantages, such as the error of habituation or anticipation. This method has not been used in this thesis.

In the method of constant stimuli, several magnitudes of the property of the stimulus are shown randomly and the observer must indicate if it was perceived or not. The main disadvantage of this method is that it may test a broader range of magnitudes to find the threshold, with the subsequent extra time. On the other hand, this method allows a complete sampling of a psychometric function with the cumulative responses of the observer and overcomes the error of expectation and habituation of the method of limits. In this thesis, this method has been used in several experiments. The method of constant stimuli was used in this thesis in Chapters 8, 9, 10, and 12.

In the method of adjustment, the subject has control of the magnitude of the psychical property, and they must vary the magnitude until is barely/not perceived (just noticeable or just noticeable difference)[226]. The main limitation of this method is that the subject must be aware to some extent of the nature of the physical property, which can add some complexity to the task. The method of adjustment has been used in this thesis in several experiments.

2.5.2. Adaptive methods

Classical methods are often considered inefficient as they must test several magnitudes of the physical property to complete the psychometric function and usually start far from the threshold[227]. The main objective of adaptive methods is to concentrate the magnitude as much as possible near the threshold. Among the many adaptive procedures developed, this thesis is focused mainly on two: up-down staircases and QUEST.

In the staircase method, the magnitude changes in fixed steps. The magnitude of the physical property usually begins far from the prior thresholds. If the observer perceives the physical property, the magnitude decreases in one step. If the observer does not perceive the psychical magnitude, the magnitude increases one step. Then, the staircase converges to the threshold. There are variants of the staircase method, with different step sizes depending on the response[227]. In this thesis, the staircase method was used in a variant where the observer has coarse and fine steps. It was used in Chapters 4, 5, 6, and 11.

The QUEST (QUick Estimation by Sequential Testing) method estimates the threshold using Bayesian statistics[228]. The adaptive QUEST algorithm computes the magnitude of the next physical property that meets the maximum likelihood estimate of the threshold, with a prior estimation of the possible threshold. QUEST algorithms were used in this thesis in Chapters 3 and 13.

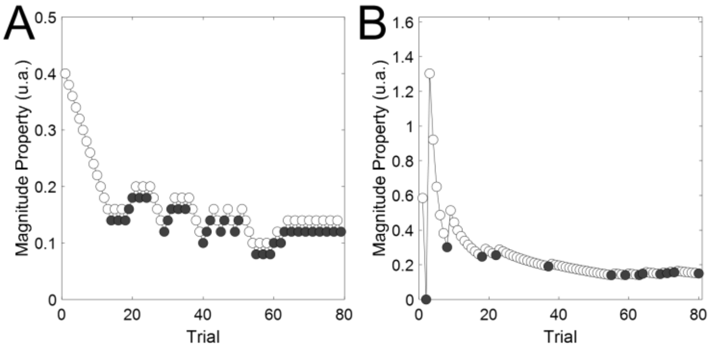

Figure 2.5. Difference between classical and adaptive methods for estimating the threshold. White points represent correct responses and black points wrong responses. **A**. Staircase method. **B**. QUEST method.

2.5.3. Scoring method

In a scoring method, the subject grade the physical property of a stimulus. In some experiments of this thesis, observers judged the optical quality of different stimuli by seeing through different optical corrections.

The MAS-2EV (Multifocal Acceptance Score to Evaluate Vision) method[229] was used to evaluate the optical quality for different monovision corrections. In this method, observers provide a score from 0 to 10 on a set of natural images. This metric was used in Chapter 7 as a measure of eye dominance.

The Visual Analogue Scale (VAS) is a metric in which the subject graded their comfortability with different optical corrections by drawing a mark on a 10 cm length line, from 0 to 100. The proportion of the length of the mark in cm compared to 10cm is comfortability. This metric was used in Chapter 6 as a measure of comfort with the prescription using the Direct Subjective Refraction method.

2.6. Displays

To carry out the experiments described in this thesis, different displays were used. Below, there is a technical description of the different displays. The spectral emission was measured by the author of the thesis using a spectrometer (Ocean Optics, USB4000-Fiber Optic Spectrometer, 200-1100nm, Orlando, USA). Figure 2.6 shows the spectrum emission for red, green, and blue channels of each display.

<u>2.6.1.1.VIEWPixx</u>

VPixx VIEWPixx LED monitors (VPixx Tecnologies Inc., Saint Bruno de Montarville, Canada) have a size of 52.2x29.1cm, a spatial resolution of 1920x1080 pixels, a native refresh rate of 120Hz, and maximum luminance of 105.9cd/m^2 in scanning backlight mode.

<u>2.6.1.2. HP EliteDisplay</u>

EliteDisplay E240 23.8’’ monitor (HP Inc, Palo Alto, USA) has a size of 55.72x34.22cm, a spatial resolution of the display was 1920x1080 pixels and a refresh rate was 60Hz. The maximum luminance of the monitor was 250cd/m^2.

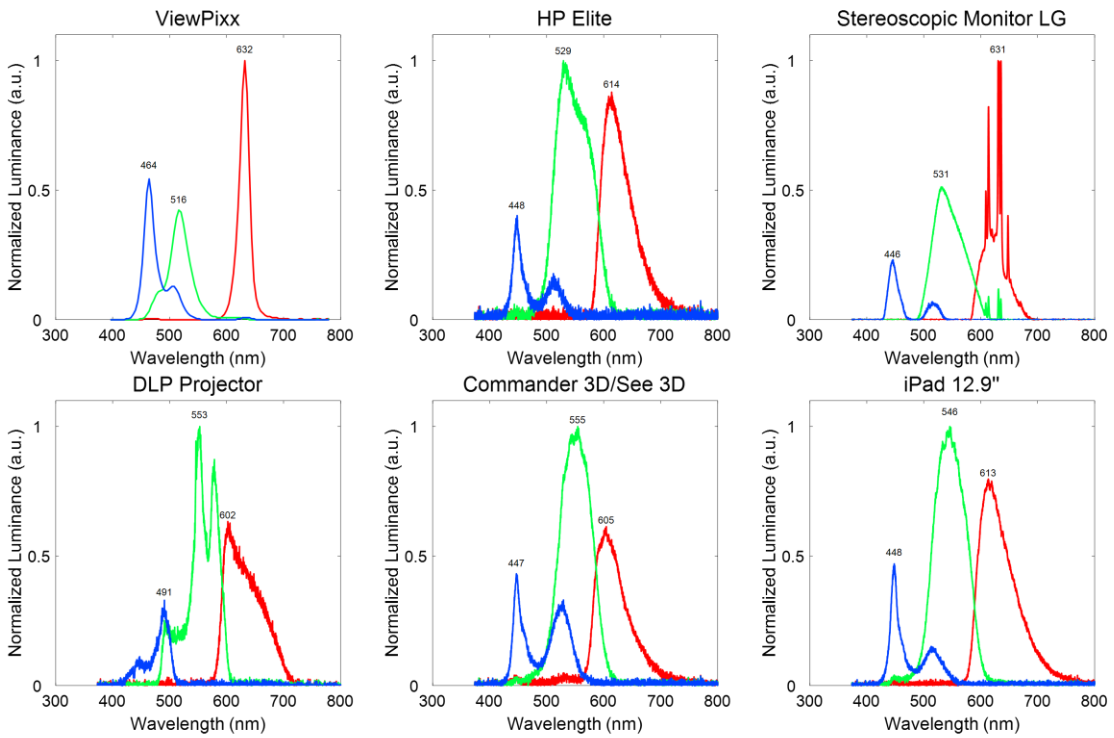

Figure 2.6. Spectral emission of the displays used in this thesis. The wavelength at maximum emission was displayed for each channel. Data was normalized with the maximum emission of each display. In red, the red channel emission, in green, the green channel emission, and in blue, the blue channel emission.

2.6.1.3. DLP Projector

A digital light projector (DLP PJD7820HD, ViewSonic, USA) was used in combination with a flat white reflecting screen to present stimuli. The distance from the projector to the screen was 0.4 meters, adjusted to provide the 1920x1080, the same number of pixels as the auxiliary screen, providing a sharp image with high luminance (500 cd/m^2 if set to white).

2.6.1.4. 3D UK UHD LG

The stereo-3D UK UHD 49” screen (LG49UH850V, LG, Seoul, North Korea) has a size of 110.4x64.5cm, a spatial resolution of the display was 3840x2160 pixels and a refresh rate was 60Hz (i.e., 60Hz/eye). The maximum luminance of the monitor was 400cd/m^2. After filtering by the glasses, only 3840x1080 interlaced pixels reached each eye. The effective luminance of the monitor for each eye was slightly less than 200cd/m^2.

2.6.1.5. iPad Pro 12.9 (3rd generation)

The iPad Pro 12.9’’ 3rd generation (Apple, Palo Alto, USA) has a Liquid Retina screen of 28.06x21.49 cm size, a spatial resolution of 2732x2048 pixels, and a refresh rate of 120 Hz. The maximum luminance of the screen is 600cd/m^2.

2.6.1.6. Commander 3D

The tablet Commander 3D 10.1’’ (Commander 3D, Toronto, Canada) has a size of 21.75x13.6cm, a refresh rate of 30Hz, and a spatial resolution of the display of 1920x1200 pixels that was reduced to 960x1200 interlaced pixels for each eye in horizontal 3D mode. The maximum luminance of the screen is 8.75cd/m^2 [230]. The tablet is driven by a PowerVR SGX544 Graphics card.

2.6.1.7. See3D

The tablet See3D 10.1'' (See3D Tablet Corporation, Toronto, Canada) has a size of 11.53x7.21cm, a refresh rate of 30Hz, and a spatial resolution of the display of 1920x1200 pixels that was reduced to 960x1200 interlaced pixels for each eye in horizontal 3D mode. The tablet is driven by an Adreno GPU 650 Graphics card. The spectral emission of this display is the same as Commander 3D.

2.7. Summary of the setups and experiment

A summary of the setups used in this thesis is described in Table 2.1, along with the psychophysical procedure, the display, and the chapter of the thesis where it was used.

Table 2.1. Summary of the setups used in this thesis, along with the experiment, psychophysical procedure, display, and chapter in which it was used.

Setup	Experiment	Psychophysical procedure	Display	Chapter
Lineal 4f system	Blur perception	QUEST	HP Elite	3
		Staircase	DLP projector	4
Head-mounted 4f system	Blur perception	Staircase	LG 49'' UHK	5
			Custom developed	6
	Binocular vision	Scoring	LG 49'' UHK	7
		QUEST	See 3D	13
Haploscope I (HI)	Binocular vision	Constant stimuli	ViewPixx	8
Haploscope II (HII)	Binocular vision	Staircase	ViewPixx	11
Stereoscopic Monitor (SM)	Binocular vision	Scoring	LG 49'' UHK	7
		Constant stimuli	LG 49'' UHK	9, 10
		QUEST	LG 49'' UHK	13
Lenticular Lenses (LLT)	Binocular vision	Constant stimuli	iPad 12.9''	12
Parallax Barrier I (PBI)	Binocular vision	Scoring	Commander 3D	7
Parallax Barrier II (PBII)	Binocular vision	QUEST	See 3D tablet	13

2.8. Models of perception

In this thesis, several models have been used to explain some features of human visual perception. This section describes their mathematical description and their use in this thesis.

2.8.1. Spatial contrast sensitivity function (SCSF)

The Spatial Contrast Sensitivity Function described the sensitivity to changes in contrast for different spatial frequencies. In this thesis, the model described by Mannos et al.[231] for the SCSF has been used.

$$S_s(f_s) = d\left(a + \frac{f_s}{f_{s0}}\right) e^{-\left(\frac{f_s}{f_{s0}}\right)^c} \qquad 11$$

where $S_s(f_s)$ is the CSF, a, c, and d are parameters, f_{s0} is the spatial frequency at the peak of sensitivity f_s is the spatial frequency. Parameter d modulates the gain of the curve, parameter a the shape of the low-frequency region, and parameter c the steepness of the high-frequency fall. Figure 2.7A shows the effect of varying parameter a while keeping the others constant ($c = 1, d = 10, f_{s0} = 4$) on the CSF. Figure 2.7B shows the effect of varying parameter c while keeping the others constant ($a = 0.01, d = 10, f_{s0} = 4$) on the CSF.

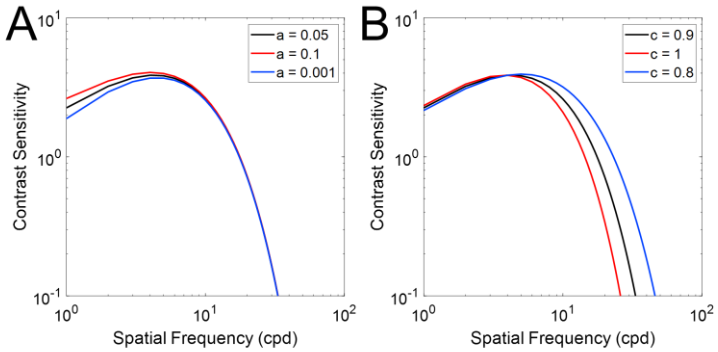

Figure 2.7. Spatial Contrast Sensitivity Function (SCSF). Based on Mannos et al.[231] model. **A**. Influence of the parameter a on the SCSF. **B**. Influence of parameter c on the SCSF.

2.8.2. Temporal Contrast Sensitivity Function (TCSF)

The temporal contrast sensitivity function (TCSF) describes the sensitivity to temporal changes in contrast. The model developed by Watson[62] considers the TCSF as the difference between two filters, one describing a sustained mechanism and the other a transient mechanism. The total filter, $ft(t)$, is

$$\begin{gathered} f(t) = \varepsilon \cdot [f_1(t) - \zeta \cdot f_2(t)] \\ f_1(t) = u(t) \cdot (\tau \cdot (n_1 - 1)!)^{-1} \cdot \left(\frac{t}{\tau_1}\right)^{n_1} \cdot e^{-(t/\tau_1)} \\ f_2(t) = u(t) \cdot (\kappa\tau \cdot (n_2 - 1)!)^{-1} \cdot \left(\frac{t}{\tau_2}\right)^{n_2} \cdot e^{-(t/\tau_2)} \end{gathered} \qquad 12$$

where ε is a gain factor, ζ is the transience factor, τ is a time constant and κ is the ratio of the time constant for the second filter over the first filter, and n_1 and n_2 are the number of stages. The Fourier transform of the filter ($f(t)$) computes the amplitude and phase response in the frequency domain. The amplitude response represents the temporal sensitivity ($S_T(f_t)$) in temporal frequency (f_t) of the human visual system

$$S_T(f_t) = FT\big(f(t)\big) \qquad 13$$

The parameters of the model have a different influence on the TCSF. Parameter ε modulates the gain of the curve, parameter ζ influences the transient mechanism, τ_1 and τ_2 the vertical and horizontal shift, and n_1 and n_2 the steepness of the transition band. Figure 2.8A shows the effect of varying parameter ζ while keeping the others constant ($\varepsilon = 1, \tau = 3, \kappa = 1.33, n_1 = 8, n_2 = 9$) on the TCSF. Figure 2.8B shows the effect of varying parameter τ_1 while keeping the others constant ($\varepsilon = 1, \zeta = 1, \kappa = 4, n_1 = 8, n_2 = 9$) on the TCSF. Figure 2.8C shows the effect of varying parameter τ_2 while keeping the others constant ($\varepsilon = 1, \zeta = 1, \tau = 4, n_1 = 8, n_2 = 9$) on the TCSF. Figure 2.8D shows the effect of varying parameter n_1 while keeping the others constant ($\varepsilon = 1, \zeta = 1, \tau = 3, \kappa = 1.33, n_2 = 9$) on the TCSF. Figure 2.8E shows the effect of varying parameter n_1 while keeping the others constant ($\varepsilon = 1, \zeta = 1, \tau = 3, \kappa = 1.33, n_1 = 8$) on the TCSF.

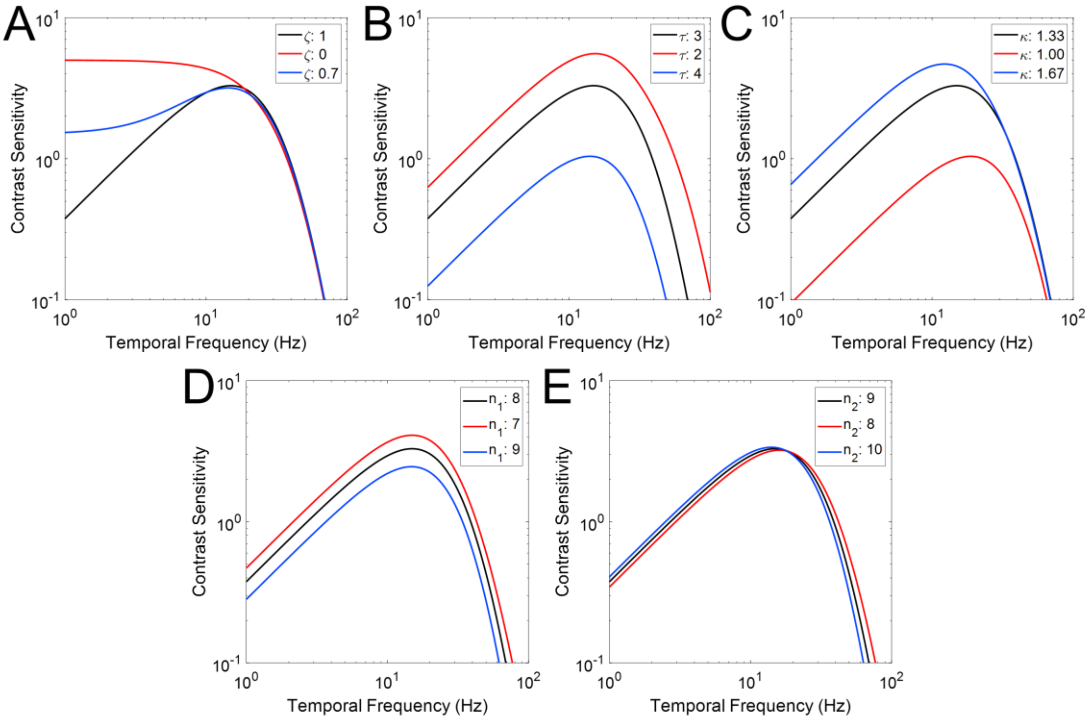

Figure 2.8. Temporal Contrast Sensitivity Function (TCSF). Based on Watson[62] model. **A**. Influence of the parameter ζ on the TCSF. **B**. Influence of parameter τ on the TCSF. **C.** Influence of parameter κ on the TCSF. **D.** Influence of parameter n_1 on the TCSF. **E.** Influence of parameter n_2 on the TCSF.

2.9. Measurements with volunteer subjects and patients

In this thesis, 100 volunteer subjects from research institutions and 33 patients from clinical sites participated in the experiments, a total of 133 people. Of the total, 77 of them participated in experiments in the CSIC, 22 at the University of Pennsylvania, and 33 in Hospital Clinico San Carlos. These number does not include pilot measurements.

Each study followed the protocol and experiments conformed to the tenets of the Declaration of Helsinki, and the approvals were granted by the corresponding Ethical Committee. In this thesis, the clinical studies got approval from the CSIC Biomedical Ethics Committee, the University of Pennsylvania Institutional Review Board, and the Research with drugs Ethical Committee of the Hospital Clinico San Carlos. Subjects and patients signed an informed consent after receiving an explanation of the nature and implications of the study and before starting the measurements.

Chapter 3. Spatiotemporal defocus sensitivity function

This chapter reports, for the first time, the spatiotemporal defocus sensitivity function of the human visual system, which describes the spatial and temporal sensitivity, and therefore perceptual thresholds, to defocus changes. This new function is inspired by the very well-known spatiotemporal contrast sensitivity function. This chapter describes a model for the spatiotemporal defocus sensitivity function and both its scientific relevance and its clinical application.

This chapter is based on the article by Victor Rodriguez-Lopez et al. *"The spatiotemporal defocus sensitivity function of the human visual system"* submitted to *Journal of Vision (2022)*. The co-authors are William Geisler and Carlos Dorronsoro.

The work was presented as a poster contribution at the International OSA Network of Students (IONS) conference in Barcelona in 2019, and partially as an oral contribution by Carlos Dorronsoro at the Association for Research in Vision and Ophthalmology Conference (ARVO), in Vancouver in 2019.

The contribution of the author of the thesis was the conceptualization and design of the study with all co-authors, the literature research, the design of the experiments in collaboration with Carlos Dorronsoro, the collection and analysis of the data, the writing of the chapter in collaboration with Carlos Dorronsoro, and the editing of the chapter in collaboration with all co-authors.

3.1. Introduction

Throughout the last decades, there has been a huge amount of research regarding the spatiotemporal properties of the human visual system, providing a good description of our limits of visibility, as well as invaluable fundamental scientific knowledge[61,62,70,232]. The Spatial Contrast Sensitivity Function (SCSF), known as CSF in the scientific literature, defines the sensitivity to modulation in contrast, i.e., the minimum contrast visible for different spatial frequencies. The typical SCSF is a curve with maximum sensitivity between 3-6 cycles per degree (cpd), and falling more rapidly in high than in lower spatial frequencies (see Figure 2.7 in section 2.8.1)[52,54]. Common cutoff spatial frequencies, i.e., the maximum spatial frequency visible at maximum contrast (1), lie between 30 and 40 cpd.

On the other hand, the perception of temporally modulated contrast is described in the Temporal Contrast Sensitivity Function (TCSF)[61,62]. When observing an object changing over time, the visual system might perceive said temporal change (flicker) or not (fusion). The TCSF is a similar curve to SCSF, although in the temporal domain. The maximum of the TCSF is found at around 10 cycles per second (Hz), falling more rapidly for high than for low temporal frequencies with a higher ratio than the SCSF (see Figure 2.8 in section 2.8.2). The cutoff temporal frequency that defines the perceptual boundary between flicker and fusion is known as the contrast Critical Fusion Frequency (CFF). The CFF is well known to be around 50-70Hz, depending on the features of the stimulus[62].

The SCSF and the TCSF can be combined in the spatiotemporal contrast sensitivity function (STCSF), which defines what is visible, at the same time, in the space and time domains. Robson[70] measured STCSF for the first time, studying the contrast thresholds of a stimulus for different spatial and temporal frequencies. The limits of the spatiotemporal perception define the ‘window of visibility’[71], a region of the spatiotemporal domain that determine the limits for the perception of visible and fused images.

Contrast sensitivity has been extensively described both in the temporal and the spatial domains because contrast is determinant in visual perception. Another important feature of vision is defocus. Defocus could be considered as a contrast modulation but affecting differently to different spatial frequencies[76]. Essentially, defocus filters high spatial frequencies more than mid and low spatial frequencies, and as the amount of defocus increases, more high frequencies are removed[233].

Some studies have measured the sensitivity to temporal changes in defocus, although only at low temporal frequencies. Walsh et al.[234] found that the maximum sensitivity of 0.1 D occurred for low spatial frequency stimuli, although their hardware limited the temporal frequency to 4Hz. Mathews et al.[235] also measured the sensitivity to temporal changes of defocus, but for even lower temporal frequencies (from 0.2 to 0.8 Hz) and fixed peak-to-valley defocus changes of 0.5 D and 2.0 D. However, a complete study of the temporal sensitivity to defocus, including higher temporal frequencies, has not been addressed due to considerable limitations on the hardware, mainly restricted to the use of mechanical parts to induce the required changes in optical defocus. Other studies have evaluated changes in onscreen blur, by computationally manipulating digital images[236].

Fortunately, modern technologies such as optotunable lenses allow fast and precise changes in optical power, overcoming the limitations of traditional setups. Optotunable lenses are widely used in the field of artificial vision[237], where temporal changes of the plane in focus are often needed. Autofocus systems are a representative example. Other emerging technologies use tunable lenses at high speeds. SimVis[238] uses a temporal multiplexing approach to simulate multifocal ophthalmic corrections by superimposing several images corresponding to different optical powers. If the temporal frequency is fast enough, the multifocal image is perceived as static. At the temporal frequency used, 50 Hz, no flicker perception is perceived. Additionally, a new subjective refraction method to estimate the refractive error of an eye (i.e., myopia, hyperopia, and astigmatism), called Direct Subjective Refraction (presented in Chapter 4 of this thesis), produces flicker cues on purpose to guide the estimation of the refractive error[159], producing changes in defocus at 15 Hz. These novel technologies invite further investigation of the spatiotemporal aspects of defocus sensitivity.

In this study, we investigated the behavior of the visual system to changes in defocus for different temporal and spatial frequencies and natural and artificial stimuli. We report the Temporal Defocus Sensitivity Function (TDSF), and the Spatial Defocus Sensitivity Function (SDSF), and we combine both in the Spatiotemporal Defocus Sensitivity Function (STDSF), described for the first time. We also investigated the impact of accommodation in the measurement of the TDSF.

3.2. Methods

In this study, we measured the Spatiotemporal Defocus Sensitivity Function (STDSF), using an optotunable lens generating sinusoidal Temporal Defocus Waves (TDW). A two-interval forced-choice (2IFC) implemented in an adaptive QUEST psychophysical algorithm was used to determine the peak-to-valley defocus changes threshold for several temporal frequencies and spatial frequencies.

3.2.1. Observers

Seven observers participated in the experiment, aged from 22 to 28 years old (25±2.6 on average). All of them had healthy stereovision (<40 arc seconds) and no color vision abnormalities. Their maximum visual acuity with their current prescription, measured with standard optometry techniques, was 0.0 logMAR or higher. Observers performed the experiments wearing their usual ophthalmic prescription if any. Three of the observers wore contact lenses, two wore glasses and two did not need any optical compensation. Only the left eye was measured.

3.2.2. Experimental setup

An optotunable lens, able to modify its optical power in response to an electric signal, is the active element generating sinusoidal TDW with different peak-to-valley defocus changes and temporal frequencies. To compensate for the dioptric distance to the display, the center of the TDW was always 1.00D, thus the defocus of the wave changed sinusoidally around that value (Figure 3.1A). We used a liquid-membrane optotunable lens (EL-10-30-TC, Optotune, Switzerland) that enables accurate variations in optical power in temporal regimes up to 100 Hz[239]. The optotunable lens is optically projected onto the pupil plane of the observer's eye via a 4f-projection optical system (Figure 3.1A).

The stimulus was displayed on an EliteDisplay E240 23.8'' monitor (HP Inc, Palo Alto, USA) with a size of 55.72x34.22cm, a spatial resolution of 1920x1080 pixels, and a refresh rate of 60Hz. The monitor was driven by an NVIDIA Quadro P4000 dual Graphic card. The physical distance from the eye's pupil to the first lens is 45 cm, and from the optotunable lens to the screen is 1m. While the actual distance from the pupil of the eye to the monitor is 1.25m, the effective optical distance is 1m. This optical setup allows changes in retinal blur (defocus) without displacements nor changes in magnification.

The maximum luminance of the monitor was 250cd/m^2. The effective luminance of the monitor, after passing through the optical system, was around 25cd/m^2.

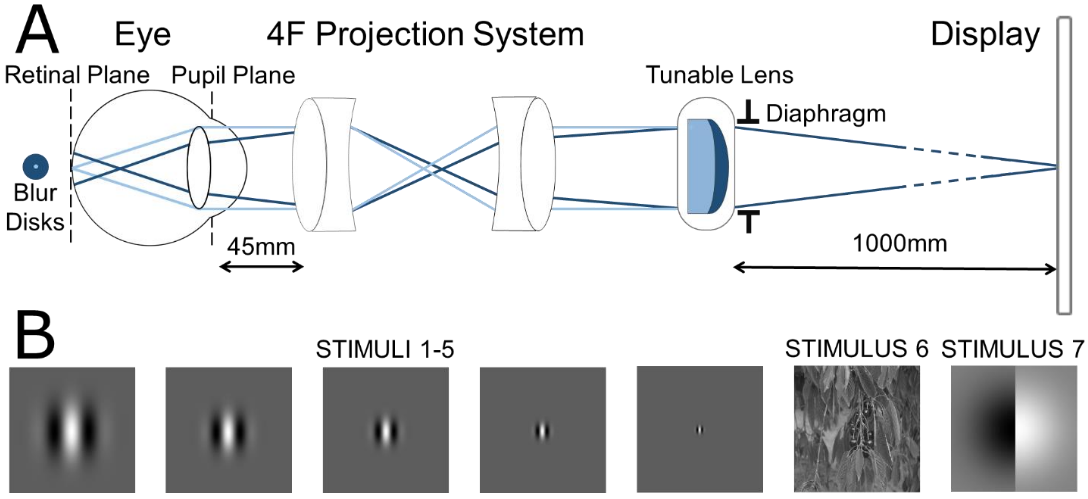

Figure 3.1. Setup for the experiment. **A**. Schematic representation of the optical system. It shows the retinal blur change produced by optical power change induce by the optotunable lens. The optotunable lens is projected onto the pupil's eye using a 4f optical system. If the stimulus is defocused for the observer (in most situations) a large blur disk is produced on the retina (dark green). If the optotunable lens focuses the stimulus on the retina (light green), the blur disk produced is minimum. With this configuration, the optical power of the optotunable lens produces defocus blur in the image, without changing the position or the magnification. **B**. Stimuli for the experiment. All stimuli subtended 4 degrees of visual field. Stimuli 1-5: Gabor patches of 2, 4, 8, 16, and 32 cpd. The size of the Gabor changed across spatial frequencies. Stimulus 6: natural image patches of vegetables, fruits, bushes, and trees. An example of the patch used in this study is shown. Stimulus 7: gaussian edge of 0.5deg of standard deviation in X and Y.

3.2.3. Stimuli

Seven stimuli were used during the experiments all of them subtending 4 degrees of visual field. (Figure 3.1B). In stimuli 1-5, we used Gabor patches of 2, 4, 8, 16, and 32 cycles per degree (cpd), equally spaced in a logarithmic scale of spatial frequency. Stimulus 6 was selected from a natural images database[240] of well-focused images with the same contrast and luminance, conformed of fruits, vegetables, bushes, and trees. Stimulus 7 was a gaussian edge. During the experiments, all the stimuli were displayed on the monitor over a gray background.

3.2.4. Experiments and procedures

We used sinusoidal Temporal Defocus Waves (TDW; periodic sinusoidal variations in optical defocus) to measure perceptual thresholds to temporal changes in defocus, i.e., the minimum peak-to-valley defocus (change in defocus) producing a sensation of flicker. The measurements were repeated for different temporal frequencies and different stimuli.

To find the threshold, we used a QUEST Bayesian adaptive procedure[228] in a two-interval forced choice (2IFC) task over 30 trials. As illustrated in Figure 3.2, in each trial, two different TDW are displayed, a reference TDW and a testing TDW, randomly assigned to the first or the second interval. Both TDWs have the same defocus peak-to-valley defocus change and therefore produce the same amount of retinal blur, but the reference TDW has a reference temporal frequency of 62.5Hz, which is always perceived static, and the other one, the testing TDW, has the testing temporal frequency that may or may not produce flicker.

In each trial, the same stimulus was shown in both intervals of 1.7 seconds each. A gray screen was displayed for 0.5 seconds during a transition period between intervals. Sound cues were provided at the beginning of each interval. The task of the subject was to indicate, using a keyboard, in which of the two intervals the stimulus was perceived flickering: left-arrow for the first interval and right-arrow for the second interval.

The response was considered correct if the subject selected the testing TDW, and incorrect if the subject selected the reference TDW. During the experiment the QUEST algorithm suggested the peak-to-valley defocus change of the next trial, based on all the previous responses of the observer. The peak-to-valley of the TDW was changed in variable steps ranging from a maximum peak-to-valley change of 4.5D (determined by the range of the tunable lens) to a minimum of 0.0D (no change in defocus) and precision of 0.01D. Completing each QUEST staircase took about 3 minutes.

For each stimulus (the 5 Gabor patches, the natural image, the gaussian edge), seven testing temporal frequencies logarithmically spaced between 1.4 to 45Hz were measured in random order (1.4, 2.8, 5.5, 11, 22.1, 31.3 and 44.2 Hz). The number of cycles within the interval duration was always an integer number. The reference temporal frequency TDW was set to 62.5Hz in all cases, because i) the critical flicker frequency of the temporal contrast sensitivity function, for similar experimental luminance conditions, is always below 60 Hz[62]; and ii) pilot experiments with maximum TDW peak-to-valley observing a laser spot providing high luminance and contrast, as well as an expanded defocus Point Spread Function (due to coherence), showed no defocus flicker perception above 50 Hz.

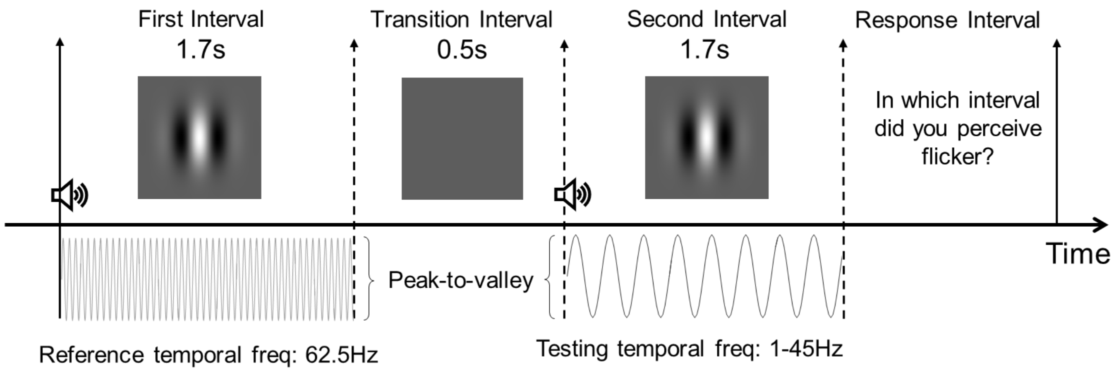

Figure 3.2. Trial sequence for the experiment. For a particular condition (stimulus 1 shown as an example), reference temporal frequency is displayed in the first interval and the testing temporal frequency in the second interval (in the experiment is randomized). Miniature speakerphones represent sound cues. Peak-to-valley defocus change threshold is found after 30 trials.

We defined the Defocus Critical Fusion Frequency (DCFF) as the threshold separating defocus flicker perception and defocus fusion. For temporal frequencies beyond the DCFF, defocus flicker is not perceived, and the image is observed fused, perceived as static. We considered that the DCFF should be calculated with a peak-to-valley defocus change of 3.D, the maximum defocus in a conventional visual scenario with objects at different distances: from optical infinite to near vision -considered at 33cm-.

Stimuli were generated with MATLAB (Math-works Inc., Natick, USA). Custom firmware was developed to control the electronics driving the optotunable lens. PsychToolbox 3[241] was used to synchronize the control of the tunable lens with the randomized stimulus presentation and the auditive signals, capturing the response of the subject and calculating the peak-to-valley change of the TDW for the next iteration.

The position of the subject was stabilized with a bite bar. Subjects aligned themselves in X and Y axes with the entrance pupil of the optical system using a micrometric system, a square TDW changing defocus between 0 and 2D at 15Hz, and a white cross over a gray background as an alignment stimulus. The alignment task is finding the XY position of the pupil producing minimum flicker (maximum superposition between images for different optical powers), corresponding to the optical axis of the projection system. As mentioned, subjects wore their optical correction to compensate for their refractive error during the experiments. The accommodation was free, except in control experiment 2. To remove acoustic cues (sounds produced by the optotunable lens), subjects wore earphones and listened to music during the experiments.

We performed one main experiment and two control experiments.

3.2.4.1. Experiment 1. Spatiotemporal defocus sensitivity experiment

We measured the peak-to-valley defocus change threshold for seven temporal frequencies ranging from 1.2-45 Hz and for all stimuli (Figure 3.1B). Pupil size was not fixed.

3.2.4.2. Control Experiment 1. Pupil size reduction

Other residual cues besides defocus introduced by the tunable lens, such as magnification or image displacement, might potentially contribute to the perception of defocus flicker. To isolate the impact of those residual cues, we reduced the pupil size of the eye to 1 mm using a diaphragm projected onto the pupil of the eye, substantially reducing the retinal blur induced by defocus due to the decrease of the defocus disk. The peak-to-valley defocus change threshold was then measured for the same seven temporal frequencies as in the main experiment. This control experiment was only performed for stimulus 6 (natural images, Figure 3.1B).

3.2.4.3. Control experiment 2. Paralyzed accommodation

As accommodation was functional during the main experiment, small fluctuations of the accommodation may affect defocus flicker perception. In this control experiment, we instilled cycloplegic drugs (tropicamide 1%, second drop instilled 10 minutes after a first drop, and 30 minutes before the experiment) to paralyze the accommodation. To reduce the increase in pupil size due to the cycloplegic drugs, we kept a 4-mm pupil diameter by using a diaphragm projected onto the pupil of the eye. Control experiment 2 was carried out for stimulus 6 (natural images, Figure 3.1B).

3.2.5. Spatiotemporal defocus sensitivity function

To fit our experimental data, we considered well-established models of contrast sensitivity (see section 2.8). On the one hand, we considered the spatial model described by Mannos et al.[231] for the Spatial Contrast Sensitivity Function (SCSF). In their model, spatial sensitivity is defined as

$$SCSF(f_s) = d\left(a + \frac{f_s}{f_{s0}}\right) e^{-\left(\frac{f_s}{f_{s0}}\right)^c} \qquad 3.1$$

where f_S is the spatial frequency, d is a gain factor, a controls the shape of the curve, c determines the steepness of the curve for high frequencies and f_{s0} is the peak frequency. In our experiments, instead of luminance contrast for different spatial frequencies, we use the peak-to-valley defocus change for different spatial frequencies (Gabor patches).

In this study, we define for the first time the spatial defocus sensitivity function ($SDSF(f_s)$) of the human eye, as the sensitivity to the presence of defocus for different spatial frequencies.

To describe the $SDSF(f_s)$, we used a model similar to the one used by Mannos for the $SCSF(f_s)$ (Equation 3.1), but with different parameters (d_D, a_D, f_{s0D}, and c_D) that are now adapted to the presence of defocus and to the sensitivity of the observer to that defocus

$$SDSF(f_s) = d_D \left(a_D + \frac{f_s}{f_{s0D}}\right) e^{-\left(\frac{f_s}{f_{s0}}\right)^{c_D}} \quad 3.2$$

On the other hand, we considered the temporal model described by Watson for the TCSF[62]. The temporal sensitivity is modeled as the difference between two temporal filters, one corresponding to low temporal frequencies and the other to high temporal frequencies, modulated by a gain factor. The total filter, $ft(t)$, defines the impulse response in the temporal domain with the following equation

$$ft(t) = \varepsilon \cdot [f_1(t) - \zeta \cdot f_2(t)] \quad 3.3$$

where ε is a gain factor, ζ is the transience factor, and $f_1(t)$ and $f_2(t)$ represent each filter.

$$\begin{gathered} f_1(t) = u(t) \cdot (\tau \cdot (n_1 - 1)!)^{-1} \cdot \left(\frac{t}{\tau}\right)^{n_1} \cdot e^{-(t/\tau)} \\ f_2(t) = u(t) \cdot (\kappa \cdot \tau \cdot (n_2 - 1)!)^{-1} \cdot \left(\frac{t}{\kappa \cdot \tau}\right)^{n_2} \cdot e^{-(t/\kappa \cdot \tau)} \end{gathered} \quad 3.4$$

where $u(t)$ is the unit step function, τ is a time constant, κ is the time constant ratio, and n is the number of stages of each filter.

Computing the Fourier transform (*FT*) of the impulse response (Equation 3.4), the amplitude and phase responses can be estimated in the temporal frequency domain. According to Watson[62], the amplitude response represents the temporal sensitivity ($S_T(f_t)$) of the human visual system (for luminance contrast)

$$TCSF(f_t) = FT\big(f(t)\big) \quad 3.5$$

In this study, we define for the first time the temporal defocus sensitivity function ($TDSF(f_s)$) of the human eye, as the sensitivity to defocus changes at different temporal frequencies. To describe the $TDSF(f_t)$, we used a model similar to the one used by Watson for the $TCSF(f_t)$ (Equations 3.4 and 3.5), but with different parameters (ε_D, ζ_D, τ_D, κ_D, n_{1D}, n_{2D}) that are now adapted to the presence of defocus and to the sensitivity of the observer to that defocus

$$\begin{gathered} f_D(t) = \varepsilon_D u(t) \tau_D e^{-\frac{\kappa_D(t+1)}{\kappa_D \cdot \tau_D}} \left[\left((n_{1D} - 1)!\right)^{-1} \left(\frac{t}{\tau_D}\right)^{n_{1D}} \right. \\ \left. - \zeta_D(\kappa(n_{2D} - 1)!)^{-1} \left(\frac{t}{\kappa_D \cdot \tau_D}\right)^{n_{2D}}\right] \\ TDSF(f_t) = FT\big(f_D(t)\big) \end{gathered} \quad 3.6$$

where $f_D(t)$ is the total filter for defocus.

In this study, both in the spatial and temporal domains, what we measured were the defocus detection thresholds, which are the inverse of defocus sensitivity. Figure 3.3 shows the process of fitting the models to the experimental data (only TDSF is shown, but we used a similar approach for the SDSF). We used the Nelder-Mead simplex optimization algorithm (direct search) for each subject and stimulus, to obtain the curve of temporal defocus thresholds in D units (minimum peak-to-valley defocus change perceived) and, by inverting it, the TDSF (in D^{-1} units).

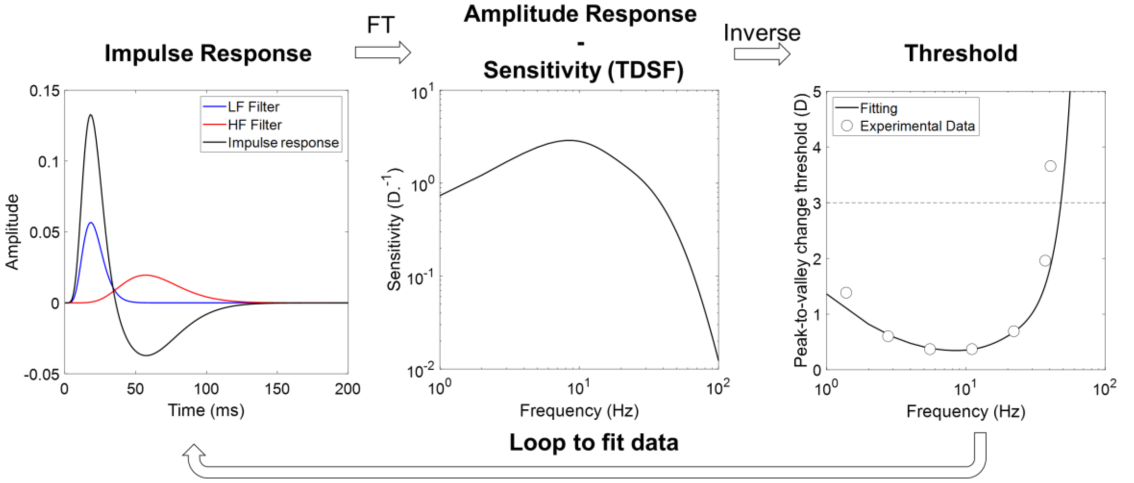

Figure 3.3. Fitting model. Process of fitting the experimental data to the model described by Watson 1986[62]. The impulse response of the system (black line in the left graph) is the difference between two filters: one for low temporal frequencies (blue line) and one for high temporal frequencies (red line). Applying a Fourier transform, we obtain the amplitude response, corresponding to the Temporal Defocus Sensitivity Function (TDSF). The inverse of the TDSF can be fitted to the experimental data.

In this study, we measured combinations of the different spatial (Gabor patches) and temporal (TDWs) conditions. To construct the spatiotemporal defocus sensitivity function (STDSF), defined as the sensitivity to the presence of defocus in the spatial and temporal domain, and to compare it with the well-known spatiotemporal contrast sensitivity function (STCSF), we used the model proposed by Lambretch et al.[73] that considers the spatiotemporal sensitivity as a non-separable function of spatial and temporal information. According to Lambretch

$$\begin{aligned} STCSF(f_s, f_t) = \alpha \Big(& SCSF_{f_{t_1}}(f_s) \cdot TCSF_{f_{s_1}}(f_t) + \beta \cdot SCSF_{f_{t_2}}(f_s) \cdot TCSF_{f_{s_2}}(f_t) \\ & + \gamma \cdot SCSF_{f_{t_2}}(f_s) \cdot TCSF_{f_{s_1}}(f_t) + \delta \cdot SCSF_{f_{t_1}}(f_s) \\ & \cdot TCSF_{f_{s_2}}(f_t) \Big) \end{aligned} \qquad 3.7$$

where α, β, γ and δ are normalization factors, $SCSF_{f_{t_1}}$ and $SCSF_{f_{t_2}}$ are the spatial sensitivities for particular temporal frequencies ($f_{t_1}$and f_{t_2}) and $TCSF_{f_{s_1}}$ and $TCSF_{f_{s_2}}$ are the temporal sensitivities for particular spatial frequencies ($f_{s_1}$and f_{s_2}), obtained previously in Equations 3.1 and 3.5, respectively. In Lambretch's model, the spatial and temporal sensitivities were selected based on the original Burbeck's description[72], selecting the spatial sensitivities for 1 and 19 Hz ($SCSF_1$ and $SCSF_{19}$) and the temporal sensitivities for 0.5 and 10 cpd ($TCSF_{0.5}$ and $TCSF_{10}$). We used this same model with different parameters to describe the spatiotemporal defocus sensitivity function ($SDCSF(f_s, f_t)$) of the human eye

$$STDSF(f_s, f_t) = \alpha_D \Big(SDSF_{f_{t_1}}(f_s) \cdot TDSF_{f_{s_1}}(f_t) + \beta_D \cdot SDSF_{f_{t_2}}(f_s) \cdot TDSF_{f_{s_2}}(f_t) + \gamma_D \cdot SDSF_{f_{t_2}}(f_s) \cdot TDSF_{f_{s_1}}(f_t) + \delta_D \cdot SDSF_{f_{t_1}}(f_s) \cdot TDSF_{f_{s_2}}(f_t)\Big) \quad 3.8$$

where α_D, β_D, γ_D, and δ_D are referred now to defocus sensitivity, $SDSF_{f_{t_1}}$ and $SDSF_{f_{t_2}}$ are the spatial defocus sensitivities for particular temporal frequencies ($f_{t_1}$and f_{t_2}) and $TDSF_{f_{s_1}}$ and $TDSF_{f_{s_2}}$ are the temporal defocus sensitivities for particular spatial frequencies ($f_{s_1}$and f_{s_2}), obtained previously in Equations 3.2 and 3.6, respectively. In our experiment, we used the spatial defocus sensitivities $SDSF_{f_{t_1}}$ and $SDSF_{f_{t_2}}$ measured for 1.1 and 22.2 Hz and the temporal defocus sensitivities $TDSF_{f_{s_1}}$ and $TDSF_{f_{s_2}}$ measured for 2 and 8 cpd.

The window of visibility, a concept defined for contrast sensitivity[71], describes the spatiotemporal boundary of contrast perception. Spatial and temporal components that lie outside the window are invisible, and those within the window are somewhat visible, depending on the spatiotemporal contrast sensitivity function. Similarly, we can define a window of defocus visibility, the spatiotemporal limits of defocus perception. We considered the boundary between visible and invisible when defocus sensitivity is below $0.3D^{-1}$.

3.2.6. Statistical analysis

To analyze the statistical significance between stimuli (Gabor patches, natural images, and edge) and main between also experiment (for natural images) and control experiments (pupil reduction and paralyzed accommodation) paired t-tests were used. We analyzed differences for each temporal frequency measured (seven in total). The statistical level to achieve statistical significance was set to 5% (p=0.05).

3.3. Results

Figure 3.4 shows a representative example of the results obtained for one subject. Figure 3.4A shows the progress of the QUEST procedure along trials for seven temporal frequencies (each one indicated with a different color) for subject 1 (S1) and a Gabor patch of 32cpd. The peak-to-valley defocus change threshold (in D) is indicated as a dot at the end of each QUEST staircase. A peak-to-valley defocus change threshold above 3.00 D (indicated with a dashed line) is considered perception without flicker, i.e., complete fusion of the temporal defocus wave. The threshold obtained for each temporal frequency and the fitting described in Equation 3.6, the inverse of the Temporal Defocus Sensitivity Function (TDSF), are shown in Figure 3.4B. The minimum threshold (i.e., maximum sensitivity) and the Defocus Critical Fusion Frequency (DCFF) are indicated with a blue and red cross, respectively. For this subject and condition, flicker is not perceived at high temporal frequencies (31.2 and 44.2 Hz). The minimum threshold is 0.25 D (corresponding to a maximum sensitivity of 4.00 D^{-1}) at 11 Hz. Figure 3.4C shows the inverse TDSF, the DCFF, and the minimum threshold for S1 and all spatial frequencies measured. The DCFF ranged from 28 to 34 Hz and the threshold from 0.21 to 0.59 D (corresponding to maximum sensitivity of 4.76 to 1.69 D^{-1}) at 8.4 to 11.6 Hz. Overall, the DCFF is around 30 Hz, and the maximum sensitivity is around 10 Hz.

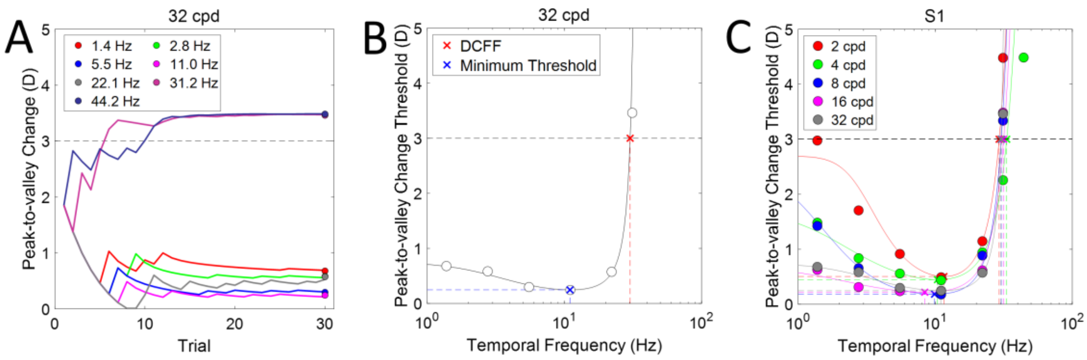

Figure 3.4. Temporal sensitivity to changes in defocus. A. Progress of the Quest procedure for different temporal frequencies, for Subject S1 and a Gabor patch of 32cpd. The endpoints of each curve represent the defocus amplitude threshold estimated after 30 trials. **B.** Thresholds obtained for each temporal frequency. The black line represents the fitting *of* Watson's model (see Equation 3.6). Minimum threshold peak-to-valley defocus change (i.e., maximum sensitivity) is displayed as a blue cross. The Defocus Critical Fusion Frequency (DCFF) is displayed as a red cross. **C.** Thresholds were obtained for each temporal frequency and all spatial frequencies measured for S1.

Figure 3.5 and Table 3.1 show the results averaged for all subjects and all stimuli measured. In Figure 3.5A, the results for the Gabor patches with different spatial frequencies. Figure 3.5B shows the results averaged across subjects for the natural images stimulus. Similarly, Figure 3.5C shows the results averaged across subjects for the edge stimulus. In Table 3.1 we show the minimum threshold, maximum sensitivity, temporal frequency of the maximum sensitivity, and the DCFF, averaged across subjects.

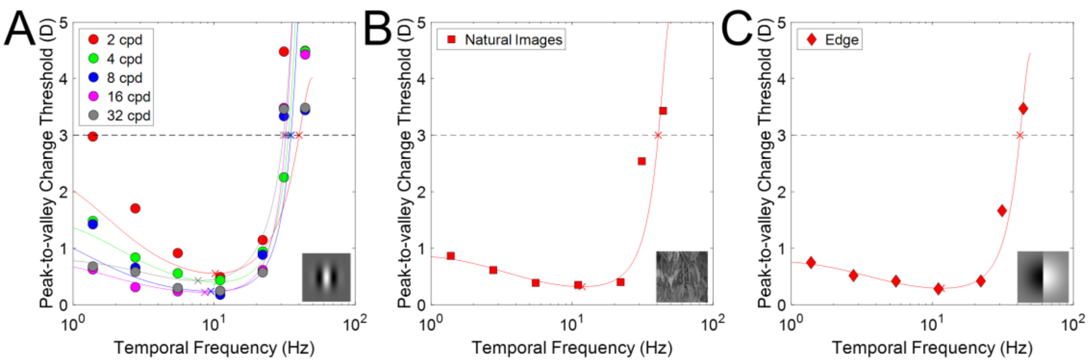

Figure 3.5. Average across subjects. A miniature *of* each stimulus is displayed in the left corner of each subplot. **A. Gabor patches.** Defocus temporal sensitivity function for Gabor patches of different spatial frequencies. Circles represent the data and lines the fitting. Red color indicates 2 cpd, red 4 cpd, blue 8 cpd, magenta 16 cpd, and gray 32 cpd. **B. Natural Images.** Defocus temporal sensitivity function for natural images condition averaged across subjects. Red squares represent the data and the red line the fitting. **C. Edge.** Defocus temporal sensitivity function for edge condition averaged across subjects. Red diamonds represent data and the red line the fitting.

Comparing the Gabor of spatial frequency with maximum sensitivity (16cpd) with natural images and edge stimulus, there is a non-significant statistical difference for any temporal frequency (paired t-test p<.05 in all comparisons).

Table 3.1. Temporal sensitivity function results for all stimuli. Minimum threshold, maximum sensitivity, temporal frequency at maximum sensitivity, and defocus critical fusion frequency averaged across subjects.

Stimulus	Minimum Threshold (D)	Maximum Sensitivity (D^{-1})	Temporal Frequency of the Maximum (Hz)	DCFF (Hz)
2 cpd	0.55	1.81	10.2	40.0

4 cpd	0.40	2.50	10.5	33.7
8 cpd	0.25	4.00	9.4	32.3
16 cpd	0.22	4.54	8.6	32.2
32 cpd	0.43	2.33	7.7	31.0
Natural Image	0.32	3.13	11.8	40.9
Edge	0.29	3.44	11.6	41.9

Control experiments

Figure 3.6A shows the results averaged across subjects for the normal experiment (in red), for control experiment 1 (pupil reduction, in green), and control experiment 2 (paralyzed accommodation, in dark yellow). The DCFF for pupil reduction and paralyzed accommodation is found at 22.3 and 36.1Hz and the minimum threshold is found at 0.50D (2.00D^{-1}) at 3.6Hz and 0.34D (2.94D^{-1}) at 7Hz, respectively. For low temporal frequencies, the minimum threshold is slightly lower (higher sensitivity) for both control experiments, and for medium and high temporal frequencies the minimum threshold is higher (lower sensitivity) for control experiments. For control experiment 1, paired t-tests report non-significant differences for low temporal frequencies (1.4 and 2.8Hz, $p>.05$) but significant differences for temporal frequencies higher than 2.8Hz ($p<.05$). For control experiment 2, paired t-tests report non-significant differences for all temporal frequencies ($p<.05$).

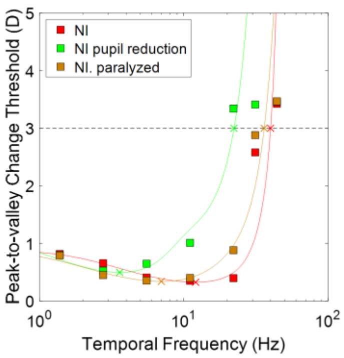

Figure 3.6. Control experiments. It shows the results for the main experiment for natural image stimulus and the control experiments. In red, the data for the main experiment, in green for the pupil reduction control experiment, and in dark yellow for the paralyzed accommodation control experiment.

Spatial Defocus Sensitivity Function

To obtain the Spatial Defocus Sensitivity Function (SDSF) we used the fitting described in section 3.2 and developed by Mannos et al.[231]. The results averaged across subjects are shown in Table 3.2 and plotted in Figure 3.7A (left plot). We did not show the results for 44.4Hz because the experimental data was above 3.0 D for all temporal frequencies and subjects.

Table 3.2. Spatial sensitivity function results for all stimuli. Minimum threshold, maximum sensitivity, temporal frequency at maximum sensitivity, and defocus critical fusion frequency averaged across subjects.

Temporal Frequency (Hz)	Minimum Threshold (D)	Maximum Sensitivity (D^{-1})	Spatial Frequency of the Maximum (cpd)	DCFF (cpd)
1.4	0.65	1.54	21.0	57.6

2.8	0.35	2.86	17.8	47.8
5.5	0.24	4.17	14.0	58.8
11.0	0.22	4.55	13.8	51.4
22.1	0.66	1.51	9.0	56.0
31.2	0.60	1.67	6.0	28.8

<u>Spatiotemporal Defocus Sensitivity Function</u>

To obtain the SDSF in (Figure 3.7A, left plot), the TDSF (Figure 3.7A, middle plot), and the spatiotemporal defocus sensitivity function (STDSF, Figure 3.7A, right plot) we used Equation 3.2, Equation 3.6, and Equation 3.8, respectively. Figure 3.7A (right plot) shows the STDSF. The parameters of the model where α_D, β_D, γ_D, and δ_D are 1, 10, -5, and 3.74, respectively. The maximum sensitivity is 4.55D^{-1} at 13.6cpd and 9.6Hz. The window of visibility for defocus (displayed as a red line) is defined as the boundaries for defocus perception and is found when sensitivity decreases to 0.3 (inverse of 3.0D), covering a region around 40 cpd to 40Hz. Table 3.3 shows the parameters of the SDSF for all temporal frequencies and the parameters of the TDSF for all spatial frequencies, shown in Figure 3.7.

Table 3.3. Parameters of the models for SDSF and TDSF. The data for the fitting was obtained from the averages across subjects for Gabor stimuli.

$\boldsymbol{SDSF(f_t)}$						
Temporal Frequency (Hz)	$\boldsymbol{d_D}$	$\boldsymbol{a_D}$	$\boldsymbol{f_{s0D}}$	$\boldsymbol{c_D}$	-	
1.38	3.27	0.01	31.36	1.77		
2.76	5.89	0.07	26.51	2.13		
5.52	10.53	0.03	17.4	1.27		
11.05	10.76	0.06	18.99	1.51		
22.10	3.40	0.14	5.62	0.67		
31.25	0.61	-0.54	0.36	0.37		
$\boldsymbol{TDSF(f_s)}$						
Spatial Frequency (cpd)	$\boldsymbol{\varepsilon_D}$	$\boldsymbol{\zeta_D}$	$\boldsymbol{\tau_D}$	$\boldsymbol{\kappa_D}$	$\boldsymbol{n_{1D}}$	$\boldsymbol{n_{2D}}$
2	2.05	0.81	6.6	0.43	8	9
4	20.81	0.97	5.52	0.93	9	9
8	49.81	0.99	6.47	0.84	8	9
16	13.89	0.91	7.25	0.71	9	10
32	3.22	0.62	8.17	0.45	8	9

Figure 3.7B shows the spatial contrast sensitivity function (SCSF, left plot), temporal contrast sensitivity function (TCSF, middle plot), and spatiotemporal contrast sensitivity function, (STCSF, right plot), to compare with the defocus sensitivity. For the STCSF the maximum is 385 at around 1cpd and 10 Hz. The window of visibility for contrast (displayed also as a red line) is found when contrast sensitivity decreases to 1 (inverse of 3.0D), covering a region around 30 cpd to 60 Hz.

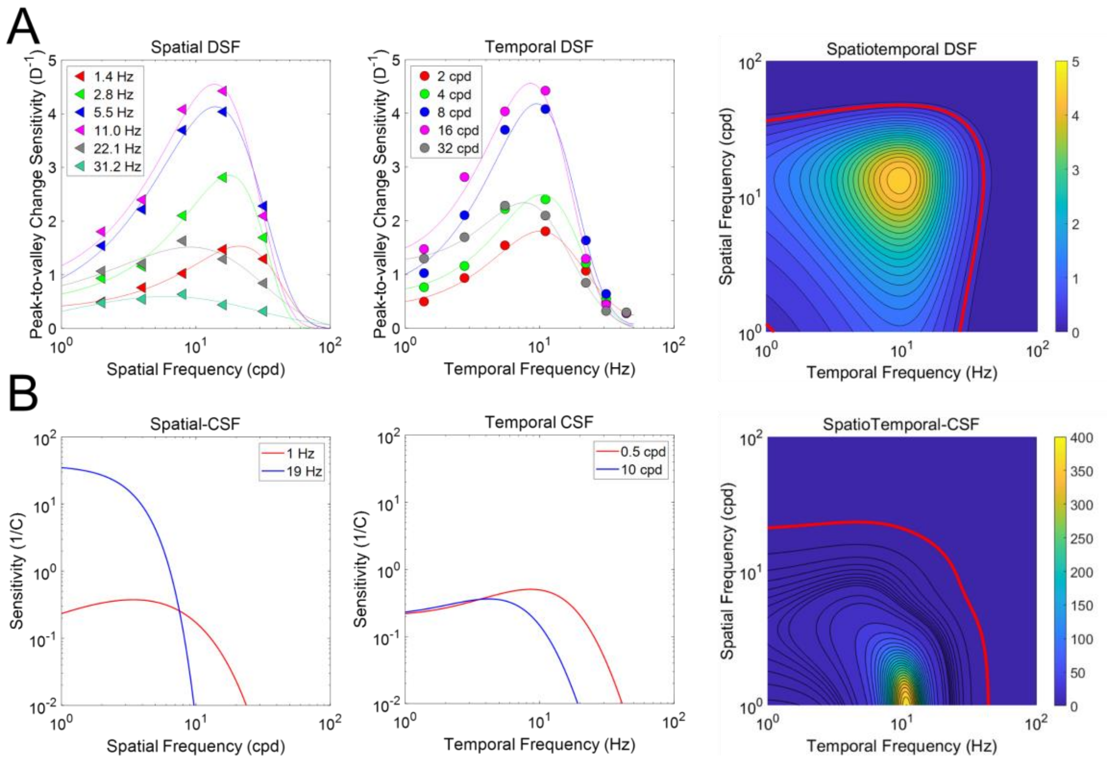

Figure 3.7. Spatiotemporal Sensitivity. A. Spatiotemporal Defocus Sensitivity Function (STDSF). It shows the spatiotemporal defocus sensitivity function from the experimental data obtained in this study, averaged across subjects and conditions. *O*n the left, the spatial defocus sensitivity function (SDSF) for different temporal frequencies. *I*n the middle, the temporal defocus sensitivity function (TDSF) for different spatial frequencies. *O*n the left, the spatiotemporal defocus sensitivity function (STDSF) contour plot. In red, the defocus window of visibility. **B. Spatiotemporal Contrast Sensitivity Function (SCDSF)**. On the left, the spatial contrast sensitivity function (SCSF) for 19 and 1 Hz temporal frequencies, based on Mannos et al.[231]. In the middle, the temporal contrast sensitivity function (TCSF) for 10 and 0.5cpd spatial frequencies, based on Watson[62]. On the right, the spatiotemporal contrast sensitivity function (STCSF), based on Lambretch et al.[73].

3.4. Discussion

Spatiotemporal defocus sensitivity function

In this study, we have measured and described, for the first time, the spatiotemporal defocus sensitivity function (STDSF). Our results report, on average across subjects, maximum sensitivity to changes in defocus at 13.6cpd and 9.6Hz. Compared with the spatiotemporal contrast sensitivity function (STCSF), the maximum sensitivity was found at a very different spatial frequency (1-2cpd) and similar temporal frequency (10 Hz). The shapes of both sensitivity curves follow the same trend and there is a shift in the spatial frequency providing the maximum sensitivity (2 cpd in contrast, 14 cpd in defocus). This result can be explained by the fact that defocus affects less at low spatial frequencies than at medium and high spatial frequencies, and therefore the detection of flicker at medium and high spatial frequencies is more sensitive. The absolute value of maximum sensitivity is much higher for contrast than for defocus (385 vs 5 D^{-1}), but this is due to the different magnitudes and units involved (contrast vs diopters).

The model described by Watson[62] to explain the temporal contrast sensitivity function (TCSF) was adapted in this study to fit the temporal defocus sensitivity function (TDSF). We obtained different results when using the model with our experimental data and the new magnitude (defocus). First, in Watson's model, the contrast Critical Flicker

Frequency (CFF) varied between 50-70 Hz, depending on the stimulus condition. However, our data yields Defocus Critical Fusion Frequencies (DCFFs) around 30-40Hz. At high temporal frequencies, the CFF is obtained at high contrast and the DCFF at high defocus values. While CFF is obtained with the maximum physical contrast (~1) DCFF is obtained at ~3D. Second, the limit for defocus changes was relatively low, as it was defined as the dioptric change between far and near vision (3.0 D). A higher dioptric limit may have shifted the DCFF to higher temporal frequencies, but 3.0D seems like a reasonable limit in vision as larger defocus changes are unusual.

Mannos et al.[231] described a model for spatial contrast sensitivity that was used in this study to find the spatial defocus sensitivity function (SDSF). After fitting, the model predicted our experimental data well. In addition, the model explained by Burbeck et al.[72] and lately refined by Lambretch et al. [73] was also used to describe the STDSF.

Influence of the pupil

For control experiment 1, reduced pupil diameter, the sensitivity at medium and high temporal frequencies (>2.8Hz) was significantly lower (higher threshold, Figure 3.6) than for the normal experiment. The result is explained by the overall reduction in retinal blur and the increase in depth-of-focus due to pupil reduction, which effectively reduces the differences in the retinal image with the different defocus levels, and therefore the sensitivity.

Flicker-detection task and accommodation

A physiological source of temporal changes in defocus is accommodation, the ability of the crystalline lens to change its optical power. Accommodation could be a very fast process, that can be activated in a few milliseconds (around 300ms[242]). However, it has been reported that the accommodative response is not able to follow changes in defocus faster than 2 Hz[9,234,243]. Beyond that frequency, the temporal response of accommodation is erratic and hardly accurate. This occurs in a blur-detection task, where the accommodation is elicited on purpose for focusing on the target (i.e., the evaluation of visual acuity). However, in this study, the task consists of flicker detection, and the accommodation response may differ.

In the results reported for control experiment 2, where the accommodation was paralyzed by instilling cycloplegic drugs, we found slightly higher sensitivity at low temporal frequencies than in the normal experiment with free accommodation (Figure 3.6), but the differences were non-significant. Besides, in control experiment 2 for medium and high temporal frequencies, the results are statistically similar. Both results suggest that accommodation does not vary during the defocus flicker detection task, even at low temporal frequencies. The varying defocus seems to deactivate accommodation, and the eye keeps its optical power stable, probably in a relaxed position.

Implications of the spatiotemporal defocus sensitivity function

The STDSF not only provides basic scientific knowledge but a theoretical framework for new technologies that make use of temporal changes in defocus. SimVis Gekko is a visual simulator, used in other chapters of this thesis, that uses optotunable lenses under a temporal multiplexing approach. It induces fast changes in defocus to project in the retina of the patient a superposition of image components that are perceived as a static multifocal image, thanks to temporal fusion. In this way, the device can provide programmable simulations of existing multifocal lens models. SimVis Gekko works at a temporal frequency of 50Hz[113,229], above all the Defocus Critical Flicker Fusions measured in this study for all conditions, and therefore defocus flicker should not be perceived. Additionally, the dynamic response of tunable lenses has been reported to be more erratic as speed increases[239]. Moreover, the temporal sensitivity to contrast decreases with age, with a shift of the maximum sensitivity to lower temporal frequencies[64]. Further studies of defocus flicker might include presbyopes, the target for multifocal corrections and SimVis Gekko.

Another recent application using fast changes in defocus, developed during this thesis (see Chapter 4), is the Direct Subjective Refraction. It is a new method for estimating the refractive error of an eye, which uses temporal changes of 15Hz to create flicker cues on purpose and to find the spherical equivalent of the eye[159]. The results of this study can be used to characterize the parameters of the new visual task that imply periodic changes in defocus.

3.5. Conclusions

In this study we have reported for the first time the spatiotemporal defocus sensitivity function of the human eye, finding a maximum of sensitivity around 14cpd and 10Hz (spatial frequency and temporal frequency) and limits of sensitivity, defined by the defocus window of sensitivity, at 40 cpd and 40 Hz. We have also demonstrated that accommodation is not stimulated while performing a defocus flicker-detection task. The spatiotemporal defocus sensitivity function described in this study has implications for new technologies that make use of fast changes in defocus in their working principles.

Chapter 4. The Direct Subjective Refraction

This chapter describes the development of a new method for estimating the spherical equivalent of the refractive error of the eye, which we call the Direct Subjective Refraction (DSR). It uses an optotunable creating temporal defocus waves that interact with the longitudinal chromatic aberration of the eye, producing flicker and chromatic distortions that are minimum when the mean optical power of the wave matches the spherical equivalent of the eye. In this chapter, the DSR working principle is described and the result of the DSR method is compared with an unsupervised version of the traditional subjective refraction (UTSR) and with the traditional subjective refraction method (TSR).

This chapter is based on the article by Victor Rodriguez-Lopez et al. *"The Direct Subjective Refraction: Unsupervised measurements of the subjective refraction using defocus waves"*, available as a preprint in *BioXrv (2021)* and submitted to *Translational Vision Science Technology (2022)*. The co-authors of the article are Alfonso Hernandez-Poyatos and Carlos Dorronsoro.

The contribution of the author of the thesis was the conceptualization and design of the study in collaboration with Carlos Dorronsoro, the literature research, the design of the experiments in collaboration with Carlos Dorronsoro, the collection of the data in collaboration with Alfonso Hernandez-Poyatos, the analysis of the data, the writing of the chapter and the editing of the chapter in collaboration with Carlos Dorronsoro.

This work was presented as an oral contribution at the Association for Vision and Research in Ophthalmology (ARVO) meeting in 2019 in Vancouver. The work was considered a hot topic at the meeting, among the best 1% of all the contributions to the conference. It also received media coverage during said conference. Also, it was presented as an invited talk in Optica Vision & Color Summer Data Blast Session (online) 2022.

4.1. Introduction

The previous chapter has explored the perceptual limits of the human visual system to spatial and temporal changes in defocus. During the experiments in that study, we found an unexpected illusion that happened at medium temporal frequencies on high contrast black-and-white edges: some colors, that were not in the stimulus, appeared on the black side of the edges. They looked like a flickering rainbow. We performed more experiments to test different hypotheses aiming at explaining the reason behind this phenomenon, and we found out that those effects were due to the longitudinal chromatic aberration of the eye, interacting with the defocus wave. Later, we improved the stimulus to maximize the chromatic effects generated, and to measure the refractive state of an eye. This chapter addresses the development of the technique and the first measurements in volunteer subjects.

The gold standard to assess the refractive error of an eye is subjective refraction[91,244]. This procedure is probably the most frequent procedure performed in eye care clinics. In fact, subjective refraction is performed on most patients, both to identify the best optical correction for each eye, and to provide a first approach to the general state of the eyes and the visual system.

Traditionally, objective refraction instruments (retinoscopes, autorefractors) are used to provide a first approximation to the patient's refraction, which has to be subsequently refined[91]. The subjective refraction procedure thus begins by adding more positive power, usually +1.00 diopter (D), to the starting point to induce myopic defocus, and then reducing said addition in steps of 0.25D until the best visual acuity is reached. This method, known as fogging, is used to relax the eye, reducing the impact of accommodation in the measurement. Other subjective refraction techniques, such as the duochrome test or Jackson's Cross Cylinders (JCC), can refine the result.

Different technologies have been used to support subjective refraction procedures. The most common, trial frames, manual phoropters, and digital phoropters, provide high correlations and non-significant differences[139].

The subjective refraction procedure usually takes more than 6 minutes[161] and can be much longer depending on the collaboration of the patient. The subjective nature of the subjective refraction implies deviations in the measurement result. The standard deviation across measurements performed by the same optometrist (the intraoptometrist variability) ranges between 0.20 and 0.32D[124,127,143–145]. The influence of the optometrist, determined by the standard deviation across measurements performed by different optometrists evaluating the same eye (the interoptometrist variability) has been reported to be as high as 0.38D[127,128,145,146,245,246].

In clinical practice, faster measurements imply increasing variability. New procedures and technologies have tried to displace this trade-off and provide faster measurements without affecting performance[161].

In an attempt to reduce the measurement time and facilitate both the task of the patient and the complexity of the procedure, many objective refraction technologies, that do not require subjective responses from the patient, have been improved throughout the years.

Autorefractors provide a direct measurement of the refractive error of the patient. Classic autorefractors project optical objects (typically dots or rings) onto the eye and obtain the refractive state of the eye from the analysis of the retinal image (typically the size or the blur of the image), using different technologies such as infrared lasers, LEDs, superluminescent diodes, Badal systems, CCD or CMOS cameras[123]. Many of them also incorporate fogging algorithms. Moreover, new technologies based on wavefront analysis have emerged over the years[25]. Several studies have reported very high repeatability of autorefractometers, with a standard deviation of repeated measurements ranging from ±0.12 to ±0.37D[124–127].

Other studies have reported significant differences in spherical equivalent between autorefractometers and subjective refraction. Thibos et al.[25] studied the precision of 33 different metrics derived from the wavefront aberration map of the eye, to predict the spherical equivalent of the refractive error. They found mean absolute differences on the spherical equivalent, compared with the subjective refraction, ranging from ±0.25 to ±0.48D, giving birth, in 2004, to wavefront autorefractometry, a discipline that has provided several autorefraction technologies over the years[125,127–133]. Modern autorefractometers provide mean absolute differences ranging from ±0.55 to ±0.24D, depending on the autorefractometer[129,134]. A recent review[135] analyzed four portable autorefractors and reported that QuickSee provides the lowest mean absolute difference (±0.21D)[136]. Many other studies have compared subjective refraction with different types of autorefractors, reporting similar differences[126,128,130–133]. To summarize, both classic autorefraction and wavefront-based autorefraction provide high repeatability, with wavefront autorefractors providing better predictions of the spherical component of the subjective refraction (mean absolute deviations between ±0.25 and ±0.50D). Other objective tools, such as deep-learning algorithms[137], have been used to predict the spherical refractive error from retinal fundus images, but their outcomes are still far from other objective techniques (±0.91D with respect to the subjective refraction).

Interestingly, the outcome of subjective refraction is better visually accepted than the outcome of autorefraction[245,247] with higher visual acuity reported with subjective refraction than with autorefraction[248,249].

Some recent developments advance toward self-refraction and unsupervised subjective refraction. Sheedy et al.[127] compared an automatic subjective refraction system, the Topcon BV-1000 with computerized forced-choice questions, autorefraction, and with traditional subjective refraction. The virtual subjective refraction[141] was proposed as a semi-automatic subjective refraction method that combines wavefront-based objective refraction providing a starting point, and an algorithm driving a virtual-reality system and processing the responses of the subject. The EYER method[140] combines a wavefront autorefractor and a phoropter to, based on the answers of the subjects to specific questions, change the lenses of a phoropter and obtain the refractive error subjectively. Leube et al.[152] tested an unsupervised self-refraction procedure based on the shift of a pair of Alvarez lenses to compensate for the spherical refractive error. Rotation of the lenses also allows the compensation of astigmatism. Wisse et al.[154] tested a web-based tool (different letter tests and algorithms) to measure the refractive error. These methods report mean absolute differences in subjective refraction between ±0.41 and ±0.21D. Furthermore, Elliot[244] suggested questionnaires based on patient satisfaction and preference[250]. The main inconvenience is that this procedure is time-consuming because it implies testing different corrections for several days until the patient feels satisfied with the prescription

As already mentioned**,** accommodation is an important issue in refractive error evaluation, common to objective and subjective refraction techniques, especially in young populations[130]. Different strategies aimed at reducing its impact. Even with the fogging method, traditionally used in subjective refraction, and later incorporated into certain objective methods, mild or higher hyperopias are often missed. Cycloplegic drugs can null the influence of accommodation, although they produce other unwanted effects such as pupil dilation, visual discomfort, or photophobia. Zadnik et al.[124] reported a higher standard deviation (lower repeatability) in cycloplegic subjective refraction versus non-cycloplegic subjective refraction (±0.48 vs ±0.32D). Additionally, Choong et al.[251] and Rauscher et al.[252] reported, in a population of 117 and 201 children, respectively, that cycloplegic autorefraction was more accurate than non-cycloplegic, which gives more myopic outcomes (~0.5D). Overcorrection of myopia or undercorrection of hyperopia, mainly provoked by accommodation, can produce asthenopia and headache[253]. Those symptoms could be eliminated with a better estimation, insensitive to accommodation, of the refractive error.

The current trend[161] is to direct the evaluation of the refractive error toward automatic unsupervised methods, that minimize: 1) miscommunications between the clinician and the patient; 2) the measurement variability; 3) the measurement time; 4) the influence of accommodation (without the need of cycloplegic drugs). Subjective methods are likely to achieve results that are closer to the traditional subjective refraction, which is nowadays still considered the universal gold standard in the evaluation of refractive error.

4.2. The Direct Subjective Refraction concept

The Direct Subjective Refraction (DSR), a new concept proposed in this study, is a subjective method to obtain the spherical equivalent of an eye, i.e., the optical power needed to compensate for the spherical refractive error. It is based on inducing rapid and periodic temporal changes in the optical power of an eye (Temporal Defocus Waves; TDWs) and therefore producing periodic temporal changes in the focus state of the retinal image while maintaining its position and magnification[254]. These fast periodic changes in defocus produce periodic changes in retinal blur and the visual perception of flicker in the image, which is minimum when the mean optical power of the TDW corresponds to the spherical equivalent of the subjective refraction of the eye. The flicker increases as the mean optical power of the TDW moves away from the spherical equivalent becoming more and more myopic or hyperopic.

In this method, the stimulus is made of different chromatic components, for example, blue and red monochromatic components and combinations of them. Due to the Longitudinal Chromatic Aberration (LCA) of the eye, each monochromatic component is focused at a different axial position relative to the retina. The TDW interacts with the LCA producing color distortions in the stimulus and differences in the flicker of the different chromatic components. These color distortions are minimum, again, when the mean optical power of the TDW matches the spherical equivalent of the eye. Interestingly, the color distortions are different on both sides of the focus.

The task of the observer in the DSR method is to minimize 1) the flicker in the stimulus and 2) the color distortions. Both perceptual effects are dynamic, concurrent, and very apparent to the observer. As a result, the two perceptual effects used in the minimization task reinforce each other to converge to a common focus, making the task easy for the observer. Around the focus, flicker and color distortions are image features perceptually stronger than the static blur commonly used to guide the traditional subjective refraction. In other words, the dual minimization task used in DSR is more sensitive than the one used in the traditional subjective refraction (blur reduction) and less affected by accommodation. In this study, we will demonstrate that the results obtained with the DSR method are more robust, precise, and direct (providing faster and more repeatable measurements) than those obtained with the traditional method.

4.2.1. Working principle

Figure 4.1 describes the working principle of DSR, based on the dynamic interactions between the LCA of the eye and the fast temporal variations of optical power induced by the TDW (Figures 4.1A, 4.1B, and 4.1C). The through-focus retinal images of the edges of a stimulus are very different across chromatic components due to LCA (as an example: red monochromatic edge through focus in Figure 4.1D; blue monochromatic edge in Figure 4.1E; magenta bi-chromatic edge -red plus blue- in Figure 4.1F). The periodic alternation in defocus generated by the TDW produces quick variations in blur that are perceived as periodic luminance changes, i.e., flicker. At a given defocus, the blur is different for each chromatic component, and the different spread of light produces energy unbalances, changing the color around the edges of the stimulus (Figures 4.1G and 4.1H). The observer subjectively selects their refraction by adjusting the mean value of the TDW (i.e., their refractive state) until those perceptual effects -flicker and color artifacts- are reduced to a minimum.

Six representative through-focus planes are considered in Figure 4.1, numbered 1 to 6, and shown as dashed lines in Figures 4.1A, 4.1B, and 4.1C. The TDW is represented by two bold dashed lines indicating the two planes of alternating focus. Figures 4.1A, 4.1B, and 4.1C represent three different refractive states in which the TDW has different mean optical powers with respect to the retina.

In Figure 4.1A, one of the alternating optical powers of the TDW corresponds to the blue focus of the eye (plane 2) -where the blue components of the stimulus are sharp-, and the other one places the stimulus in front of the retina (plane 1). In this situation, the best focus of the eye (in between the blue and the red foci) would lay behind the retina. This eye is, therefore, in a hyperopic refractive state. The alternation between planes 1 and 2 induced by the TDW produces: i) More average blur in red image components than in blue image components; ii) More flicker perception in red image components -where blur is suprathreshold in both planes 1 and 2- than in blue image components -were blur is subthreshold in plane 2 and small in plane 1-, and; iii) A reddish halo within the dark side of magenta edges, and blueish halo within the bright side (Figures 4.1F, 4.1G and 4.1H) in both planes 1 and 2. The reason is that in an edge between magenta and black, the red light is spread more than the blue light. On the dark side of the magenta edge, the additional red produces a reddish halo (Figure 4.1G, planes 1 and 2), and on the bright side, the missing red produces a blueish halo (Figure 4.1H, planes 1 and 2).

Figure 4.1C represents the opposite situation. It could represent the same eye, but with more average optical power in the TDW. One of the optical powers corresponds to the red focus (plane 5), and the other one projects the stimulus behind the retina (plane 6). Because the best focus of the eye would lay in front of the retina (between the blue and the red foci), this eye is in a myopic refractive state. In this other case, the observer experiences: i) More blur in blue than in red; ii) More flicker in blue than in red, and; iii) A blueish halo within the dark side of the magenta edge, and a reddish halo within the bright side (Figures 4.1G and 4.1H, planes 5 and 6).

Figure 4.1B shows the particular situation in which the eye is in focus (it could represent, again, the same eye). In this perfectly corrected eye is focused in between the blue focus -in front of the retina- and the red focus -behind the retina-. The two optical powers of the TDW correspond to planes 3 and 4, very close and at either side of the best retinal focus. The mean optical power of the TDW matches the retinal plane and therefore the eye represented is in an emmetropic state. Consequently: i) blue and red components have similar amounts of blur, ii) similar small flicker in blue and red components, and iii) blue and red light are barely spread and the difference is hardly noticeable. The color distortions in magenta edges disappear with the fast alternation because no color dominates the other.

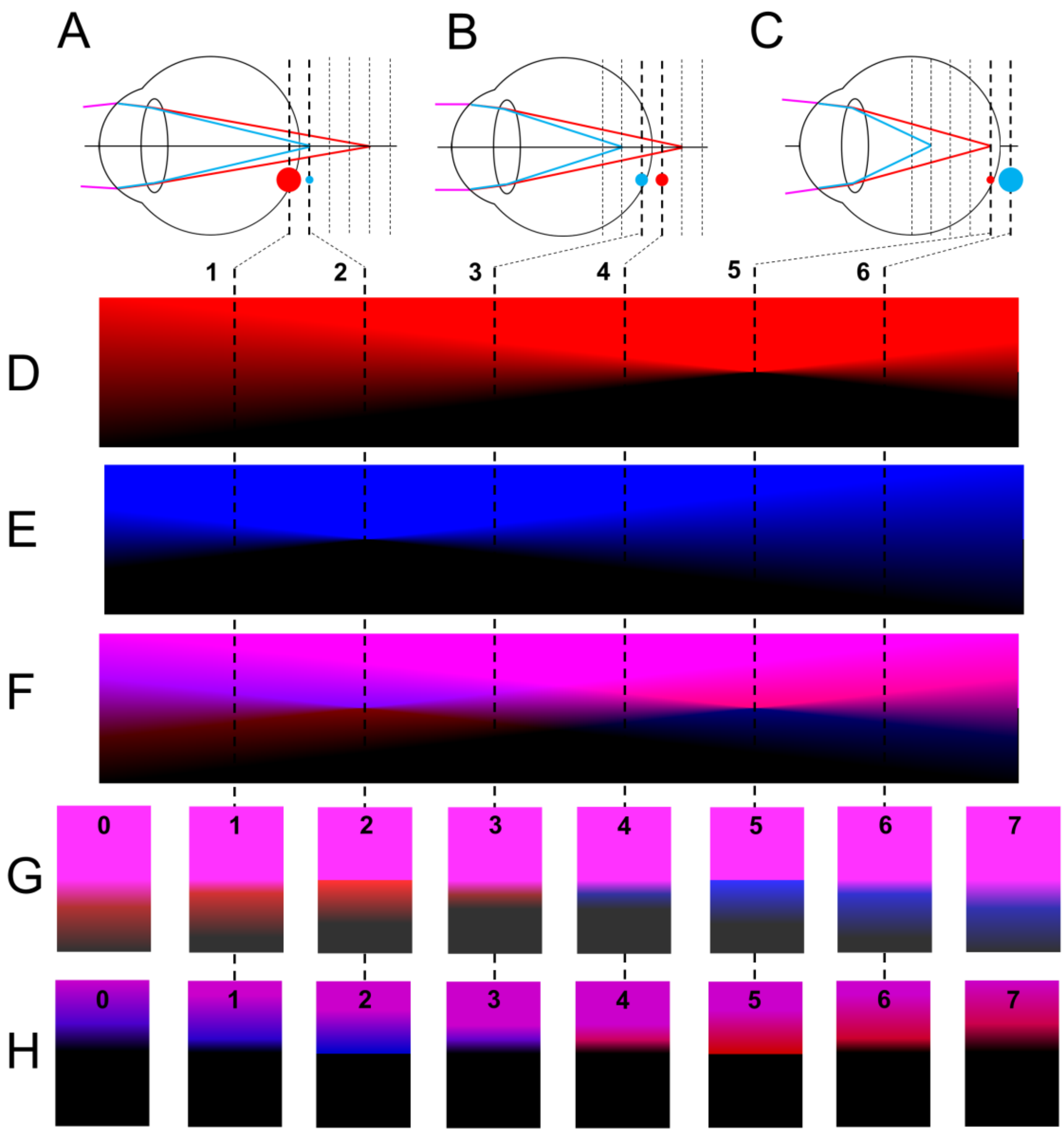

Figure 4.1. Working principle of the Direct Subjective Refraction. The perception of the stimulus depends on the mean optical power of the TDW, which changes the plane of focus in the retina. **A.** Schematic representation of an eye in a hyperopic state for a given mean value of the TDW. Six optical planes are represented with dashed lines (1 to 6). The two optical powers of the TDW are represented with bold dashed lines: one of them, plane 2, corresponds to the blue focus of the eye and the other one, plane 1, is defocused. **B.** Eye in an emmetropic state with respect to the TDW. It could be the same eye, but with more mean optical power in the TDW. The two optical powers of the TDW correspond to planes 3 and 4, very close and at either side of the retina, i.e., similarly defocused. **C.** Eye in a myopic state with respect to the TDW. It could be the same eye, but with even more mean optical power in the TDW. The two optical powers of the TDW correspond to planes 5, red focus of the eye, and 6, defocused. **D.** Representation of the through-focus blur, induced by defocus, for a red edge. Only plane 5 is in focus. **E.** Through-focus blur for a blue edge, with plane 2 in focus. **F.** Through-focus blur for a magenta edge (red plus blue). The different defocus in the blue and red components induce color distortions that are different on the hyperopic and myopic sides of the retina, and on the bright and dark sides of the edges. **G.** Images corresponding to planes 1 to 6 (and also to additional planes 0 and 7) of a magenta edge with high contrast and brightness, represent the vision of an eye not completely adapted to a bright display. The observers perceive color distortions on the dark side of the edges: reddish tint on the hyperopic side of the retina and blueish tint on the myopic side. **H.** Same images, but with lower contrast and brightness, corresponding to an eye not completely adapted to a dim display. Color distortions are now better perceived on the bright side of the edges: now the tint is blueish on the hyperopic side of the retina, and reddish on the myopic side. In this figure, for illustration purposes, the

amplitude of the TDW was only one-third of the chromatic difference of focus between the blue and the red wavelengths. However, the effect will be magnified by a larger amplitude, producing a bigger change in the image of the edges.

Blur, flicker, or color artifacts keep increasing for higher amounts of myopia (position 0) or hyperopia (position 7). In summary, when the eye is defocused in a TDW scheme, not only does the amount of blur increase as defocus increases but also, more noticeably, the amount of flicker and color distortions. Even a slight residual defocus results in an increase in these effects. The color distortion is different at both sides of the focus of the eye (blueish tint of black objects if myopic defocus, reddish if hyperopic; Figure 4.1G). Therefore, color artifacts not only indicate the amount of defocus, but also an unambiguous cue of the defocus sign. Furthermore, the fast change in defocus produced by the TDW also has a beneficial effect on distracting accommodation. The accommodation system is no longer able to follow the (quick) changes in optical power and the image cannot be focused. Therefore, the unstable nature of the image does not provide a cue for the activation of the accommodation mechanism.

This study proposes Direct Subjective Refraction as a new unsupervised subjective refraction method to overcome some of the limitations of the existing objective and subjective refraction methods. In this work, different stimuli have been designed and tested, in combination with the TDW (Figures 4.3 and 4.4), to maximize the perceptual effect and the sensitivity of the dual task (minimization of flicker and color distortions). In this method, the task is so straightforward for the patients that they can perform the minimization routine by themselves. The practitioner's intervention is reduced to explaining the perceptual task at the beginning of the test and supervising the result. This research also explores the limits of an unsupervised version of traditional subjective refraction, expected to result in a faster procedure, but inaccurate.

4.3. Methods

4.3.1. Optical System

The active part of the optical system is an optotunable lens, a lens able to change its optical power in response to an electric signal. The optotunable lens used in this study is based on liquid-membrane technology (EL-10-30-TC, Optotune, Dietikon, Switzerland), enabling precise changes in optical power up to 100 Hz[238,255]. The TDW is produced by a SimVis simultaneous vision simulator that uses a 4f-projection optical system to optically conjugate the optotunable lens with the pupil plane of the eye of the observer (Figure 4.2A). The distance from the eye pupil to the first lens is 45mm. The distance from the optotunable lens to the stimulus is 1 meter. The total distance from the real position of the eye to the screen is 1.25m.

The display was a combination of a digital light projector (DLP PJD7820HD, ViewSonic, USA) and a flat white reflecting screen. The distance from the projector to the screen was 0.4 meters, providing a sharp image with high luminance (500 cd/m^2 if set to white). The spectral emission is shown plotted in Figure 4.2D.

Custom routines were programmed in Matlab (Math-works Inc., Natick, USA) to operate the custom driver based on Arduino electronics (Arduino Nano 3; Arduino, Turin, Italy) controlling the optical power of the optotunable lens and implementing the TDW. Matlab, in combination with Psychtoolbox[241], was also used to design and present the stimuli and to perform the perceptual task.

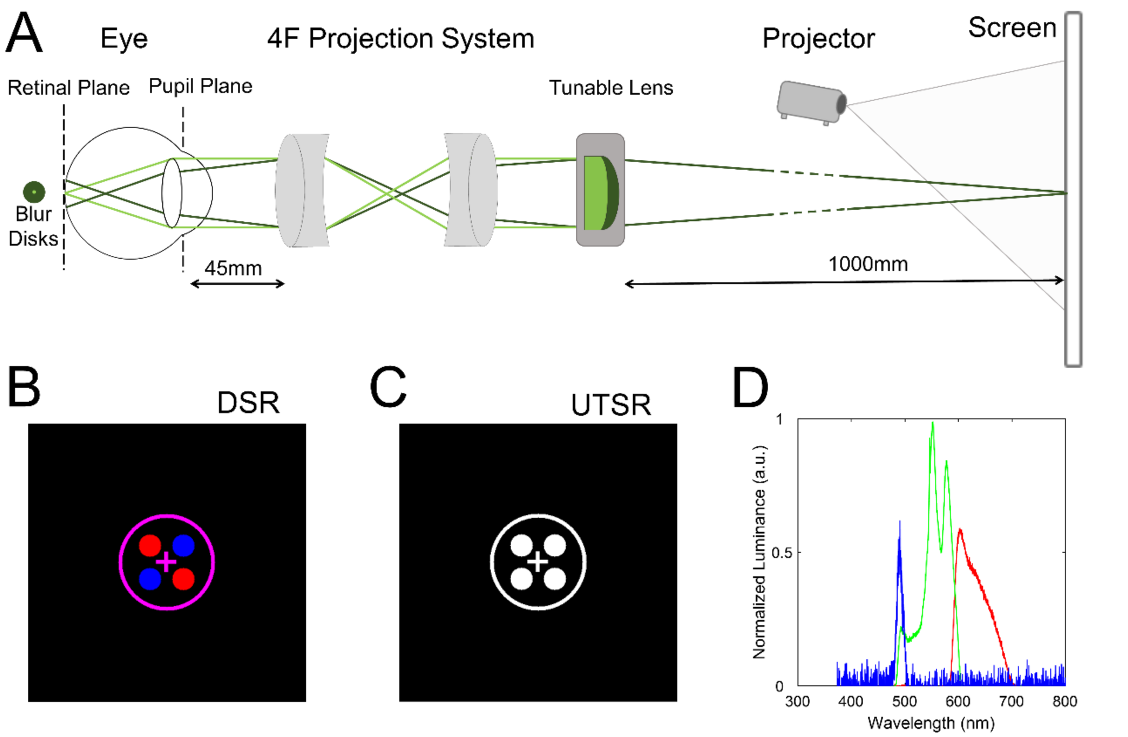

Figure 4.2. Setup of the study. A. Schematic representation of the optical system of the Direct Subjective Refraction. It shows how inducing optical powers with the optotunable lens changes the retinal blur. The 4f optical system projects the optotunable lens on the pupil plane of the eye. In most situations, the stimulus is defocused for the observer, producing a large blur disk on the retina (dark green). In the particular situation when the optotunable lens focuses the stimulus on the retina (light green), the blur disk is minimum. DSR uses fast variations in optical power. With this configuration, the optical power of the optotunable lens produces defocus blur in the image, without changing the position or the magnification. The sizes and distances displayed are not proportional to the real optical system. **B.** Stimulus used to perform the DSR task. **C.** Stimulus used to perform UTSR task. **D.** Spectral emission of the light source (DLP) for blue, green, and red components.

4.3.2. Temporal Defocus Wave (TDW)

We performed pilot experiments on experienced subjects to refine the design of the stimuli, and to find the parameters of the TDW that maximized the perceived flicker and the intensity of the chromatic distortions outside the best focus. The stimulus is described in the Experiments section (4.3.4 and 4.3.5) and is shown in Figure 4.2B. The temporal frequency of the TDW was set to 15 Hz, corresponding to the maximum perceptual sensitivity to defocus flicker[256]. The peak-to-peak amplitude of the TDW was set to 0.50D producing a good balance between measurement sensitivity and precision.

With those optimal parameters of the TDW, flicker and chromatic distortions are almost negligible in focus (if the TDW oscillates between planes 3 and 4 in Figure 4.1), but very apparent out of focus. With smaller amplitudes, the two images of each pair are very similar, and the subject has difficulties perceiving flicker even outside the best focus. With larger amplitudes, the two images are very different in luminance and flicker is very noticeable, even in focus.

4.3.3. Subjects

Twenty-five subjects, 15 females and 10 males, between the ages of 48 and 23 (29.9±7.3 on average), participated in the study. All participated in Experiment 1, and five of them also participated in Experiment 2. The average age of the subjects that participated in Experiment 2 was 29.2±8.8 years. No color abnormalities were found, tested with

Ishihara chromatic test. All subjects had normal visual acuity (VA; ≤0.0 logMAR) wearing their usual correction. Experiments were performed with the room lights switched off.

Objective refraction was measured using an ARK-1 autorefractometer (ARK1, Nidek, Gamagori, Japan). The refractive error (in spherical equivalent) ranged from -6.75 to +1.50D (-1.62±2.32D on average) with a distribution of eight emmetropes (±0.50D or refractive error), fourteen myopes (<-0.50D) and three hyperopes (>+0.50D). Subjects were free to accommodate, except in Experiment 2 where the accommodation was paralyzed using cycloplegic drugs.

A bite bar provided centration stability during the experiments. Fixation was provided by the stimuli. Only the left eye was measured. The right eye was occluded with an eyepatch.

The experimental protocols were approved by the Spanish National Research Council (CSIC) Bioethical Committee and were in compliance with the Declaration of Helsinki. Written informed consent was provided by all subjects.

4.3.4. Experiment 1

Figure 4.2B shows the stimulus used to evaluate DSR. This stimulus was designed to intensify the perception of flicker and chromatic artifacts at both sides of the focus. It comprises four circles arranged like the corners of a square, alternatively red (RGB coordinates [1 0 0]) and blue ([0 0 1]), on a black background ([0 0 0]). The diameter of the circles is 1º. They are surrounded by a thin magenta ring ([1 0 1]; 4.7º of visual angle). The stimulus also contains a magenta cross in the center, for fixation.

The interaction between the DSR stimulus, the TDW, and the LCA of the eye, produces flicker and chromatic distortions depending on the mean optical power of the TDW. The flicker of the blue dots is preponderant when the mean power of the TDW changes the refractive state of the eye to myopia, while the flicker of red dots becomes more visible in hyperopia. In emmetropia, flicker is minimum and similar to red and blue dots. In the DSR stimulus, chromatic artifacts appear in the magenta components (the fixation cross and the surrounding ring), which are shifted to blue in myopia and red in hyperopia.

The DSR task consisted in simultaneously minimizing the two concurrent effects in the image induced by the TDW: the flicker and the chromatic distortions. Subjects increased or decreased the mean power of the TDW using a keyboard, in coarse or fine steps of 0.25D or 0.10D, respectively.

To compare with the DSR, subjects also performed an Unsupervised Traditional Subjective Refraction (UTSR) task, a version of the Traditional Subjective Refraction (TSR) used in clinical practice. The stimuli designed for UTSR (Figure 4.2C; UTSR) is a black-and-white version of DSR (Figure 4.2B), in which magenta, blue and red colors are replaced with white ([1 1 1]). The task of the subject was to minimize the blur (defocus) of the stimulus, changing the optical power of the optotunable lens via keyboard (same steps as in DSR) until the stimulus was perceived sharp. In this case, the explanation of the task did not require a video presentation and therefore it was faster than in DSR.

The explanation preceding the experiment took about 1 minute for the DSR task and 0.5 minutes for the UTSR task. The time elapsed between the explanation and the conclusion of the unsupervised tasks was recorded in both methods.

Subjects wore their current prescription throughout the experiments (delivered by spectacles or contact lenses). Both in DSR and UTSR, the spherical equivalent was estimated averaging across 10 repetitions, each one following a staircase procedure with a different starting point: 5 of them myopic, from -0.20D to -1.00D, and the other 5 hyperopic, from +0.20D to +1.00D. The precision of the method was estimated as the standard deviation across repetitions. As subjects wore their spectacles or contact lenses, both tasks measure residual refraction, i.e., deviations regarding their current correction. But the results, obtained from different myopic and hyperopic starting points, are representative of arbitrary refractive errors. After the measurements, visual acuity was checked with the spherical equivalent obtained with the DSR task.

4.3.5. Experiment 2

In Experiment 2, five subjects performed the same procedure and using the same experimental setup as in Experiment 1, but with the accommodative response paralyzed after the instillation of cycloplegic drugs (tropicamide 1%, three drops instilled in intervals of 10 minutes each). Experiment 2 was performed after Experiment 1, beginning 10 minutes after the instillation of the third dose (around 45 min after Experiment 1).

Statistical Analysis

To analyze the statistical significance of the differences between the results of the different experiments, we used Wilcoxon signed-rank tests to compare the results of Experiment 1 vs 2. Additionally, to compare groups with different refractive errors (myopes, hyperopes, and emmetropes), we also used a Mann-Whitney U-test for different sample sizes.

To evaluate the agreement between DSR and UTSR tasks versus the TSR, we used Bland-Altman plots. The statistical level to achieve statistical significance was set to 5% (p=0.05). For each subject, we considered each repetition of the DSR and UTSR task as a different measurement of residual refraction. Additionally, paired t-tests and correlation coefficients were also used to compare myopic and hyperopic starting points in the DSR and UTSR tasks. Matlab (Math-works Inc., Natick, USA) was used to perform the analysis.

4.4. Results

Figure 4.3 depicts a few representative examples of the measurements performed. Each panel shows the progress along trials (staircase) of every repetition for subject 1, Experiments 1 and 2, and both tasks, DSR and UTSR. Red lines represent hyperopic starting points and blue lines myopic starting points. The X-axis represents the trial number. The Y-axis represents the mean optical power of the TDW, in diopters, for the Direct Subjective Refraction (DSR; examples in panels A and C) and the optical power, for the Unsupervised Traditional Subjective Refraction (UTSR; example in panels B and D). Subjects wore their usual correction while performing the experiments (spectacles or contact lenses) and therefore the result of each repetition (red or blue dots), or the average (solid black line in the center of the gray band indicating the standard deviation), represent the residual refraction over their usual correction.

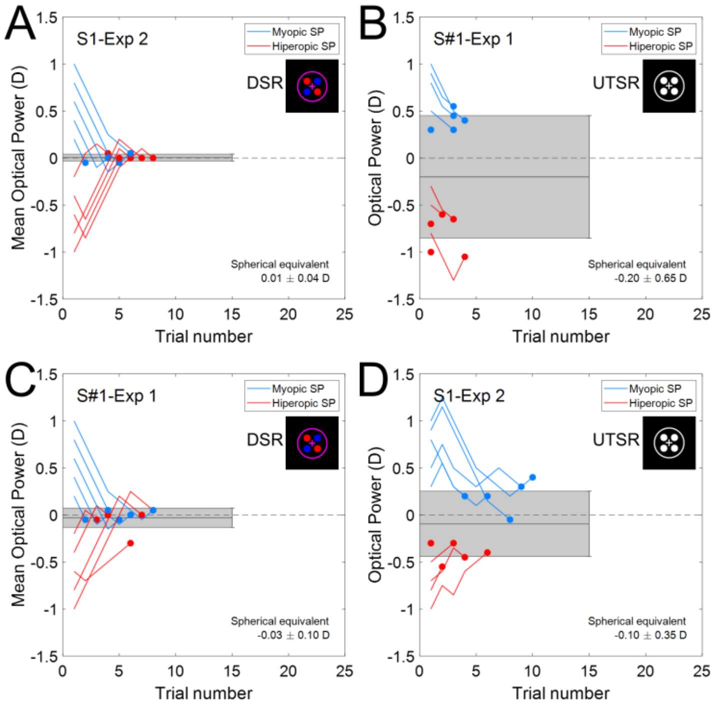

Figure 4.3. Progress of DSR and UTSR tasks one subject (S1) and Experiments 1 and 2. Each panel shows the progress of a subject while performing a visual task (DSR or UTSR) to obtain the subjective refraction. Blue lines represent repetitions with myopic starting points and red lines with hyperopic starting points. The filled dot at the end of each line indicates the residual refraction for that repetition. The gray bar indicates the mean and the standard deviation of the residual refraction across repetitions. These values are indicated in the left-bottom corner of each panel. A miniature of the stimulus used in each example is shown in the upper-right corner. **A.** Evolution of the mean optical power of the TDW (in D) versus the trial number for S1 performing the DSR task in Experiment 1. **B.** Optical power (in D) versus the trial number for Experiment 1 while performing the UTSR task. **C.** DSR task in Experiment 2 (paralyzed accommodation). **D.** UTSR task for Experiment 2.

Figure 4.3A illustrates the DSR task for subject S1 performed in Experiment 1. All repetitions converge to the best spherical equivalent with a standard deviation of ±0.10D. This value is lower than the finest optical power step available in eyecare clinics (±0.25D). Figure 4.3B shows the corresponding UTSR task for the same subject and experiment. In this case, there is no convergence, and the standard deviation is much higher ±0.65D, indicating that the unsupervised blur-detection task is dramatically affected by accommodation: hyperopic defocus (red lines) can be compensated with accommodation and the subject (25 years old) perceives the stimulus instantly sharp. Due to the depth of focus of the eye, myopic defocus is also very soon perceived as sharp. Figure 4.3C shows the results of the DSR task for the same subject (S1) for Experiment 2 (cycloplegic drugs). Paralyzing the accommodation results in an even lower standard deviation ±0.04D) with the same spherical equivalent (-0.03D in Experiment 2 vs 0.01D in Experiment 1). This suggests that, at least in this subject, accommodation was barely influencing the outcome of the DSR task in Experiment 1 (where the accommodation was free). Figure 4.3D shows the results for the UTSR task for S1 and accommodation paralyzed. Now, hyperopic defocus, which was accommodated when accommodation was free (Figure 4.3B), cannot be compensated. Therefore, the standard deviation of UTSR with cycloplegic drugs is much lower (±0.35D). Further analysis will show the result for all the subjects measured with and without paralyzed accommodation.

The convergence of the subject to a unique result in the DSR task, regardless of the starting point for each repetition (myopic and hyperopic), is consistent across subjects and experiments and proves that the accommodative response, although functional, is not elicited during the DSR task. The quick and abrupt changes in optical power produced by the TDW seem to unfasten the accommodation mechanism from the stimulus. The DSR visual task does not require paying attention to blur and concentrates the attention of the patient on luminance flicker and chromatic distortions. Besides, the task takes place in presence of a dynamic baseline blur that cannot be eliminated, and that seems to make accommodation unproductive. On the contrary, as already mentioned and shown in the examples of Figures 4.3B and 4.3D, which are representative of the responses of all subjects, the UTSR task is severely affected by accommodation.

Figure 4.4 shows the spherical equivalent obtained from the DSR (red) and the UTSR (blue) tasks, for all subjects in Experiment 1 (free accommodation) and Experiment 2 (cycloplegia). The position of the bar indicates the mean across repetitions and the length, with one standard deviation at each side of the mean. The average spherical equivalent obtained with the DSR task, across subjects shows a myopic shift of -0.33D. The DSR method detects significant residual refractions in 80% of the subjects (measurements significantly different from zero, the usual correction of the subjects, using a 0.9 significance level, i.e., red bars not touching the zero). UTSR average spherical equivalent has a lower myopic shift (-0.15D) and captures significant residual refractions in only 12% of the subjects.

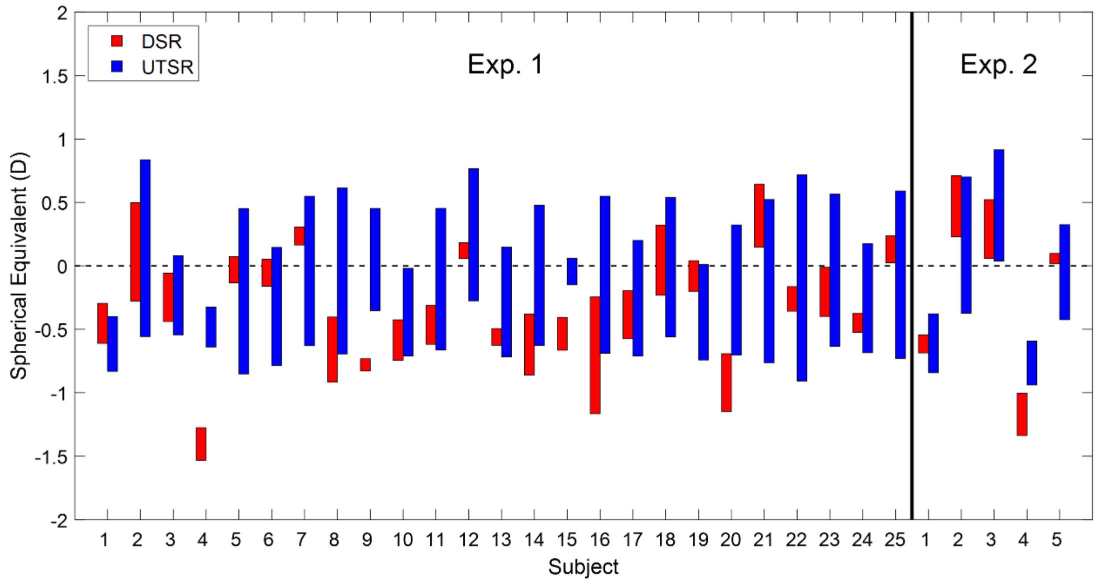

Figure 4.4. Spherical equivalent and standard deviation for all subjects and experiments. Each bar is centered on the spherical equivalent and its length represents twice the standard deviation. Red bars correspond to the DSR task and blue bars to the UTSR task.

Analyzing separately the results of DSR from the two experiments, the average spherical and average standard deviation equivalent across subjects are -0.33±0.17D for Experiment 1 and -0.19D±0.15D for Experiment 2. Interestingly, when accommodation is paralyzed (Experiment 2), the average absolute residual error for UTSR (0.41D) is comparable to that found in DSR (0.36D on average across experiments, 0.52D in Experiment 2). For DSR measurements, a Wilcoxon signed-rank test for the same subjects in Experiment 1 vs 2 reports that the differences in mean spherical equivalent were not statistically significant (*p*>.05), indicating that, in our sample, paralyzing the accommodation does not induce significant differences.

Figure 4.5 directly plots the standard deviation across repetitions for each subject and experiment, providing a closer look at the repeatability of the DSR and UTSR tasks. The horizontal dashed lines indicate the average standard deviation across subjects. To compare with the literature, we also plotted the intraoptometrist variability (averaged from[124,127,143]) with a dark green line and the interoptometrist variability (averaged from[125,127,128,146,245,246]) with a light green line. On average, the standard deviation for the DSR task (±0.17D) is 64% lower than that of the UTSR task (±0.47D), 57% lower than the traditional interoptometrist variability (±0.39D), and 39% lower than the intraoptometrist variability (±0.28D). Across the four experiments, the standard deviation for the DSR task is lower than that for the UTSR task in 96.7% of the subjects, lower than the interoptometrist variability in 93.3% of the subjects, and lower than the intraoptometrist variability in 90% of the subjects. These results evidence the higher repeatability (i.e., precision) of the DSR task compared to the corresponding UTSR task in the same conditions and compared to the traditional subjective refraction methods. Minimizing flicker and chromatic distortions happens to be more precise than judging blur.

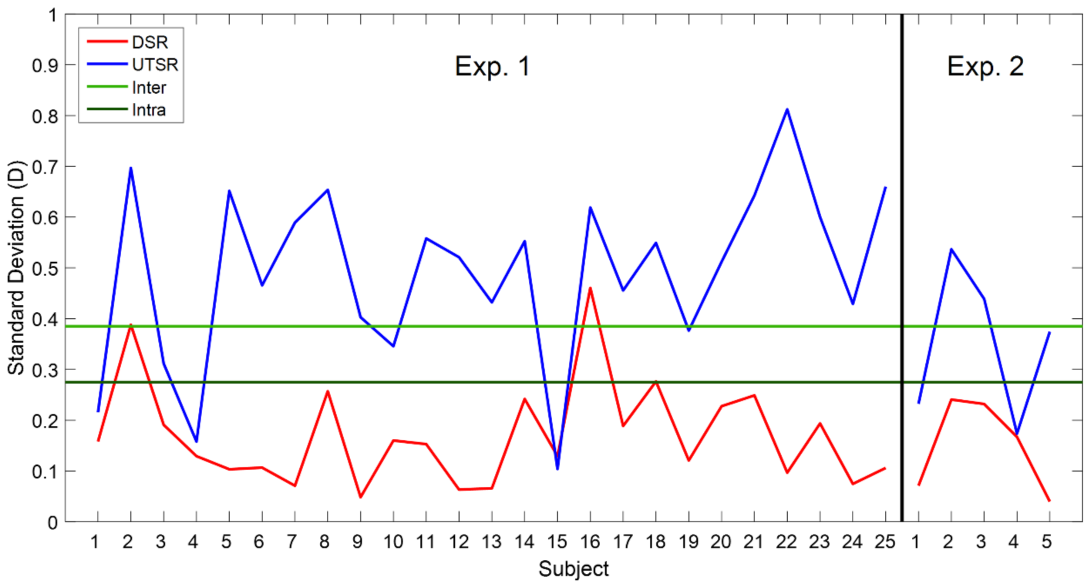

Figure 4.5. The standard deviation for all subjects and experiments. The standard deviation for the DSR (red curve) and UTSR (blue curve). The horizontal dashed red and blue lines indicate the average standard deviations across subjects for the DSR task and the UTSR task, respectively. The horizontal light green line indicates the interoptometrist variability (traditional subjective refraction) and the dark green light the intraoptometrist variability, both extracted from the literature.

To compare the results obtained with the DSR task and the UTSR task with the Traditional Subjective Refraction (TSR), we performed different Bland-Altman analyses. Figure 4.6A shows the Bland-Altman plot for the DSR versus the TSR, pooling the data of all repetitions for Experiment 1 (non-cycloplegic subjects). We found a strong correlation (r=.99; p<.05) and an offset of -0.33D. Figure 4.6B shows the corresponding plot for UTSR (r=.98; p<.05). For UTSR we found similar correlations, and a lower offset (-0.15D), but these results could be artifactual. As we already know from Figures 4.3B and 4.3D, the result of each UTSR repetition is strongly affected by the starting point. Since the set of starting points is uniformly distributed within the ±1D range at both sides of the TSR of the subject, the average UTSR outcome could be artificially determined by the average of all starting points and therefore matching the TSR. To explore this potential effect, we performed additional Bland-Altman analyses with subsets of samples on the myopic and hyperopic sides. Figures 4.6C and 4.6D correspond to starting points within the +0.8 to +1.0D range (maximum myopia; DSR and UTSR), and Figures 4.6E and 4.6F to starting points within the -1.0 to -0.8D range (maximum hyperopia; DSR and UTSR). The correlation coefficients are high in all cases (r=.99, p<.05). However, while the DSR offset only changes 0.14D from myopia to hyperopia, the UTSR offset changes as much as 1.23D. The superimposed Limits of Agreement (LOAs, 95% Confidence Interval) along the interval of starting points for DSR are -1.19 to +0.59D (difference 1.78D) and for UTSR -1.53 to +1.20D (difference 2.73D).

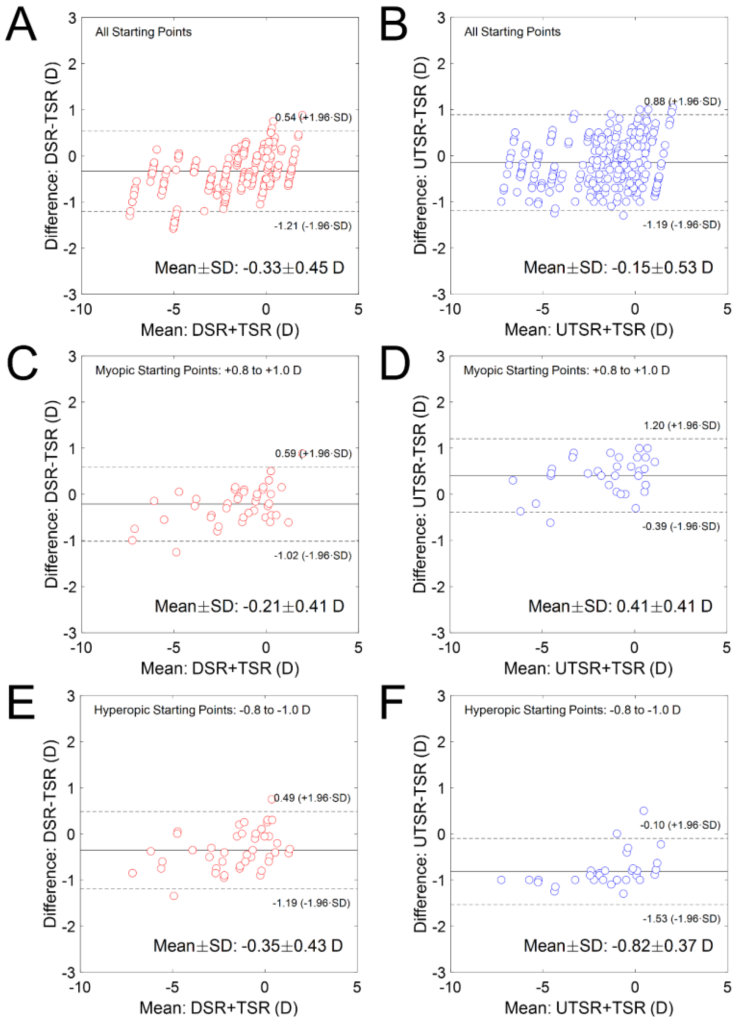

Figure 4.6. Bland-Altman analysis for Experiment 1. Each panel shows a Bland-Altman plot, indicating the Limits of Agreement (LOAs, 95% Confidence Interval), mean, and standard deviation of the sample. **A.** Plot comparing DSR and TSR for all starting points. **B.** Plot comparing UTSR and TSR for all starting points. **C.** Plot comparing DSR and TSR only for highly myopic starting points (+0.8 to +1.0D). **D.** Plot comparing UTSR and TSR only for highly myopic starting points (+0.8 to +1.0D). **E.** Plot comparing DSR and TSR only for highly hyperopic starting points (-1.0 to -0.8D). **F.** Plot comparing UTSR and TSR only for highly hyperopic starting points (-1.0 to -0.8D).

Removing the offset (-0.33D) between DSR and TSR provides a comparison closer to the final implementation of the technique: a similar analysis to Figure 4.6A, averaging across repetitions and compensating the offset, provides a standard deviation in the residual refraction of ±0.45D and LOAs of ±0.87D. But the variabilities across subjects and between DSR and TSR reported in this study (standard deviations and LOAs) are not only attributable to variability and disparities in the DSR but also include all sources of residual refractive error for TSR (used as a baseline): interoptometrist variability, tolerances of glasses and contact lenses, under or overcorrections in the subjects, refraction changes with time, etc. However, the comparison between DSR and UTSR confirms the enormous dependence of the UTSR results on the starting point, due to the well-known detrimental effect of accommodation (in the absence of fogging strategies), which was free and fully functional during Experiment 1 (except for two subjects, S1 and S19, that were partially functional due to presbyopia).

The DSR refraction provided higher or similar values of visual acuity in all the subjects than the usual refraction of the patients (TSR refraction), but it was not significantly different (paired t-test p>.05).

The spherical equivalent obtained from the TSR and the objective refraction are strongly correlated, and not statistically different (paired t-test p>.05). Bland-Altman analysis of the objective refraction compared to the TSR reports a slightly positive deviation of +0.12D and a mean absolute difference of ±0.54D. The LOAs are -0.93 to +1.17D (difference of 2.1D).

Figure 4.7A explores the effect of accommodation further. The results of the DSR task for all hyperopic starting points (average of all hyperopic repetitions) are directly plotted against the results for all myopic starting points (average of all myopic repetitions), both for DSR (each red symbol indicates a subject) and UTSR (blue symbols). For DSR, the correlation between hyperopic and myopic starting points is very high (r=.94, p<.05) and there is a small but significant statistical difference between them (0.08D on average; paired t-test p<.05). On average, the residual refraction and the standard deviation obtained with myopic starting points is -0.27±0.15D and with hyperopic starting points is -0.35±0.14D. The similarity of the results obtained with hyperopic and myopic starting points with the DSR task demonstrates that this task is barely affected by accommodation and that the method is very precise both for small amounts of myopia and hyperopia. In contrast, for the UTSR method, the correlation is low (r=.03, p>.05) between myopic and hyperopic starting points, which provide radically different results (0.17±0.23D and -0.47D±0.30D, an average difference of 0.47D, paired t-test p<.05). As expected, the unsupervised UTSR method, consisting of a blur-detection task without fogging, with a comparable stimulus, and in the same setup, is severely affected by accommodation, which not only affects repeatability, but also the final spherical equivalent measured, especially in hyperopic patients.

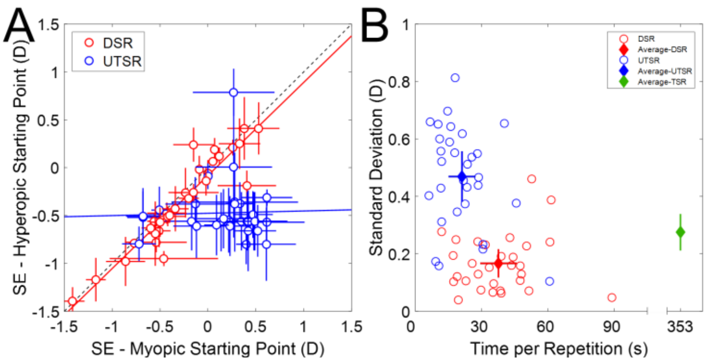

Figure 4.7. Comparison between DSR and UTSR tasks. A. Analysis of myopic and hyperopic starting points for DSR and UTSR. Spherical equivalent obtained from the average of all hyperopic starting points versus the spherical equivalent obtained from the average of all myopic starting points for DSR (red) and UTSR (blue) tasks and all experiments. The error bars indicate the standard deviation across repetitions. **B. Precision and time to perform the tasks.** Standard deviation across repetitions vs the time per repetition for DSR (red), UTSR (blue), and TSR. For TSR, the standard deviation is the intraoptometrist error and the average time is extracted from the literature. The filled diamonds indicate the average across subjects.

Experiment 2 provides additional information about the effect of accommodation. Five subjects carried out the experimental session of Experiment 2 (including the DSR and the UTSR tasks), but under the effect of cycloplegic drugs, paralyzing their accommodation. Considering the low number of subjects, the correlation between Experiments 1 and 2 (in spherical equivalent) was very high for DSR (r=.92, p<.05), but low and not significant for UTSR (r=.74, p>0.05). The slope (ideally 1) was 1.05 for DSR and 1.33 for UTSR). Interestingly, cyclopegia produced a constant shift (y-intercept) of 0.23D in the DSR results, similar and opposite to the average spherical equivalent reported in Experiment 1. The standard deviation was lower for Experiment 2 than for Experiment 1, both for UTSR (on average ±0.35 vs ±0.41D), and DSR (±0.19 vs ±0.15D), but not significant (paired t-tests p>.05 in both cases).

The ideal method to perform subjective refraction would provide a good balance between measurement time and variability. Figure 4.7B shows a scatter plot of the standard deviation in the measurement versus the average time per repetition for all subjects and experiments. We observe two clear clusters: the results for UTSR -blue open circles- have extremely low measurement times but high standard deviations, while the results for DSR -red open circles- have intermediate measurement times and low standard deviations. DSR is more precise than the TSR (intra-optometrist standard deviation ±0.28D±0.06[124,127,143–145]) and, of course, the UTSR. On average, the UTSR task takes 21±12 seconds per repetition with an average standard deviation of ±0.47±0.18D -solid blue diamond- and the DSR task takes 38±16 seconds per repetition with a standard deviation of ±0.17±0.10D -solid red diamond-. The DSR (also the UTSR) is much faster than the TSR (green diamond), which takes around 350 seconds (almost 6 minutes) according to previous studies[123,139–142]. However, the DSR method only provides the spherical equivalent of the refraction while the TSR provides a complete prescription (sphere and astigmatism) in both eyes. A fairer comparison of times should include the measurement of the spherical equivalent and astigmatism using the DSR method.

Finally, we investigated if the refractive error of the subject influences the DSR method. We divided the subjects into three groups, based on their current correction: hyperopes (>+0.50D; 3 subjects), myopes (<-0.50D; 14 subjects), and emmetropes (±0.50 D; 8 subjects). The results of a Wilcoxon rank-sum test do not show statistically significant differences between the three groups (p>0.05 in all comparisons). Therefore, in our groups of subjects, the refractive error is a statistical variable that does not influence the results.

4.5. Discussion

Direct Subjective Refraction

Subjective refraction is a ubiquitous procedure in eye care clinics. Despite being cumbersome and time-consuming on some occasions, it has not advanced much in decades. Some technologies such as automated phoropters have made the procedure easier but have not improved significantly the methodology[161]. Objective refractors, as wavefront autorefractors, now provide good approximations to subjective refraction but have not been able to replace it[248,249].

Subjective visual tasks are inherently slow, they entail a large series of trials, each one requiring a perceptual judgment from the observer (blur detection, blur preference, or letter identification in the case of subjective refraction) and a decision by the practitioner. But the situation is worse in subjective refraction than in other visual tasks. Traditional Subjective Refraction (TSR) begins by displacing the starting point far away from the best estimation available, usually provided by objective refraction (or sometimes by a lensometer), to the myopic side. This long detour in the through-focus trajectory, called fogging, is inefficient in terms of trials, but allows to deal with accommodation, and also provides the direction of focus. An ideal method to measure the subjective refraction would provide a shortcut toward the final spherical equivalent of the patient, using the lowest number of perceptual judgments: only a few steps separating the patient's subjective focus from the one measured objectively.

In this study we have presented the Direct Subjective Refraction (DSR), novel technology and methodology to measure the spherical equivalent of the refractive error of an eye, that disentangles, to a large extent, the accommodation mechanism, and that provides the patient with a visual hint of the direction of focus. The starting point can be the best estimation provided by objective refraction, and the spherical equivalent can be found directly. The number of trials (perceptual judgments) is reduced, and each one is straightforward and not supervised, producing faster measurement times than the TSR (Figure 4.7B). The DSR task is direct in the sense that color provides an unambiguous cue for the direction of the next step in the staircase (color distortions are different on both sides of the retina: blueish on the myopic side, and reddish on the hyperopic side).

In the last steps of the TSR, the practitioner checks if power changes of ±0.25D improve the visual acuity or visual comfort, sometimes using colored backgrounds (such as the duochrome test). These final checks inspired the development of the DSR method. The DSR performs 15 of those optical power changes per second, during the duration of the measurement and in every step of the subjective staircase leading to the spherical equivalent. Besides, 15 Hz is a frequency providing maximum temporal sensitivity to flicker[256], and therefore optimal for the task, although out of reach for the accommodative system. Hence, DSR provides a much stronger perceptual cue (in fact two concurrent and reinforcing signals: flicker and color) than TSR and is isolated from accommodation (because blur, the main clue for the accommodative system is no longer involved in the task), allowing straightforward measurements for the patients without requiring the guidance of the clinician. Our results show that the DSR method provides a precise, accurate, and fast estimation of the spherical equivalent of subjective refraction.

To put the results of the DSR task in the appropriate context, we have confronted them with comparable data of TSR obtained from the literature, and with the UTSR (Unsupervised Traditional Subjective Refraction) task. UTSR is a quick version of TSR, also depending on blur judgments but unsupervised and without fogging techniques. UTSR can also be considered a black-and-white and static version of the DSR. In this study, TSR was the current prescription for the subjects.

As seen in Figures 4.3-5, UTSR has more variability in the spherical equivalent (standard deviation ±0.47D) than TSR (±0.28D). At the same time, with DSR we found (Figure 4.5A) subclinical variability across repetitions in the spherical equivalent (±0.17D) and an average offset -0.33D compared to the correction worn by the subjects. This offset, although small, is clinically relevant. However, it has minor importance because it represents a systematic shift in the measurements (as discussed below) that could ultimately be compensated with a correction factor.

Accommodation and the Direct Subjective Refraction method
Accommodation is a potential cause of variability and systematic shifts during any subjective refraction technique (also during objective refraction). To study the effect of accommodation in the UTSR and DSR tasks, we included different starting points in the different repetitions, simulating different amounts of myopia or hyperopia in the same subject. We found that UTSR is undoubtedly affected by dynamic accommodation. In contrast to the TSR procedures used in clinics, that implement different strategies to reduce the impact of accommodation and reach the center of the depth of focus interval, UTSR is not protected against accommodation and results in important variabilities due to offsets that depend on the starting point: between +0.41D if the starting point is myopic, and -0.82D if hyperopic (Figure 4.6). Hyperopic starting points can be accommodated (red points in Figure 4.3A and Figure 4.3C), bringing the image into focus and finishing the staircase prematurely, leaving a negative offset (underestimating the correction). Similarly, depth of focus produces positive shifts in myopic defocus

(overestimating the correction) because subjects judge the image sharply before reaching the maximum optical quality and stop the staircase fractions of a diopter in front of the best focus (blue points in Figure 4.3B and Figure 4.3D). A direct comparison of the different starting points simulating myopia or hyperopia (Figure 4.6, Figure 4.7A) reinforces the finding that DSR is unaffected by the accommodative response, which spoils the UTSR measurements.

As seen in the examples in Figure 4.3, the DSR task forces the subject to reach the best focus and the staircases oscillate on both sides of it, removing the positive offset associated with myopic starting points. Figure 4.7A suggests that, at the same time, the accommodation mechanism is to a large extent deactivated during the DSR measurements. Defocus is present in the stimulus during DSR, as in UTSR, and is certainly perceived by the subject, but it is not part of the DSR task. The accommodation of the eye remains fixed because the fast change induced by the TDW prevents its activation. Other studies have shown that accommodation varies as much as 0.5D with flickering light at relevant frequencies for this study (between 10 and 20 Hz) in monochromatic stimuli[257–259] and chromatic stimuli[260]. However, there are substantial differences in the methodologies of those studies. On the one side, the task of the subjects was to fixate the stimulus and therefore elicit on purpose the accommodation response. In the DSR method, flicker is the main cue and accommodation should not be elicited. On the other hand, these studies used stimuli flickering in luminance, not in defocus. Walsh et al.[234] tested the threshold to defocus changes, but mechanical limitations only allowed temporal frequencies up to 4Hz and they did not find any influence of accommodation. The fast defocus alternation in the image does not provide a fixed reference to focus and does not elicit accommodation. Nevertheless, more research on the effect of accommodation for flickering defocus stimulus should be addressed.

Offset in the outcome of the Direct Subjective Refraction method

However, the small offset found could still be attributed to a small remaining residual accommodation (tonic accommodation). Being stable and largely unaffected by the stimulus, we could refer to this accommodative state as the ‘resting position’ of the eye, in a ‘dark focus’ of ‘tonic accommodation’ closer than infinity, previously reported in conditions where the accommodation is lost, for example in night myopia[9,261,262].

Experiment 2 corroborated these findings. Results before and after cycloplegia provided insignificant correlations with UTSR (and slope 1.33) but were highly correlated for DSR (and with slope 1.05). Paralyzing accommodation also had the effect of reducing the measurement variability to its lowest value (±0.15D on average; in DSR). Although promising, these findings should be confirmed in a higher number of patients.

Accommodation to the stimulus can be discarded as an explanation for the offset found in DSR, but several other reasons could provide a plausible explanation. For example, DSR contains the implicit assumption that the spherical equivalent lies in the intermediate position (in diopters) between the red focus and the blue focus (Figure 4.1). Therefore, changes in the spectral composition of the stimulus (spectral width and position of the red and blue peaks) could shift the spherical equivalent measured with DSR. Besides, the relationship between wavelength and focus position in diopters (the LCA curve) is not lineal[42,263], and the monochromatic wavelength-in-focus for subjective refraction changes with the subject[264], predicting the polychromatic spherical equivalent from monochromatic measurements difficult to model[265]. Furthermore, even the gold standard, the polychromatic spherical equivalent measured with TSR, can change with the color temperature of the white light used. Moreover, the variability of any subjective measurement (TSR, DSR, UTSR) is extremely related to the subjective depth of focus, not only for optical reasons (aberrations) but for neuronal reasons[266].

Instrument myopia (an effect also related to accommodation) or pupil size effects due to relatively low ambient light levels during the measurements, such as potential focus shifts due to spherical aberration or depth of focus increments, could also be blamed for this small but significant offset between DSR and TSR. The magnitude of most of the mentioned effects, separately, could be higher than the offset found in our measurements[264–266]. The calibration of the instrument and the fidelity of the TDW to the nominal power, as well as the distances involved in the optical setup, were checked before the measurements, and the potential deviations in optical power could be considered negligible[237]. Still, further research of all these hypotheses under clinical conditions in a large number of patients will allow the development of strategies to null or compensate for the offset.

The fogging techniques required to reduce the influence of accommodation make TSR tiresome for the subject and the practitioner and increase the measurement time. TSR is indeed a time-consuming procedure, reported taking almost 6 minutes per subject, on average[139–141]. An unsupervised version of the traditional procedure, the UTSR, is very quick, taking about 21 seconds per repetition. However, it has low precision, with repeatability across subjects of ±0.47D, and systematic deviations that depend on the starting point. The DSR method, insensitive to accommodation by design, does not require fogging strategies. It is not only a very precise (±0.17D) and accurate procedure (-0.33D without offset compensation), but also fast: it takes less than 40 seconds to be performed, on average. The fastest subject took only 12 seconds per repetition, and the slowest, 90 seconds. The short measurement time (plus only 1.5 minutes of explanation) allows thorough training and would allow several repetitions, although only a few are needed (probably two, one for training and approximation and another one for refinement), given the high repeatability of the method. An assessment of the reliability of Experiment 1 supports these conclusions, as it reports a Cronbach's Alpha value of 0.979 -with a reliability factor of 0.95- estimates that only the first 4 repetitions are not redundant.

Further developments in the Direct Subjective Refraction

In this study, we measured the spherical equivalent, but not the amount of astigmatism in the subjective correction. Moreover, we measured the subjects with their usual corrections on, therefore reducing the amount of astigmatism, if present, to a residual value. Pilot experiments have shown that the DSR task can be performed in presence of astigmatism[267], at least up to one diopter but presumably more. This promising result suggests that the DSR approach described could also have the potential for fast and unsupervised measurement of subjective refraction including astigmatism. For that, the current method should be refined with new stimuli, oriented features, and new measurement protocols considering flicker and chromatic distortions in different orientations.

Some autorefractors have achieved comparable repeatability in non-cycloplegic eyes as the one reported here with DSR, and are evolving into hand-held and binocular instruments[268]. But DSR is a subjective method to measure the spherical equivalent, and as such with true potential to replace TSR with a faster and more direct approach. The DSR technology is as simple as projecting an optotunable lens onto the eye and can be easily implemented in portable binocular devices, hand-held or even wearable[229,255,269], potentially substituting phoropters or trial frames in clinical centers or screening campaigns outside the clinic.

4.6. Conclusions

The Direct Subjective Refraction presented here is a straightforward and unsupervised new subjective method to obtain the spherical equivalent of an eye. Direct Subjective Refraction overpasses existing subjective methods in terms of accuracy, precision, and measurement time, with the potential to become a new paradigm in the measurement of subjective refraction.

Chapter 5. The Direct Subjective Refraction: measurement of astigmatism

This chapter described the extension of the Direct Subjective Refraction method to measure the astigmatic component of the refractive error. Several pilot experiments were carried out to verify the suitability of the method to capture the astigmatism component of the refraction. Then, a comparison with the Traditional Subjective Refraction was carried out.

The co-authors of this study are Eduardo Esteban and Carlos Dorronsoro. The contribution of the author of the thesis was the literature research, the conceptualization, and design of the study in collaboration with Carlos Dorronsoro, the design of the experiments in collaboration with other co-authors, the collection of the data in collaboration with Eduardo Esteban, the analysis of the data, and the writing and editing of the chapter.

This work was presented as an oral contribution at the Association for Vision and Research in Ophthalmology (ARVO) virtual meeting in 2021.

5.1. Introduction

The previous chapter described the Direct Subjective Refraction method, a new method for obtaining the refractive error of an eye. However, only the spherical equivalent could be obtained. In this chapter, we extend the method to the estimation of astigmatism, by changing the stimulus and the procedure.

The Refractive error of the eye is fully described with the amount of spherical equivalent and the amount and orientation of astigmatism. As already mentioned in section 1.3.3, in clinical practice the workflow for evaluating the refractive error begins with objective refraction, providing a first estimation of the final refraction, which is later refined with the subjective refraction[91,161]. Of that first objective estimation, the angle of astigmatism is much more reliable than the amount of spherical equivalent or the amount of astigmatism[144].

Astigmatism is the difference in the refractive error in different axes, produced by the different curvature along two principal axes. Astigmatism is characterized by the dioptric amount of the difference (cylinder power) and the principal axis (the axis with more optical power, i.e., more myopic, usually called axis) and it is reported as the [cylinder @ principal axis]. The cylinder and axis of astigmatism are usually assessed by objective methods, based on keratometry, corneal topography, wavefront aberration, or Scheimpflug methods[270], with high repeatability. Retinoscopy can also be used to evaluate astigmatism, with similar repeatability to other objective methods (±0.20 standard deviation)[271]. Another study found that astigmatism estimation is more reliable with cycloplegic autorefraction (repeatability of ±0.14D of standard deviation), followed by non-cycloplegic autorefraction (±0.18D), while non-cycloplegic retinoscopy reported the lowest repeatability (±0.52D)[272]. Overall, the repeatability of astigmatism with different objective methods ranges from ±0.10D to ±0.52D[138,270–273].

Astigmatism can also be evaluated in traditional subjective refraction. On one hand, to find out the orientation of the astigmatism clinicians use the clock dial (Figure 5.1A). In the presence of astigmatism, some lines will appear thicker or with more contrast than others, indicating the orientation. The dial clock method can be useful if lacking an objective method. On the other hand, to refine the amount and orientation of astigmatism, the most extended method is Jackson's Cross Cylinders (JCC) using the stimulus shown in Figure 5.1B. The repeatability of astigmatism found with the subjective refraction ranges from 0.10 to 0.35D[144,145].

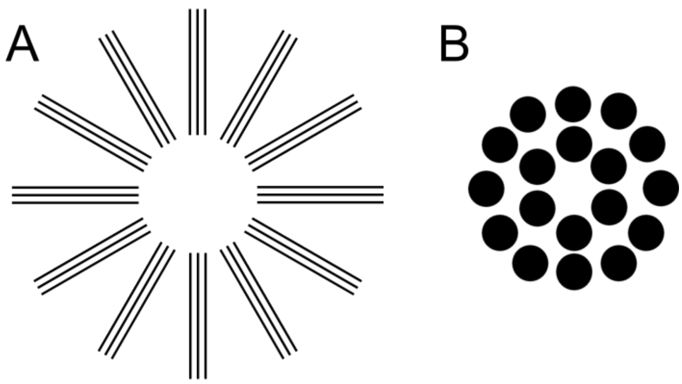

Figure 5.1. Stimuli used for astigmatism estimation in the traditional subjective refraction method. **A.** Clock dial stimulus. **B.** Jackson's Cross Cylinders stimulus.

The goal of this study is to adapt the Direct Subjective Refraction method to measure the astigmatic component of the refraction, and to demonstrate its use in pilot experiments with voluntary subjects. Finally, an additional goal was to compare the results of the new method with the results of the traditional subjective refraction method in the same subjects.

5.2. Methods

The approach followed to find the amount of astigmatism with the DSR method, is to measure the refractive error in the two principal axes and compute the difference. To do so, some improvements in the stimulus used, the setup, and the procedure followed in the previous chapter were carried out.

5.2.1. Developments

5.2.1.1. Stimulus design

The stimulus for the spherical equivalent was conformed of different circles of blue, red, and magenta components (Figure 5.2A). The new stimulus for the estimation of astigmatism contains similar arrangements and colors, but the features of the stimulus are now lines instead of circles, oriented to the angle of astigmatism that is being measured (Figure 5.2B). The new stimulus for astigmatism comprises 2 pairs of blue lines (4 lines) of 1.43x0.06º size located at both sides of the center and on the diagonal, and another 2 pairs of red lines (4 lines) of the same size located on the opposite position of the blue lines, and two magenta lines of 3.55x0.16º size located above and below the central lines. In total, the stimulus subtended 3.55x0.8º. The magenta fixation cross of the center in the stimulus for spherical equivalent (Figure 5.2A) was replaced by a fixation dot, which subtends 0.18º, to avoid the impact of astigmatism (Figure 5.2B).

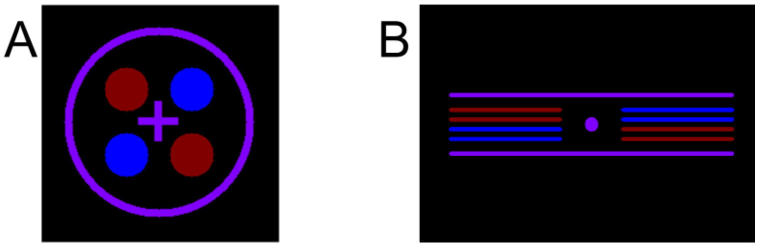

Figure 5.2. Stimuli used in the DSR method. **A.** Stimulus used for the measurement of the spherical equivalent described in Chapter 4. **B.** Stimulus used for the measurement of astigmatism. In this case, oriented at 90º.

5.2.1.2. Setup

The setup also improved compared to the one used in Chapter 4. The Temporal Defocus Wave (TDW) generator was now SimVis Gekko (same optical system but miniaturized with mirrors and head-mounted, see Figure 2.1 in Chapter 2) that allowed measurement procedures closer to those expected in a clinical environment. The subject's head position was stabilized with a chinrest, avoiding the need for a bite bar. Besides, being binocular, SimVis Gekko allowed measurements in both eyes without realignment.

The stimulus was presented on a white flat screen by a DLP projector (PJD7820HD, ViewPort). Although this setup is not optimal due to the broad spectral emission of each chromatic channel (see Figure 2.6 in section 2.6.1.2), is ideal for designing and developing the stimulus, in particular regarding the position and shape of its components. Custom routines were programmed in MATLAB (Math-works Inc., Natick, USA) to control SimVis Gekko and the optical power of its optotunable lenses. In combination with

Psychtoolbox[241], MATLAB was also used to design and present the stimuli and perform the perceptual task and collect data from subjects.

5.2.2. Procedure

The psychophysical procedure is the same that was described in Chapter 4. Objective refraction (OBR) using the ARK-1 autorefractometer (ARK1, Nidek, Gamagori, Japan) was considered the starting point of the DSR refraction. The axes to measure with the DSR method are determined by the principal axis (and the orthogonal) provided by the autorefractometer. The refractive error for each axis was estimated by averaging 4 repetitions, each one following a staircase procedure with a different starting point (added to the outcome of the autorefraction): -1.00, -0.50, +0.50, and +1.00D. The high repeatability of the results for DSR described in Chapter 4 allowed us to reduce the number of repetitions from 10 to 4, based on a reliability estimation (see section 4.4). In total, astigmatism is found with the DSR method from 16 repetitions (8 for each eye, 4 for each axis). The 8 repeated measurements for each eye (4 repetitions for each axis) were randomized. As in Chapter 4, the DSR task consisted in simultaneously minimizing the two concurrent effects in the image induced by the TDW: the flicker and the chromatic distortions. Chromatic distortions affected more the red components when the mean of the TDW was on the hyperopic side of the retina and affected more the blue components when the mean of the TDW was on the myopic side of the retina. The parameters of the TDW were 15Hz of temporal frequency and 0.25D of amplitude. Subjects increased or decreased the mean optical power of the TDW using a keyboard, in coarse or fine steps of 0.25D or 0.10D, respectively. The difference between the refractive error of both axes provides the amount of astigmatism, and the average across them provides the spherical equivalent. The experiment was performed without supervision (the experimenter only explained the task before the experiment), and accommodation was free. Figure 5.3 shows the process, and an example measurement, for an amount of astigmatism of 0.57D with its principal axis (myopic axis) at 160º.

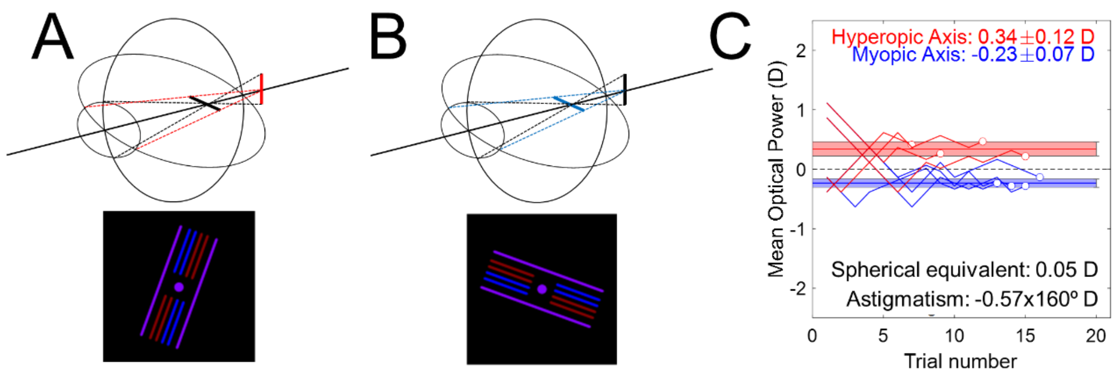

Figure 5.3. Estimation of astigmatism with the DSR method in a subject with mixed astigmatism. A. Evaluation of the hyperopic axis, oriented at 70º. **B.** Evaluation of the myopic axis, oriented at 160º. **C.** DSR results. Mean optical power at 0D represents the retina. The myopic axis lies below 0 (-0.23D, which means before the retina in A), and the hyperopic axis above 0 (+0.34D, which means behind the retina in B). The amount of astigmatism in this patient is -0.57D at 160º.

5.2.3. Pilot experiments

One trained researcher (27 years old) participated in pilot experiments to refine the parameters of the TDW and the stimuli. Three pilot experiments were performed, including 1) induction of an extra 0.75D amount of astigmatism in the principal axis to find out if the method is sensitive to changes in astigmatism; 2) changes in the monochromatic colors from blue and red (Blue/Red; B/R stimulus), to red and green (Red/Green; R/G stimulus) and; 3) test with cycloplegic drops to evaluate the impact of the accommodation on the DSR method for estimating astigmatism. Three cycloplegic drops (tropicamide 1%) were instilled every 10 minutes and measurements began 10 minutes after the third instillation. The astigmatism component of the refraction obtained with the DSR method was used to compare across experiments.

5.2.4. Experiments

Four patients participated in this study (age 31.0±11.4 years old). The astigmatic component of the refraction of the subject was obtained with the DSR method. The final refraction reported was the combination of the sphere obtained with the autorefraction and the additional amount of astigmatism obtained with the DSR method.

We also measured the traditional subjective refraction (TSR) following the procedure described in Chapter 2 (see section 2.4). The starting point of the TSR was also the measurement of the autorefractometer. The refraction obtained with TSR was the combination of the sphere of the autorefraction and the amount of astigmatism obtained with the TSR method.

To compare between refractions, the astigmatic component in power vector notations[24] was compared (J_0, J_{45}) using Bland-Altman analysis. We also evaluated the visual function provided by the DSR and the TSR refractions measuring the visual acuity (VA), the stereoacuity using the Titmus test, and a direct comparison of the perceived comfort between both refractions. This comparison was carried out by testing the refractions with trial lenses in two different trial frames. Additionally, we compared the time taken for DSR and TSR to be performed. To obtain a refraction from the DSR method, at least one measurement for both axes and both eyes is needed. To calculate the total amount of time for the DSR refraction, we considered the time taken on average across repetitions for each axis and for both eyes and the time measured for explaining the task to the subject. For the TSR method, we measured the time since the clinician began the evaluation of the first eye until the binocular adjustment.

5.2.5. Statistical analysis

To evaluate the agreement between the astigmatism obtained with the DSR and TSR refractions we used Bland-Altman analysis for the J_0 and J_{45} components of the refraction. For each subject, we considered each repetition of the DSR task as a different measurement. Paired t-tests were used to compare the J_0, J_{45}, VA, and stereoacuity for both refraction methods. The statistical level to achieve statistical significance was set to 5% (p=0.05).

5.3. Results

5.3.1. Pilot experiments

Effect of inducing astigmatism

In this pilot experiment, we measured the effect of inducing astigmatism in one axis to evaluate the capability of the Direct Subjective Refraction method to capture that extra amount of astigmatism. Figure 5.4 shows the result for one subject and both eyes. Figure 5.4A shows the results without any induced astigmatism (the refraction obtained with the DSR method adapted to the measurement of astigmatism). The DSR measurement detects a subclinical amount of residual astigmatism in both eyes of the subject (-0.08D in LE and -0.11D in RE). Figure 5.4B reports the result with 0.75D of induced astigmatism in the myopic axis (170º for the left eye and 20º for the right eye for this subject). As can be observed, astigmatism measured increases to -0.70D in LE (0.62D increment) and -

0.81D in RE (0.70D difference). Moreover, the main change is produced in the myopic axis, the one in which the astigmatism was induced (from -0.14 to -1.01D in the left eye and from 0.21 to -0.54D in the right eye). This result suggests that the DSR method can successfully capture differences in astigmatism. In addition, the standard deviation for all axis was lower than ±0.15D (±0.09D on average across axis, eyes, and conditions). However, these were pilot experiments on one experienced subject. The performance of this visual task must be demonstrated in more subjects and eventually in patients.

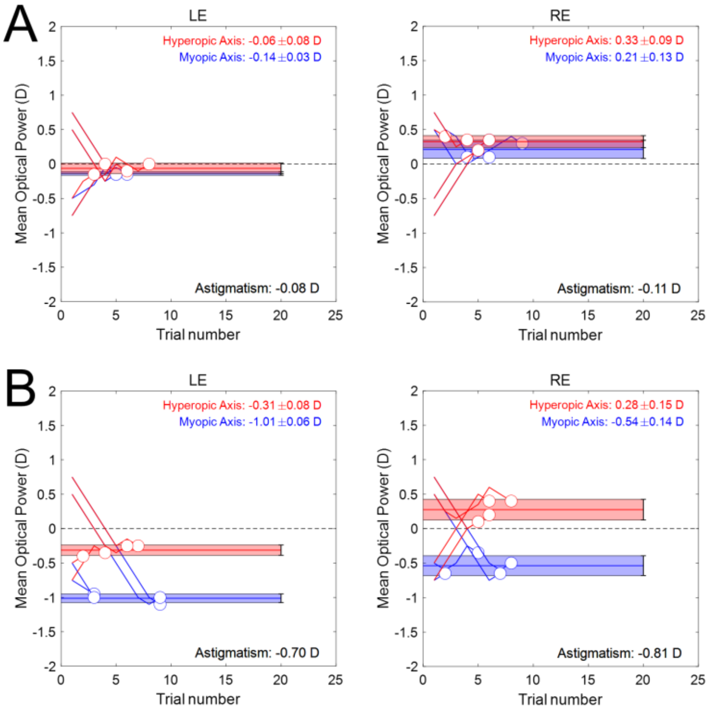

Figure 5.4. Effect of inducing astigmatism in the result of the DSR method. The plots show the mean optical power of the TDW for each trial number. The endpoint of each staircase is indicated as a white dot and represents the refraction obtained in each repetition. The shaded horizontal bars represent the average and the standard deviation across 4 repetitions for each axis (in red, hyperopic axis; in blue, myopic axis). Left plots indicate the results for the left eye and right plots for the right eye. **A.** DSR method without induced astigmatism. **B.** DSR method with induced astigmatism of 0.75D in the myopic axis (extra +0.75D at 170º in the left eye and +0.75D at 20º).

<u>Effect of the chromatic components of the stimulus</u>

In this pilot experiment, the goal was to test if changing the stimulus developed originally from Blue/Red (B/R) to Red/Green (R/G) resulted in a different outcome. In Figure 5.5 we show the difference between the B/R and R/G for one subject. The difference found in terms of astigmatism was negligible -0.19 to -0.10D in the left eye and -0.36 to -0.30D in the right eye for B/R and G/R. In terms of standard deviation, both B/R and G/R provide highly repeatable measurements (±0.05D and ±0.02 on average across axes and eyes). However, in terms of the spherical equivalent, the difference between B/R and R/G was around 0.4D in both eyes, with B/R providing more myopic results.

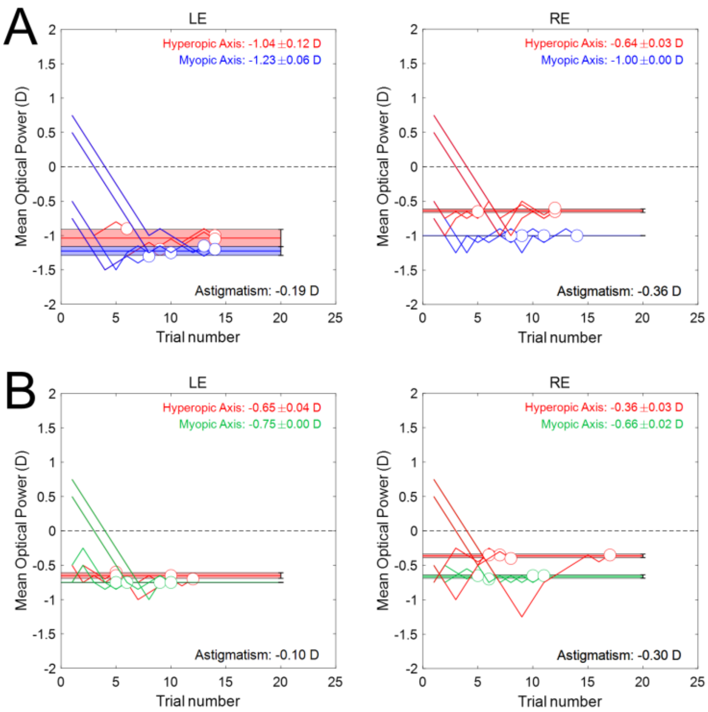

Figure 5.5. Effect of changing the chromatic components of the stimulus in the result of the DSR method. A. Results using B/R stimulus. **B.** Results using R/G stimulus.

Effect of accommodation

In Figure 5.6 we show the result of paralyzing the accommodation with the DSR method for both eyes and the same non-presbyopic subject (27 years old), with the B/R stimulus (upper plots, Figures 5.6A and 5.6B) and the R/G stimulus (lower plots, Figures 5.6C and 5.6D). For the B/R stimulus, the amount of astigmatism barely changes with accommodation free (from -0.19 to -0.08D in the left eye and -0.36 to -0.34D in the right eye, for free and paralyzed accommodation conditions, respectively), although there is a change in the spherical equivalent of the right eye higher than 0.3D, similar to the findings in Chapter 4 (see Figure 4.6). For the R/G stimulus, the astigmatism amount changes more pronouncedly in the right eye (from -0.3 to -0.06D, free and paralyzed accommodation conditions, respectively) although with subclinical importance, but barely changes in the left eye (from -0.10 to -0.09D, free and paralyzed accommodation). Similarly, there is a small hyperopic shift in the spherical equivalent of the right eye (0.3D) but no change in the left eye. Remarkably, the standard deviation for each axis is kept low: ±0.05D on average across axes, eyes, stimuli, and conditions, and below ±0.12D in all cases.

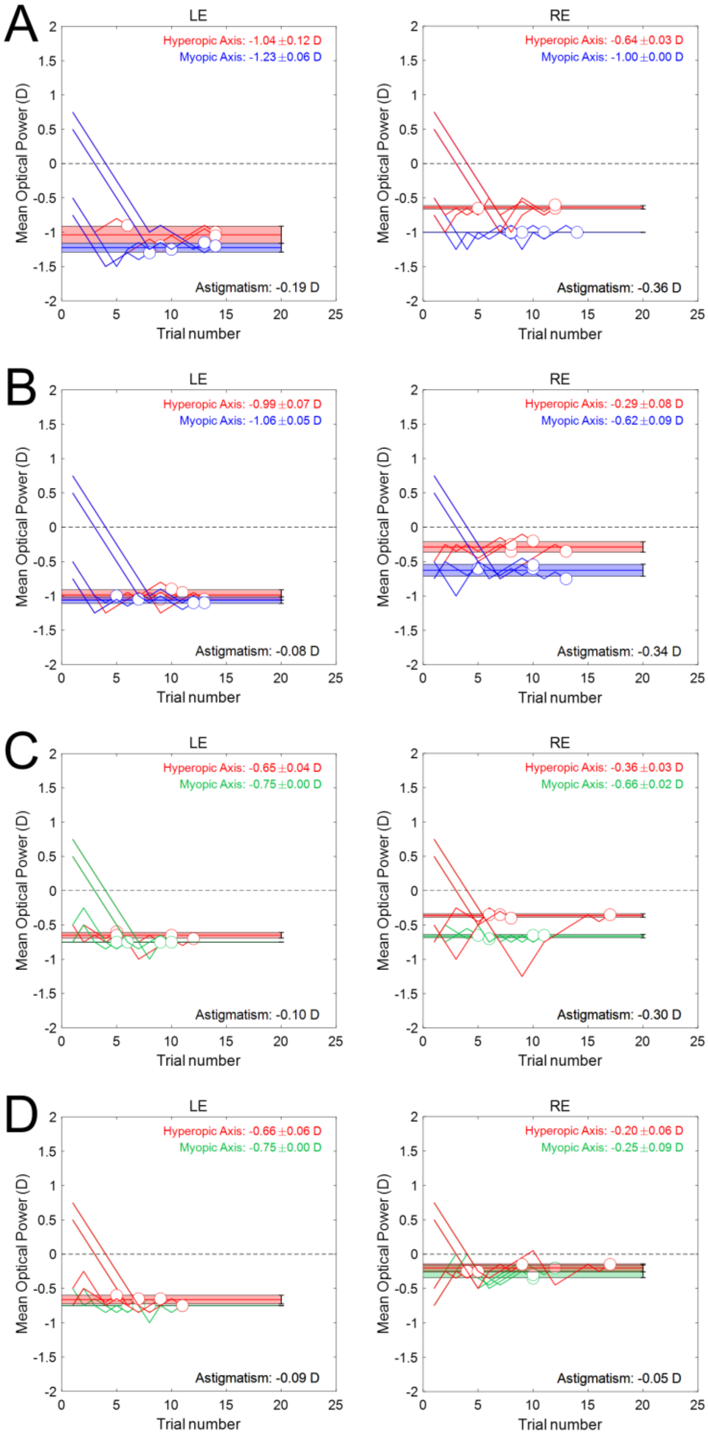

Figure 5.6. Effect of paralyzing accommodation in the result of the DSR method. A. Results with free accommodation using B/R stimulus. **B.** Results with paralyzed accommodation using B/R stimulus. **C.** Results with free accommodation using G/R stimulus. **D.** Results with paralyzed accommodation using G/R stimulus.

5.3.2. Comparing the Direct Subjective Refraction with the Traditional Subjective Refraction

Figure 5.7 shows the result of the DSR method for all subjects. The DSR method captures the amount of astigmatism with high repeatability. On average across eyes and subjects, the amount of astigmatism was 0.28±0.21D. In terms of performance, the average standard deviation across axes and eyes were 0.14, 0.09, 0.27, and 0.18D for S1, S2, S3, and S4, respectively.

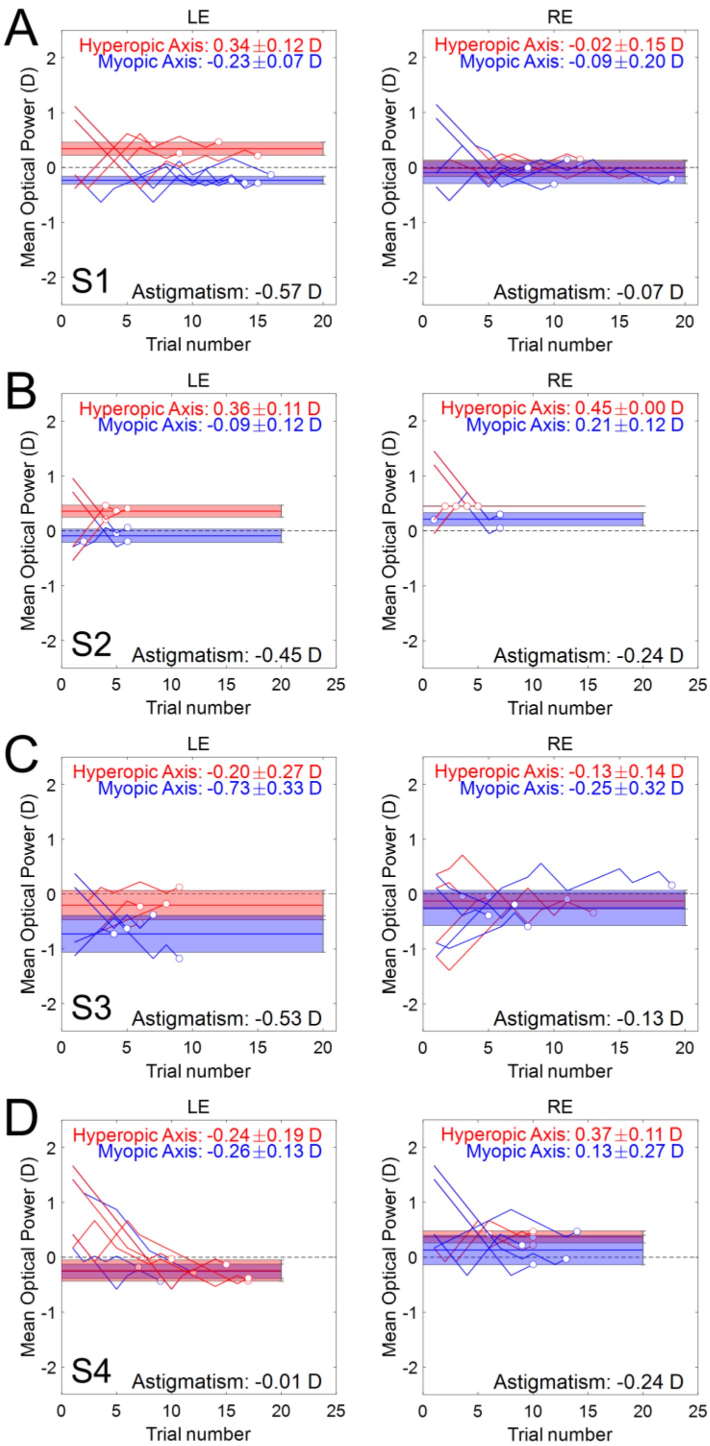

Figure 5.7. Results of the DSR method. A. Subject 1. The angle of astigmatism of the myopic and hyperopic axis for the left eye was 170º and 80º, respectively. The angle of astigmatism of the myopic and hyperopic axis for the right eye was 20º and 110º, respectively. **B. Subject 2.** The angle of astigmatism of the myopic and hyperopic axis for both eyes eye was 55º and 145º, respectively. **C. Subject 3.** The angle of astigmatism of the myopic and hyperopic axis for the left eye was 110º and 20º, respectively. The angle of astigmatism of the myopic and hyperopic axis for the right eye was 75º and 165º, respectively. **D. Subject 4.** The angle of astigmatism of the myopic and hyperopic axis for the left eye was 155º and 65º, respectively. The angle of astigmatism of the myopic and hyperopic axis for the right eye was 25º and 115º, respectively.

Figure 5.8 shows the Bland-Altman plots of the DSR method vs. the TSR method for horizontal and oblique astigmatism components in power vector notation (J_0 and J_{45}, respectively). In the DSR, 4 repetitions are performed for each axis, while for TSR we only performed it twice. We have included the result for all repetitions and both eyes in the analysis. For the J_0 component (Figure 5.8A), the difference is close to 0 (-0.05±0.13D) between TSR and DSR (Limits of Agreement (LOAs) of [-0.29, 0.20]D) being non-significantly different (paired t-test *p*>.05). For the J_{45} component (Figure 5.8B), the difference is -0.01±0.06 between methods (LOAs of [-0.12, 0.10]D), without any statistical difference (paired t-test *p*>.05).

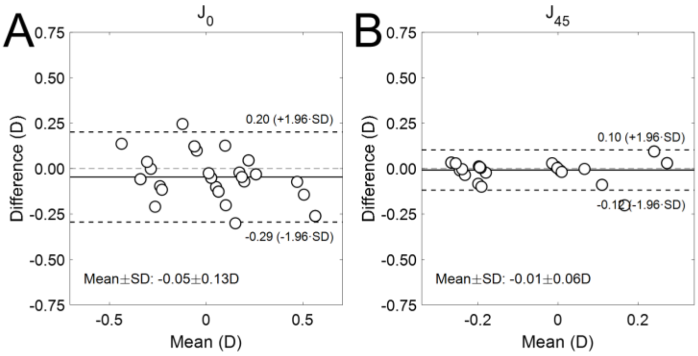

Figure 5.8. Bland-Altman analysis for TSR vs OBR refractions. Each panel shows a Bland-Altman plot, indicating the Limits of Agreement (LOAs, 95% Confidence Interval), mean, and standard deviation of the sample. **A.** Plot comparing J_0 component for both eyes. **B.** Plot comparing J_{45} component for both eyes.

In terms of time and repeatability, however, both methods provide very different results. Figure 5.9 shows the repeatability as a function of time. The repeatability of the DSR measured was the average standard deviation across eyes and axis for each subject, and the repeatability for the TSR was obtained from the literature[161]. As shown in Figure 5.9, DSR reduced measurement time, compared to the TSR, by a factor higher than x10, on average (2.48 vs 14.45min) and was almost twice more repeatable (standard deviation ±0.17 vs ±0.28D).

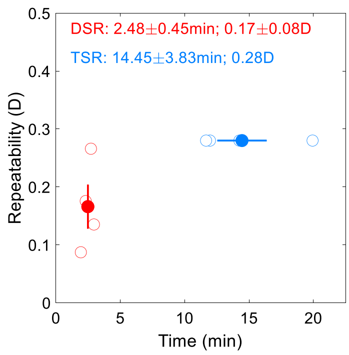

Figure 5.9. Time vs. repeatability. Empty dots indicate the result for each subject and filled dots indicate the average across subjects. In red, the DSR method. In blue, the TSR method.

We also evaluated the visual function with both methods (DSR and TSR) by measuring visual acuity (VA) and stereoacuity. The VA averaged across subjects for both DSR and TSR was -0.1 logMAR and was not statistically significantly different (paired t-test *p*>.05). Stereoacuity was also very similar for DSR and TSR (on average, 30±11.5 and 28±9.8 arc seconds, respectively) and there was no statistically significant difference (paired t-test *p*>.05). In the direct comparison of preference between correction, 50% of subjects preferred the DSR prescription and 50% of the subjects preferred the TSR prescription.

5.4. Discussion

Direct Subjective Refraction for astigmatism

In this study, we have demonstrated that the Direct Subjective Refraction (DSR) method could be used in the estimation of the amount of astigmatism, a key component of the refractive error not measured in previous versions of the DSR (Chapter 4). In this chapter, we have shown that the DSR method is very repeatable (±0.17D on average) and quick (each repetition taking 37 seconds), in agreement with the results of previous measurements, focused on the spherical equivalent (Chapter 4).

In the comparison of the DSR method with the traditional subjective refraction (TSR) in terms of astigmatism, there is barely any difference between them (J_0: -0.05±0.13D; J_{45}: -0.01±0.06D). Other novel subjective refraction methods have reported higher differences compared to the TSR, ranging from ±0.07 to ±0.39D in the J_0 component and from ±0.07 to ±0.31D in the J_{45}[127,128,140–142,152]. In this sample size, the encouraging results of the DSR overpass the outcomes of other subjective refraction methods but these results must be addressed in a higher sample size.

With the refraction obtained with the DSR and the TSR in trial lenses in a trial frame, the visual function evaluated with the visual acuity and the stereoacuity was statistically similar in both methods (paired t-test p>.05) and the direct comparison between refractions showed that 50% of the patients preferred either DSR or TSR. A preference of 50% suggests that both TSR and DSR and undistinguishable and the results are encouraging. However, the sample size is small. A confirmation of these results in a larger sample size is needed to yield conclusions about the potential of the DSR.

We have also shown that the influence of accommodation on the estimation of astigmatism is negligible. However, the amount of spherical equivalent with free accommodation is 0.3D more myopic than with paralyzed accommodation, in agreement with previous results (Figure 4.7, Chapter 4). Besides, pilot experiments have shown that the method can capture the amount of astigmatism very accurately when adding extra astigmatism to the refractive error of the subject's eye (Figure 5.4).

In addition, the change of the stimulus from a Blue/Red (B/R) version to a Red/Green (R/G) seems to not influence the astigmatism amount, although it changes the amount of spherical equivalent (Figure 5.5). We can speculate that the result, being undesirable, is not so unexpected. We assume that the spherical equivalent lies in between the two-color components used in the stimulus. Changing one (or the two) color components induces an overall spectral shift and a potential change in the spherical equivalent. Considering the model described by Thibos et al.[45] of the chromatic aberration of the eye and the maximum spectral emission of the red, green, and blue components of the projector (602, 552, and 490nm, respectively; see Figure 2.6, Chapter 2), the spectral shift is 0.15D, half the shift found. In this subject, the result does not match the model. However, the display used in this study (projector and white screen) has a broad spectral width for red, green, and blue components and therefore is not optimal for investigating the effect of the chromatic components. A display with customized RGB channels, with narrow spectral bandwidths, can help to understand the effect of different colors in the DSR task or even to perform the DSR task.

Although with encouraging results, these pilot experiments were performed on only one experienced subject. Measurements in a larger sample size will help to better describe these results and to yield proper conclusions.

Limitations of the DSR method for astigmatism
DSR method had been previously developed to measure the spherical equivalent component of the refractive error of an eye (Chapter 4). In this study, we have extended the procedure to also measure the astigmatism component. However, a complete prescription must include both spherical equivalent and astigmatism. The next step in the development of this method should aim at evaluating the whole refractive error to provide a complete prescription.

In clinical practice, the refractive error is often evaluated with objective refraction as a starting point and then the traditional subjective refraction is performed. During this process, both the amount and orientation of the astigmatism are evaluated. In this study, the DSR method depends exclusively on the autorefraction to estimate the orientation of astigmatism. Although it has been reported that the angle of the axis provided by the autorefractometer is highly correlated with the angle estimated later with the TSR[144], a DSR-based procedure for defining or refining the angle of astigmatism might help to provide a better estimation. However, it is a challenging goal and may be out of reach now, as autorefractors are fast and reliable in determining the angle of astigmatism and are widespread in eyecare clinics.

5.5. Conclusions

In this chapter of the thesis, we have demonstrated the feasibility of the Direct Subjective Refraction method to measure the astigmatic component of the subjective refraction using an oriented version of the stimulus previously designed for the estimation of spherical equivalent. The performance of the method for the measurement of astigmatism is very similar in terms of repeatability, accuracy, and measurement time to that obtained in Chapter 4 for the spherical equivalent. The results of this proof of concept in subjects with experience in visual studies is encouraging to develop a more sophisticated method to provide a complete prescription with the Direct Subjective Refraction method and to test it in real patients.

Chapter 6. Clinical measurements with the Direct Subjective Refraction

This chapter covers further developments of the Direct Subjective Refraction method to provide a complete description of the refractive state of the eye, including spherical equivalent and astigmatism in the same measurement. In this chapter, the initial table-top setup evolved to a portable prototype, based on a wearable device and miniaturized display, able to measure the full spherocylindrical eye prescription in clinical environments.

This chapter is based on the article in preparation entitled *“The Direct subjective refraction method: fast and accurate subjective measurements of the refractive error”,* in which Victor Rodriguez-Lopez is the first author. Other co-authors are Eduardo Esteban, Daniel Pascual, Nerea Arejita and Carlos Dorronsoro.

The contribution of the author of the thesis was the conceptualization and design of the study in collaboration with Carlos Dorronsoro, the literature research, the design of the experiments in collaboration with Eduardo Esteban, the collection of the data in collaboration with Nerea Arejita, the analysis of the data, the writing of the chapter and the editing of the chapter in collaboration with all the co-authors.

6.1. Introduction

The Direct Subjective Refraction (DSR) method has been described in previous chapters for the isolated measurement of the spherical equivalent (Chapter 4) and astigmatism (Chapter 5). Preliminary results have demonstrated that this methodology allows self-refraction of the spherical equivalent and astigmatism in less than one minute each, with unprecedented repeatability in both measurements (±0.17D). The potential of this new methodology has already been shown in laboratory studies with volunteer subjects, but the performance of real patients still needs to be demonstrated in clinical environments. This chapter describes the evolution of the setup to a portable device and the results of the first joint measurements of spherocylindrical error with DSR in clinical environments.

The Direct Subjective Refraction (DSR) method used in previous chapters had important limitations. The main technological limitation refers to the setup, in which the optotunable lens creating the Temporal Defocus Waves (TDW) was part of an optical system mounted on an optical board, with all the complexities associated with on-bench systems, requiring continuous realignment and recalibration. Besides, the alignment of the eye with respect to the optical axis of the optical system was carried out with a bite bar, something very uncomfortable for the subjects as it requires big efforts to avoid any movement and frequent re-alignments. An RGB projector on a white screen was used to present the stimulus. This projector generates color components with large spectral widths and with low luminances, which can potentially make the task harder.

Since its invention, the ultimate goal of this method has been its use in clinical environments. This chapter brings the method closer to the clinic by 1) reengineering the initial prototype (head-mounted TDW generator and LED-based display), 2) optimizing the parameters of the task and the psychophysical procedure, and 3) improving the measurement technique. Finally, measurements in two clinical environments were performed, exploring the clinical use of this technology and obtaining valuable feedback from real patients.

6.2. Methods

6.2.1. Estimation of the eye prescription

The Direct Subjective Refraction (DSR) task remains the same as in Chapters 4 and 5: subjects (or patients, in some parts of this chapter) must minimize the flicker and chromatic artifacts guided by the reddish or blueish cues on the stimulus shown. The psychophysical procedure is the same as the one already described in previous chapters. However, in this chapter, the full spherocylindrical notation of the refractive error is directly obtained from DSR measurements in only two axes, the principal axes identified by autorefractometry, each measurement consisting of 4 repetitions of a staircase procedure. The spherical equivalent and the amount of astigmatism are subsequently obtained as the average and the difference across the results of axes, respectively.

6.2.2. Clinical prototype

6.2.2.1. Hardware improvement

The hardware was improved from a table-top in-line monocular optical system with a projector-screen display to a miniaturized head-mounted and binocular optical system with a custom high-luminance monochromatic LED display.

The SimVis Gekko was used as the generator of Temporal Defocus Waves (TDW). The optical system of the SimVis Gekko uses mirrors to twist the optical path and reduce the overall length of the system, maintaining the optical path[113]. Additionally, SimVis Gekko is binocular, wearable, head-mounted, see-through, and has a large visual field (almost 20º for each eye). Another advantage is that the connection is wireless.

The display was changed completely compared to previous versions of the technology. The commercial DLP projector of the previous system was replaced by a custom display of LEDs, comprising high-luminance highly monochromatic LEDs (LUXEON Rebel Color Line series, Lumileds, Schiphol, The Netherlands). Considering the spectral sensitivity function of the human visual system[274,275] and the LED peaks of emission from technical specifications, three LEDs were selected to create the Blue, Green, and Red stimuli, with peaks of sensitivity at 470, 530, and 627 nm, respectively. Figure 6.1 shows the spectral emission of the three selected LEDs, their spectral sensitivity, and the corresponding focus shift according to the LCA curve of the phakic human eye based on the chromatic eye model described by Thibos et al.[45] (Equation 1.3, Chapter 1).

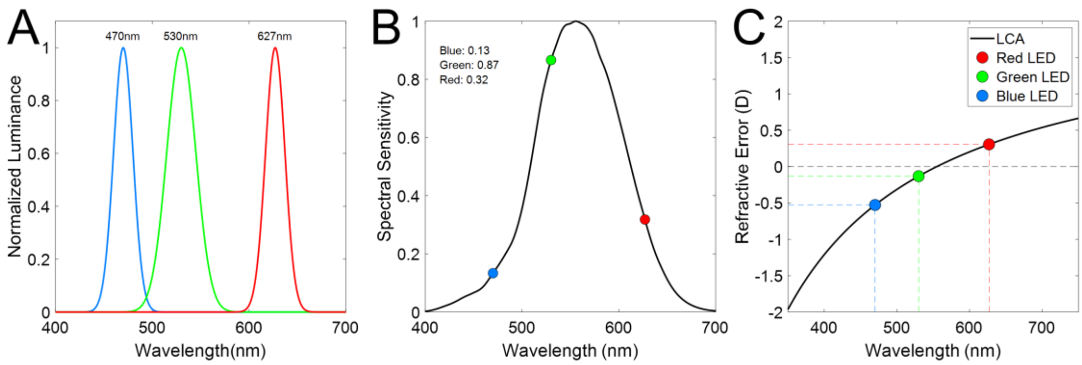

Figure 6.1. LEDs used for the display. **A.** Normalized spectral emission of the Blue, Green, and Red LEDs. **B.** Photopic spectral sensitivity normalized (black line) and the position of the LEDs according to their maximum emission. **C.** Longitudinal Chromatic Aberration (LCA, black line) and the position of the LEDs according to their maximum emission.

Figure 6.2 shows the clinical prototype developed. We developed a display for spherical equivalent measurements (Figure 6.2A) and another display for full prescription measurements (Figure 6.2B). In this chapter, we describe the technology development of both, although we did not perform measurements using the spherical equivalent display. The main component is the display made of narrow banded monochromatic LEDs soldered to a printed circuit board (PCB). The rectangular black housing contains the electronics needed to control the power of the LEDs. The display is held by a mount to allow changing the configuration of the stimulus and is mounted in a swing to allow slanting the angle of the display to match the visual axis of the observer. Besides, in the full prescription display (Figure 6.2B), the display is also joined to a servomotor to allow changing the orientation of the stimulus. Each component is described in detail below.

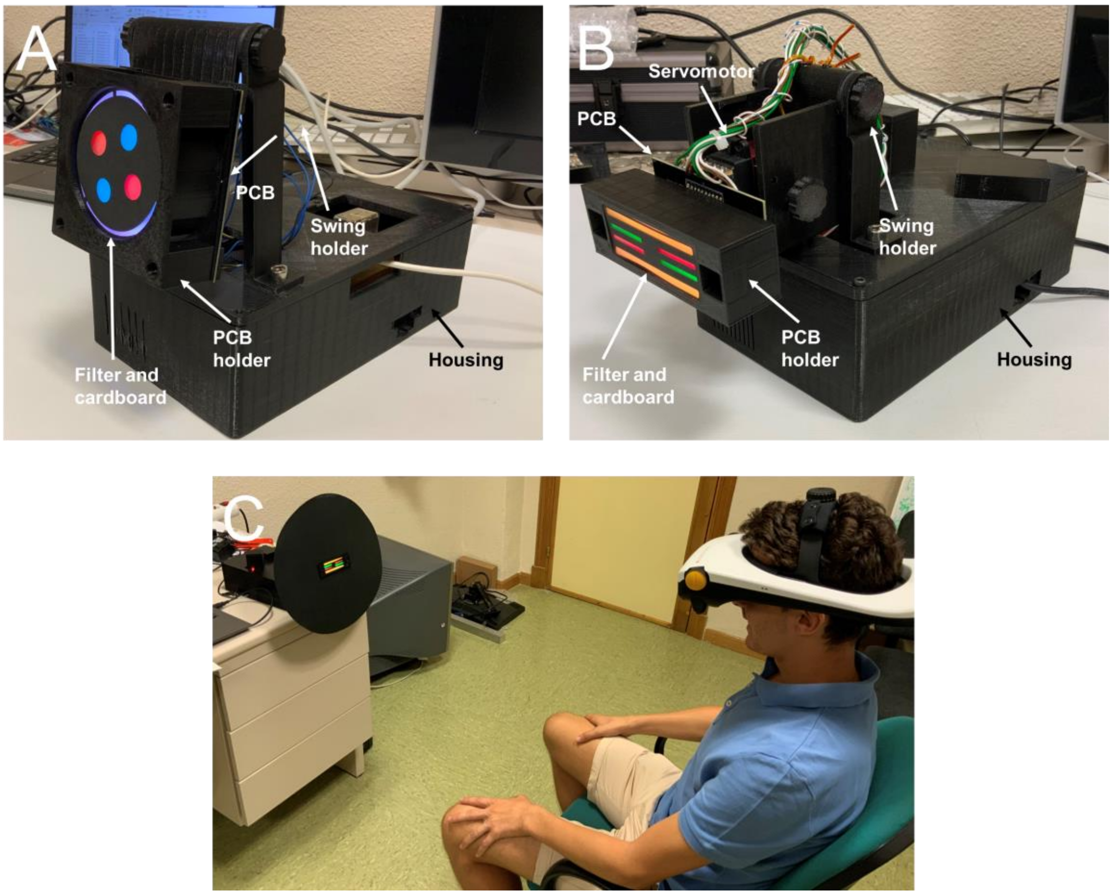

Figure 6.2. Image of the clinical prototype. A. For spherical equivalent. **B.** For full prescription. C. Patient performing the DSR experiment with the clinical prototype. During the measurements, the lights were off.

The LEDs were assembled in a custom printed circuit board (PCB), designed specifically for this thesis (with the help of Daniel Pascual). The PCB for spherical equivalent measurements with LEDs soldered is shown in Figure 6.2A, and the PCB for full prescription measurements with LEDs soldered is shown in Figure 6.2B. The size of the PCB and the position of the LEDs were designed to match the dimensions of the stimulus displayed onscreen in previous studies (Figures 4.2 and 5.2), subtending the same visual degrees at 1m distance. The PCB allows controlling the power emission of the LEDs by groups, adapting the stimulus to the visual task.

The PCB for the spherical equivalent was conformed of a group of 4 LEDs for each circle (4 circles in total, 2 of one monochromatic color and 2 of another monochromatic color) and a surrounding biochromatic ring with 18 alternating LEDs of the two monochromatic colors (Figure 6.3A). The PCB had 6 independent channels to control the LEDs: one channel to control the 2 inner monochromatic circles of one color, another channel to control the inner circles of the other monochromatic color, and another two channels to control each half of one monochromatic color of the bichromatic ring, and the remaining two channels to control each half of the other monochromatic color of the bichromatic ring.

The PCB for the full prescription was conformed of a group of 7 LEDs for each line (4 lines in total, 2 of one monochromatic color and 2 of another monochromatic color) and two surrounding bichromatic lines with 14 alternating LEDs of the two monochromatic colors (Figure 6.3B). The PCB had 6 independent channels to control the LEDs: one channel to control the 2 inner monochromatic lines of one color, another channel to control the inner lines of the other monochromatic color, another two channels to control one monochromatic color of the bichromatic line, and the remaining two channels to control the other monochromatic color of the bichromatic line.

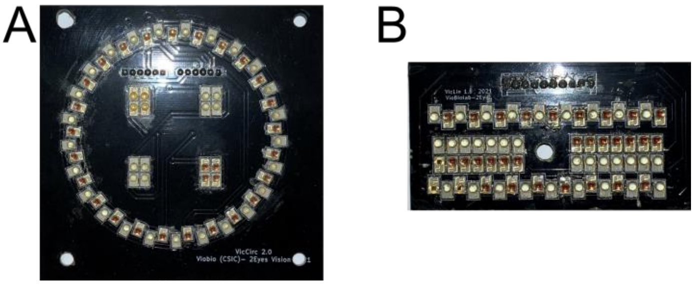

Figure 6.3. PCBs for controlling the stimuli. A. PCB for the spherical equivalent experiment. **B.** PCB for the full prescription experiment.

The fixed position of the LEDs limits the shape of the stimulus. Therefore, the mount for the PCB not only holds the PCB to a slanting system but also allows the creation of different stimulus designs using a diffusor filter and printed cardboards. Different design patterns for the spherical equivalent and the full prescription stimuli were modeled and laser-printed on cardboards, which allowed a high-precise definition of the edges of the stimuli. Figure 6.4 shows the three designs printed for the spherical equivalent (S) stimulus and the five designs printed for the full prescription (P) stimulus.

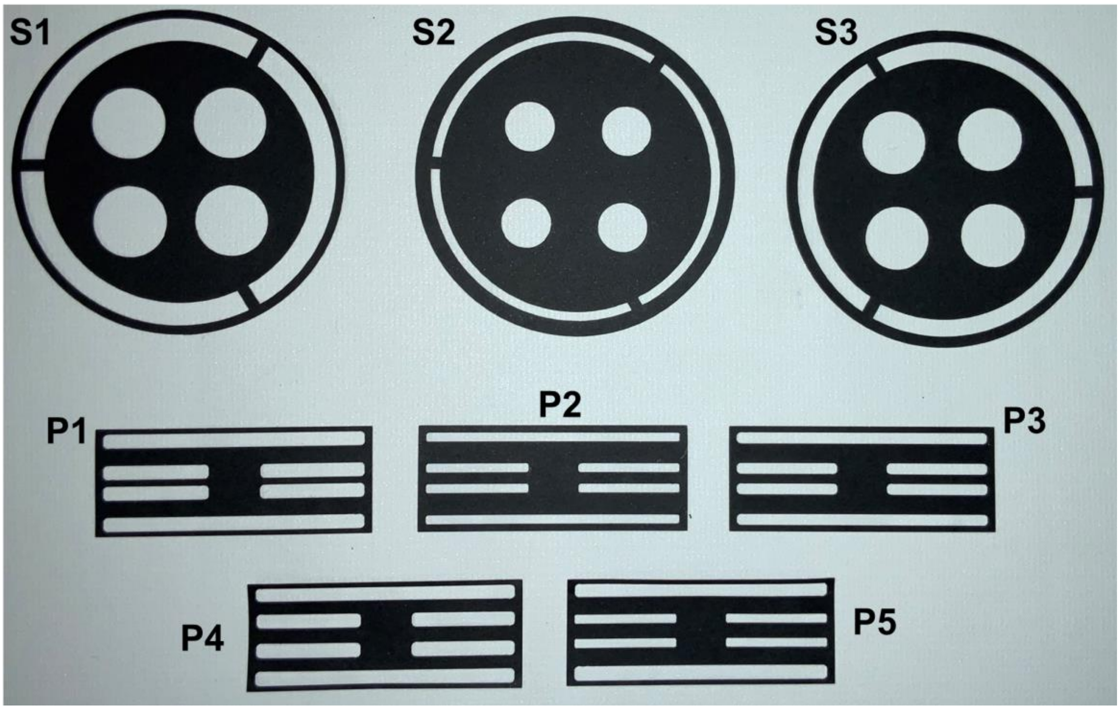

Figure 6.4. Image of the laser-printed cardboard designs for spherical equivalent and full prescription. Designs S1, S2, and S3 correspond to the spherical equivalent display, and P1, P2, P3, P4, and P5 to the full prescription display.

Different combinations of LEDs were configured to create different stimuli: Blue/Red (B/R), Red/Green (R/G), and Green/Blue (G/B). The PCB for each stimulus has the same structure and only the distribution of LEDs changes. The luminous power emission of each display was calibrated using a PowerMeter (Coherent, Santa Barbara, USA).

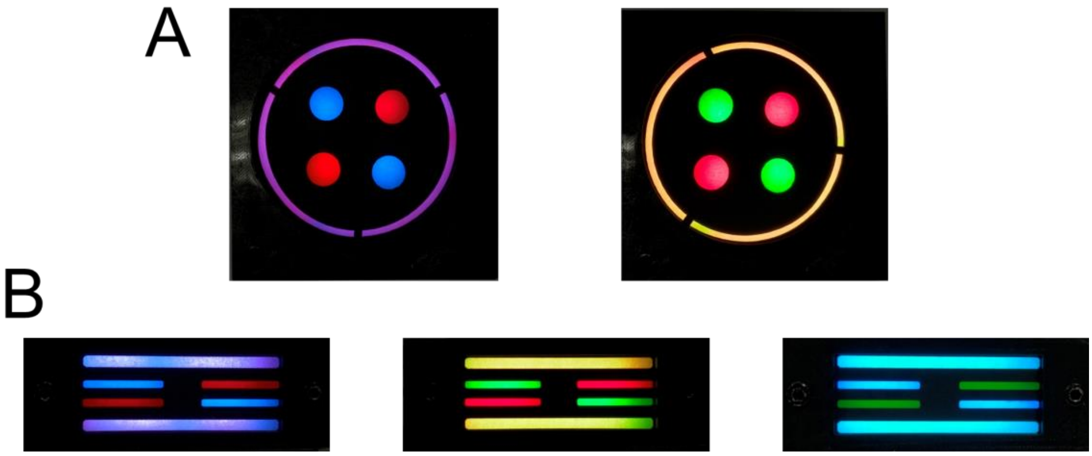

Figure 6.5. Stimuli designed with LED display. A. Spherical equivalent stimuli (from left to right, Blue/Red and Red/Green). **B.** Full prescription stimuli (from left to right, Blue/Red, Red/Green, and Green/Blue).

The PCB received voltage controlled by an Arduino Nano 3 (Arduino, Turin, Italy). All the electronic components were soldered to a circuit board. For allocating the board, the housing was designed using 3D modeling and later 3D-printed in black plastic. Different housings were designed for the spherical equivalent stimulus and the full prescription stimulus. The main components of the housing were 1) a box for setting on the power source and the electronic circuit, 2) a tap with threads for placing a holder for the LEDs PCB which could slant the structure to align its center with the gaze of the observer (and for a servo motor for rotating the LEDs PCB for evaluating different axes of the refractive error in the full prescription stimulus), and 3) a holder for the PCB that also allowed to create specific patterns with laser-printed cardboards. Besides, the box had openings for wires of the power source and the USB connection and several parallel slits to avoid overheating the power source. Figure 6.6 shows the components of the clinical prototypes of the different components and an image of the assembled housing once 3D printed.

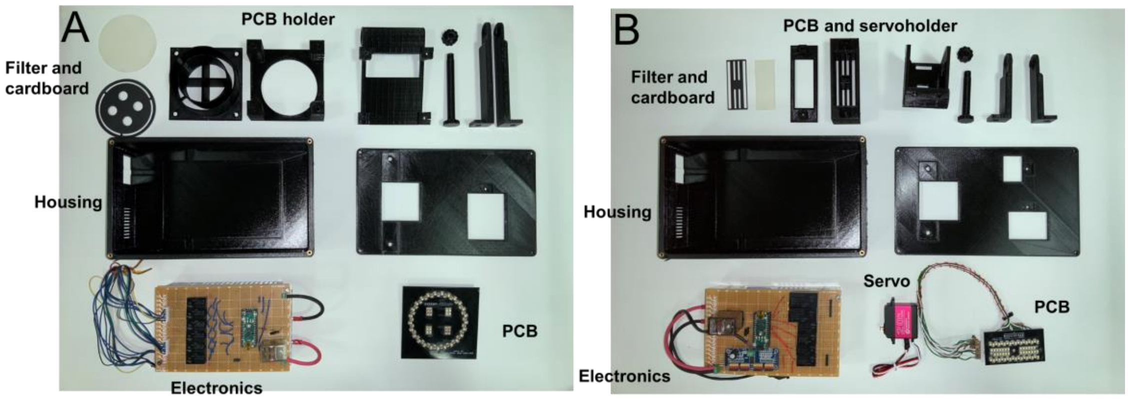

Figure 6.6. Carving-up of the clinical prototype. A. Spherical equivalent. **B.** Full prescription.

The different components of the housing were joined using metal screws in threads previously 3D modeled. To assure that the power source was as tight as possible to avoid undesirable movements while carrying it, polystyrene plastic was placed on both sides of the power source.

Table 6.1. Comparison of the features of the starting optical system and the evolution to a clinical prototype for the Direct Subjective Refraction.

Feature	On-bench Setup (previous chapters)	Clinical Prototype (this chapter)
Optical system	In-line	Miniaturized using SimVis Gekko
Eye	Monocular	Binocular
Alignment and fixation	Bite bar	Wearable
Display	Projector + white screen broad spectral bandwidth	Custom board of LEDs with narrow spectral bandwidth and high luminance
Connection	USB	Bluetooth

6.2.2.2. Software improvement

In terms of software, specific routines in MATLAB were developed to run the new display (the power supplied to the LEDs) and to rotate the display using the servo motor. Additionally, Psychtoolbox[241] was used to collect the response of the subjects. A GUI (Graphical User Interface) was developed to facilitate the data collection in patients from the clinical environment. This GUI allowed us to introduce the objective refraction obtained from the autorefractometer and to calculate the final prescription based on the result of the DSR.

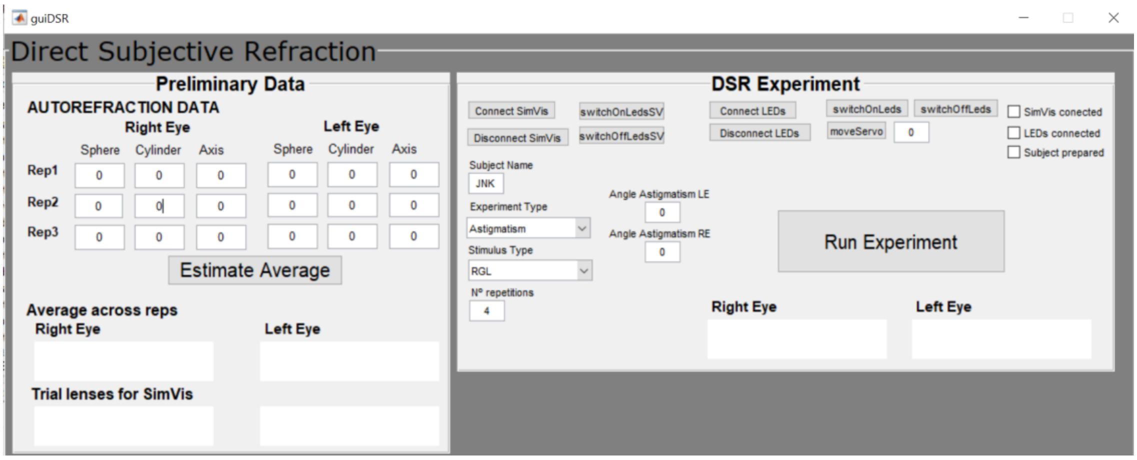

Figure 6.7. Graphical User Interface (GUI) for performing the Direct Subjective Refraction method in a clinical environment using a clinical prototype. The functions included estimation of the average across repetitions of the objective refraction, the starting point for the DSR method, connection to the display, connection to SimVis Gekko, performing the spherical equivalent experiment, and the full prescription experiment, among others.

6.2.3. Pilot experiments

Several pilot experiments were carried out to refine the parameters of the TDW and the stimulus. The goal of these pilot experiments performed in the laboratory was to define the parameters of the experiment to be performed afterward in clinical sites. In these pilot experiments, we used the full prescription display.

6.2.3.1. Parameters of the temporal defocus wave (TDW)

The parameters of the TDW in the starting setup were 0.25D of amplitude and 15Hz of temporal frequency. This pilot experiment aims at optimizing the DSR task by maximizing the perceived flickering and the intensity of the chromatic distortions out of best focus. Five subjects judged qualitatively the differences perceived in changing the amplitude to 0.25D, 0.375D, and 0.50D while keeping the frequency fixed at 15Hz, and the differences perceived in changing the temporal frequency to 10, 15, and 20 Hz while keeping the amplitude fixed at 0.50D, using the B/R stimulus.

6.2.3.2.Overall luminance of the stimulus

The luminance of the new display could show many different light levels. The goal of this pilot experiment was to evaluate the influence of the overall luminance level on the performance of the DSR method. Five levels of overall luminance were measured: 10, 20, 30, 40, and 50 lumens (lm). The parameters of the TDW were 15 Hz and 0.25D of temporal frequency and amplitude, respectively, using the R/G stimulus. The spherical equivalent of each condition was used to compare the results. Figure 6.8 shows an image of the overall luminance change for the R/G stimulus.

Figure 6.8.Stimuli for the overall light level experiment. A. Stimulus with an overall luminance of 10 lm. **B.** Stimulus with an overall luminance of 30 lm. **C.** Stimulus with an overall luminance of 50 lm.

6.2.3.3. Chromatic balance

Chromatic balance refers to the luminance difference between the monochromatic colors in each eye, reducing the luminance of one monochromatic color while keeping the other monochromatic color unperturbed. The stimulus used was R/G with an overall luminance of 30 lm. Parameters of the TDW were 15Hz of temporal frequency and 0.50D of amplitude. Condition (or chromatic balance factor) is defined as the difference between the luminance of the monochromatic red and the monochromatic green (Equation 6.1). Negative values indicate that the monochromatic green dominates and positive values that the monochromatic red dominates. Conditions measured ranged from -0.50 (less red, more green) to +0.50 (less green, more red) in steps of 0.25. Spherical equivalent was used to compare across conditions. Figure 6.9 shows an image of the chromatic balance for the R/G stimulus.

$$CB = L_R - L_G \qquad 6.1$$

where CB means chromatic balance factor, L_R luminance of red component, and L_G luminance of green component.

Figure 6.9. Stimuli for chromatic balance experiment. A. Stimulus with a chromatic balance factor of -0.50. **B.** Stimulus with a chromatic balance factor of 0.00. **C.** Stimulus with a chromatic balance factor of 0.50.

Different stimulus

Three monochromatic LEDs were selected as candidates for the display. Theoretically, the dioptric difference between each of them varies, according to the LCA (Figure 6.1C), and may result in a different outcome. To test this hypothesis, 3 stimuli were designed: R/G, B/R, and G/B. The DSR method was performed with 15Hz of temporal frequency, 0.50D of amplitude, and 30 lm of luminance. Seven subjects participated in the R/G and B/R and four of them also in the G/B. The average spherical equivalent across subjects was used to compare the difference between subjects. Figure 6.4B shows an image of the different stimuli.

As the stimuli were different, the perceptual effects also varied slightly. In the B/R stimulus, reddish chromatic distortions appear when the mean of the TDW is on the hyperopic side of the retina and bluish chromatic distortions appear when the mean of the TDW is on the myopic side of the retina. In the R/G stimulus, reddish chromatic distortions appear when the mean of the TDW is on the hyperopic side of the retina and greenish chromatic distortions appear when the mean of the TDW is on the myopic side of the retina. In the G/B stimulus, greenish chromatic distortions appear when the mean of the TDW is on the hyperopic side of the retina and blueish chromatic distortions appear when the mean of the TDW is on the myopic side of the retina.

6.2.4. Experiment in clinical sites

After the selection of the best parameters for the experiment in pilot experiments, patients were recruited and measured at two clinical sites, a public hospital (Hospital Clinico San Carlos, Madrid, Spain) and the optometrist office in the research center (Instituto de Optica, Madrid, CSIC). The inclusion criteria were age range 18-75 years old, no ocular pathologies different from refractive error, spherical refractive error range from +6.00D to -10.00D and astigmatism <3.50D, and ocular transparent media. The exclusion criteria included visual acuity lower than 0.30 logMAR, history of strabismus, diplopia, other binocular vision abnormalities, iris coloboma, ocular surface pathologies or scars, systemic diseases or current medical prescription affecting the ocular health, and aphakic subjects. Measurements took less than 1 hour and were performed by an optometrist with more than 2 years of experience. The study followed the tenets of the Declaration of Helsinki. Study protocols were approved by the Hospital Clinico San Carlos Ethical Review Board. Subjects signed a consent form after receiving an explanation of the nature and possible consequences of the study.

<u>6.2.4.1. Refraction methods</u>

The refraction was obtained by three methods, Objective Refraction (OBR), Traditional Subjective Refraction (TSR), and Direct Subjective Refraction (DSR). The visual function with the refraction of each of them was compared after the evaluation.

The OBR was obtained using the autorefractometer BIO Huvitz Keratometer (Huvitz, Gunpo, South Korea). The average across 3 repetitions provided the final refraction and the standard deviation provided a measure of repeatability. The time taken to carry out all the repetitions was recorded with a chronometer. The measurement time of the OBR refraction was estimated as the average across three repetitions. As in clinical practice, the result of the OBR refraction was used as the starting point of the TSR and the DSR refractions.

The TSR was obtained following the conventional method for obtaining the subjective refraction described in section 2.4. In summary, the TSR method evaluated first the left eye, then the right eye, and finally a binocular adjustment. The result of the OBR was the starting point. The time taken to evaluate each of the phases was recorded with a chronometer. Measurement time for the TSR refraction was estimated as the addition of the time taken in every three phases. The measurement was carried out in a trial frame.

The DSR refraction was obtained using the setup described in the previous section for full prescription measurements. The DSR method requires alignment of the optical system, as well as a detailed explanation with demos that simulate the flicker effect before starting the measurement. To modify the TDW and perform the DSR method, patients were instructed in the DSR task and had the control of a keyboard. The average across 4 repetitions for each axis provided the refractive error, and the standard deviation provided the repeatability. First, the left eye was measured, then the right eye. The result of the OBR was considered the starting point. The time taken to explain the tasks and the demos were recorded with a chronometer, and the time taken for the DSR method in each eye (average time across 4 repetitions, for each axis) was recorded using MATLAB. Measurement time for the DSR refraction was the addition of the explanation, the demos, and the time of the DSR method.

6.2.4.2. Visual function

Usually, the suitability of any refraction is evaluated using mainly visual acuity. In this study, visual acuity, stereoacuity, perceptual visual quality with two tests, and refraction preference were performed.

Visual Acuity (VA) was measured using Sloan letters optotype in Stereoscopic Monitor (SM, LG49UH850V with a spatial resolution of 3840x2160 pixels) and the software Optonet (Cheshire, Reino Unido), in the left eye, the right eye, and in both eyes. For the TSR refraction, VA was already obtained during the method. The VA measurement was taken with the final refraction in trial glasses with trial lenses.

Stereoacuity was measured using a custom test consisting of 4 squares of 2.5x2.5 visual degrees made of random dot white squares of 0.12x0.12 visual degrees over a gray background. Of the 4 squares, only one of them had disparity and was therefore perceived in depth with crossed disparity (in front of the screen). The test consisted of images with disparities ranging from 1000 to 100 arc seconds in steps of 100, from 100 to 40 arc seconds in steps of 10, and from 40 to 0 in steps of 5 arc seconds. The test was presented on a TFT Toshiba monitor 13.3'' (Toshiba Portege Z30, Toshiba, Tokyo, Japan) at 40cm distance.

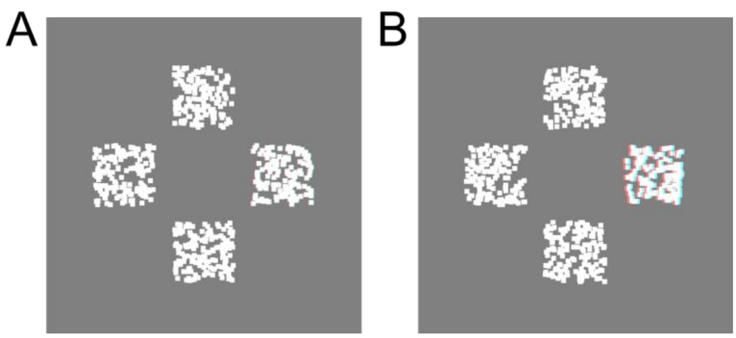

Figure 6.10. Custom stereoacuity stimulus using the anaglyph method. Green is perceived by the left eye and red by the right eye. **A**. Disparity of 60 arc seconds. **B.** Disparity of 300 arc seconds.

Visual quality was tested by presenting a natural image with different daily visual scenes[229] and was graded using the Visual Analogue Scale (VAS), where patients indicated their comfort from 0 to 100 on a black line 10cm long. The stimulus was presented in a TFT Toshiba at 1m distance.

6.2.4.3. Refraction preference

Overall satisfaction with the different refractions was directly compared using trial lenses in trial glasses looking at letters optotype of 0.2 logMAR size smaller than the maximum visual acuity of each patient. Refractions were compared in pairs: OBR vs. TSR, TSR vs. DSR, and DSR vs OBR.

6.2.4.4. Feedback about the Direct Subjective Refraction method

To obtain valuable feedback from patients about the DSR method, several questions were asked before finishing the visit:

1. Overall, what do you think about the Direct Subjective Refraction method?

2. Would it be easier if I (the clinician) press the buttons on the keyboard instead of you (the patient), or you feel comfortable?
3. Would you wear glasses prescribed with this new method?
4. Did you find useful the simulation DEMOs showed before for understanding and then performing the task?
5. Did you find it useful to perform a DEMO of the DSR task before beginning the actual measurement?

6.2.5. Statistical analysis

In the pilot experiments, the differences between conditions were evaluated with the spherical equivalent obtained in each. Besides, an ANOVA-n-way was used to evaluate the statistical significance of the condition, using the spherical equivalent average across subjects. In the experiment in clinical patients, the agreement among refraction methods was evaluated using Bland-Altman plots. Also, paired t-test was used to evaluate statistical differences. To analyze the statistical significance between groups of different sizes (age, clinical site), Mann-Whitney U-test was used. The statistical level to achieve statistical significance was set to 5% (p=0.05).

6.3. Results

6.3.1. Pilot Experiments

<u>Parameters of the temporal defocus wave (TDW)</u>
All subjects reported that, when varying the amplitude of the TDW between 0.25, 0.375, and 0.50D, at a temporal frequency of 15 Hz, the maximum flickering perception out of best focus was with 0.50D. Besides, while changing the temporal frequency to 10, 15, and 20Hz, subjects reported that the flicker was better perceived at 10Hz. Therefore, the optimum parameters of the TDW were 0.50D and 15Hz.

<u>Overall luminance of the stimulus</u>
Figure 6.11 shows the spherical equivalent (Figure 6.11A) and the amount of astigmatism (Figure 6.11B) obtained as a function of the overall luminance level for the left eye (circles) and right eye (squares) for one subject. The spherical equivalent averaged across luminance levels was -0.91±0.14 and -0.22±0.12D for the left and the right eye, respectively. The absolute amount of astigmatism averaged across luminance levels was 0.48±0.13D and 0.11±0.07D for the left and right eyes, respectively. There was no correlation between spherical equivalent and overall luminance (r=.27, p>.05) or astigmatism and luminance (r=.35, p>.05), suggesting that the overall luminance level does not affect the measurement. Besides, the subject subjectively preferred to perform the task at 30 lm, as it provided sufficient light without dazzle. Other subjects that did not perform this systematic study but evaluated the task with different light levels, also identified 30 lm as the preferred level. Thus, 30 lm was selected as the overall luminance level for the experiments.

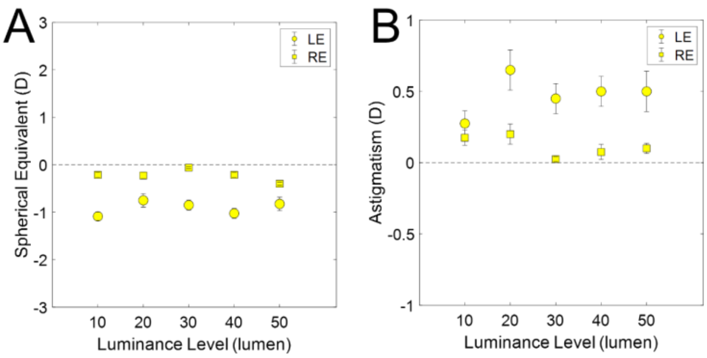

Figure 6.11. Overall luminance pilot experiment. Spherical equivalent as a function of the luminance level. Error bars indicate the average standard deviation across repetitions for both axes (error bars in A and B for each datapoint are the same, although the y-axis limits differ). Circles mean left eye and squares mean right eye. **A.** Spherical equivalent. **B.** Astigmatism.

Chromatic balance

In this experiment, the luminance of one monochromatic color was changed while keeping the other fixed. Negative values of the chromatic balance factor indicate more amount of green than red and positive values that the amount of red was higher than green (Equation 6.1). Figure 6.12 shows the spherical equivalent (Figure 6.12A) and the amount of astigmatism (Figure 6.12B) as a function of the chromatic balance for the left (circles) and right eye (squares) and one subject. The spherical equivalent averaged across conditions is -0.62±0.12D and -0.3±0.06D for the left eye and right eye, respectively. There was no correlation between spherical equivalent and chromatic balance factor (r=.66, p>.23) or astigmatism and luminance (r=-.40, p>.49), suggesting that chromatic balance factor does not influence the result. The absolute amount of astigmatism averaged across luminance levels was 0.23±0.16D and 0.12±0.07D for the left and right eyes, respectively. In this case, the subject was more comfortable performing the task with more amount of red than green (condition +0.50). The visual system is more sensitive to green light, and the red channel multiplier must compensate for the excess brightness perceived in the green channel.

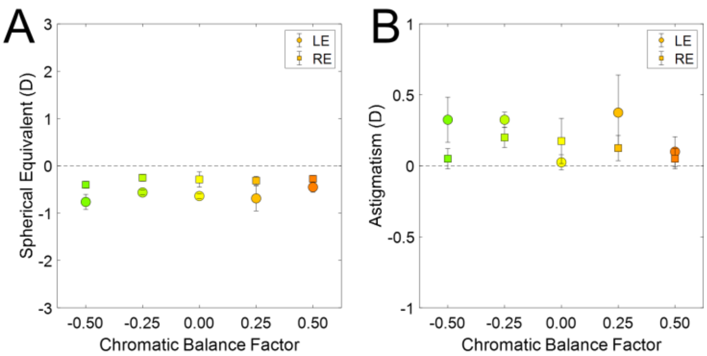

Figure 6.12. Chromatic balance pilot experiment. Spherical equivalent as a function of the chromatic balance factor. Error bars indicate the average standard deviation across repetitions for both axes (error bars in A and B for each datapoint are the same, although the y-axis limits differ). Circles mean left eye and squares mean right eye. Colors mean chromatic difference condition (the greener the more proportion of green in the stimulus, the redder the more proportion of red on the stimulus). **A.** Spherical equivalent. **B.** Astigmatism.

Different stimulus

The spherical equivalent (Figure 6.13A) averaged across subjects for Blue/Red (B/G), Red/Green (R/G), Green/Blue (G/B) was -0.59±0.60D, -0.50±0.64D, and -0.65±0.41D for the left eye, respectively, and -0.50±0.64D, -0.59±0.60D, and -0.65±0.41D, respectively, for the right eye. There was no statistical difference between the different stimuli (paired t-test *p*>.05 for comparison between B/R vs. R/G and both eyes, and Mann-Whitney U-test *p*>.05 for comparison between B/R and R/G vs. G/B stimulus for both eyes).

The absolute amount of astigmatism (Figure 6.13B) averaged across subjects for B/R, R/G, and G/B was 0.49±0.77D, 0.25±0.30D, and 0.27±0.27D for the left eye, respectively, and 0.43±0.27D, 0.35±0.51D, and 0.12±0.08D, respectively, for the right eye. There was no statistical difference between the different stimuli (paired t-test *p*>.05 for comparison between B/R vs. R/G and both eyes, and Mann-Whitney U-test *p*>.05 for comparison between B/R and R/G vs. G/B stimulus for both eyes, except for R/G vs. G/B in the right eye, which reports statistically significant differences *p*<.05).

The average standard deviation across subjects for B/R was ±0.24 and ±0.31D, for the left and the right eye, R/G was ±0.27D and ±0.14D, for the left and the right eye, and G/B was ±0.23D and 0.20D for the left and the right eye. Results suggest that R/G is the stimulus that subjects performed better, which corresponds to the subjective preference of the subjects that, in general, reported that the task was more easily performed with the R/G stimulus.

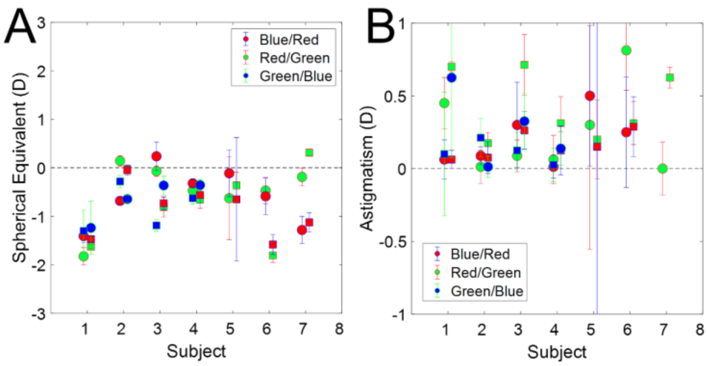

Figure 6.13. Different stimuli pilot experiment. Error bars indicate the average standard deviation across repetitions for both axes (error bars in A and B for each datapoint are the same, although the y-axis limits differ). Circles mean left eye and squares mean right eye. Blue edge and red filling mean Blue/Red (B/R) stimulus. Red edge and green filling mean Red/Green (R/G) stimulus. Green edge and blue filling mean Green/Blue (G/B) stimulus. **A.** Spherical equivalent for each subject. **B.** Astigmatism for each subject.

6.3.2. Direct Subjective Refraction method for prescription

In total, 40 patients were recruited. Seven of them were discarded because they were not able to perform the DSR task within the 1-hour timeframe of the measurements. Of the 33 remaining patients (age 34.9±11.6 years old), 18 were evaluated at the Hospital Clinico San Carlos (Madrid, Spain) and 15 in the optometry office of the Institute of Optics (Madrid, Spain). Visual acuity was >0.1 logMAR in all subjects. One subject reported color dyschromatopsia (protanopia), discovered while performing the DSR task, but he was able to perform the task without problems (see section 6.4).

Figure 6.14 shows two example subjects performing the DSR task for the left and right eye. Each graph shows the mean optical power of the TDW as the experiment progress, for different repetitions (4 repetitions per axis). Green lines represent the myopic axis and red lines the hyperopic axis. The endpoint of each line represents the final point of each repetition, where the subject perceived minimum flicker and chromatic distortions. The average and standard deviation across repetitions (endpoints) are displayed as a shaded green or red bar, depending on the axis evaluated. The starting point was the objective refraction. Figure 6.14A shows one representative subject that performs the task with a very low standard deviation, where all the repetitions for each axis converge to a common point (average standard deviation across axes and eyes 0.09D). Figure 6.14B shows a representative example of a subject that did not perform well, likely due to a misunderstanding of the task, resulting in an average standard deviation (across axes and eyes) of 0.89D. As can be seen, this subject seems to press buttons randomly, without any logic, which explains the result obtained.

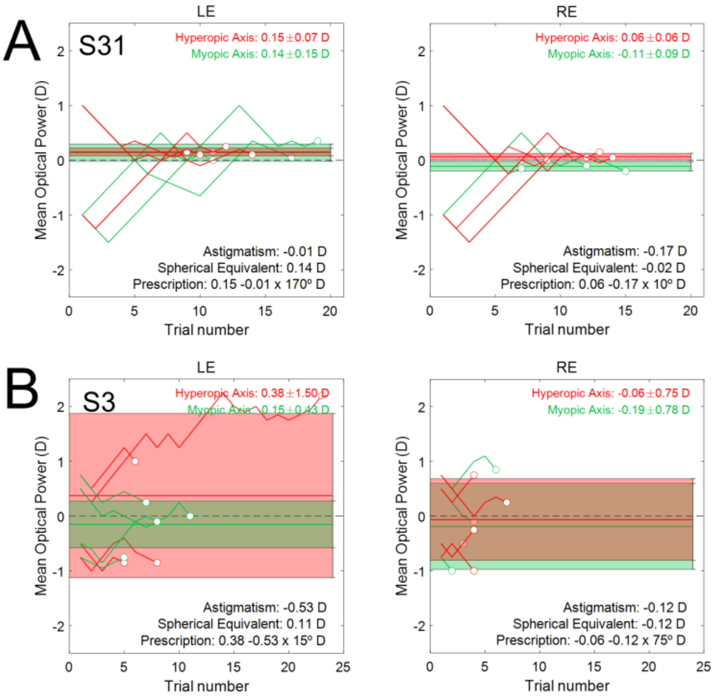

Figure 6.14. Direct Subjective Refraction provides a complete prescription. A. Subject who performed very well in the DSR task (S31). **B.** Subject that did not perform correctly the DSR task (S3).

<u>Analysis by groups</u>

Figure 6.15 shows the standard deviation of all subjects, sorted. The standard deviation of each subject was estimated as the average across axes and eyes. We divided subjects into 3 regions. The green region included subjects with a standard deviation equal to or below 0.28D (the intra-optometrist error of the traditional subjective refraction from the literature[161]). The yellow region included subjects with a standard deviation higher than 0.28D and lower than twice the intraoptometrist error (±0.56D). The red region included subjects with a standard deviation higher than twice the intraoptometrist error (0.56D).

In the protocol for all refractions, the left eye was first evaluated, and then the right eye. Some subjects reported that were more confident while performing the DSR task in the second eye (right eye). Therefore, we analyzed if any training effect could be inferred by comparing the average standard deviation for all subjects in the left eye versus the right eye. The averages were 0.54±0.29D and 0.46±0.4D, for the left and the right eye, respectively, although no statistical difference was found (paired t-test p>.05), suggesting no learning effect.

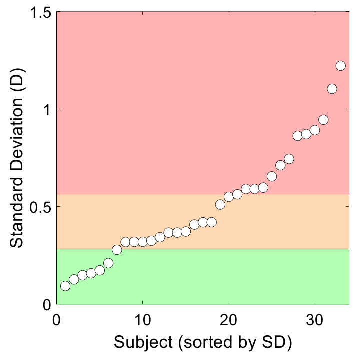

Figure 6.15. Standard deviation of the DSR refraction for all subjects, sorted by standard deviation. Three regions are indicated: green region (SD<0.28D), yellow region (0.28>SD>0.56), and red region (>0.56D).

Figure 6.16 shows the standard deviation for all subjects evaluated at the Hospital Clinico San Carlos (HSCS) site and for all subjects evaluated at the Institute of Optics (IO-CSIC) site. The average standard deviation across subjects was 0.54±0.24D and 0.41±0.38D for HSCS and IO-CSIC. Although the average is slightly lower for the IO-CSIC venue than for the HSCS venue, differences were not statistically significantly different (Mann-Whitney U-test *p*>.05).

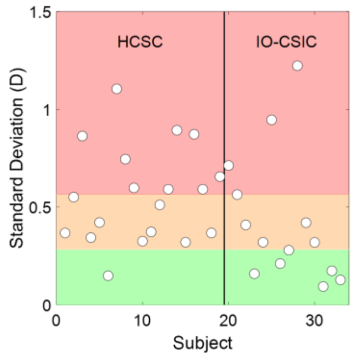

Figure 6.16. Standard deviation of the DSR refraction for all subjects, differentiating between venues. Left side: subjects measured at Hospital Clinico San Carlos (HCSC). Right side: subjects measured at Institute of Optics (IO-CSIC).

Figure 6.17 shows the average standard deviation sorted by age. Three groups were considered: young, lower than 30 years old, pre-presbyope, between 30 and 45 years old, and presbyope, older than 45 years old. The average standard deviation for the young group is 0.38±0.24D, for the pre-presbyope group is 0.51±0.16D, and for the presbyope group 0.71±0.31D. Mann-Whitney U-test for different sample sizes reports a non-significant difference between young and pre-presbyope groups and between pre-presbyope and presbyope groups (*p*>.05) and reports a significant difference between young and presbyope groups (*p*<.05).

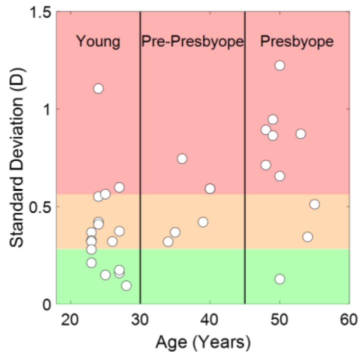

Figure 6.17. Standard deviation of the DSR refraction for all subjects, differentiating age groups: young (<30 years old left), pre-presbyope (between 30 and 45 years old, middle), and presbyope, (>45 years old, right).

<u>Comparison of refraction methods</u>

Figure 6.18 shows in power vector notation (spherical equivalent, M, horizontal astigmatism, J_0, and oblique astigmatism, J_{45}) the refraction obtained for all subjects with the Objective Refraction (OBR) method. The average and standard deviation across subjects for M were -1.18±1.98D and -1.42±2.31D for the left and the right eye, respectively; for J_0 is 0.21±0.54D and 0.17±0.38D for the left and the right eye, respectively; for J_{45} is -0.05±0.26D y 0.04±0.33D for the left and the right eye, respectively.

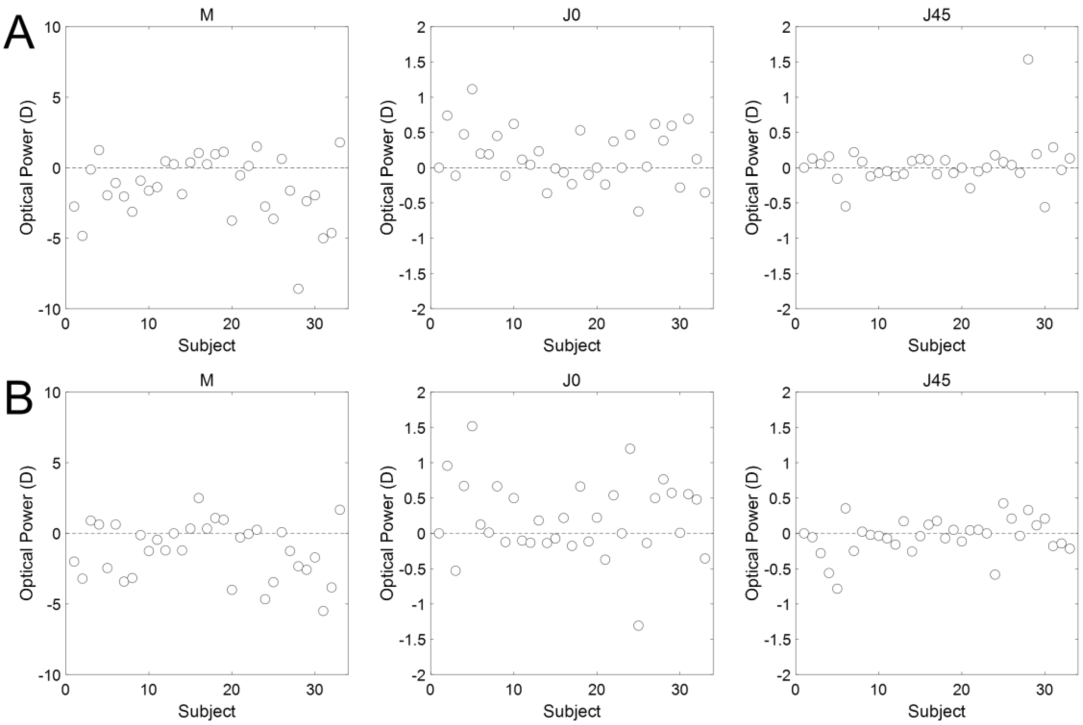

Figure 6.18. Results of the Objective Refraction (OBR) for all subjects. A. Left eye. **B.** Right eye.

Figure 6.19 shows the refraction obtained for all subjects with the Traditional Subjective Refraction (TSR) method. The average and standard deviation across subjects for M were -1.0±1.89D and -1.18±2.1D for the left and the right eye, respectively; for J_0 is 0.22±0.44D and -0.14±0.36D for the left and the right eye, respectively; for J_{45} is -0.05±0.21D and 0.03±0.25D for the left and the right eye, respectively.

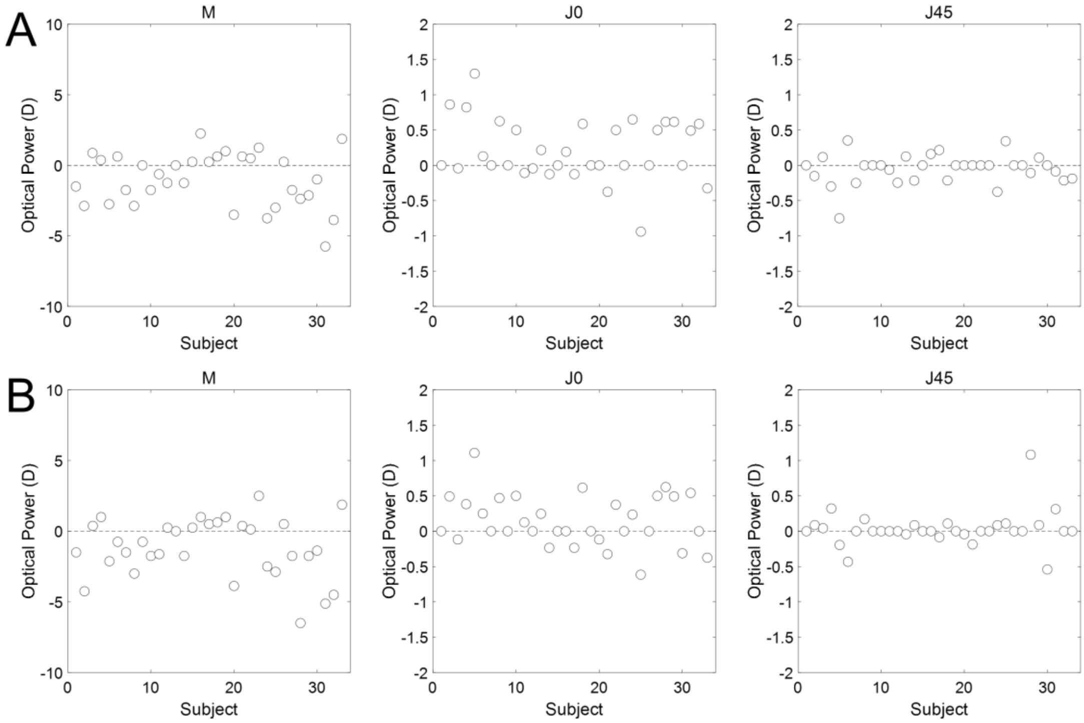

Figure 6.19. Results of the Traditional Subjective Refraction (TSR) for all subjects. A. Left eye. **B.** Right eye.

Figure 6.20 shows the refraction obtained for all subjects with the Direct Subjective Refraction (TSR) method. The average and standard deviation across subjects for M -1.77±1.97D and -1.83±2.02D for the left and the right eye, respectively; for J_0 0.26±0.60D and 0.24±0.64D for the left and the right eye, respectively; for J_{45} is 0.0±0.40D and -0.03±0.28D for the left and the right eye, respectively.

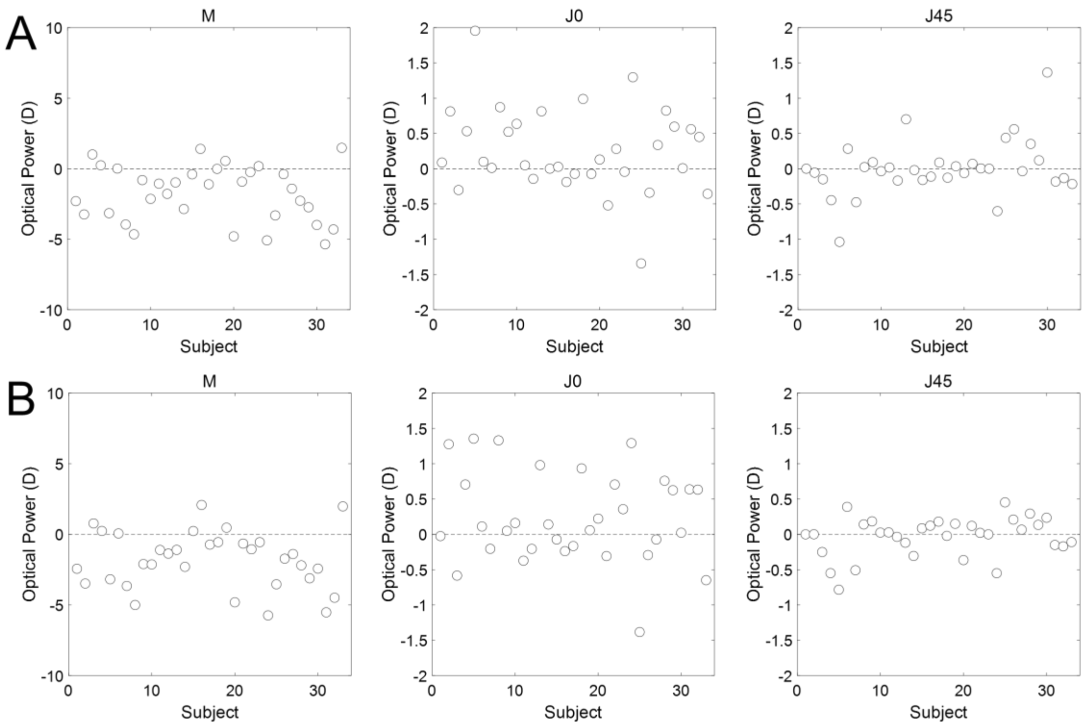

Figure 6.20. Results of the Direct Subjective Refraction (DSR) for all subjects. A. Left eye. **B.** Right eye.

The following figures show the comparison between refraction methods using Bland-Altman analysis, which plots the difference versus the mean of the methods compared, indicating in the figure the Limits of Agreement (LOAs) and the mean and standard deviation of the difference.

Figure 6.21 shows the Bland-Altman plots of the objective refraction (OBR) vs. the traditional subjective refraction (TSR). The result obtained for M component was -0.18±0.48D (LOAs: [-1.12 to 0.77]D) and -0.24±0.52D (LOAs: [-1.27 to 0.79]D) for the left and right eye, respectively; for J_0 component -0.01±0.17 D (LOAs: [-0.34 to 0.32]D) and 0.03±0.10D (LOAs: [-0.18 to 0.23]D) for the left and right eye, respectively; and for J_{45} component 0.00±0.14D (LOAs: [-0.27 to 0.28]D) and 0.01±0.12D (LOAs: [-0.22 to 0.24]D) for the left and right eye, respectively.

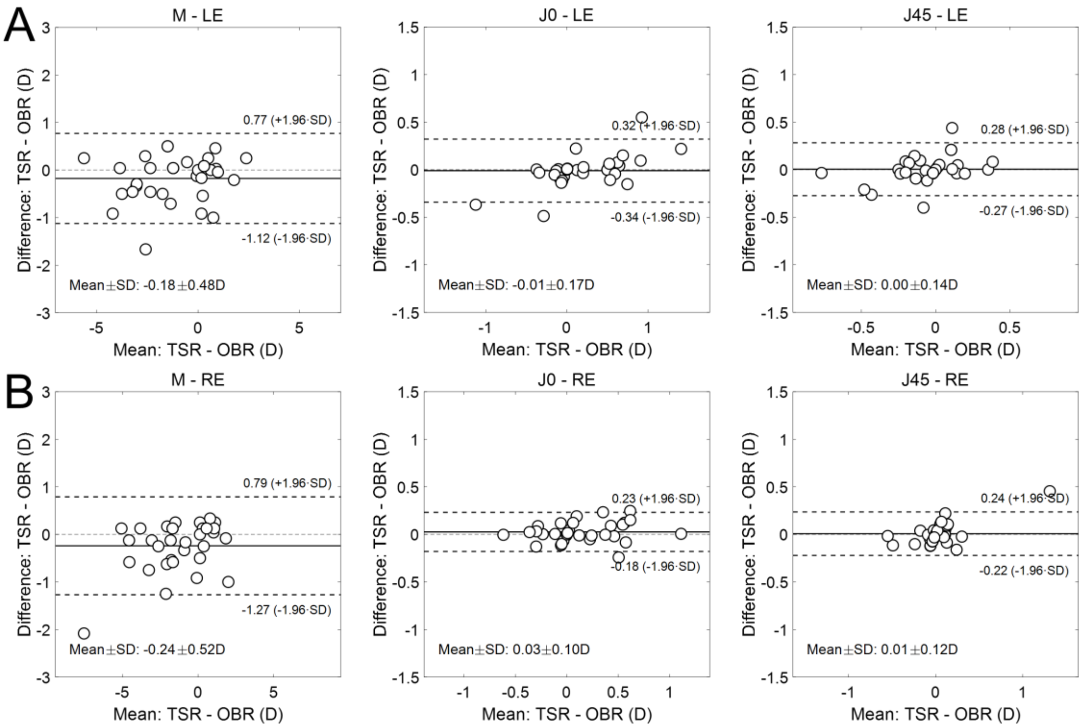

Figure 6.21. Bland-Altman analysis for TSR vs OBR refractions. Each panel shows a Bland-Altman plot, indicating the Limits of Agreement (LOAs, 95% Confidence Interval), mean, and standard deviation of the sample. **A.** Plot comparing M, J_0, and J_{45} for the left eye. **B.** Plot comparing M, J_0, and J_{45} for the right eye.

Figure 6.22 shows the Bland-Altman plots of the TSR vs. the Direct Subjective Refraction (DSR). The result obtained for M component was -0.77±0.71D (LOAs: [-2.16 to 0.63]D) and -0.66±1.36D (LOAs: [-3.33 to 2.02]D) for the left and right eye, respectively; for J_0 component -0.04±0.28D (LOAs: [-0.50 to 0.59]D) and 0.10±0.43D (LOAs: [-0.74 to 0.93]D) for the left and right eye, respectively; and for J_{45} component 0.06±0.31D (LOAs: [-0.56 to 0.67]D) and -0.06±0.38D (LOAs: [-0.80 to 0.68]D) for the left and right eye, respectively.

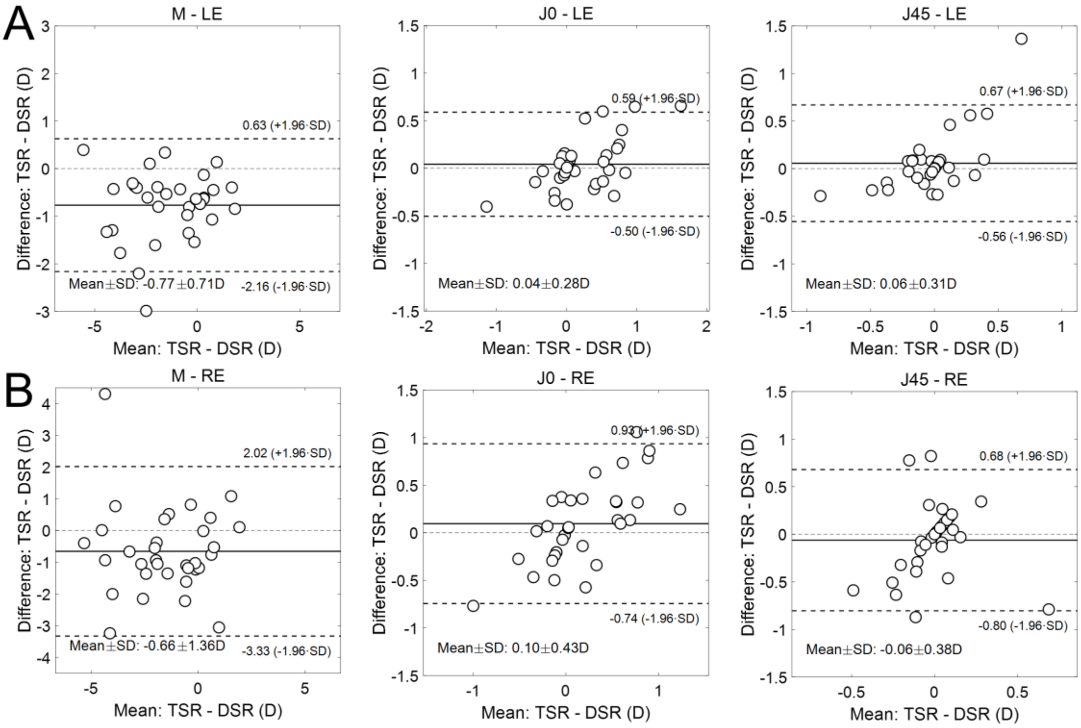

Figure 6.22. Bland-Altman analysis for TSR vs DSR refractions. Each panel shows a Bland-Altman plot, indicating the Limits of Agreement (LOAs, 95% Confidence Interval), mean, and standard deviation of the sample. **A.** Plot comparing M, J_0, and J_{45} for the left eye. **B.** Plot comparing M, J_0, and J_{45} for the right eye.

Figure 6.23 shows the Bland-Altman plots of the OBR vs. the DSR. The result obtained for M component was -0.59±0.55D (LOAs: [-1.68 to 0.49]D) and -0.42±1.60D (LOAs: [-3.55 to 2.72]D) for the left and right eye, respectively; for J_0 component 0.05±0.22D (LOAs: [-0.39 to 0.49]D) and 0.07±0.42D (LOAs: [-0.76 to 0.90]D)for the left and right eye, respectively; and for J_{45} component 0.05±0.25D (LOAs: [-0.43 to 0.54]D) and -0.07±0.44D (LOAs: [-0.93 to 0.79]D) for the left and right eye, respectively.

In the comparison between all components of the refraction (M, J_0, J_{45}), both eyes (left and right eye), and all the refraction methods (OBR, TSR, DSR), there were no statistical significance differences (paired t-test in all comparison p>.05) except when comparing M obtained with the OBR, TSR, and DSR for the left eye and comparing M obtained with OBR vs TSR and with TSR vs DSR (paired t-test in all comparison p<.05).

In terms of time taken per repetition, for the OBR the time was estimated as the average across 3 measurements, for the TSR the time was measured while performing the task, and for the DSR was estimated as the addition of the time for alignment, for explaining the task, and the average across repetition for the two axes and each eye. The average time per repetition took 0.63±0.27min for OBR, 9.52±2.26 min for TSR, and 3±0.45 min for DSR, being statistically significantly different (paired t-test p<.05). For all subjects, the OBR method was the fastest, then DSR method and the slowest was TSR method.

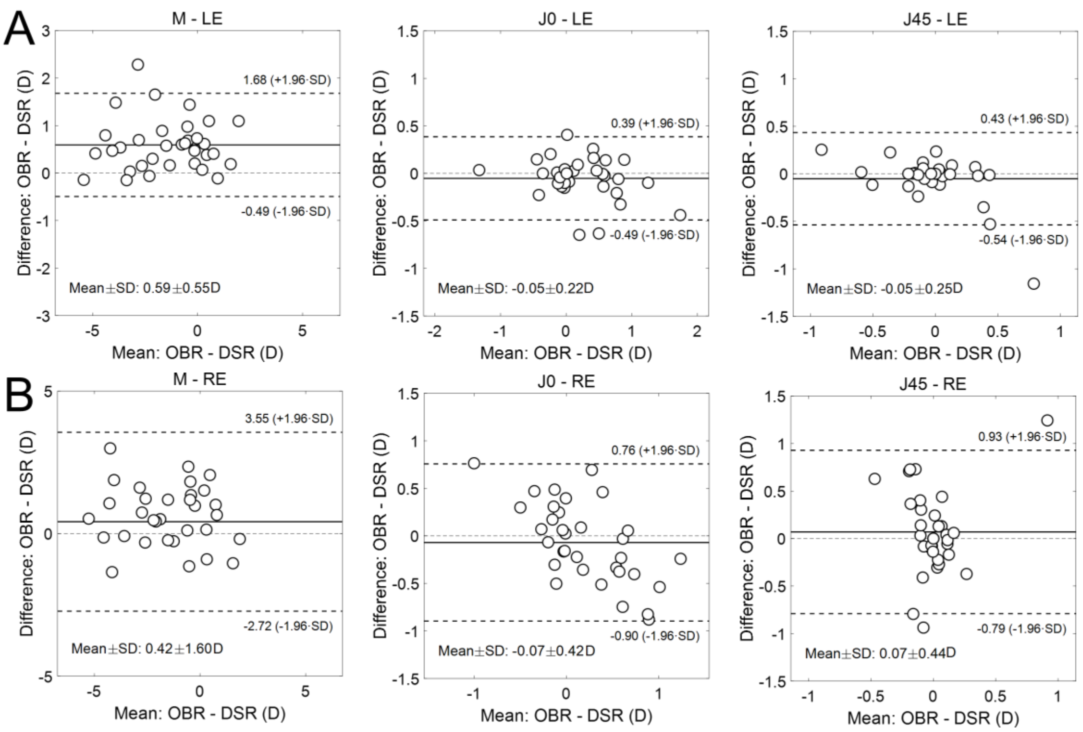

Figure 6.23. Bland-Altman analysis for OBR vs DSR refractions. Each panel shows a Bland-Altman plot, indicating the Limits of Agreement (LOAs, 95% Confidence Interval), mean, and standard deviation of the sample. **A.** Plot comparing M, J_0, and J_{45} for the left eye. **B.** Plot comparing M, J_0, and J_{45} for the right eye.

The optical quality obtained with each refraction method was very similar. For visual acuity (VA), the average and standard deviation across subjects were -0.08±0.06, -0.08±0.05, and -0.04±0.16 logMAR for OBR, TSR, and DSR, respectively. Besides, there was no statistical significance difference among them (paired t-test p>.05 in all comparisons). For stereoacuity, the average and standard deviation across subjects were 188.79±254.13, 179.24±255.23, and 205±264.83'' for OBR, TSR, and DSR, respectively. There was no statistical significance difference between refraction methods (paired t-test p>.05 in all comparisons). For the Visual Analogue Scale (VAS) test, the average and standard deviation across subjects were 8.71±0.83, 8.69±1.34, and 6.38±2.64 cm for OBR, TSR, and DSR, respectively. There was a statistical significance difference between DSR vs. TSR and DSR vs. OBR (paired t-test p<.05) and no statistical significance difference between TSR vs. OBR (paired t-test p>.05). When directly comparing the prescription obtained with the different refraction methods, 57% subjects preferred the TSR over the OBR; 64% preferred the TSR over the DSR, and 50% preferred the DSR over the OBR.

<u>Analysis of patients performing the DSR task correctly</u>

To account for the effect on patients that understood and performed the task correctly, we analyzed the results of only (7) patients with an average standard deviation lower than 0.28D (Figure 6.15, green region). Comparing the Bland-Altman plots only for the DSR and TSR methods (Figure 6.24), the result obtained for the M component was -0.34±0.53D (LOAs: [-1.39 to 0.70]D) and -0.63±1.44D (LOAs: [-3.45 to 2.20]D) for the left and right eye, respectively; for the J_0 component -0.10±0.13D (LOAs: [-0.36 to 0.16]D) and -0.03±0.42D (LOAs: [-0.84 to 0.79]D) for the left and right eye, respectively; and for the J_{45} component 0.06±0.23D (LOAs: [-0.39 to 0.51]D) and 0.05±0.40D (LOAs: [-0.73 to 0.84]D) for the left and right eye, respectively. In all components for both the left and the right eye, the standard deviation of the difference improved (improvement higher in the left eye). The most remarkable improvement is the one found in the M component of the left eye, from -0.77±0.71D to -0.34±0.53D, similar to the results reported in Chapter

4 for the measurement of the spherical equivalent. There were non-significant differences among all components of refractions (paired t-test $p>.05$ in all comparisons).

In terms of visual function, average visual acuity was the same for all refraction methods (-0.11 logMAR), VAS metric reported averages of 9.10±0.77, 8.89±1.29, and 7.92±1.52 cm for OBR, TSR, and DSR, with non-significant differences among them (paired t-test $p>.05$ in all comparisons). When directly comparing the prescription obtained with the different refraction methods, 57% of the subjects preferred the OBR over the TSR; 57% preferred the DSR over the TSR, and 80% preferred the DSR over the OBR.

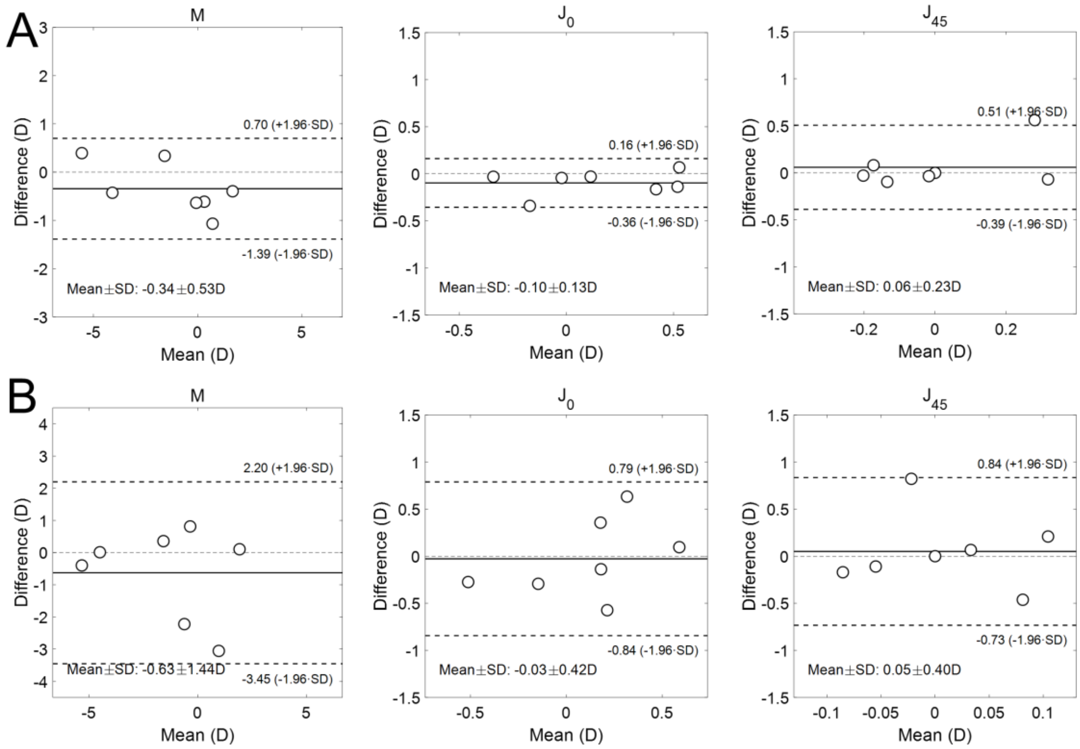

Figure 6.24. Bland-Altman analysis for TSR vs DSR refractions for subjects with an average standard deviation in the DSR refraction lower than 0.28D. Each panel shows a Bland-Altman, indicating the Limits of Agreement (LOAs, 95% Confidence Interval), mean, and standard deviation of the sample. **A.** Plot comparing M, J_0, and J_{45} for the left eye. **B.** Plot comparing M, J_0, and J_{45} for the right eye.

Feedback from the patients

After finalizing all the experimental measurements, we asked the patients several questions to obtain feedback about the Direct Subjective Refraction method. For the question '*In overall, what do you think about the Direct Subjective Refraction method in terms of difficulty?*', 53% of the patients considered the task easy, 40% hard, and 7% medium difficulty. For the question '*Would it be easier if I (the clinician) press the buttons on the keyboard instead of you (the patient), or do you feel comfortable?*', 93% of the patients were comfortable with pressing the buttons. For the question '*Would you wear glasses prescribed with this new method?*', 40% of the patients would, 40% would not, and 20% were not confident enough to provide an answer. For the questions '*Did you find useful the simulation DEMOs showed before for understanding and then performing the task?*' and '*Did you find it useful to perform a DEMO of the DSR task before beginning the actual measurement?*', 93% of the patients found it useful for performing later the task.

6.4. Discussion

This study reports the first use of the direct subjective refraction method in a clinical environment. Many technological developments were required to accomplish this goal, most of them described in section 6.2 of this chapter. The technology evolved in the direction of a clinical product. The first steps were replacing a commercial display and an on-bench setup with a custom and portable LED display and a wearable device for optical manipulation. This study also reports the process followed to select the optimal parameters of the psychophysical method, that improved the performance of the DSR task.

Direct Subjective Refraction method

In pilot experiments, we have demonstrated that changing the overall luminance of the custom display (Figure 6.11), the proportion of monochromatic colors (Figure 6.12), and the monochromatic components (Figure 6.13), do not substantially affect the outcome of the DSR task. This result suggests that the Direct Subjective Refraction method provides a robust measurement independent of the chromatic features of the stimulus.

In the DSR method, age seems to play a role. We have found that young patients perform statistically better than presbyope subjects (Figure 6.17). In addition, the 7 patients discarded were presbyopes (older than 54 years). This influence of age in the DSR task may be explained by an increase in the scattering (due to a less transparent crystalline lens, or even to a subclinical cataract[10,11]) or by the increasing of the spherical aberration[276,277]. Both effects will decrease the optical quality and increase the depth of focus, and therefore decrease the sensitivity to defocus. Moreover, it has been reported that the peak of the temporal contrast sensitivity function (TCSF), usually around 10 Hz, is shifted to lower temporal frequencies in older subjects[64]. In the DSR method, the temporal frequency of the TDW was 15Hz, which may have produced a lower sensitivity in this group of patients.

One of the patients in the study was identified as color-blinded (protanopia) while performing the DSR measurements (he was previously unaware of his optical condition). He was able to perform the DSR task, although with moderate performance (SD ±0.87 and ±0.27D in the left and right eye, respectively). The DSR task is based on minimizing flicker and chromatic distortions produced by the TDW that appeared in the red or the green components, depending on the position of the TDW with respect to the retina. In this case, the chromatic distortions were not perceived by the patient, but, due to the different spatial locations of the red and green components, he was able to perceive the flicker changing from one location to another. Some studies have also found that color-blinded subjects were able to perform stereoacuity tests based on anaglyph filters, but with a decrease in their performance, similar to what was found in this study[278,279]. Although more tests need to be performed, this result suggests that the DSR task is also possible in patients with color-blind conditions.

Seven patients were able to perform the DSR task with maximum repeatability. We believe that these patients understood the task perfectly and, during the demos, they were able to perceive when green components or red components individually, knowing exactly what to do. In this sample, perceived visual quality evaluated with the VAS metric was slightly higher with the TSR refraction (8.89±1.29 cm) than with the DSR refraction (7.92±1.52 cm), there was no statistically significant difference. However, in direct comparisons, the DSR refraction was preferred over the TSR refraction in 57% of the patients. However, only 7 out of 33 (21%) were able to perform correctly. This result, although encouraging to demonstrate the potential implementation of the DSR method in the clinic, shows that further investigation is needed to understand why some patients could not even perform the task, or why others reported low repeatability (high standard deviation).

6.5. Conclusions

This chapter shows the first use of the Direct Subjective Refraction method in a clinical environment with real patients. We have developed a new clinical prototype and demonstrated that patients of all ages (older than 18 years old) can perform the visual task. But we have also identified some difficulties in the task and the method, affecting an important number of patients, that need to be overpassed by improving the technology, using personalized parameters of the temporal defocus wave and developing new measurement protocols. Although the technology needs more maturation, this chapter already shows a strong potential of the DSR method for clinical measurements.

Chapter 7. Monovision corrections and eye dominance

In this chapter, we have measured the impact of eye dominance in the selection of the best monovision correction.

This chapter is based on the article by Victor Rodriguez-Lopez et al. *"Ocular dominance measurements and monovision correction preference"* submitted to *Translational Vision Science and Technology* (2022). The co-authors of the study are Xoana Barcala, Amal Zaytouny, Carlos Dorronsoro, Eli Peli, and Susana Marcos.

The contribution of the author of the thesis was the conceptualization and design of the study with Susana Marcos, Carlos Dorronsoro, and Xoana Barcala, the literature research in collaboration with Susana Marcos, the design of the experiments in collaboration with Carlos Dorronsoro, the collection and analysis of the data in collaboration with Amal Zaytouny, the writing of the chapter in collaboration with Susana Marcos and the editing of the chapter in collaboration with all co-authors.

This work was presented as a virtual oral contribution by Xoana Barcala at the Association for Vision and Research in Ophthalmology (ARVO) virtual meeting in 2021.

7.1. Introduction

Previous chapters have tackled different aspects of dynamic blur and its use for estimating the refractive state of the eye. This chapter uses programable blur to improve the prescription of monovision, one of the most popular solutions for presbyopia, that induces static interocular blur differences. Particularly, the chapter studies the role of ocular dominance in monovision corrections.

Monovision is a widespread treatment strategy for presbyopia, the age-related loss of dynamic focusing of the eye from distance to near vision. Conventional monovision clinical practice involves correcting the dominant eye for distance[167–169] and the non-dominant eye for near.

Numerous tests for ocular dominance have been proposed in the literature and a few are performed clinically, yet it is not clear whether the dominance that they capture is relevant to the prescription of monovision. The tests used can be grouped into three categories[170]: 1) binocular rivalry tests; 2) determining the eye with better visual acuity, contrast sensitivity, or other measures of visual functioning; and 3) sighting dominance, which identifies the eye that is selected to look at a (distant) target (such as the 'hole in the card' test[171]). While the results of tests within each category are generally matching, provided that the conditions of the tests are comparable, there is a high degree of disagreement across categories.

Blur suppression is supposedly easier in the nondominant eye[280,281]. For this reason, several proposed ocular dominance tests rely on finding the eye that best suppresses the signals that contain artifacts (such as blur) and assigns the contralateral eye to be the dominant eye (sensory dominant by inhibition). When images provided to the left and right eye are so dissimilar that they cannot be fused, the observer experiences alternating suppression and dominance of each monocular stimulus. Traditional psychophysical tests based on binocular rivalry measure the relative duration of the period of dominance in each eye, which may be considered a measurement of eye dominance (see Evans 2007[97] for a review). There have been proposals to use rivalry tests to identify the dominant eye in the clinic, for possible applications in monovision management. Yang et al.[282] developed a new interocular suppression technique based on measured reaction times to the presence of Gabor patches on Mondrian noise. However, the dominant eye identified by binocular rivalry methods appears to depend on the variables of the test[283] and the retinal location[284]. These tests (modified version by Squier[285]) failed to capture systematic changes in the laterality of ocular dominance when comparing distance to near targets in patients with anisometropia[286], as would have been expected in subjects with a difference in interocular blur. Furthermore, features of the visual stimulus (size, contrast, brightness, color) in the test (generally Gabor patches of different orientations) appear to influence the dominance strength[283], as they may be eliciting different mechanisms[48].

Examples of studies showing discrepancies across tests include Coren and Kaplan[172] (13 tests on 54 normal subjects), Seijas et al.[173] (9 tests on 51 patients), Ross et al.[174] (4 tests on 8 patients), and Garcia-Perez and Peli (5 tests on 40 subjects). In extreme cases (for example, amblyopes or subjects with severe monocular impairment), it is expected that the eye used for aiming a target matches that with better optics or visual function[174]. However, several studies show that, in general, contrast sensitivity is not necessarily worse in the weaker eye than in the stronger eye, measured using a binocular rivalry test[287]. There is also strong evidence that the sighting eye dominance and sensory dominance do not necessarily reside in the same eye of an individual[175,288]. This supports some hypotheses that sighting eye dominance does not even have a relevant underlying physiological cause and may just be the result of a 'habit'[170].

The clinical literature on the impact of the choice of the eye on the outcomes of monovision is contradictory, likely as a result of the lack of a well-defined test for ocular dominance and even a conclusive definition of eye dominance itself (and whether this is unique to a patient). Malott et al.[289] speculated that agreement between the dominant eye determined by identifying the eye that was most sensitive to blur and by sighting dominance enhanced the chances of successful monovision adaptation. However, given the frequent lack of correspondence between those dominance test results, the conclusion seems to be questionable and in conflict with the views of others who find that a strong dominance may be associated with unsuccessful monovision correction[290]. Along the same lines, Seijas et al.[173] concluded that in general there is no strong dominance in normal patients. The authors inferred that the monovision is usually well tolerated but should be avoided in patients with clear dominance. It is likely that the poor predictability of sighting eye dominance also explains the unexpected results in high myopic eyes pseudophakic patients of Xung et al. (in a prospective randomized study)[291] and Zhang et al. (in a retrospective study)[292] who found no statistical difference in visual outcomes of monovision with the distance correction in the dominant eye (conventional monovision) of the distance correction in the non-dominant eye (crossed monovision).

Differences in the effect of ocular dominance on vision in patients treated with monovision may be affected by both the method to measure eye dominance and select the dominant eye and the method to measure visual outcomes. For example, Nitta et al.[293] found that monovision treatments produced larger degradation of near visual acuity and binocular contrast sensitivity at low spatial frequencies in patients with large sensory dominance imbalances but it did not degrade near stereoacuity. In general, the selection of the dominant eye appears to have a larger effect on distance binocular contrast sensitivity than on visual acuity[294].

The sensory dominance test is usually evaluated by introducing monocular blur with trial (repeating the process several times) or with contact lenses. The amount of blur used is usually +1.50D. The patient reports the eye that feels less comfortable in the presence of blur, considering that eye the dominant. With trial lenses, interocular differences in magnification may appear. Besides, the lenses must be changed manually. Contact lenses allow a more faithful representation of monovision, comparing the vision produced by changing the blur is more difficult as implies changes in the contact lenses.

Binocular, simultaneous, vision simulators allow the presentation of monovision corrections[29]. The SimVis Gekko is a head-mounted simulator using optotunable lenses which are projected on the eye's pupil plane, allowing a rapid shift between conventional (distance vision in the dominant eye) and crossed monovision (near vision in the dominant eye). The system allows subjects to see the real world, or images projected on a display (distance or near) through the selected correction. In earlier studies[229,295], we introduced the Multifocal Acceptance Score (MAS-2EV), a rapid, clinically suitable test that uses natural images to assess perceived visual quality with presbyopic corrections (multifocal lenses, monovision, and modified monovision) at near/distance, day/night conditions.

In this study, we present a two-interval forced choice preference procedure (Preferential test) through the SimVis Gekko as a potential sensory eye dominance test to directly select the optimal monovision combination and the strength of the eye dominance based on the repeatability of the preferred choice. For monovision prescription, this could be taken as a measure of the eye dominance that is relevant for monovision, as well as an indicator of the importance of eye selection in each patient (expectedly higher in patients with large dominance strength). We also used MAS-2EV to test perceived visual quality with conventional and crossed monovision. We compared eye dominance at distance and near using the preferential test and the MAS-2EV scoring test. We examined the differences in the dominant eye selection and monovision prescription from these tests in comparison with sighting dominance (hole in the card) and clinical sensory dominance tests.

7.2. Methods

7.2.1. Subjects

Twenty early presbyopic subjects (51.5±5 years old) participated in the study. All subjects had normal stereovision (<40 arc seconds), normal color vision, and no history of eye surgery or eye disease. The spherical component of the refractive error ranged between -2.50 and +2.50D and the cylindrical component from -0.75 to 0.00D. The required addition for near vision ranged from +1.25 to +2.25D, determined as the minimum addition needed to achieve 0.00 logMAR visual acuity with a near vision eye chart. Subjects were habitually corrected for distance with spectacles or contact lenses and 14 of them used a near aid to read. None of the subjects had their presbyopia corrected with monovision. The study followed the tenets of the Declaration of Helsinki. Study protocols were approved by the CSIC Institutional Review Board. Subjects signed a consent form after receiving an explanation of the nature and possible consequences of the study.

7.2.2. Apparatus

The binocular Simultaneous Vision Simulator SimVis Gekko (2EyesVision SL, Madrid, Spain)[238] was used to rapidly (in less than 0.5 seconds) change the power between both eyes of the patient. The variable optical power was induced by two optotunable lenses (Optotune Inc, Dietikon, Switzerland). Previous calibrations show a precision of 0.05D in the power induced by the system[239]. A trial lens holder was used to introduce the distance refraction of the subjects.

The Psychophysical Toolbox of MATLAB (Math-works Inc., Natick, MA, USA) was used for stimuli presentation and response collection. Custom-developed software was written in MATLAB to control the optical power in the right and left eye channels of the SimVis Gekko and to synchronize the sequence of images presented in the displays with the sequence of corrections programmed in the device.

Distance vision stimuli were presented on the Stereoscopic Monitor (SM, described in section 2.2.2), mainly based on a UK UHD 49” monitor LG49UH850V (LG, South Korea), driven by an NVIDIA® Quadro® P4000 dual Graphic card. The display spatial resolution is 3840x2160 pixels, with a refresh rate of 60 Hz, and its maximum luminance is 200 cd/m^2. This display was used for sensory eye dominance and sighting eye dominance (subject located at 4m) and to present the distance images in the Preferential test and distance Multifocal Acceptance Score (MAS-2EV) test. The subjects viewed the display at 2 meters.

Near vision stimuli were presented in parallax barrier tablet I (PBI, see section 2.2.3.2) tablet (Commander3D, Toronto, Canada), driven by a PowerVR SGX544 Graphic card. This display was used for near Preferential test and near MAS-2EV test. The subjects viewed the display at 40 cm.

7.2.3. Experiments

We measured eye dominance using two clinical methods (sighting eye dominance and sensory eye dominance, which provide a binary metric, right or left eye) and performed two tests that directly quantified the preferred combination of monovision (distance correction in the right or the left eye), using a two-interval forced choice paradigm and a perceptual scoring test. Those tests provided a magnitude of the ocular dominance strength (in a monovision correction). The monovision corrections were automatically and randomly changed using a wearable binocular simultaneous-vision simulator (SimVis Gekko) that projected optotunable lenses onto the eye's pupil. Unless otherwise noted, all tests were conducted in a room with the lights on (400 lux).

7.2.3.1. Sensory dominance

We tested sensory dominance using a clinical test that evaluates the tolerance to interocular blur difference placing a positive trial lens in front of one eye while the fellow eye is kept sharp. We performed the test with two levels of positive defocus (+1.50D and +0.50D) in front of the right and left eye alternately while the subject was looking binocularly at a distance letter stimulus of 0.2logMAR size larger than their best visual acuity. The subject had to indicate the eye that appears more bothered by defocus blur, which is considered the dominant eye. This procedure was repeated three times (randomly assigning the first eye where the trial lens was placed) for the two levels of defocus. The order of the first level of defocus evaluated was also randomized. The dominant eye was determined if the subject selected two or three times the same eye. The result of the test was recorded as -1 for left eye dominance and 1 for right eye dominance. The sensory dominance test was only performed for distance vision, and it took typically 45 seconds for each blur level, in total, 1.5 minutes.

7.2.3.2. Sighting eye dominance

We measured sighting eye dominance using the "hole in the card" method[171]. Subjects were asked to look at a stimulus (an optotype of 0.2 logMAR size larger than their best visual acuity) at distance with both eyes open through the hole in the card held in both hands. Then, the experimenter covered each eye individually and the subject had to indicate if the letter disappears when either the right or the left eye was covered. The dominant eye is the one where the letter did not disappear when covered. In this study's notation, -1 indicates left eye dominance, and 1, right eye dominance. The sighting eye dominance test was performed only for distance vision, and it took typically under 60 seconds to be performed.

7.2.3.3. Preferential test

Subjects had to indicate whether the perceived quality of an image is preferred with the monovision correction (+2.00D) induced in the left eye (ML) or the right eye (MR) in a Two Interval Forced-Choice (2IFC) task. In each trial, the monovision correction was induced in one eye for 1.5s, then the monovision correction was flipped to the other eye for 1.5s. An inter-interval gray screen was presented for 0.7s between trials. The eye in which monovision was firstly induced was randomized for each trial.

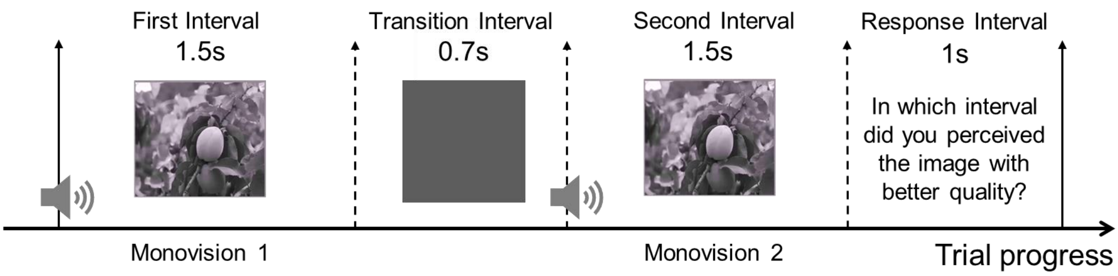

Figure 7.1. Trial sequence in the Preferential test. A representative trial of the test is shown. In each interval, a monovision condition (randomly MS or MR) is presented during 1.5s, separated by a gray field (during 0.7s) and an auditory tone (gray speaker). Subjects were given 1s to respond between trials. The example shows one of the 26 natural images used. The test consisted of 52 trials.

Subjects judged a total of 26 different natural images extracted from the "Barcelona Calibrated Images Database"[240], and generally contained scenes of vegetation and fruits (1/f spatial spectrum). Images were grayscale and subtended an 8x8 deg field both for distance and near vision. The display for distance vision was physically located 2-m from the subject, but optically at infinity by use of +0.50D lenses in the trial lens holder of the SimVis Gekko. The near distance was 40cm. Subjects viewed the same image twice in each trial, in counterbalance order, for a total of 52 trials, therefore assessing their preference for ML or MR for 26 natural images. Eye dominance strength is defined as the proportion of trials that the subject prefers monovision in one eye. For distance vision, a stronger preference for ML indicates right-eye dominance (1) and a preference for MR indicates left-eye dominance (-1). For near vision, a stronger preference for ML indicates left-eye dominance (-1) and for MR indicates right-eye dominance (1). The Preferential test was performed for distance and near vision and took about 7 minutes to be run for each distance.

<u>7.2.3.4. Multifocal Acceptance Score</u>

The Multifocal Acceptance Score to Evaluate Vision (MAS-2EV) is a multi-component metric to measure the subjectively perceived quality of natural images with a given presbyopic correction[229]. Previous work has demonstrated the use of MAS-2EV both in combination with contact lenses and with corrections simulated in the SimVis Gekko to assess perceived quality with multifocal lenses, standard monovision, or modified monovision[229,295]. Subjects judged the perceived quality of images at two distances and two illumination conditions (Distance-Day; Distance-Night; Near-Day; Near-Night). Images for every distance and illumination condition represented usual visual activities. The distance images subtended 27x15 deg and were presented in the distance monitor. The near images subtended 5.5x3.5 deg and were presented in the near tablet. The room lights were turned off for the Distance-Night and Near-Night conditions. For the Distance-Night component, two white LEDs are superimposed on the headlights of a car in the left image of the Distance-Night stimulus to simulate glare.

In every component, each subject scored the perceived image quality on a scale from 0 to 10, although data are reported normalized from 0 to 1, for comparison purposes with other tests. Each scoring was repeated three times (final scores are obtained as the average across repetitions). The four components are plotted in a polygon, where the left-upper corner represents the score for Distance-Night, the right-upper corner for Distance-Day, the bottom right corner for Near-Day, and the left-bottom corner for Near-Night.

The MAS-2EV test was performed for three different corrections: distance vision in both eyes (FF), and monovision with +2.00 D in the left eye (ML) and in the right eye (MR).

The SimVis Gekko was used to automatically induce the FF, ML, and MS corrections. For a given correction, the scoring of 3 conditions takes about 2 minutes.

The difference between MAS-2EV for MR minus ML (Equation 7.1) defines a metric that indicates MAS-2EV score dominance (left or right eye) in a monovision correction and is calculated for distance and near (averaging the day and night scores).

$$difMAS = MAS_{MR} - MAS_{ML} \qquad 7.1$$

7.2.3.5. All experiments

To compare between experiments, each test provides a value varying from -1 to 1, as explained in each section. For conventional tests (sighting and sensory) the eye dominance can only be binary, -1 (left-eye dominance) or 1 (right-eye dominance). For the Preferential Test and MAS-2EV, the eye dominance value can vary continuously within said range, providing a metric for Eye Dominance Strength (EDS). If strength falls between -0.1 and 0.1, it is said that the eye does not have a clear dominance[294]. Values between -1 and -0.1 indicate left-eye dominance and between 0.1 and 1 indicate right-eye dominance.

7.2.4. Statistical Analysis

Paired t-tests and correlation coefficients are used to compare between same measurements performed for distance and near vision, in all experiments. The Chi-square test is used to compare the results of the clinical dominance tests, $p<0.05$ is considered significant. Reliability analysis is performed for the Preferential Test to estimate the number of trials needed to obtain a Cronbach alpha value of 0.9. Point-biserial correlation coefficient and two-tailed unpaired t-test with equal variances for the correlation coefficient were estimated to assess the association between clinical tests (binary response) and psychophysical tests.

7.3. Results

We compared the eye dominance identified by two clinical tests with the monovision preference (perceptual preference and perceptual scoring tests). The Eye Dominance Strength (EDS) was defined as the magnitude of perceived quality with conventional monovision relative to crossed monovision. Results are shown with subjects ordered according to the EDS estimated from the Preferential test.

Sensory and Sighting eye dominance

Figure 7.2 shows the eye dominance evaluated with the blur tests (sensory eye dominance) with 1.50D and 0.50D tolerance and the ‘hole-in-the-card’ test (sighting eye dominance). We found right-eye dominance in 45% of the subjects using the sensory dominance test with +1.50D, 60% using the sensory dominance test with +0.50D, and 60% using the sighting eye dominance test. Comparing both sensory tests, 75% of the subjects selected the same eye dominance ($X^2(1)=5.69$, $p<.05$). Sensory dominance and sighting dominance agreed in 75% of the subjects for 1.50D ($X^2(1)=5.69$, $p<.05$) and in 60% for 0.50D ($X^2(1)=0.56$, $p>.05$). Only 55% subjects selected the same eye using all three clinical tests.

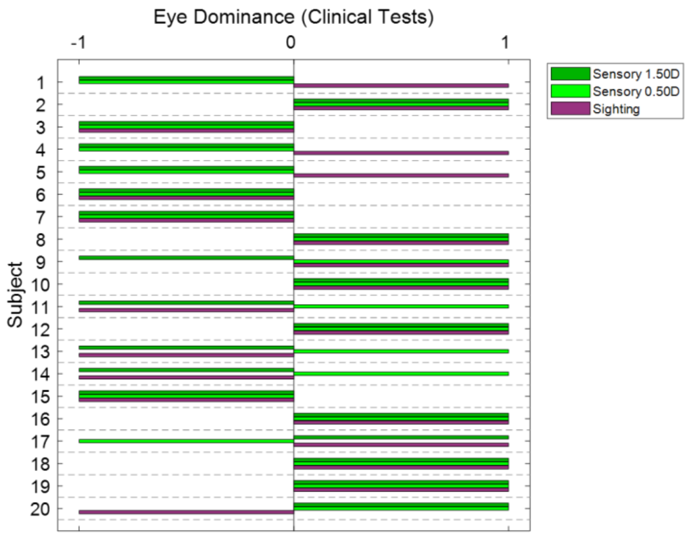

Figure 7.2. Eye dominance for clinical eye dominance tests for all subjects. -1 stands for left-eye dominance and +1 for right-eye dominance. Dark and light green bars represent sensory eye dominance using + 1.50D and +0.50D blur, respectively, and dark magenta represents sighting eye dominance.

Preferential test and monovision

The preferential test was a 2IFC task between conventional monovision and crossed monovision (for a near addition of +2.00D). Figure 7.3 shows an example of results for S19 for distance vision (Figure 7.3A) and near vision (Figure 7.3B). This subject shows a clear preference for monovision in the left eye (ML) at distance, i.e., addition in the left eye, and full distance correction in the right eye, indicative of right eye dominance. Conversely, some subjects do not show a clear preference (weak dominance), i.e., S9 in Figures 7.4C and 7.4D.

Figure 7.3E shows the EDS for distance vision (blue bars) and Figure 7.3F shows the eye dominance for near vision (red bars) for all subjects. According to this metric, four subjects (20%) showed weak eye dominance (fall within the ±0.1 gray band), three of them both at distance and near vision. Filled bars indicate left-eye dominance and empty bars right-eye dominance according to the clinical sensory test (with +1.50D blur). There was a mismatch between the eye dominance identified by the clinical sensory test and the Preferential test in 6 subjects (4 with strong Preferential dominance: S2, S13, S14, S15) at distance vision and 4 subjects at near vision. We averaged the Preferential test EDSs of subjects clinically identified as left eye and right eye dominance, respectively, with the different tests. For distance vision, the average EDS with the Preferential test for subjects that had left-eye dominance was -0.2 and for right-eye dominance was +0.34 (for sensory eye dominance +1.50D, Figure 7.3E subplot), -0.25 and +0.24, respectively, for sensory eye dominance +0.50D, and +0.07 and +0.03, respectively, for sighting eye dominance. For near vision, the average EDS with the Preferential test for left-eye and right-eye dominance was -0.18 and +0.21, respectively, for sensory eye dominance +1.50D (Figure 7.3F subplot), -0.22 and +0.14, respectively, for sensory eye dominance +0.50D, and +0.02 and -0.02, respectively, for sighting eye dominance.

Figure 7.3G plots the EDS obtained with the Preferential test for near vision versus that for distance vision, showing a highly statistically significant positive correlation (r=.86; p<.05). A paired t-test shows a non-significant difference (p>.05) between the Preferential EDS for distance and near, suggesting the test could be equally applicable at both distances to select the best eye for monovision correction.

A reliability test estimated a Cronbach Alpha value of 0.941 for distance and 0.976 for near vision. Considering 0.9 as a value that guarantees the reliability of the data, the number of trials could be reduced to 30 in the distance vision test and 12 in the near vision test. Reducing the number of trials to the minimum number still estimating EDS reliably could reduce the time of performance of the Preferential test to less than 4 minutes for distance, and less than 2 minutes for near.

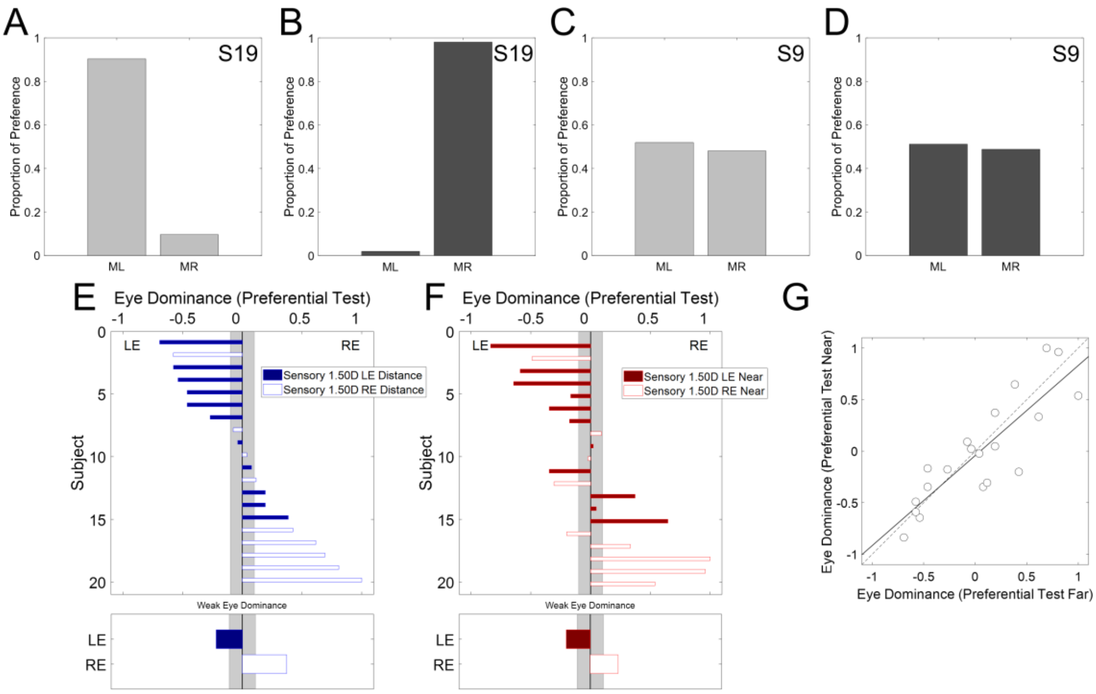

Figure 7.3. Preferential test eye dominance. **A.** Proportion of preference for monovision in the left eye (ML) and monovision in the right eye (MR) for distance vision and subject S19. **B.** Proportion of preference for ML and MR for near vision and subject S19. This subject has a strong monovision preference and, expectedly, high Eye Dominance Strength (EDS). **C.** Proportion of preference for ML and MR for distance vision and subject S9. **D.** Proportion of preference for monovision ML and MR for near vision and subject S9. This subject is a representative example of weak monovision preference and, expectedly, low EDS. **E.** Preferential test EDS for distance vision (all subjects). Filled blue bars indicate that the subject selected left-eye dominance with the clinical Sensory dominance test with 1.50D and empty blue bars that the subject selected right-eye dominance. The shaded gray band indicates weak dominance (±0.1). Results above 0.1 indicate right-eye dominance, and below -0.1 indicate left-eye dominance. Bottom subplot represents the average Preferential test EDS across subjects that selected left-eye dominance with clinical Sensory dominance test with 1.50D (filled blue bar) and right-eye dominance (empty blue bar). **F.** Preferential EDS for near vision (all subjects). Filled red bars indicate that the subject selected left-eye dominance with the clinical Sensory dominance test with 1.50D and empty red bars that the subject selected right-eye dominance. Bottom subplot represents the Preferential test EDS across subjects that selected left-eye dominance with clinical Sensory dominance test using 1.50D (filled red bar) and right-eye dominance (empty red bar). **G** Relationship between Preferential Test EDS for distance and near vision.

MAS-2EV and monovision

In Multifocal Acceptance Score to Evaluate Vision (MAS-2EV) test, subjects subjectively graded their perceived visual quality for 4 different stimuli and scenes, providing a multi-component description of their perception, for different corrections[229,295]. We tested three different corrections: both eyes corrected for distance vision (FF); monovision in the left eye (ML), and monovision in the right eye (MR). Figure 7.4A shows an example of a MAS-2EV polygon for S19. Each line represents a different correction (FF-black line, ML-dark gray line, and MR-light gray line). For FF correction, as expected in presbyopes, near vision scores decrease compared to distance vision scores (score for distance vision was 0.98 and for near vision 0.47 -averaged across the day and night components-). In this subject, the MAS-2EV polygon for ML is notably different than that for MR. For ML correction, the perceptual score for distance vision (average night and day) is 0.62, while for MR it is 0.78. Both ML and MR improve vision at near compared to the FF correction (0.75 and 0.57), but MR is largely preferred at distance. Conversely, other subjects (for example S11, shown in Figure 7.4B) do not show significant differences between MR and ML, while still showing a small visual degradation at distance (0.88 and 0.83, respectively) and a significant improvement over FF in near (0.77 and 0.78, respectively).

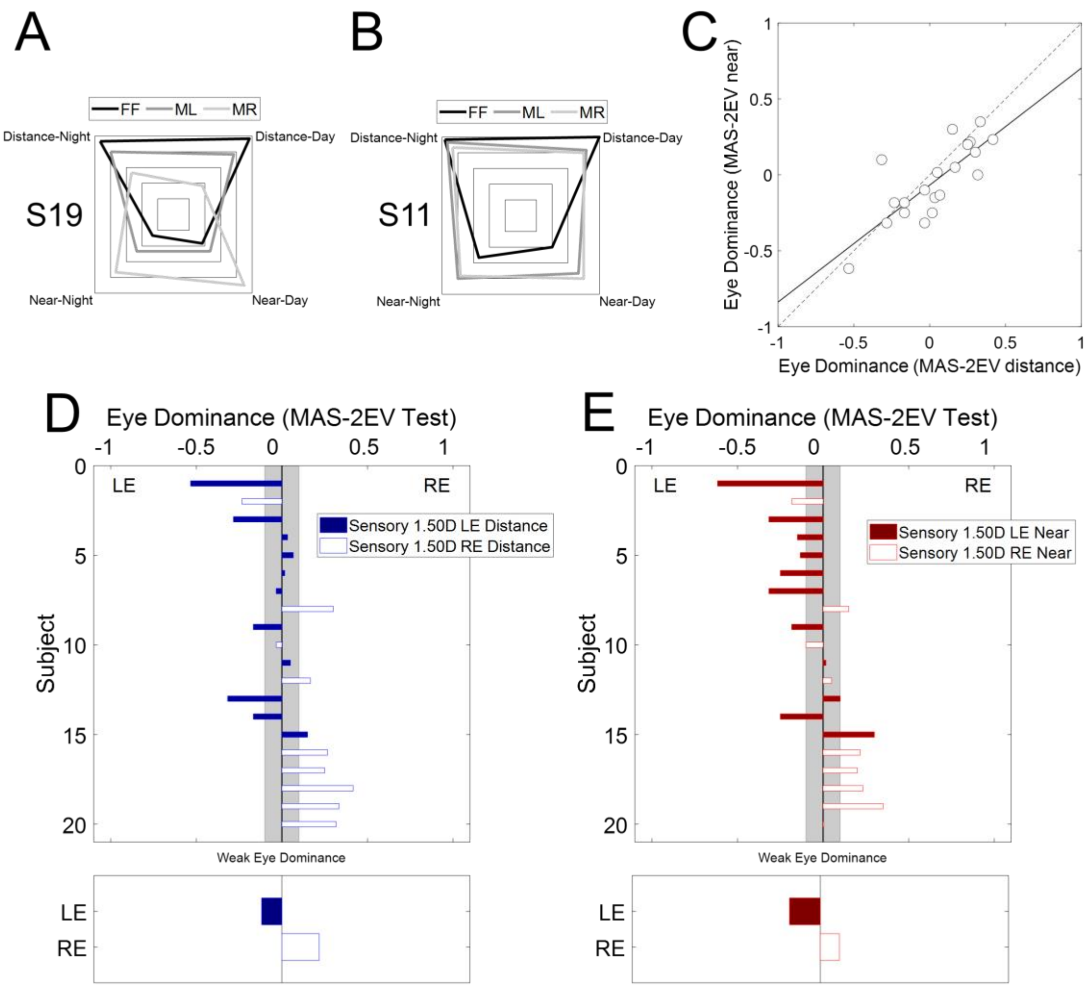

Figure 7.4. MAS-2EV test eye dominance. A & B. MAS-2EV polygons for two subjects. Lines represent the scores for FF (black), monovision in the left eye (ML, dark gray), and monovision in the right eye (MR, light gray). Subject S19 (A) shows a large degradation at distance with MR, and significant differences between ML and MR (high Eye Dominance Strength (EDS)); S11 (B) shows small differences between ML and MR (low EDS). **C.** Relationship between MAS-2EV eye dominance for distance vision versus near vision. **D.** MAS-2EV test EDS for all subjects for distance. Filled blue bars indicate that the subject selected left-eye dominance with the clinical Sensory dominance test with 1.50D and empty blue bars that the subject selected right-eye dominance. The shaded gray band indicates weak dominance (±0.1). Bottom subplot represents the average of the MAS-2EV test EDS across all subjects that selected left-eye dominance with clinical Sensory dominance test using 1.50D (filled blue bar) and right-eye dominance (empty blue bar). **E.** MAS-2EV test EDS for all subjects for near vision. Filled red bars indicate that the subject selected left-eye dominance with the clinical sensory dominance test with 1.50D and empty red bars that the subject selected right-eye dominance. Bottom subplot represents the average of MAS-2EV test EDS across subjects that selected left-eye dominance with clinical sensory dominance test using 1.50D (filled red bar) and right-eye dominance (empty red bar).

The difference between the score given for MR and the score given for ML provided a metric for estimating eye dominance strength using MAS-2EV (*difMAS*, Equation 7.1). This metric is equivalent to the Preferential test, but the main difference is that subjects gave scores instead of choosing forcibly between monovisions. Figures 7.4D and 7.4E plot the results of the MAS-2EV test EDS for distance vision (blue bars) and near vision (red bars), respectively. As in Figures 7.3E and 7.3F, filled bars indicate left-eye dominance and empty bars right-eye dominance according to the clinical sensory test (+1.50D blur). We averaged the MAS-2EV eye dominance strengths of subjects clinically identified as left-eye and right-eye dominance. For distance vision, the average MAS-2EV test EDS for subjects that had left-eye dominance was -0.11 and for right-eye dominance was +0.2 (for sensory eye dominance +1.50D, Figure 7.4D subplot), -0.04 and +0.08, respectively for sensory eye dominance +0.5 D, and -0.03 and +0.07, respectively for sighting eye dominance. For near vision, the average of EDS with the MAS-2EV test for left-eye and right-eye dominance was -0.16 and +0.1, respectively, (for sensory eye dominance +1.50D, Figure 7.4E subplot), -0.16 and +0.3, respectively, for sensory eye dominance +0.50D, and -0.09 and -0.01, respectively, for sighting eye dominance. As in the Preferential test, there is a high statistical correlation between the eye dominance for distance and near using the MAS-2EV metric (r=.77; p<.05), and a non-significant statistical difference between the eye dominance selection for the two distances (paired t-test; p>.05), as shown in Figure 7.4C.

Correspondence between tests

Figures 7.4E, 7.4F, 7.5D, and 7.5E represent EDS based on the Preferential test and MAS-2EV (all subjects) for distance vision, with filled and empty bars indicating left- and right-eye dominance obtained with clinical sensory eye dominance with 1.50D, respectively. Negative values along the y-axis of each graph represent the strength of left-eye dominance from the different tests and positive values of right-eye dominance. We performed analysis by averaging the EDS obtained from the Preferential and MAS-2EV of all subjects with the same sign of sensory EDS with 1.50D, sensory dominance with 0.50D, and sighting eye dominance. The only tests that show a statistically significant correlation between them are sensory dominance 1.50D with the Preferential test and MAS-2EV, and sensory dominance 0.50D with the Preferential test (see Table 7.1).

Table 7.1. Statistical analysis of the association between clinical tests (binary response) and psychophysical tests. We show the point-biserial correlation coefficient (r) and two-tailed unpaired t-test with equal variances for the correlation coefficient (t-statistic (t) and p-value (p)). Statistical significance difference is indicated with two asterisks (**).

	Sensory 1.50D	**Sensory 0.50D**	**Sighting**
Preferential Test EDS	r = .53 t = 2.74 p < .05**	r = .47 t = 2.35 p < .05**	r = -.04 t = -0.18 p = .86
MAS-2EV test EDS	r = .6 t = 3.30 p < .05**	r =.23 t = 1.03 p > .32	r = .20 t = 0.91 p = .38

Figure 7.5 shows the eye dominance strengths obtained from MAS-2EV versus the Preferential test. There is a statistically significant correlation between the EDS obtained from either test, both for distance (r=.70; p<.05) and near (r=.76; p<.05). Paired t-tests indicate non-statistical differences between the dominance from both tests at distance (p>.05) or at near (p>.05).

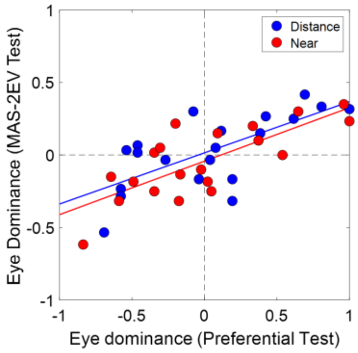

Figure 7.5. Correspondence between the Preferential and the MAS-2EV eye dominance tests. Blue dots indicate distance vision and red dots near vision.

Eye dominance and monovision

Considering the Preferential test a reference for selection of the eye to treat for monovision, we have tested how selection from other tests would have impacted the success of a monovision correction. The estimation was performed for distance vision because the clinical tests are performed for distance vision only. We removed from the analysis the 6 subjects that showed weak eye dominance provided by MAS-2EV test. By this definition, the Preferential test (Figure 7.6, blue circle) shows 100% success. Choosing the eye to treat monovision based on clinical eye sensory dominance (1.50D or 0.50D blur) would result in a successful treatment in 64% of the patients. Choosing the eye to treat monovision based on clinical sighting eye dominance would result in a successful treatment only in 43% of the patients. In contrast, the test based on MAS-2EV results in agreement with the Preferential test in 79% of the subjects. MAS-2EV appears the most time-effective measurement, as scoring direct and crossed monovision for one condition (Distance-Day) takes only 1 minute.

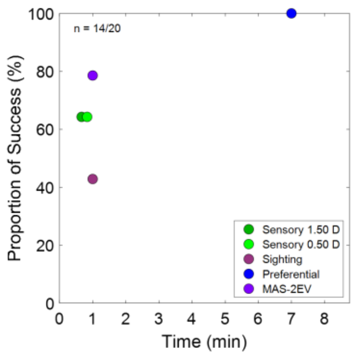

Figure 7.6. Proportion of successful patients. Proportion of subjects in whom the result of eye dominance provided for each test agreed with the results provided by the Preferential test, considered as the reference for monovision selection. The time to perform sensory eye tests with 1.50D or 0.50D is 45 seconds, although they are plotted shifted for visualization purposes.

7.4. Discussion

Eye dominance is measured in clinical practice with conventional clinical tests such as sighting and sensory tests. As numerous studies in the literature[172–175], we have also found that sighting eye dominance does not consistently match dominance obtained from sensory dominance tests (whether using lower or higher blur magnitude). In our study, only 55% of the subjects reported the same dominance with the three tests most used in the clinic.

Several authors have turned their attention to binocular rivalry tests to identify eye dominance and have proposed versions of the psychophysical paradigm of this test that could be amenable in clinical practice[282]. Identifying the eye that best suppresses artefactual blur may be a good indicator for the eye to give the near addition in a monovision treatment. However, the typically high-contrast targets used in binocular rivalry tests make them little related to the natural visual content that the subjects are exposed to in the real world. Besides, the fact that results from these tests may be affected by physical features of the stimulus[283] and may target different types of dominance poses a question on the suitability of tests based on the binocular rivalry to select the optimal monovision approach.

Instead, our proposed tests chose to directly evaluate monovision and to select placing the reading addition in the right or left eye based on the subject's perceptual response (in a two-interval forced choice comparison in the Preferential Test, or perceptual scoring as in the MAS-2EV test). The use of natural images conveys a more realistic depiction of the distance real world than high contrast optotypes or Gabor patches used in the psychophysical binocular rivalry tests of dominance. While evaluation of the effect of image size, spatial frequency content, image brightness, or chromatic features on the identification of the eye dominance using this test is pending, our results suggest that the selection is robust, given the large correspondence obtained between independent measurements at distance and near vision. The Preferential test used monochromatic images (plants, trees, fruits) subtending an 8-deg field, while the MAS-2EV test used color images (faces, urban landscapes, signs) subtending a 27-deg field. Moreover, MAS-2EV test was performed under two levels of illumination (day and night). Despite all these differences, there is a highly statistically significant correlation between the eye dominance selected by these tests (Figure 7.5). Furthermore, while binocular rivalry tests and clinical eye sensory tests have shown a lack of predictability of eye dominance at near vision from eye dominance measured at distance vision[285], the eye dominance from both the Preferential test and MAS-2EV test measured at both distance and near visions show a high degree of correlation (Figure 7.3G and Figure 7.4C).

Unlike conventional tests in the clinic that provide a binary identification of the dominant eye (right or left), the Preferential and MAS-2EV tests provide a measurement of the eye dominance strength (EDS). The MAS-2EV test is fast and allows evaluating perceived quality with several presbyopic corrections, including multifocal corrections[229]. In our subject cohort, 70% of the subjects showed clear differences in the perceptual judgment of conventional and crossed monovision (indicating strong eye dominance), while 30% showed weak dominance. The clinical literature is inconclusive on whether the patients with strong or weak eye dominance are the most suitable candidates for successful monovision. Nevertheless, having a graded metric to discern eye dominance appears highly valuable for clinical management and as a tool in further studies. On the one hand, it allows identifying patients for whom careful selection of the eye to treat for distance and for near is more critical. On the other hand, it allows assessing whether the same selection would hold with other visual stimuli, near add magnitude, or lens designs.

Subjects were instructed to judge the perceived quality of images based on their natural appearance and a higher degree of comfort. Judgments are highly repetitive at least in those subjects that appear to have stronger dominance (in fact, the dominance strength in the Preferential test is based on the repeatability of the response). Likely, the ability to suppress blur with either the conventional or crossed monovision is the underlying mechanism in the perceived quality judgment, although this remains to be investigated. In addition, the assumption by which the success of a prescribed monovision treatment relies solely on optimizing perceptual image quality at distance remains to be tested. Other perceptual factors not considered in this study include the effect of monovision on stereovision[97], claimed by some authors to be a key factor in monovision success[296], which could be added to the tests proposed in this study. Also, tests were performed for fixed monovision near addition (+2.00D). An interesting question is to what extent the identified eye dominance may be altered with a higher/lower near addition. Another open question is whether eye dominance may change after adaptation to a given monovision correction[297]; making the eyes initially selected for distance and near respectively eventually less important.

Key to the implementation of the proposed eye dominance tests has been the use of the SimVis Gekko. This system allows programming and rapid alternation between corrections enabling short measurement times and making them suitable for clinical use. Besides the mentioned advantages of this binocular visual simulator and, unlike trial lens frames or even automatic phoropters, the correction is applied in a plane conjugate to the pupil of the eye, avoiding magnification imbalances or prismatic effects. Furthermore, while the current study has only made use of monofocal lens corrections (and a single power change in the optotunable lens), the SimVis Gekko is conceived as a simulator of multifocal corrections, with the optotunable lens operating under the principle of temporal multiplexing[238]. The Preferential test and MAS-2EV can be easily adapted, as shown in laboratory work[229,238,255] to include other presbyopia correction modalities (e.g., modified monovision or multifocal corrections) in the comparison. We have shown that the application times of the proposed tests (a few minutes) are compatible with reasonable clinical chair times.

7.5. Conclusions

In this chapter of the thesis, we have reported discrepancies between the clinical sensory eye dominance test and sighting eye dominance in selecting the dominant eye, confirming the results of the literature. In the context of monovision corrections, perceptual preference or perceptual scoring of naturalistic stimuli allow the direct identification of the eye for treating monovision and a measurement of the strength of eye dominance. Although the effect of specific features of the stimulus on the eye dominance identification and strength remains to be investigated, the high repeatability of the test and the consistency between the measurements at near and far suggest that natural stimuli rather than artificial stimuli are well suited for testing eye dominance and monovision preference. The use of a head-mounted binocular simultaneous vision simulator, in combination with psychophysical procedures, allowed a fast and precise identification of the monovision preference, providing a useful framework for clinical practice.

Chapter 8. The Reverse Pulfrich effect: first report of the optical illusion

This chapter describes the discovery and the scientific and clinical implication of the Reverse Pulfrich effect, a new version of a 100-year-old optical illusion called the Pulfrich effect, produced by interocular differences in blur between the eyes. Those blur differences, common in monovision prescriptions, cause a previously unknown motion illusion that makes people dramatically misperceive the distance and three-dimensional direction of moving objects. The effect occurs because blurry and sharp images are processed at different speeds. For moving objects, the mismatch in processing speed causes a neural disparity, which results in misperceptions. In this chapter, a method to compensate for said motion illusions, anti-Pulfrich monovision corrections, is also described.

This chapter, in collaboration with the University of Pennsylvania, is based on the published article by Johannes Burge et al. *“Monovision and the misperception of motion”* published in *Current Biology (2019)*. The co-authors are Victor Rodriguez-Lopez and Carlos Dorronsoro.

The anti-Pulfrich monovision corrections principle is protected by a US patent *“Anti-Pulfrich monovision ophthalmic correction”*. The co-inventors of the patent are Johannes Burge, Carlos Dorronsoro, and Victor Rodríguez-Lopez.

The work was presented as an oral contribution by Victor at the 8th Iberian Conference of Perception (Spain, 2019). Besides, the co-author Johannes Burge presented an oral contribution at the Vision Science Society (VSS) Meeting in Florida in 2019 and the 43rd Annual Interdisciplinary Conference (AIC) in Wyoming in 2019.

This work was also covered by the media in several press releases (Philadelphia Inquirer, PennToday, CSIC) and in the American Science Journal.

The contribution of Victor was the conceptualization and design of the study and the literature research in collaboration with all the co-authors, the design of the experiments in collaboration with Johannes Burge, the collection and analysis of the data, and the preparation of the chapter in collaboration with all co-authors.

8.1. Introduction, results, and discussion

The previous chapter studied monovision, and in particular the selection of the most suitable eye for far and for near vision. This chapter studies the influence of the interocular blur differences produced by that prescription asymmetry between the eyes in the depth perception of moving stimuli.

In the year 2020, nearly two billion people will have presbyopia worldwide[298]. Presbyopia, a natural part of the aging process, is the loss of focusing ability due to the stiffening of the crystalline lens inside the eye[9]. All people develop presbyopia with age, so the number of affected people increases as the population ages. Without correction, presbyopia prevents people from reading and from effectively using a smartphone.

Many corrections exist for presbyopia. Reading glasses, bifocals, and progressive lenses are well-known examples. Monovision and multifocality provide spectacle independence. With monovision, each eye is fitted with a lens that sharply focuses light from a different distance, providing ‘near vision’ to one eye and ‘far vision’ to the other. Monovision thus causes differential blur in the left- and right-eye images of a target at a given distance. For patients in which the correction is successful, the visual system suppresses the lower-quality image and preferentially processes the higher-quality image[280,299,300]. The consequence is an increase in the effective depth of field without many of the drawbacks of other corrections (e.g., the ‘seam’ in the visual field caused by bifocals). As mentioned in section 1.3.1.2, despite its drawbacks (degrades stereoacuity[98,99] and contrast sensitivity[96] and can cause difficulties in driving[97,100]) many people prefer monovision corrections[102].

Ten million people in the United States currently have a monovision correction. The number of candidates will increase in the coming years. The population is aging and monovision is the most popular contact lens correction for presbyopia amongst the baby boomers[102]. To put it in context, there are approximately 123 million presbyopes in the USA[103]. Approximately 12.9 million of these presbyopes wear contact lenses, and 4.5 million (35%) of these contact lens wearers have monovision corrections[301,302]. Approximately 30 million presbyopes have had surgery to implant intraocular lenses, and approximately 5.1 million (17%) of these surgical patients have received monovision corrections[303]. Together, this results in approximately 9.6 million presbyopes with monovision corrections only in the USA. A full understanding of the effects of monovision on visual perception is critical, both for sound optometric and ophthalmic practice and for the protection of public safety. Unfortunately, there is no literature on how the differential blur induced by monovision impacts motion perception, a critical ability that supports successful interaction with the environment[304].

We investigated the impact of differential blur on motion perception by measuring the Pulfrich effect, a stereo-motion phenomenon first reported nearly 100 years ago[305]. When a target oscillating horizontally in the frontoparallel plane is viewed with unequal retinal illuminance or contrast in the two eyes, the target appears to move along an elliptical trajectory in depth (Figure 8.1A). The effect occurs because the image in the eye with lower retinal illuminance or contrast is processed more slowly than the image in the other eye[203,208,218,305–308]. The mismatch in processing speed causes a neural binocular disparity, a difference in the effective retinal locations of target images in the two eyes[309,310], which results in the illusory motion in depth.

Do interocular blur differences, like interocular illuminance and contrast differences, ¿cause misperceptions of motion? More specifically, does blur slow the speed of processing and cause a Pulfrich effect? In the Classic Pulfrich effect, if the retinal illuminance or contrast in the left eye is decreased, observers perceive ‘front left’ motion (i.e., clockwise motion from above; Figure 8.1A). However, we find that when the left eye is blurred, observers perceive 'front right' motion (Figure 8.1B). Thus, instead of a Classic Pulfrich effect, differential blur causes a Reverse Pulfrich effect.

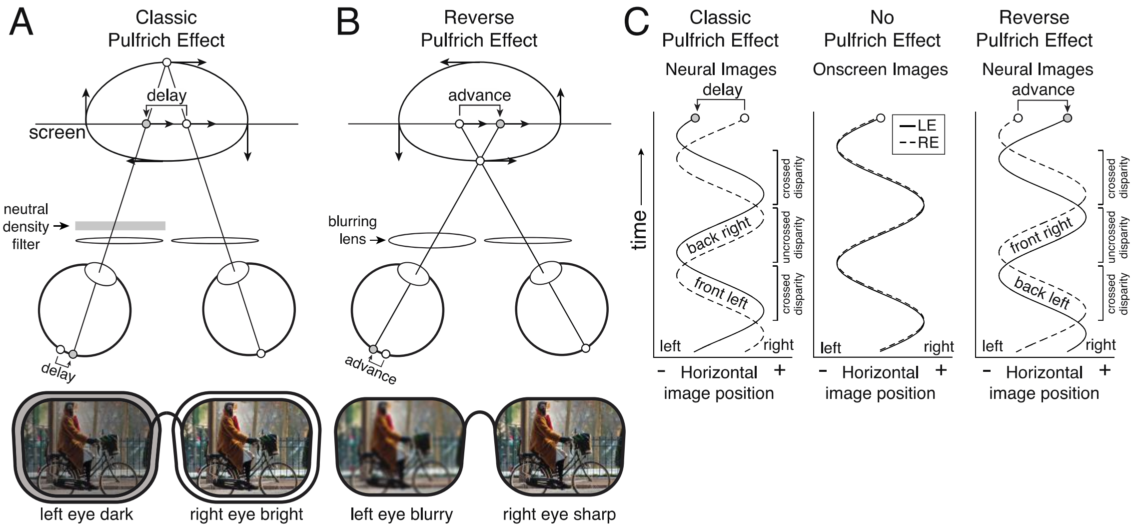

Figure 8.1. Classic and Reverse Pulfrich effects. A. Classic Pulfrich effect. A neutral density filter in front of the left eye causes sinusoidal motion in the frontoparallel plane to be misperceived in depth (i.e., clockwise motion from above: 'back right', 'front left'). The effect occurs because the response of the eye with lower retinal illuminance (gray dot) is delayed relative to the other eye (white dot), causing a neural disparity. **B. Reverse Pulfrich effect**. A blurring lens in front of the left eye causes illusory motion in depth in the other direction (i.e., counterclockwise from above: 'back left', 'front right'). The effect occurs because the response of the eye with increased blur (gray dot) is advanced relative to the other eye (white dot), causing a neural disparity with the opposite sign. **C.** Effective neural image positions in the left and right eye as a function of time for the Classic Pulfrich effect, no Pulfrich effect, and the Reverse Pulfrich effect.

The discovery of the Reverse Pulfrich effect implies an apparent paradox. Blur reduces contrast and should therefore cause the blurry image to be processed more slowly, but the Reverse Pulfrich effect implies that the blurry image is processed more quickly (Figure 8.1C). At first, this finding appears at odds with a large body of neurophysiological and behavioral results. Low contrast images are known to be processed more slowly at the level of early visual cortex[95,311–313] and the level of behavior[94,96].

The paradox is resolved by recognizing two facts. First, optical blur reduces the contrast of high spatial frequency image components more than low-frequency image components[51,314–316]. Second, extensive neurophysiological[317,318] and behavioral[94,96] literature indicate that high spatial frequencies are processed more slowly than low spatial frequencies, all else equal. Together, these facts suggest that the blurry image is advanced in time relative to the sharp image because the high spatial frequency components in the sharp image decrease the speed at which it is processed. Thus, a new version of a 100-year-old illusion is explained by known properties of the early visual system.

The Pulfrich effect has been researched extensively since its discovery. The effect is elicited by interocular luminance differences[305] and interocular contrast differences[218]. For a given interocular difference, the effect size depends on overall luminance[203,208,319] and dark adaptation[206–208]. In the late 1990s and early 2000s, a flurry of work debated what the effect reveals about the neural basis of stereo and motion encoding[320–324]. But it is not known whether the Pulfrich effect occurs under conditions similar to those induced by monovision corrections. In this study, we tackle two main questions: Do interocular blur differences, like interocular illuminance and contrast differences, cause misperceptions of motion? More specifically, does blur slow the speed of processing and cause a Pulfrich effect?

To measure the Reverse Pulfrich effect, we performed a one-interval two-alternative forced choice (2AFC) experiment. We used trial lenses to induce interocular differences in blur, and a haploscope for the dichoptic presentation of moving targets (Figure 8.2A). On each trial, a target oscillated from left to right (or right to left) while the observer fixated on a central dot. The onscreen interocular delay of the target images was under experimenter control. If the onscreen interocular delay is zero, onscreen disparity specifies that the target is moving in the plane of the screen. If the onscreen delay is non-zero, onscreen disparity specifies that the target is moving on an elliptical trajectory outside the plane of the screen. Observers reported whether the target was moving leftward or rightward when it appeared to be in front of the screen. Human observers made these judgments easily and reliably.

For a given difference in focus error, we measured the proportion of trials that observers reported ‘front-right’ as a function of the onscreen interocular delay. In each condition, performance was summarized with the point of subjective equality (PSE), the 50% point on the psychometric function (Figures 8.2B and 8.2C). The PSE specifies the onscreen delay required to make the target appear to move in the plane of the screen (i.e., no motion in depth).

The magnitude of the Reverse Pulfrich effect increases systematically with the difference in focus error between the eyes (Figure 8.2B, white circles; Figure 8.6A). (Discrimination thresholds also increase with interocular differences in focus error[325]; Figure 8.2C, Figure 8.6B). Negative differences in focus error indicate conditions in which the left-eye retinal image is blurry and the right-eye retinal image is sharp. In these conditions, the left-eye onscreen image must be delayed (i.e., negative PSE shift) for the target to be perceived as moving in the screen plane. Conversely, positive differences in focus error indicate that the left-eye retinal image is sharp and the right-eye retinal image is blurry. In these conditions, the right-eye onscreen image must be delayed (i.e., positive PSE shift). The results indicate that the blurrier image is processed faster than the sharper image. For the first human observer, a $\pm$1.5D difference in focus error caused an interocular difference in processing speed of $\pm$3.7ms (Figure 8.2B).

As a control, we measured the Classic Pulfrich effect. To do so, we systematically reduced the retinal illuminance to one eye while leaving the other eye unperturbed (see section 8.2). As expected, the pattern of PSE shifts reverses (Figure 8.2B, gray squares; Figure 8.6A). When the left eye’s retinal illuminance is reduced, the left-eye onscreen image must be advanced in time for the target to be perceived as moving in the plane of the screen, and vice versa. Consistent with Classic findings, these results indicate that the darker image is processed more slowly than the brighter image.

Why does the Reverse Pulfrich effect occur? To test the hypothesis that the blurry image is processed faster because the high spatial frequencies in the sharp image slow its processing down (see above), we ran an additional experiment with two critical conditions. In the first condition, the onscreen stimulus to one eye was high-pass filtered while the other stimulus was unperturbed. High-pass filtering artificially sharpens the image by removing low frequencies, increases the average spatial frequency, and should decrease the processing speed relative to the original. In the second condition, the onscreen stimulus to one eye was low-pass filtered (Figures 8.3A and 8.3B) while the other was unperturbed. Low-pass filtering removes high frequencies, approximates the effects of optical blur, and should increase the speed of processing relative to the original unperturbed stimulus. Results with high- and low-pass filtered stimuli should therefore resemble the Classic and Reverse Pulfrich effects, respectively. The predictions are confirmed by the data (Figure 8.3C; Figure 8.6C). These differences in processing speed cannot be attributed to luminance or contrast differences because the stimuli were designed such that the low- and high-pass filtered stimuli had identical luminance and contrast (Figure 8.8). The detailed computational rules that relate frequency content to processing speed remain to be worked out and should make a fruitful area for future study.

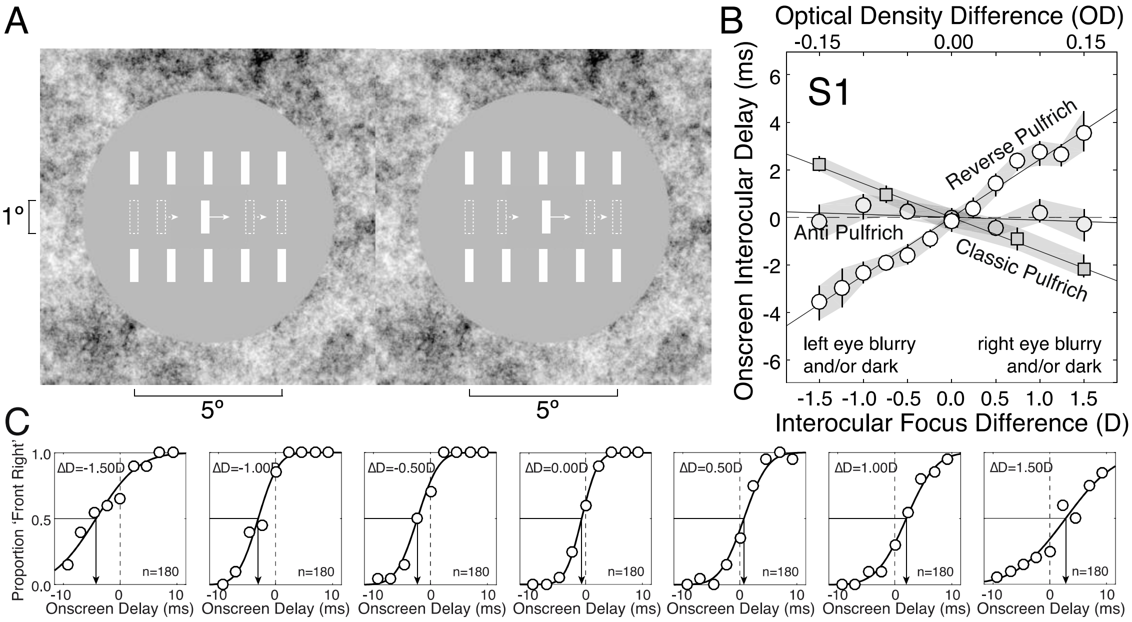

Figure 8.2. Reverse, Classic, and anti-Pulfrich effects. A. Binocular stimulus. The target was a horizontally moving 0.25x1.0º white bar. Arrows show motion speed and direction, and dashed bars show bar positions throughout a trial; both are for illustrative purposes only and were not present in the actual stimulus. Observers reported whether they saw three-dimensional (3D) target motion as 'front right' or 'front left' with respect to the screen. Stationary white 'picket fence' reference bars served to indicate the screen distance. Fuse the two half-images to perceive the stimulus in 3D. Cross- and divergent-fusers will perceive the bar nearer and farther than the screen, respectively. **B.** Points of subjective equality (PSEs) for one human observer, expressed as onscreen interocular delay relative to baseline. Interocular differences in focus error (bottom axis, white circles) cause the Reverse Pulfrich effect. Interocular differences in retinal illuminance (top axis, gray squares) cause the Classic Pulfrich effect. Appropriately tinting the blurring lens (light gray circles) can eliminate the motion illusions and act as an anti-Pulfrich prescription. (In anti-Pulfrich conditions, the optical density was different for each observer at each interocular focus difference.) Shaded regions indicate bootstrapped standard errors. Best-fit regression lines are also shown. **C.** Psychometric functions for seven of the Reverse Pulfrich conditions in B. Arrows indicate the raw PSE in each condition.

The performance of the first human observer is consistent across all observers and experiments (Figure 8.3D; Figure8.6). The interocular differences in processing speed were 1.4-3.7ms across observers for 1.5D differences in focus error and 1.5-2.1ms for 0.15OD differences in retinal illuminance. Similar effects are obtained with low- and high-pass filtering. These differences in processing speed may appear modest. But a few milliseconds difference in processing speed can lead to dramatic illusions in depth (see below).

Effect sizes vary across observers but appear correlated in each observer across conditions (Figure 8.3D). A larger pool of observers is necessary to confirm this trend. Future studies should measure the range and determine the origin of these inter-observer differences. Developing techniques that increase the speed of data collection will aid these efforts[326].

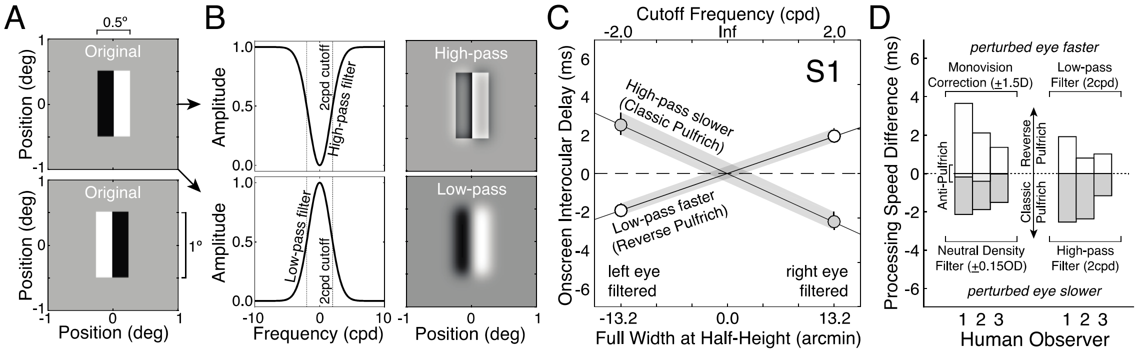

Figure 8.3. Spatial frequency filtering and the Pulfrich effect. **A.** Original stimuli were composed of adjacent black-white (top) or white-black (bottom) 0.25ºx1.00º bars. **B.** High-pass or low-pass filtered stimuli (shown only for black-white bar stimuli). High- and low-pass filtered stimuli were designed to have identical luminance and contrast (see Figure 8.8). **C** Resulting interocular delays. High-pass filtered stimuli are processed slower, and low-pass filtered stimuli are processed faster than the original unfiltered stimulus. Negative cutoff frequencies indicate that the left eye was filtered (high- or low-pass). Positive cutoff frequencies indicate that the right eye was filtered. **D** Effect sizes for each human observer in multiple conditions, obtained from the best-fit regression lines (see Figures 8.2B and 8.3C). Two manipulations resulted in Reverse Pulfrich effects (white bars): blurring one eye (left) and low-pass filtering one eye (right). Two manipulations resulted in Classic Pulfrich effects (gray bars): darkening one eye (left) and high-pass filtering one eye (right). A fifth manipulation—appropriately darkening the blurring lens (left, small light gray bars)—eliminates the Pulfrich effect and acts as an anti-Pulfrich correction.

8.1.1. Motion illusions in the real world

Monovision corrections cause misperceptions of motion. How large are these misperceptions likely to be in daily life? If the illusions are small, they will impose no impediment and can be safely ignored. If the illusions are large, they may have serious consequences. To generalize laboratory results to the real world, differences in viewing conditions must be considered. The same focus error causes less blur with smaller pupils, the same interocular difference in processing speed results in larger binocular disparities at faster speeds, and the same disparity specifies larger depths at longer viewing distances. Thus, all these factors—pupil size, target speed, and viewing distance—must be considered when predicting the severity of misperceptions that wearers of monovision corrections are likely to experience in daily life.

Consider a target object, five meters away, moving from left to right in daylight conditions. Predicted illusion sizes with different monovision corrections strengths are shown for one observer as a function of target speed (Figure 8.4A). A +1.5D difference in optical power (far lens over the left eye), a common monovision correction strength[97], will cause the distance of a target moving at 15 miles per hour to be overestimated by 2.8m. This, remarkably, is the width of a narrow street lane! If the prescription is reversed (-1.5D; far lens over right eye) target distance will be underestimated by 1.3m. Also, illusion sizes should increase with faster target speeds, stronger monovision corrections, and dimmer lighting conditions[203,208,319,327] (e.g., driving at dawn, dusk, or night; see section 8.2).

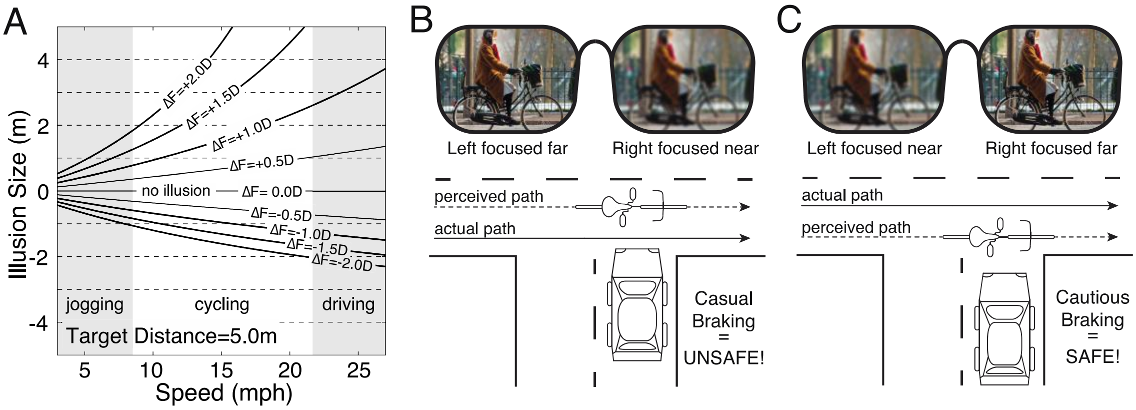

Figure 8.4. Monovision corrections and misperceptions of depth. A. Illusion size in meters as a function of speed for an object moving from left to right at 5.0m for different monovision corrections strengths (curves). Monovision correction strengths (interocular focus difference, ΔF) typically range between 1.0D and 2.0D; strengths of 0.5D are typically not prescribed, but we show them for completeness. Shaded regions show speeds associated with jogging, cycling, and driving. Illusion sizes are predicted directly from stereo-geometry (section 8.2) assuming a pupil size (2.1mm) that is typical for daylight conditions[327], and assuming interocular delays that were measured in the first human observer (see Figure 8.2B). The predictions also assume that the observer can sharply focus the target at 5.0m in one eye[9]. **B** The distance of cross traffic moving from left to right will be overestimated when the left eye is focused far (sharp) and the right eye is focused near (blurry). **C** The distance of left-to-right cross traffic will be underestimated when the left eye is focused near (blurry) and the right eye is focused far (sharp).

Illusions this large will not only be disturbing for the person wearing the monovision correction; they may compromise public safety. In countries where motorists drive on the right side of the road (e.g., USA), cars and cyclists approaching in the near lane of cross traffic move from left to right. Placing the far lens in the left eye will cause distance overestimation, which may result in casual braking and increase the likelihood of traffic accidents (Figure 8.4B). Placing the far lens in the right eye may be advisable. The resulting distance underestimation should result in more cautious braking and reduce the likelihood of collisions (Figure 8.4C). In countries where motorists drive on the left side of the road (e.g., United Kingdom), the opposite practice should be considered (i.e., far lens in the left eye). The current standard is to place the far lens in the dominant eye[97,162], but this does not appear to improve patient acceptance rate, patient satisfaction[162,328], or quantitative measures of visual performance[98]. Although the scenarios just discussed are not the only scenarios that should be considered, they may invite a reexamination of standard ophthalmic practice.

In the real world, many cues exist that tend to indicate the correct rather than illusory depths. The literature on cue combination[329,330] suggests that in cue-rich situations the magnitude of the Reverse Pulfrich effect may be somewhat reduced from the predictions in Figure 8.4A. It will be of clinical and scientific interest to precisely examine how the Reverse Pulfrich effect manifests in the rich visual environment of the real world[100]. This question could be examined with virtual- or augmented-reality headsets that can provide researchers with precise programmatic control of near-photorealistic graphical renderings.

Another implication of these results is that objects moving toward an observer along straight lines should appear to follow S-curve trajectories (Figure 8.5). These misperceptions should make it difficult to play tennis, baseball, and other ball sports requiring accurate perception of moving targets. Monovision corrections should be avoided when playing these sports.

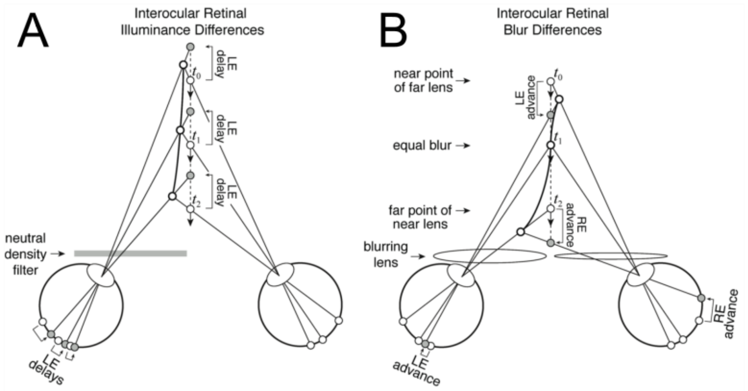

Figure 8.5. Misperception of motion towards the observer. **A.** Predicted perceived motion trajectory (bold curve), given target motion directly towards the observer (dashed line), with an interocular retinal illuminance difference. Here, a neutral density filter in front of the left eye causes its image to be processed more slowly, regardless of target distance. Stereo-geometry predicts that the target will appear to travel along a curved trajectory that bends towards the darkened eye (bold curve) rather than in a straight line. **B.** Predicted perceived motion trajectory, given target motion directly towards the observer, with an interocular blur difference. The left eye is corrected for near and the right eye is corrected for far. The eye that is processed more quickly now changes systematically as a function of target distance. When the target is far, the left eye image will be blurry and be processed more quickly. When the target arrives at an intermediate distance where both eyes will form equally blurry images, the processing will be the same in both eyes and the target will appear to move directly towards the observer. When the target is near, the right eye image will be blurry and processed more quickly. The resulting illusory motion will trace an S-curve trajectory as the target traverses the distances between the near point of the far lens and the far point of the near lens. Even more striking effects occur for targets moving towards and to the side of the observer, along oblique motion trajectories. A full description of these effects, however, is beyond the scope of the current chapter. (Note: the diagrams are not to scale.)

Eliminating monovision-induced motion illusions

Reconsidering prescribing practices is one approach to minimizing the consequences of monovision-induced motion illusions, but it is not the perfect solution. It would be far preferable to eliminate the illusions. Because increased blur and reduced retinal illuminance have opposite effects on processing speed, it should be possible to null the two effects by tinting the blurring lens. We reran the original experiment, with appropriately tinted blurring lenses for each human observer (see section 8.2). This 'anti-Pulfrich correction' eliminates the motion illusion in all human observers (Figures 8.2B and 8.3D). Of course, for a given monovision prescription, the lens forming the blurry image varies with the target distance. Anti-Pulfrich monovision corrections thus cannot work at all target distances. Tinting the near lens (blurry, dark images for far targets; sharp, dark images for near targets) will eliminate the Pulfrich effect for far targets but exacerbate it for near targets. However, because many presbyopes retain some accommodation and use it to focus the distance-corrected eye[331] the range of far distances for which motion misperceptions may be eliminated can be quite large: 0.67m to the horizon for a presbyope with 1.5D of residual accommodation. Given that accurate perception of moving targets is probably more important for tasks at far than at near distances (e.g., driving vs. reading), tinting the near lens is likely to be the preferred solution. This issue, however, clearly needs further study.

For any given monovision prescription, the lens forming the blurry image varies according to the target distance. Anti-Pulfrich prescriptions thus cannot work at all target distances. Tinting the near lens (blurry, dark images for far targets; sharp, dark images for near targets) will eliminate the Pulfrich effect for far targets but exacerbate it for near targets. However, because many presbyopes have some residual accommodation and because they tend to use it to focus the distance-corrected eye[9,331], the range of far distances over which motion misperceptions can be eliminated may be quite large: 0.67m to the horizon for a patient with 1.5D of residual accommodation. Given that accurate perception of moving targets is likely to be more critical for tasks at far distances (e.g., driving) than at near distances (e.g., reading), tinting the near lens is likely to be the preferred solution. This issue, however, clearly needs further study.

Adaptation
Previous studies have shown that blur perception changes with consistent exposure to blur[332]. Do motion illusions change as patients adapt to monovision corrections over time? This question has not been asked before. The literature on adaptation to the Classic Pulfrich effect may provide a guide, but the results are mixed. At short time scales (i.e., minutes), motion illusions remain unchanged[208] or increase[207] until reaching a steady state. At longer time scales (i.e., days), motion illusions remain the same or decrease as observers adapt to interocular differences in light level[333]. However, in these previous adaptation studies, the eye with the dark image was always the same. With a monovision correction, the eye with the blurry image varies with the target distance. Thus, it is unclear whether observers will adapt such that motion illusions caused by the Reverse Pulfrich effect will be reduced. This is an important area for future study, both for basic science and the development of successful clinical interventions.

Spatial frequency binding problem
Scientific discoveries often present new scientific opportunities. We have argued that the Reverse Pulfrich effect occurs because sharp images contain more high frequencies (i.e., fine details) than blurry images and because high frequencies are processed more slowly than low frequencies. Indeed, different spatial frequencies are processed in the early visual cortex with different latencies[317]. Thus, the frequency components of an image should appear to split apart when a target object moves, causing rigidly moving images to appear non-rigid. This percept is not typically experienced. To achieve a unified percept, the visual system must therefore have a mechanism for binding the different frequency components together.

Variants of the paradigm that we have used to measure the Reverse Pulfrich effect have great potential for investigating the visual system's solution to the spatial frequency-binding problem. The measurements have exquisite temporal precision, often within fractions of a millisecond (Figures 8.2B and 8.2C, Figures 8.3C 8.3D). This precision should prove useful for studying this fundamentally important but understudied problem in vision and visual neuroscience.

8.1.2. Results for all observers

Figure 8.6 shows the results for all observers. Figure 8.6A shows the results for Classic, Reverse, and anti-Pulfrich conditions, Figure 8.6B shows the discrimination threshold for Classic, Reverse, and anti-Pulfrich conditions and Figure 8.6C shows the results for interocular onscreen blur differences.

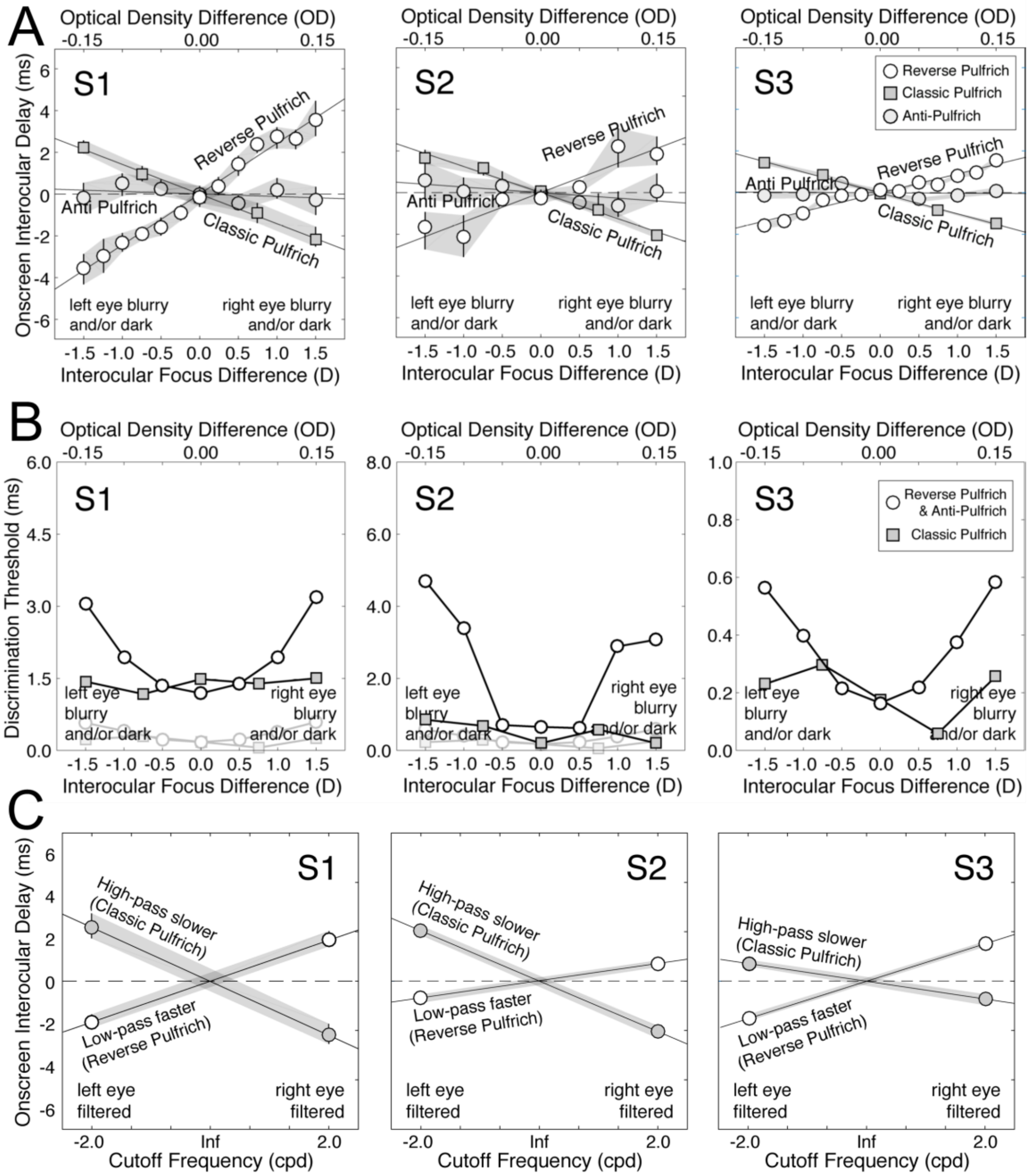

Figure 8.6. Reverse, Classic, anti-Pulfrich, and filtered stimulus conditions: Interocular delays and discrimination thresholds. **A**. Reverse, Classic, and anti-Pulfrich effects. Interocular differences in focus error cause the Reverse Pulfrich effect; the blurrier image is processed more quickly. Interocular differences in retinal illuminance cause the Classic Pulfrich effect; the darker image is processed more slowly. In the anti-Pulfrich condition, the blurry image is darkened to eliminate interocular delay. **B**. Discrimination thresholds. Thresholds for each observer ($d' = 1.0$) in the Reverse Pulfrich conditions (interocular focus differences) and the anti-Pulfrich conditions (interocular focus differences plus retinal illuminance differences) were similar and were thus averaged together (white circles). In each human observer, discrimination thresholds increased systematically with differences in interocular blur, consistent with the classic literature on how blur differences deteriorate stereoacuity[325]. These threshold functions thus provide evidence that the desired optical conditions were achieved. To reduce clutter, bootstrapped 95% confidence intervals are not plotted. In all cases but one, the confidence interval is smaller than the data point. Discrimination thresholds in the Classic Pulfrich conditions (i.e., interocular retinal illuminance differences only) are also shown (gray squares). Differences in retinal illuminance up to +0.15OD had no systematic effect on thresholds. (Note: the y-axis has a different scale for each observer to emphasize the similarities in the threshold patterns. To give a sense of scale, the Classic Pulfrich data from observer S3, the most sensitive observer, is re-plotted in the subplots for observers S1 and S2; faint circles and squares.). **C.** Interocular delays with high- and low-pass filtered stimuli for each human observer. The onscreen image for

one eye was filtered and the image for the other eye was left unperturbed. High-pass filtered images were processed slower than the unperturbed images, similar to how reduced retinal illuminances induce the Classic Pulfrich effect. Low-pass filtered images were processed faster than unperturbed images, similar to how optical blur induces the Reverse Pulfrich effect.

8.2. Methods

8.2.1. Subjects

Three human observers (two males, one female) ran in the experiment; two were authors. All human observers had normal or corrected to normal visual acuity (20/20), a history of isometropia, and normal stereoacuity as confirmed by the Titmus Stereo Test. The observers were aged 26, 31, and 40 years old and had refractive errors of -6.0, -2.0, and 0.0 diopters at the time of the measurements.

8.2.2. Apparatus

Stimuli were displayed on haploscope system I (HI, described in section 2.2.1.1). In summary, left- and right-eye images were presented on two identical VPixx VIEWPixx LED monitors controlled by the same AMD FirePro D500 graphics card with 3GB GDDR5 VRAM, to ensure that the left and right eye images were presented synchronously.

Human observers viewed the monitors through mirror cubes with 2.5cm circular openings positioned one inter-ocular distance apart. Heads were stabilized with a chin and forehead rest. The haploscope mirrors were adjusted such that the vergence distance matched the distance of the monitors. The light path from the monitor to the eye was 100cm. Anti-aliasing enabled sub-pixel resolution permitting accurate presentations of disparities as small as 15-20arcsec.

8.2.3. Stimuli

The target stimulus was a binocularly presented, horizontally moving, white vertical bar (Figure 8.2A). The target bar subtended 0.25x1.00º of visual angle. In each eye, the image of the bar moved left and right with a sinusoidal profile. An interocular phase shift between the left- and right-eye images introduced a spatial disparity between the left- and right-eye bars. The left- and right-eye onscreen bar positions were given by

$$\begin{aligned} x_L(t) &= Ecos(2\pi\omega t + \phi_0 + \phi) \\ x_R(t) &= Ecos(2\pi\omega t + \phi_0) \end{aligned} \qquad 8.1$$

where $x_L(t)$ and $x_R(t)$ are the left and right eye x-positions in degrees of visual angle, E is the movement amplitude in degrees of visual angle, ω is the temporal frequency, ϕ_0 is the starting phase which in our experiment determines whether the target starts on the left or the right side of the display, t is time, and ϕ is the phase shift between the images.

The interocular temporal shift (i.e., delay or advance) in seconds associated with a particular phase shift is

$$\Delta t = \phi/(2\pi\omega) \qquad 8.2$$

Negative values indicate the left eye onscreen image is delayed relative to the right; positive values indicate the left eye onscreen image is advanced relative to the right.

When the interocular temporal shift equals zero, the virtual bar moves in the frontoparallel plane at the distance of the monitors. When the interocular temporal shift is non-zero, a spatial binocular disparity results and the virtual bar follows a near-elliptical trajectory of motion in depth. The binocular disparity in radians of visual angle as a function of time is given by

$$\delta(t) = x_R(t) - x_L(t) = 2Esin\left(\frac{\phi}{2}\right)cos\left(2\pi\omega t + \phi_0 + \frac{\phi}{2}\right) \tag{8.3}$$

Here, negative disparities are crossed and positive disparities are uncrossed, indicating that the target is nearer and farther than the screen distance, respectively. The disparity takes on its maximum magnitude when the perceived stimulus is directly in front of the observer and the lateral movement is at its maximum speed. When the stimulus is moving to the right, the maximum disparity in visual angle is given by $\delta_{max} = 2Esin(\phi/2)$.

In our experiment, the movement amplitude was 2.5º of visual angle (i.e., 5.0º total change in visual angle in each direction), the temporal frequency was 1 cycle per second and the starting phase ϕ_0 was randomly chosen to be either 0 or π. Restricting the starting phase to these two values forced the stimuli to start either 2.5º to the right or 2.5º to the left of the center on each trial. The onscreen interocular phase shift ranged between ±216 arcmin at maximum, corresponding to interocular delays of ±10.0 ms. The range and particular values were adjusted to the sensitivity of each human observer.

Two sets of five vertical 0.25x1.00º bars in a 'picket fence' arrangement flanked the region of the screen traversed by the target bar. The picket fences were defined by disparity to be at screen distance and served as a stereoscopic reference for the observer. A 1/f noise texture, also defined by disparity to be at the screen distance, covered the periphery of the display to aid binocular fusion. A small fixation dot marked the center of the screen.

8.2.4. Procedure

The observer's task was to report whether the target bar appeared to move leftward or rightward when the stimulus was nearer than the screen in its virtual trajectory in depth. Observers fixated on the fixation dot throughout each trial. Using a one-interval two-alternative forced-choice procedure, nine-level psychometric functions were collected in each condition using the method of constant stimuli. Each function was fit with a cumulative Gaussian using maximum likelihood methods. The 50% point on the psychometric function—the point of subjective equality (PSE)—indicates the onscreen interocular delay needed to null the interocular difference in processing speed. The pattern of PSEs across conditions was fit via linear regression, yielding a slope and y-intercept. Average y-intercepts were nearly zero for each observer: 0.06ms, -0.06ms, and 0.01ms, respectively. To emphasize the differences in slope (i.e., the changes in processing speed in the slope) induced by interocular perturbations, we zeroed the y-intercepts when plotting the PSE data. Observers responded to 180 trials per condition in counter-balanced blocks of 90 trials each. All experiments were performed in MATLAB 2017b using Psychtoolbox (version 3.0.12)[241]. All analyses were performed in MATLAB 2017b. Psychophysical data are presented for each human observer. Cumulative Gaussian fits of the psychometric functions were in good agreement with the raw data. Bootstrapped standard errors are reported on all data points unless otherwise noted.

<u>Defocus and blur</u>
The interocular focus difference is the magnitude of the defocus in the right eye minus the magnitude of the defocus in the left eye

$$\Delta F = |\Delta D_R| - |\Delta D_L| \quad 8.4$$

where $\Delta D = D_{focus} - D_{target}$ is the defocus, the difference between the dioptric distances of the focus and target points. To manipulate the amount of defocus blur in each eye, we positioned trial lenses ~12mm from each eye, centered on each optical axis, between each eye, and the front of the mirror cubes of the HI system.

Human observers ran in thirteen conditions defined by interocular focus difference. (One observer, S2, ran in only seven). Each eye was myopically defocused from 0.00D to 1.50D in 0.25D steps while the other eye was kept sharp. The first six conditions defocused the left eye (0.25D to 1.50D in 0.25D steps) while leaving the right eye sharp (ΔF<0.0D). In the seventh condition, both eyes were sharp (ΔF=0.0D). The final six conditions defocused the right eye (0.25D to 1.50D in 0.25D steps) while leaving the left eye sharp (ΔF>0.0D).

In the condition in which both eyes were sharply focused, the optical distances of the left- and right-eye monitors were set to optical infinity with +1.00D trial lenses. All human observers indicated that they could sharply focus the monitor when they fully relaxed the accommodative power of their eyes. Because each trial lens absorbs a small fraction of the incident light, having a trial lens in front of each eye in all conditions ensures that retinal illuminance is matched in both eyes in all conditions. To induce interocular differences in focus error, we placed a stronger positive lens (i.e., +1.25D, +1.50D, +1.75D, +2.00D) in front of one eye. This procedure puts one eye's monitor beyond optical infinity, thus introducing myopic focus errors that cannot be cleared by accommodation. Before each run, the observer viewed a test target to confirm that he/she could focus targets at optical infinity in the 0.0D baseline condition. Undercorrected hyperopia or overcorrected myopia could place the far point of each eye beyond optical infinity, frustrating our attempts to control the optical conditions. To protect against this possibility, before running each observer, we estimated the far points of the eyes with standard optometric techniques. Then, if necessary, we adjusted the trial lens power so that the monitors were positioned at the desired optical distance.

Another potential concern is that the eyes could accommodate independently to clear the blur in each eye. However, there are several reasons to think that differential blur was successfully induced. First, positioning the optical distance of one monitor beyond optical infinity (see above) minimizes the possibility that differential optical power could be compensated by differential accommodation. Second, accommodation in the two eyes tends to be strongly coupled, especially for targets straight ahead at distances beyond 1.0m[9,331,334,335]. Third, discrimination thresholds ($d' = 1.0$) increase systematically with interocular difference in focus error, which is consistent with the literature showing that differential blur deteriorates stereoacuity[325].

8.2.4.1. Neutral Density Filters

To induce interocular differences in retinal illuminance we placed 'virtual' neutral density filters in front of the eyes. To do so, we converted optical density to transmittance, the proportion of incident light that is passed through the filter, using the standard expression $T = 10^{-OD}$ where T is the transmittance and OD is the optical density. Then, we reduced the luminance of one eye's monitor by a scale factor equal to the transmittance. We compared the performance of all observers with real and equivalent virtual neutral density filters, to find out about the accurate implementation of the virtual filters. In all observers, performance with real and equivalent virtual neutral density filters is essentially identical, suggesting that the virtual filters were implemented accurately (Figure 8.6).

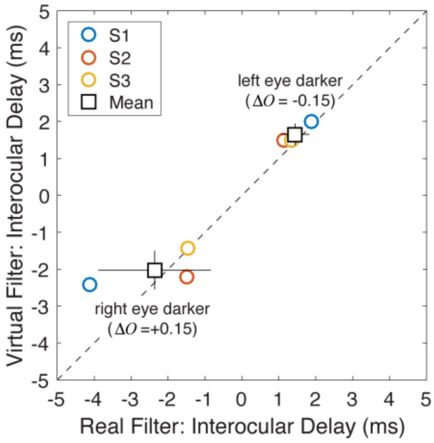

Figure 8.7. Real and virtual neutral density filters: Interocular delays. Real and virtual neutral density filters with the same optical densities (i.e., 0.15OD; 71% transmittance) caused similar delays for all human observers (colored circles) and the mean human observer (black square). Interocular differences in optical density, ΔO, are negative when the left eye retinal illuminance is reduced and positive when the right eye retinal illuminance is reduced. Error bars indicate standard deviations. The results suggest that the software implementation of the virtual neutral density filters was accurate.

The interocular difference in optical density $\Delta O = \Delta O_R - \Delta O_L$ is the difference between the optical density of filters placed over the right and left eyes. Human observers ran in five conditions with virtual neutral density filters, with equally spaced interocular differences in optical density between -0.15 and 0.15. Two conditions introduced a filter in front of the left eye (ΔO<0.00). In one condition, both eyes were unfiltered (ΔO=0.00). And two other conditions introduced a filter in front of the right eye (ΔO>0.00).

8.2.4.2. Low- and high-pass spatial filtering

To test the hypothesis that the Reverse Pulfrich effect is caused by differences in the processing speed of different spatial frequencies, we filtered the onscreen stimulus of one eye with two different frequency filters. The low-pass filter was Gaussian-shaped

$$k_{low} = e^{-0.5(f/\sigma_f)^2} \quad 8.5$$

with a standard deviation $\sigma_f = f_0/\sqrt{\ln{(4)}}$ set by the cutoff frequency f_0 so that the filter reached half-height at f_0 (i.e., 2cpd in the current experiments; see Figure 8.3). The high-pass filter complemented the low-pass filter and was given by

$$k_{high} = 1 - k_{low} \quad 8.6$$

After high-pass filtering, the mean luminance was added back in so that the high-pass and low-pass filtered stimuli had the same mean luminance.

To isolate the impact of spatial frequency content on processing speed, we modified the onscreen stimulus from the main experiment. Rather than the 0.25ºx1.00º white bar, the onscreen stimulus was changed to a 0.50ºx1.00º stimulus that was composed of adjacent 0.25x1.0º black and white (or white and black) bars (Figure 8.3A). This modification ensured that the low- and high-pass filtered stimuli had identical luminance and identical contrast (Figure 8.8). Each human observer collected 180 trials in each of eight conditions—low- vs. high-pass filtering, left- vs. right-eye filtered, black-white vs. white-black stimulus types—collected in counter-balanced order. Black-white vs. white-black stimulus types had little impact so results were collapsed across stimulus types.

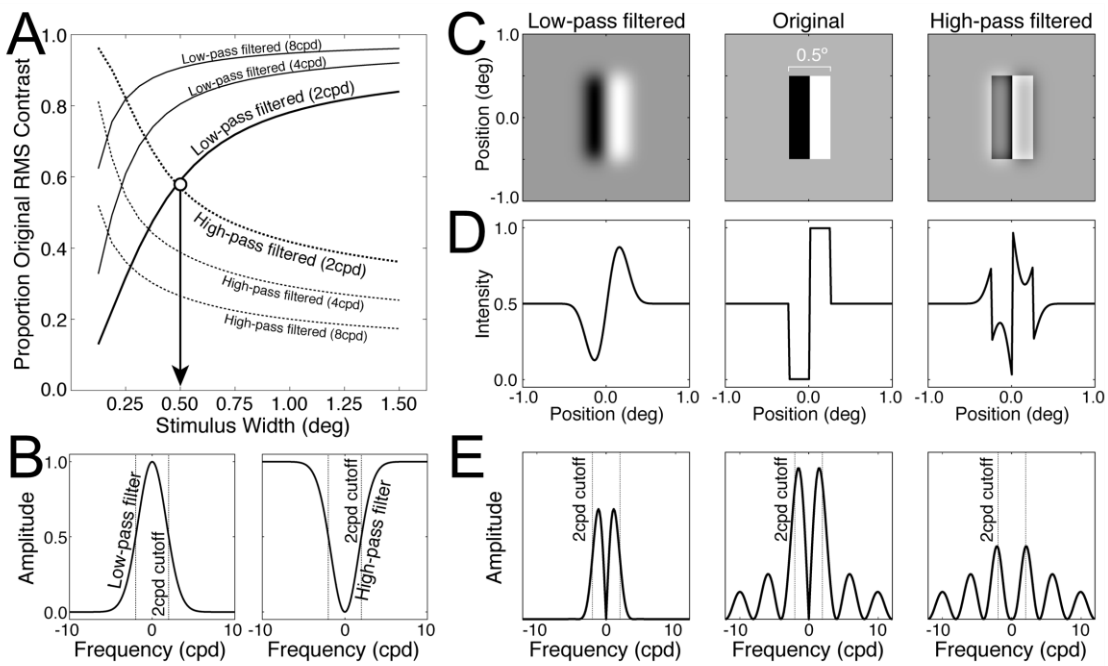

Figure 8.8. Spatial frequency filtered stimuli: stimulus construction. **A**. Proportion of original stimulus contrast after low-pass filtering vs. high-pass filtering (solid vs. dashed curves, respectively) as a function of total black-white (or white-black) bar width. The white circle and arrow indicate the stimulus width (0.5º) that equates to the root-mean-squared (RMS) contrast of the stimulus after low and high-pass filtering. Because low-pass and high-pass filtered images had identical luminance and contrast, the differential effects in Figure 8.6C cannot be attributed to luminance or contrast. **B**. Low-pass and high-pass filters with a 2cpd cutoff frequency. **C.** Low-pass filtered stimulus, original stimulus, and high-pass filtered stimulus with matched luminance and contrast. **D**. Horizontal intensity profiles of the stimuli in C. **E**. Amplitude spectra of the horizontal intensity profiles in D. Note how, for each stimulus type, the peak of the lowest frequency lobe shifts relative to the cutoff frequency of the filters.

8.2.4.3. Generalizing results to the real world

To predict the motion misperceptions that monovision will cause in the real world, it is important to account for the differences in viewing conditions that may impact illusion sizes. Although the experimental conditions were chosen based on differences in focus error, the Reverse Pulfrich effect is more directly mediated by differences in image blur. The amount of retinal image blur in each eye depends both on the focus error and on the pupil diameter. Thus, it is important to account for changes in pupil diameter that will be caused by luminance differences between the lab and the viewing conditions of interest.

The blur circle diameter in radians of visual angle is given by

$$\theta_b = A|\Delta D| \tag{8.7}$$

where θ_b is the diameter of the blur circle in radians of visual angle and A is the pupil aperture (diameter) in meters. In our experiments, we assumed a pupil diameter of 2.5mm, corresponding to the luminance during the experiment[327]. Under the geometrical optics approximation, the absolute value of the defocus $|\Delta D|$ in the blurry eye equals the absolute value of the interocular focus difference $|\Delta F|$ because one eye was always sharply focused (i.e., $min(|\Delta D_L|, |\Delta D_R|)$=0.0D) in our experiments.

The interocular delay in seconds is linearly related to each level of blur by

$$\Delta t = \alpha_{\Delta F} \frac{\theta_b}{A_{exp}} + \beta_{\Delta F} \quad 8.8$$

where $\alpha_{\Delta F}$ and $\beta_{\Delta F}$ are the slope and constant of the best-fit line to the data in Figure 8.2B, and A_{exp} is the pupil diameter of the observer in meters during the experiment. The constant (i.e., y-intercept) can be dropped assuming it reflects response bias and not sensory-perceptual bias.

For a target moving at a given velocity in meters per second, a particular interocular difference in processing speed will yield an effective interocular spatial offset (i.e., position difference)

$$\Delta x = v \Delta t \quad 8.9$$

The illusory distance of the target, predicted by stereo-geometry, is given by

$$\hat{d} = \frac{I}{(I + \Delta x)} d \quad 8.10$$

where I is the inter-pupillary distance and d is the actual distance of the target.

Combining Equations 8.7-10 yields a single expression for the illusory distance

$$\hat{d} = \left(\frac{I}{I + v|\Delta F| R \alpha_{\Delta F}} \right) \quad 8.11$$

where $R = A/A_{exp}$ is the ratio between the pupil diameters in the viewing condition of interest and in the lab when the psychophysical data was collected. Finally, taking the difference between the illusory and actual target distances $\hat{d} - d$ yields the illusion size (see Figure 8.4A).

The expression for the illusory distance can also be derived by first computing the neural binocular disparity caused by the delay-induced position difference, and then converting the disparity into an estimate of depth. The binocular disparity in radians of visual angle is given by

$$\delta = \frac{\Delta x}{d} \quad 8.12$$

The relationship between illusory distance, binocular disparity, and actual distance is given by

$$\hat{d} = \frac{I}{(I + \mathrm{d}\delta)} d \quad 8.13$$

Plugging Equation 8.12 into Equation 8.13 yields Equation 8.10. Thus, both methods of computing the illusory distance are equivalent.

8.2.5. Anti-Pulfrich monovision corrections

Reducing the image quality of one eye with blur increases the processing speed relative to the other eye and causes the Reverse Pulfrich effect. Reducing the retinal illuminance of one eye reduces the processing speed relative to the other eye and causes the Classic

Pulfrich effect. Thus, in principle, it should be possible to null the two effects by reducing the retinal illuminance of the blurry eye. The interocular delay in seconds is linearly related to each interocular difference in optical density ΔO by

$$\Delta t = \alpha_{\Delta O}(\Delta O) + \beta_{\Delta O} \quad 8.14$$

The optical density that should null the interocular delay of a given interocular focus difference is given by

$$\Delta O_0 = -\frac{\alpha_{\Delta F}}{\alpha_{\Delta O}} \Delta F \quad 8.15$$

the interocular difference in focus error scaled by the ratio of the slopes of the best-fit regression lines to the Reverse and Classic Pulfrich datasets. The optical density predicted by the two regression slopes eliminates the Pulfrich effect (Figure 8.2B, Figure 8.3D).

8.3. Conclusions

We have reported a new version of a 100-year-old illusion: the Reverse Pulfrich effect. We found that interocular differences in image blur, like those caused by monovision corrections, cause millisecond interocular differences in processing speed. For moving targets, these differences can cause dramatic illusions of motion in depth. The fact that a mismatch of a few milliseconds can yield substantial misperceptions highlights how exquisitely the visual system must be calibrated for accurate percepts to occur. The fact that these motion illusions are rare indicates how well the visual system is calibrated under normal circumstances.

Chapter 9. Reverse Pulfrich effect: contact lenses

In this chapter, we have extended the measurements of the Reverse Pulfrich effect and anti-Pulfrich corrections using contact lenses. The relevance of testing the presence of the Reverse Pulfrich effect with contact lenses is both scientific and clinical. Clinically, contact lenses are the most common method for delivering monovision corrections. Scientifically, trial lenses of different powers can cause large magnification differences between the eyes. The use of contact lenses prevents these magnification differences and allows us to confidently attribute the Reverse Pulfrich effect to only interocular optical blur differences.

This chapter is based on the published article by Victor Rodriguez-Lopez et al. *"Contact lenses, the Reverse Pulfrich effect, and anti-Pulfrich monovision corrections",* published in *Scientific Reports (2020)*. The co-authors of the study are Carlos Dorronsoro ad Johannes Burge.

The contribution of the author of the thesis was the conceptualization and design of the study and the literature research in collaboration with all the co-authors, the design of the experiments in collaboration with Carlos Dorronsoro, the collection and analysis of the data, the writing of the chapter and the editing of the chapter in collaboration with all co-authors.

This work was presented as a virtual poster contribution at the Association for Vision and Research in Ophthalmology (ARVO) virtual meeting in 2020. The author of the thesis was also interviewed by the media (Medscape Medical News) about the impact of this work on public safety once the virtual poster was presented.

9.1. Introduction

The previous chapter demonstrated that interocular differences in optical blur, like those induced by monovision corrections, have the potential to cause large errors in estimating the distance and 3D direction of moving objects. Under some conditions, the perceptual errors may be large enough to impact public safety[103]. For example, the distance to a cyclist in cross-traffic may be overestimated by nearly 9ft, the width of a narrow lane of traffic (Figure 9.1A). The illusion occurs because the image in the blurrier eye is processed more quickly by a few milliseconds than the image in the sharper eye. Blur removes high spatial frequencies (i.e., fine details) from the image[51,233,314], and high spatial frequencies are known to be processed more slowly[94,96,312,313,317,336]. Thus, the blurry image is processed more quickly because the high frequencies in the sharp image slow its processing down[103].

The Classic Pulfrich effect is induced by an interocular difference in retinal illuminance. However, darkening the image in one eye has the opposite effect of blur[305]. The darker image is processed more slowly rather than more quickly[203,208,319]. The response properties of neurons in both the retina and early visual cortex are thought to underlie the Classic Pulfrich effect[308,333]. The resulting illusions are thus similar to the illusions associated with the Reverse Pulfrich effect, except that the Classic Pulfrich effect causes distance underestimation whereas the Reverse Pulfrich effect causes distance overestimation, and vice versa (Figure 9.1B).

The previous chapter also demonstrated that anti-Pulfrich monovision corrections can eliminate the depth and motion misperceptions associated with the Reverse and Classic Pulfrich effects. The logic behind anti-Pulfrich corrections is simple. Blurry images are processed more quickly than sharp images (i.e., the Reverse Pulfrich effect). Dark images are processed more slowly than bright images (i.e., the Classic Pulfrich effect). Thus, if the blurry image is darkened appropriately, the two differences in processing speed cancel each other out and eliminate the misperceptions (Figure 9.1C). To date, however, the efficacy of anti-Pulfrich monovision corrections has been demonstrated only with interocular differences in optical power induced by trial lenses[103]. Monovision prescriptions are most commonly prescribed with contact lenses[97]. (Surgically implanted interocular lenses are the second most common[162,337,338].) Hence, it is important to demonstrate that anti-Pulfrich corrections are effective when implemented with the ophthalmic corrections that are most relevant to clinical practice.

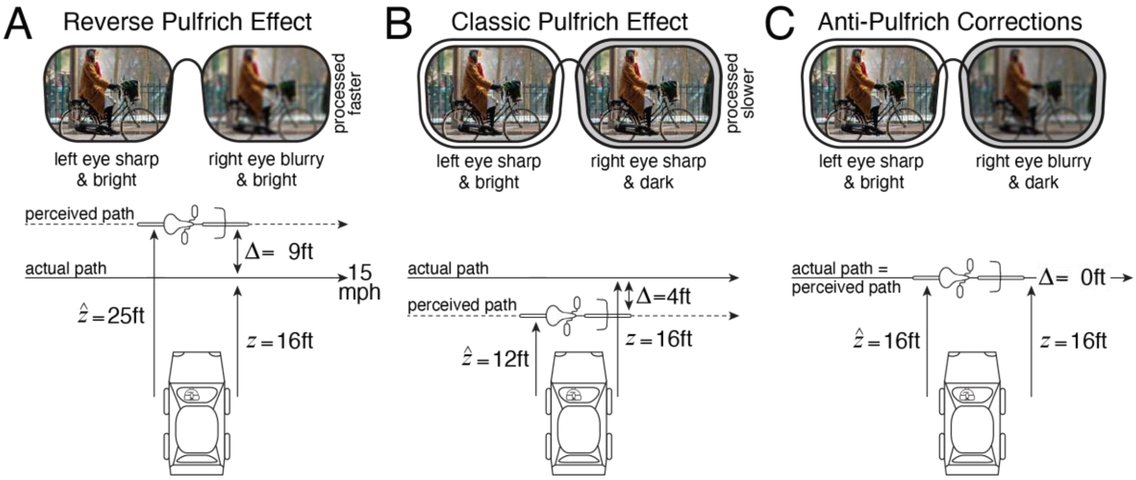

Figure 9.1. Reverse Pulfrich effect, Classic Pulfrich effect, and anti-Pulfrich monovision corrections. A. Interocular blur differences like those induced by monovision corrections cause the 'Reverse Pulfrich effect', a substantial misperception of the distance of moving objects. If the left eye is sharp and the right eye is blurred, an object moving from left to right will be misperceived as farther away than it is, and vice

versa. The blurry image is processed faster than the sharp image, causing a neural disparity that leads to depth misperceptions. In some scenarios, the distance misestimates can be substantial. Burge et al.[339] reported that, for an individual observer with a typical monovision correction strength of 1.5D, a cyclist moving left to right at 15mph at 16ft may be estimated to be at 25ft. This overestimation of 9ft is approximately the width of a narrow lane of traffic. These misperceptions occur because the blurrier eye is processed more quickly by only a few milliseconds. **B.** Interocular luminance differences cause the Classic Pulfrich effect. When both eyes are sharp, the darker eye is processed slower. If the left eye is bright and the right eye is dark, and both eyes are sharply focused, the distance to the same cyclist will be underestimated, because the darker eye is processed more slowly by a few milliseconds. **C.** Anti-Pulfrich monovision corrections can eliminate misperceptions by darkening the blurring lens. The Reverse and Classic Pulfrich effects cancel each other out.

Another reason to study the Reverse Pulfrich effect and anti-Pulfrich corrections with contact lenses is that, unlike trial lenses, contacts introduce negligible retinal magnification differences between the eyes. The retinal magnification induced by a lens increases with its optical power and its distance from the eye. Trial lenses, like eyeglasses, are positioned 10-14mm from the eye. Consequently, trial lenses of different powers induce both blur and magnification differences. The original demonstration of the Reverse Pulfrich effect thus leaves open the possibility that the Reverse Pulfrich effect could be due to interocular differences in magnification, rather than to interocular differences in blur. Although theoretical considerations and previously performed control experiments make this possibility unlikely, it should still be established empirically that differences in image magnification play no role in driving the effect.

A typical monovision correction induces a 1.50D difference in optical power between the eyes[97]. For contact lenses, which are fit directly on the cornea, this power difference translates into an interocular magnification difference of 0.4% (Figure 9.2A). For eyeglasses, which are typically positioned 10-14mm from the cornea, the same power difference translates into a magnification difference of between 1.5% and 2.1% (Figure 9.2B). Magnification differences of this size are thought to cause visual discomfort and other clinical issues[340]. This is the reason that monovision is most often implemented with contact lenses, surgically implanted interocular lenses, and laser corneal surgery, all of which induce negligible magnification differences.

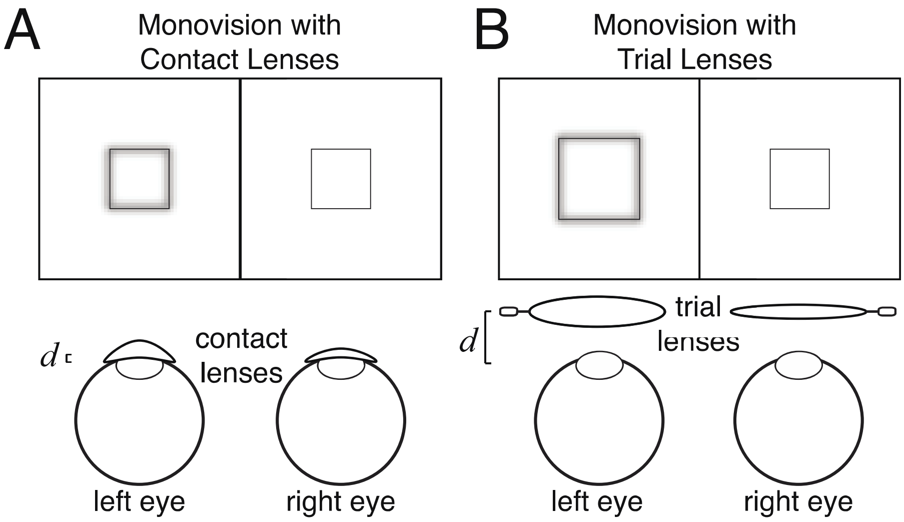

Figure 9.2. Magnification differences with contacts and trial lenses. A. Contact lenses with different power in the two eyes create interocular differences in blur with negligible interocular differences in magnification. Contact lenses produce negligible image magnification because they are fitted directly on the cornea. The distance *d* between the contact lens and the entrance pupil of the eye is quite small. **B.** Trial lenses with different powers in the two eyes create interocular differences in blur with non-negligible magnification differences between the eyes. Trial lenses produce substantially more image magnification than contact lenses of the same power because the distance between the lens and the entrance pupil is considerably larger (i.e., 10-14mm).

Measuring the Reverse Pulfrich effect with contact lenses has the benefit of i) isolating the impact of blur from the potential impact of magnification on processing speed, ii) testing for misperceptions in the optical conditions most similar to those induced by eye care practitioners, and iii) advancing towards a clinically applicable anti-Pulfrich correction.

9.2. Methods

9.2.1. Participants

Two male and two female observers between the ages of 25 and 30 participated in the experiment (27.1±2.1 years); all were in good ocular health. Anisometropia, a difference in refractive error between the eyes, was equal to or lower than 0.50D in all observers. The amount of astigmatism was subclinical in all observers but one, who had astigmatism of 0.50D. Visual acuity was normal or corrected-to-normal (i.e., visual acuity of 0.00 logMAR or better) in both eyes of each observer. Stereoacuity was also normal, as assessed with the Titmus stereo test (i.e., stereoacuity better than or equal to 30arcmin). The experimental protocols were approved by the Spanish National Research Council (CSIC) Bioethical Committee and were in compliance with the Declaration of Helsinki. All participants provided written informed consent.

9.2.2. Apparatus

The stimulus was displayed on the Stereoscopic Monitor (SM, see section 2.2.2), consisting of a stereo-3D UK UHD 49” monitor (LG49UH850V, LG) driven by an NVIDIA Quadro P4000 dual Graphic card. Passive circular polarization glasses selectively passed the appropriate image to each eye. The spatial resolution of the display was 3840x2160 pixels. After filtering by the glasses, only 3840x1080 interlaced pixels reached each eye. Combined with a transmittance of slightly less than 1.0, the effective luminance of the monitor for each eye was slightly less than 200cd/m^2.

The observer viewed the monitor from 2m, with his/her head stabilized by a chin and forehead rest. Observers viewed the display through custom-built mounts for trial lenses. The mounts were horizontally and vertically adjusted so that the optical element was centered along the line of sight of each eye.

9.2.3. Stimuli

The stimulus was the same stimulus used in Chapter 8 (see Figure 8.1). The target stimulus was a 0.25x1.00º white vertical bar that oscillated horizontally on a gray background (Figure 9.3A). The target bar traversed one cycle of a cosinusoidal trajectory during each trial. The left- and right-eye onscreen bar positions in degrees of visual angle were given by

$$\begin{gathered} x_L(t) = Ecos(2\pi\omega(t + \Delta t) + \phi_0) \\ x_R(t) = Ecos(2\pi\omega t + \phi_0) \end{gathered} \quad 9.1$$

where E is the movement amplitude in degrees of visual angle, ω is the temporal frequency, ϕ_0 is the starting phase, t is time, and Δt is the onscreen delay between the left- and right-eye target images. The onscreen interocular delay controlled whether stereo information specified ‘front left’ or ‘front right’ motion (Figure 9.3B). Note that we did not temporally manipulate when left- and right-eye images were presented onscreen. Rather, we calculated the effective binocular disparity given the target velocity and the desired onscreen delay on each time step, appropriately shifted the spatial positions of the left- and right-eye images to create an equivalent disparity, and presented these disparate images synchronously on each monitor refresh.

The onscreen binocular disparity associated with a given interocular delay as a function of time was given by

$$\delta(t) = x_R(t) - x_L(t) = 2Esin\left(\frac{\phi}{2}\right)cos(2\pi\omega(2t + \Delta t) + \phi_0) \tag{9.2}$$

where negative disparities are crossed (i.e., nearer than the screen) and positive disparities are uncrossed (i.e., farther than the screen).

9.2.4. Procedure

Each moving bar stimulus was presented as part of a one-interval two-alternative forced-choice (2AFC) procedure. The task was to report, via a key press, whether the target bar was moving leftwards (‘front left’) or rightwards (‘front right’) when the bar appeared to be in front of the plane of the screen. Nine evenly spaced levels of onscreen interocular delay between -10 and 10 milliseconds were presented with the method of constant stimuli. Twenty trials per level were collected for a total of 180 trials per condition.

The proportion ‘front right’ responses were recorded as a function of onscreen interocular delay and fit with a cumulative Gaussian via maximum likelihood methods. The point of subjective equality (PSE) indicates the onscreen interocular delay necessary to make the target appear to move within the screen plane. The PSE is opposite in sign and equal in magnitude to the neural difference in processing speed between the eyes.

Data were collected from each human observer in five different experiments; each experiment had multiple conditions (see below). In a given experiment, data was collected across all conditions in counterbalanced blocks of 90 trials each. Each block took approximately 2.5 minutes to complete. Experiment 1 measured the impact of interocular blur differences induced by contact lenses. Experiment 2 measured the impact of interocular blur differences induced by trial lenses. Experiment 3 measured the impact of interocular luminance differences between the eyes. Experiment 4 measured the efficacy of anti-Pulfrich monovision corrections with contact lenses. And Experiment 5 measured whether interocular magnification differences impact processing speed.

9.2.5. Optical Conditions in the Experiments

To determine the lens powers needed to induce the desired focus error and the resulting optical blur in each eye, we performed three separate steps. First, using standard methods of subjective refraction, we measured and corrected each observer to ensure that uncorrected refractive errors did not compromise the desired optical conditions. Second, we added a distance compensation power to set the optical distance of the screen to optical infinity; given that the actual distance of the screen was 2m, the required distance compensation power was +0.5D. Third, in each eye, we chose an optical power equal to the desired focus error (i.e., the excess power); the excess power was either positive or equal to zero. Importantly, adds excess optical power to a screen already at optical infinity position the optical distance of the screen beyond optical infinity. Thus, even when accommodation is in its most relaxed state, with a positive excess power the target image was focused in front of the retina. Our procedure, therefore, renders accommodation unable to compensate for the desired focus error caused by the excess optical power. The total optical power of the associated lens is thus given by

$$P = EP + CP + R_x \tag{9.3}$$

where EP is the excess power (i.e., the desired focus error), CP is the compensation power, and R_x is the refractive error of the human observer, all of which are expressed in diopters. Combining the total amount of optical power in one lens instead of using multiple lenses minimizes potential interocular differences due to reflections and transmission.

In experiments with contact lenses, the total optical power (Equation 9.3) was delivered with ACUVUE Moist monofocal soft contact lenses (Johnson & Johnson Vision Care, Jacksonville, USA). In the experiment with trial lenses, the excess and compensation powers were delivered with a trial lens, and the refractive error of each human observer was compensated for by their spectacles. In all other experiments, the total power was delivered by a single contact lens. The human observers had different amounts of myopia. Hence, across observers and experimental conditions (see below), the nominal power of the contact lenses ranged from -2.75D to +0.75D.

9.2.5.1. Image magnification

The relative magnification—the magnification caused by an ophthalmic lens relative to the naked eye—depends both on the power of the lens and on the distance of the lens to the entrance pupil of the eye. Under the thin lens approximation, which is appropriate in the present circumstances, image magnification M is given by

$$M = \frac{1}{1 - d \cdot P} \qquad 9.4$$

where d is the distance of the lens in meters to the entrance pupil and P is the power of the lens in diopters.

9.2.5.2.Luminance, optical density, and transmittance

To induce the required differences in retinal illuminance, we reduced the luminance of the perturbed eye's onscreen image by a scale factor equivalent to the transmittance of a neutral density filter with a particular ocular density. The transmittance is given by

$$T = 10^{-OD} \qquad 9.5$$

where OD is the optical density of the filter. We have previously verified that this procedure (using 'virtual' neutral density filters) yields results that are equivalent to using real neutral density filters[103].

9.2.5.3. Interocular differences in focus error, optical density, and magnification

The interocular difference in focus error (i.e., optical power) is defined as the difference in excess optical power between the eyes

$$\Delta F = EP_R - EP_L \qquad 9.6$$

where EP_L and EP_R are the excess optical powers in diopters of the left and right eyes, respectively. In experiments having conditions with non-zero differences in focus error (Experiments 1, 2, and 4), excess power (i.e., EP>0.0D) was induced in one eye only - the perturbed eye- while the other eye was kept sharply focused on the screen distance (i.e., EP=0.0D). All observers reported that the nominally sharp eye was subjectively well focused before measurements began. In these experiments, the interocular difference in focus error ranged from -1.5D to 1.5D.

The interocular difference in luminance is quantified by the interocular difference in optical density

$$\Delta O = \Delta O_R - \Delta O_L \qquad 9.7$$

where ΔO_L and ΔO_R are the optical density of the neutral density filters in the left and right eyes. In experiments having conditions with non-zero interocular differences in optical density (Experiments 3 and 4), the luminance in one eye was reduced whereas the other eye was left unperturbed. In these experiments, the interocular difference in optical density ranged from -0.15OD to 0.15OD. An optical density of 0.15OD corresponds to a transmittance of 70.8%.

The interocular difference in onscreen magnification is given by

$$\Delta M = M_R - M_L \qquad 9.8$$

where M_L and M_R represent the magnification associated with the left- and right-eye images, respectively. In the experiment that manipulated magnification differences onscreen (Experiment 5), the interocular difference in magnification ranged from -3.6% to 3.6%. Magnification differences of this size are twice the magnification difference induced by trial lenses differing by 1.5D in optical power.

9.2.5.4. Quantifying differences in processing speed from differences in blur and luminance

The interocular difference in processing speed was measured for interocular differences in focus error ranging from -1.5D to 1.5D and interocular differences in optical density ranging from -0.15OD to -0.15OD. The interocular difference in processing speed (i.e., interocular delay) is linearly related to the interocular difference in the focus error

$$\Delta t = \alpha_{\Delta F} \cdot \Delta F + \beta_{\Delta F} \qquad 9.9$$

where $\alpha_{\Delta F}$ and $\beta_{\Delta F}$ are the slope and intercept of the best line fit via least squared regression[103]. Just as with blur differences, the interocular delay is linearly related to the difference between the optical densities of the virtual filters in the two eyes. Specifically,

$$\Delta t = \alpha_{\Delta O} \cdot \Delta O + \beta_{\Delta O} \qquad 9.10$$

ΔO is the interocular difference in optical density, and $\alpha_{\Delta O}$ and $\beta_{\Delta O}$ are the slope and the intercept of the best line fit via linear regression. Linear regression was similarly used to fit the pattern of interocular delays with interocular differences in magnification.

9.2.5.5. Anti-Pulfrich monovision corrections

The interocular differences in processing speed caused by a unit difference in optical power (i.e., $\alpha_{\Delta F}$) and a unit difference in optical density (i.e., $\alpha_{\Delta O}$) can be used to determine the luminance difference required to null processing speed differences caused by an arbitrary difference in optical power. Setting the first terms on the right-hand sides of Equations 9.9 and 9.10 equals to each other and solving for the interocular difference in optical density yields the optical density difference that will achieve the anti-Pulfrich correction. Specifically,

$$\Delta O_0 = -\frac{\alpha_{\Delta F}}{\alpha_{\Delta O}} \Delta F \qquad 9.11$$

Negative values indicate that the transmittance of the left lens should be reduced to achieve an anti-Pulfrich correction. Positive values indicate that the transmittance of the right lens should be reduced.

9.2.5.6. Summarizing effect sizes

To compare effect sizes across experiments and human observers, we report interocular delays in a particular condition estimated from the best-fit lines in each experiment, rather than using the raw PSE data itself. We used this approach for two reasons. First, this approach has the advantage of minimizing the effect of measurement error. Second, in experiments with blur differences (Experiments 1, 2, and 4), not all observers collected data in identical conditions. Some collected data with a maximum interocular difference in focus error (i.e., optical power) of ±1.5D while others collected data with a maximum difference of ±1.0D; some observers had difficulties performing the task with the larger difference. To compare interocular delays across observers at the power difference associated with the most commonly prescribed monovision correction strength (i.e., 1.5D), we extrapolated using the best-fit lines to the data (Equation 9.9).

9.3. Results

Interocular differences in processing speed were measured in five separate experiments in each of the four human observers. The same experimental paradigm was used to collect data across all five experiments. First, we describe the experimental details that were common across the experiments. Then, we describe each experiment. As a group, the experiments seek to establish: i) that contact lenses of different powers can induce the interocular mismatches in processing speed that underlie the Reverse Pulfrich effect, ii) that anti-Pulfrich corrections with contact lenses are effective in eliminating the Reverse Pulfrich, and iii) that interocular differences in image magnification relevant to monovision have no impact on interocular differences in processing speed.

To measure interocular differences in processing speed, human observers collected data in a one-interval two-alternative forced-choice (2AFC) experiment. On each trial, observers viewed a dichoptically presented vertical target bar that oscillated horizontally in the frontal plane (Figure 9.3A) while fixating a central dot (not shown). When the onscreen interocular delay is zero, onscreen disparity specifies that the target is moving in the plane of the screen. When the onscreen interocular delay is negative, the left-eye image onscreen trails the right-eye image onscreen, and onscreen disparity specifies that the target is following an elliptical trajectory outside the plane of the screen that is clockwise when viewed from above (‘front left’ motion). When the onscreen interocular delay is positive (i.e., an onscreen advance), the left-eye image onscreen leads the right-eye image onscreen, and onscreen disparity specifies that the target is following an elliptical trajectory outside the plane of the screen that is counter-clockwise when viewed from above (‘front right’ motion; Figure 9.3B).

The task was to choose, on each trial, whether the target appeared to be undergoing ‘front right’ or ‘front left’ motion. In each condition, the proportion of times each observer chose ‘front right’ was plotted as a function of onscreen delay. This raw data was fit with a cumulative Gaussian function in each condition. Data and fits for the first human observer in the first experiment are shown in Figure 9.3C. The point of subjective equality (PSE) indicates the onscreen delay necessary for the observer to report ‘front right’ on half of the trials (black arrows). This onscreen delay (or advance) of the left-eye onscreen image relative to the right-eye onscreen image is equal in magnitude and opposite in sign to the neural advance (or delay) induced by the image perturbations. Each experiment examines whether a particular interocular difference in image properties (i.e., a particular perturbation of the image in one eye) causes interocular differences in processing speed.

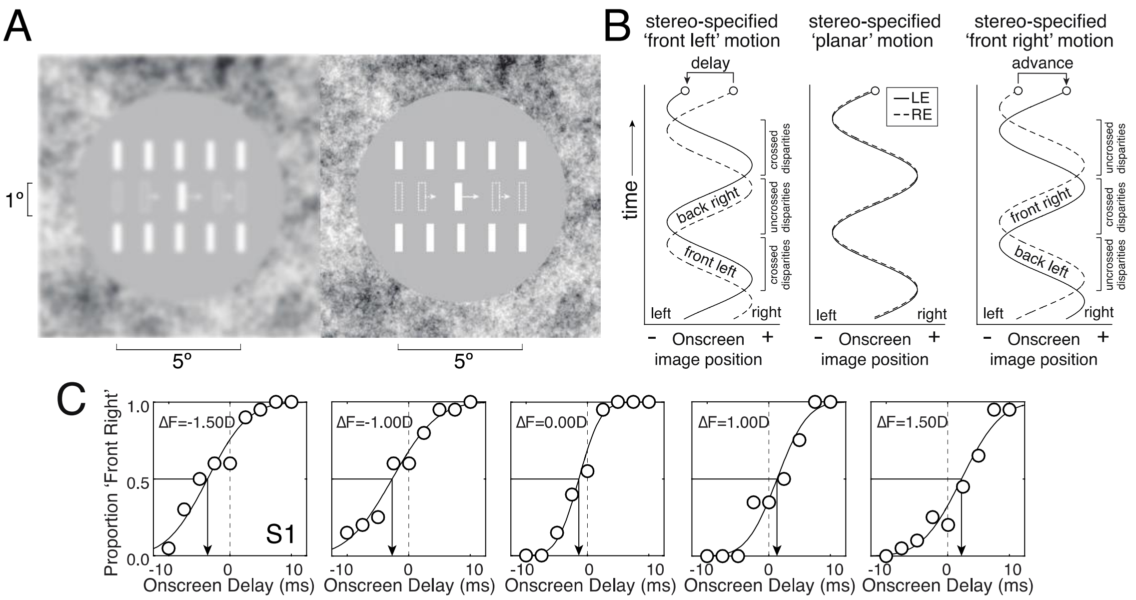

Figure 9.3. Binocular stimulus, time-course of stimulus presentation, and psychometric functions. **A**. The target was a dichoptically presented horizontally moving white bar. The left-eye image is blurred to simulate the optical blur that was induced in the experiment; no onscreen blur was present in this experiment. White arrows show target motion, speed, and direction. Dashed bars show example stimulus positions throughout a trial. Arrows and dashed bars are both for illustrative purposes and were not present in the actual stimulus. Fuse the two half-images to perceive the target bar in 3D on one frame of the movie. Cross-fusers will see a depiction of 'front right' motion on this frame. Divergent-fusers will see 'back right' motion on this frame and would answer 'front left' for the complete one-cycle trial. **B**. Left-eye and right-eye onscreen horizontal image positions as a function of time (solid and dashed curves, respectively) when the left-eye image was delayed onscreen, coincident with, or advanced onscreen relative to the right-eye image. **C**. The task was to report whether the target bar appeared to be moving 'front left' or 'front right' with respect to the screen. Psychometric functions for the first human observer as a function of onscreen delay in five conditions in Experiment 1. Each condition had a different interocular difference in focus error (i.e., ΔF=[-1.5D, -1.0D, 0.0D, 1.0D, 1.5D]). The point of subjective equality (PSE, black arrows) changes systematically with the difference in focus error, indicating that the difference in focus error systematically impacts the neural differences in processing speed between the eyes.

Experiment 1: Contact Lenses

Experiment 1 measures the interocular differences in processing speed caused by blur differences induced by soft contact lenses having different powers. As mentioned earlier, contact lenses of different powers cause negligible interocular differences in magnification. Contact lenses thus isolate differences in optical blur from the possible confounding magnification differences caused by trial lenses (Figure 9.4A). This experiment will determine whether the Reverse Pulfrich effect occurs when interocular blur differences are not accompanied by interocular differences in magnification. It will also determine whether the Reverse Pulfrich effect is caused by the most commonly used delivery system for monovision prescriptions.

One eye—the perturbed eye—was fit with a contact lens that blurred the stimulus. The other eye was fit with a contact lens that sharply focused the stimulus. As expected, we found that contact lenses of different powers cause a Reverse Pulfrich effect. When the left eye is blurred, a target stimulus oscillating in the frontal plane with no onscreen delay is incorrectly perceived as undergoing 'front right' motion in depth. The Reverse Pulfrich effect occurs because the image in the blurrier eye is processed more quickly than the image in the sharper eye (Figure 9.4B). To null this effect, the left eye must be delayed onscreen by an amount equal in magnitude but opposite in sign to the advance in neural processing speed.

Data from the first human observer is shown in Figure 9.4C. When the left eye was at its blurriest and the right eye was sharp (i.e., ΔF=-1.5D), the left-eye stimulus had to be delayed onscreen by 2.8ms from baseline. When the left eye was sharp and the right eye was at its blurriest (i.e., ΔF=1.5D), the left-eye stimulus had to be advanced onscreen by 3.1ms from baseline. A similar pattern of results was found for all four human observers (Figure 9.10A). Across observers, the blurrier eye was processed 1.9ms faster on average (SD=1.0ms).

These mismatches in processing speed imply that monovision corrections, which are most often delivered by contact lenses, can cause substantial misperceptions of motion[103]. Optometrists and ophthalmologists should consider making their patients aware of these motion illusions when prescribing monovision, just as it is commonplace to mention the decreases in stereoacuity that are associated with monovision[98,325,341].

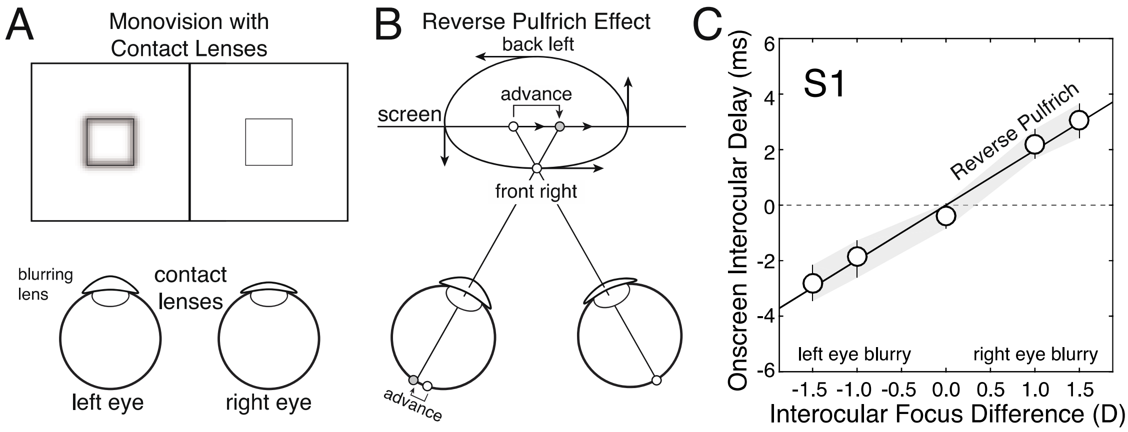

Figure 9.4. Reverse Pulfrich effect with contact lenses (Experiment 1). A. Stimulus conditions with contact lenses. Contact lenses of different powers cause interocular differences in blur, but no differences in magnification. The differences in optical power (i.e., focus error) ranged from -1.5D to 1.5D, which are common monovision correction strengths. **B.** The interocular difference in blur causes a mismatch in processing speed between the eyes—the blurrier image is processed more quickly—which leads to the Reverse Pulfrich effect. Horizontal oscillating motion in the frontal plane is perceived as 'front right' elliptical motion in depth (i.e., counterclockwise when viewed from above). **C.** Onscreen interocular delays required to null neural differences in processing speed induced by differences in optical power between the eyes for the first human observer. Error bars indicate 68% confidence intervals from 1000 bootstrapped datasets. See Figure 9.10A for data from all human observers.

Experiment 2: Trial Lenses

Experiment 2 measures the interocular differences in processing speed induced by trial lenses having different powers. As mentioned earlier, trial lenses with different powers cause non-negligible magnification differences—1.8% for a 1.5D difference—in addition to blur differences (Figure 9.5A). Experiment 1 demonstrated that magnification differences are not necessary for the Reverse Pulfrich effect to occur. But magnification differences could, in principle, interact with blur differences to strengthen or weaken the Reverse Pulfrich effect. One might also hypothesize that increased magnification in one eye will increase the speed of processing relative to the other eye; magnification shifts the image spectrum to lower spatial frequencies, and low spatial frequencies are processed more quickly than high spatial frequencies all else equal[94,96,103].

To examine these issues, we re-ran each human observer in conditions that were identical to those in Experiment 1, except that trial lenses, instead of contact lenses, induced the optical blur differences. The perturbed eye was fit with a trial lens that blurred the stimulus. The other eye was fit with a trial lens that sharply focused the stimulus.

Again, the blurrier eye was processed more quickly, causing a Reverse Pulfrich effect (Figure 9.5B).

Data from the first human observer is shown in Figure 9.5C. The onscreen interocular delay that is required to null the Reverse Pulfrich effect changes linearly with the interocular difference in focus error, just as with contact lenses. In this observer, when the left eye was at its most blurry (ΔF=-1.5D), the left-eye image had to be delayed onscreen by 3.1ms. When the right eye was most blurry (ΔF=+1.5D), the left eye had to be advanced onscreen by 2.7ms. Again, a similar pattern of results was found for all human observers (Figure 9.10B). Across observers, the blurrier eye was processed 2.1ms faster on average (SD=0.5ms). These findings replicate the primary result of Burge et al.[339].

To check whether magnification differences had any influence on the size of the Reverse Pulfrich effect, we plotted the effect size measured with trial lenses in each condition against the effect size measured with contact lenses in the same condition, for all observers (Figure 9.5D). Trial lenses and contact lenses yielded very similar effect sizes that were tightly correlated across all human observers (r=.96; p<.05). The magnification differences caused by trial lenses, while large enough to impact some aspects of binocular processing (see section 9.4) are too small to cause the spatial-frequency-mediated differences in processing speed hypothesized above. The magnification differences caused by trial lenses do not influence the size of the Reverse Pulfrich effect caused by blur differences.

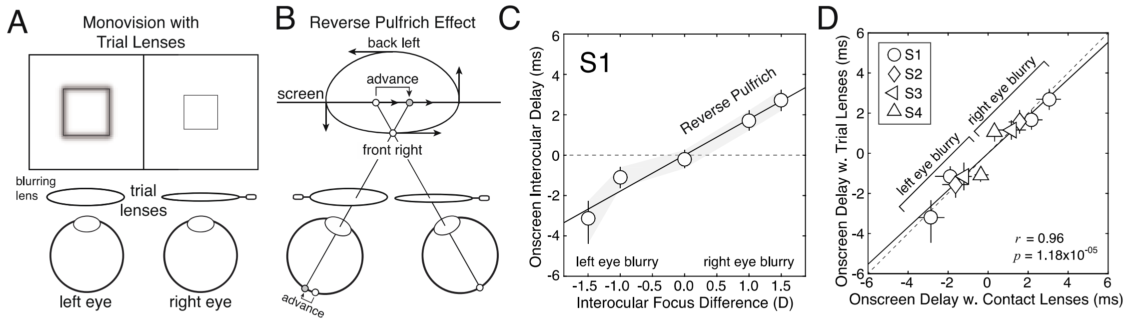

Figure 9.5. Reverse Pulfrich effect with trial lenses (Experiment 2). A. Stimulus conditions with trial lenses. Trial lenses of different powers cause interocular differences in blur and magnification. The differences in optical power (i.e., focus error) ranged from -1.5D to 1.5D. **B.** The interocular difference in blur causes a mismatch in processing speed between the eyes—the blurrier image is processed more quickly—which leads to the Reverse Pulfrich effect. Horizontal oscillating motion in the frontal plane is perceived as 'front right' elliptical motion in depth (i.e., counterclockwise motion when viewed from above). **C.** Onscreen interocular delays required to null neural delays induced by differences in optical power between the eyes in the first human observer. Error bars indicate 68% confidence intervals from 1000 bootstrapped datasets. See Figure 9.10B for data from all human observers. **D.** Onscreen interocular delays from trial lenses vs. contact lenses for each observer (symbols) in all conditions measured. Processing delays induced by contacts and trial lenses with equivalent power differences are nearly identical; the best-fit regression line has a slope of 0.92 (solid line). The magnification differences caused by the trial lenses do not affect processing speed.

Experiment 3: Luminance Differences

Experiment 3 measures the interocular differences in processing speed caused by luminance differences between the eyes. This experiment is useful for two reasons. First, measuring the decrease in processing speed caused by darkening the image in one eye is necessary to test whether anti-Pulfrich monovision corrections are effective with contact lenses. Second, replicating results from the classic literature increases confidence that the current paradigm is producing valid results.

The image to one eye—the perturbed eye—was darkened onscreen by a factor equivalent to the transmittance of a neutral density filter with a particular optical density

(Figure 9.6A). The other eye was left unperturbed. Both eyes were sharply focused on the stimulus. As expected, a luminance difference between the eyes causes the Classic Pulfrich effect; the darker image is processed more slowly. For a target stimulus oscillating in the frontal plane with no onscreen delay, the percept is of 'front left' motion in depth (Figure 9.6B).

Data from the first human observer is shown in Figure 9.6C. Just as with the Reverse Pulfrich effect, the onscreen interocular delay required to null the Classic Pulfrich effect changes linearly with the interocular difference in optical density. But the sign of the slope relating to the difference is now negative instead of positive. When the left eye was darkest (i.e., ΔO=-0.15OD), the left-eye image had to be advanced onscreen by 1.8ms to null the neural delay. When the right eye was darkest (i.e., ΔO=+0.15OD), the left eye had to be delayed onscreen by 2.1ms to null the neural delay. Again, similar results were found for all observers (Figure 9.10C). Across observers, the darker eye was processed 1.6ms more slowly on average (SD=0.5ms).

Currently, it is unknown whether the interocular mismatches in processing speed induced by luminance and blur differences are mediated by common (or partially shared) neural mechanisms. To help constrain the answer to this question, we examine whether the Classic and Reverse Pulfrich effect sizes were correlated amongst observers.

Figure 9.6D plots the onscreen interocular advance (or delay) required to null the neural delay (or advance) caused by interocular differences in luminance and blur. The onscreen advances and delays are shown for focus error differences and optical density differences with magnitudes of 1.0D and 0.15OD, respectively. Other conditions yield similar results. (Note: to quantify the effect of blur differences on neural delay we averaged the Reverse Pulfrich effect sizes for each observer across Experiments 1 and 2.)

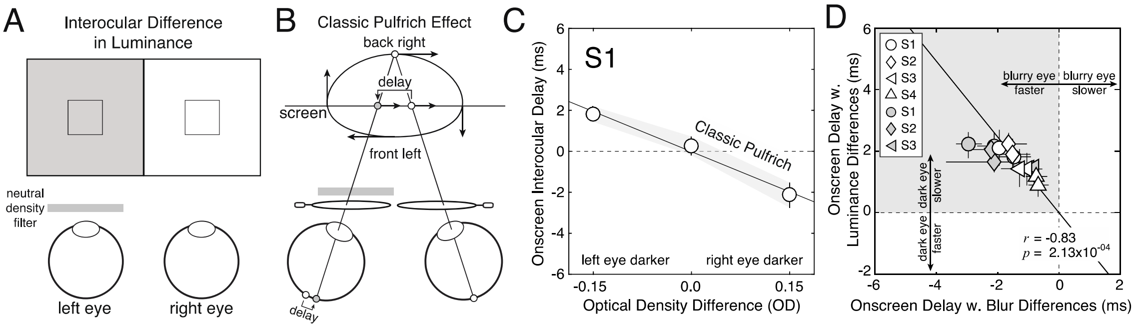

Figure 9.6.Classic Pulfrich effect with luminance differences (Experiment 3). A. Stimulus conditions with interocular luminance differences. The image in one eye was darkened onscreen by a factor equal to the transmittance of a neutral density filter with a particular optical density; the other eye was left unperturbed. The differences in optical density ranged from -0.15OD to 0.15OD, corresponding to a 30% transmittance difference between the left and right eyes. **B.** The luminance differences cause a mismatch in processing speed between the eyes—the darker image is processed more slowly. The Classic Pulfrich effect results. Horizontal oscillating motion in the frontal plane is misperceived as 'front left' elliptical motion in depth (i.e., clockwise motion when viewed from above). **C.** Onscreen interocular delays required to null the neural delays induced by luminance differences in the first human observer. Error bars indicate 68% confidence intervals from 1000 bootstrapped datasets. See Figure 9.10C for data from all human observers. **D.** Interocular delays induced by luminance differences (i.e., ΔO =0.15OD) are plotted against interocular delays induced by blur differences (i.e., $|\Delta F|$=1.0D) in individual observers from the current study (white symbols) and Burge et al.[103] (gray symbols). To isolate the factor of interest—the similarity of effect size due to interocular differences blur and luminance—we plot onscreen delays with respect to the perturbed eye rather than with respect to the left eye. In individual observers, the size of the Reverse and Classic Pulfrich effects are correlated (*r*=-.83; *p*<.05).

Observers with large Reverse Pulfrich effects tended to have large Classic Pulfrich effects (*r*=-.94, *p*<.05). For the particular conditions considered, the best-fit line indicates that an optical density difference of 0.15OD caused interocular delays that were 23%

larger than a focus error difference of 1.0D. However, one must be careful not to place too much interpretative weight on a correlation computed from a very small number of observers. Accordingly, we included data from three additional observers from a previously published paper to increase the power of the analysis. Data from the current experiments are shown as white symbols. Data from Burge et al. (2019) is shown as gray symbols. A similar trend is present in the previous dataset (r=-.88; p=<.05). Across both datasets, the correlation was strong (r=-.83; p<.05). More data must be collected before drawing a firm conclusion, but the preliminary evidence suggests that the size of the Reverse Pulfrich effect is correlated with the size of the Classic Pulfrich effect in individual observers. If this preliminary evidence holds up, the result may be useful in attempts to understand the neurophysiological mechanisms that underlie these effects.

Experiment 4: Anti-Pulfrich Corrections with Contact Lenses

Experiment 4 measures whether anti-Pulfrich monovision corrections delivered with contact lenses can eliminate the interocular differences in processing speed that cause the Reverse Pulfrich effect. The logic of an anti-Pulfrich correction is simple. Decreasing luminance and increasing blur have opposite effects on processing speed; by tinting the blurring lens, it should be possible to simultaneously null the two effects for a large range of target distances (Figure 9.7A). The efficacy of anti-Pulfrich monovision corrections has been demonstrated previously with trial lenses[103]. Here, we show that anti-Pulfrich corrections work with contact lenses.

To determine the optical density of the filter that is appropriate to pair with a particular focus error, we compared how blur and luminance differences impacted processing speed in each human observer. The ratio of the slopes of the best-fit regression lines in Experiments 1 and 3 (see Figures 9.4C, 9.6C, and Equation 9.11) specifies the optical density required to null the change in processing speed due to a given blur difference. We found that appropriately darkening the blurry image successfully eliminates the mismatches in processing speed and restored veridical depth and motion perception (Figure 9.7B).

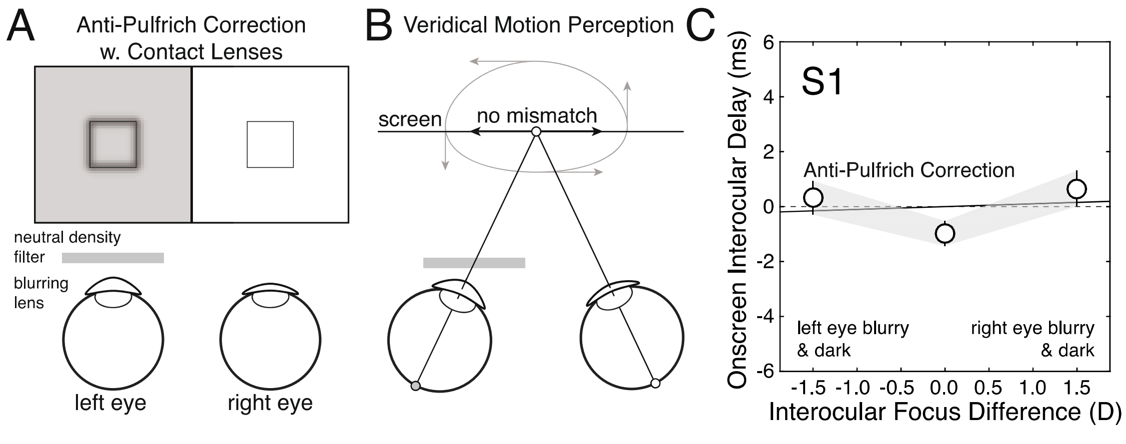

Figure 9.7. Anti-Pulfrich corrections with contact lenses eliminate the Reverse Pulfrich effect (Experiment 4). A. Stimulus conditions for anti-Pulfrich monovision corrections. Darkening the image in the blurrier eye can eliminate the interocular differences in processing speed otherwise caused by blur. **B.** Restoring the parity of processing speed eliminates the misperceptions associated with the Reverse Pulfrich effect (dashed ellipse and arrows) and restores the veridical perception of moving objects (solid arrows). **C.** Onscreen interocular delays are no longer required to null misperceptions of motion in depth because anti-Pulfrich corrections (i.e., appropriately tinting the blurring lens) eliminates interocular differences in processing speed caused by blur alone. Error bars indicate 68% confidence intervals from 1000 bootstrapped datasets. Appropriately tinting the near contact lens in a pair of contact lenses delivering a monovision correction could eliminate the misperceptions of distance and 3D direction for far-moving objects. See Figure 9.10D for data from all human observers.

Data from the first human observer is shown in Figure 9.7C. The anti-Pulfrich correction with contact lenses was successful at nulling the Reverse Pulfrich effect in this observer. With an anti-Pulfrich correction, the interocular difference in processing speed that was caused in this observer by contact lenses with a 1.5D difference in optical power was reduced from 2.9ms to 0.1ms in this observer. Similarly successful results were obtained for all human observers (Figure 9.10D). The average interocular difference in processing speed for a 1.5D difference in optical power was reduced from 1.9ms to -0.1ms (SD=0.3ms).

The first observer required the largest difference in optical density to null the Reverse Pulfrich effect. Nulling the Reverse Pulfrich effect for a 1.5D interocular difference in optical power required an interocular difference in optical density of 0.23OD. An optical density of 0.23OD corresponds to a transmittance of 59% (Equation 9.5). Across observers, the required transmittance in the dark lens ranged from 59% to 89%. For reference, a standard pair of sunglasses transmits only 25% of the incoming light (i.e., an optical density of 0.60). Thus, the required difference in transmittance required between the eyes for a successful anti-Pulfrich correction is rather slight.

Experiment 5: Magnification Differences

Experiment 5 measures whether magnification differences between the images in the two eyes can cause processing speed differences. The results of Experiments 1 and 2 showed that magnification differences caused by monovision corrections do not impact processing speed when differences in optical blur are present. The current experiment tests directly whether magnification differences can cause differences in processing speed when blur differences are absent.

Onscreen interocular differences in magnification were introduced, while both eyes were kept sharply focused and equally bright (Figure 9.8A). The onscreen magnification difference was either equal (1.8%) or double (3.6%) the magnification difference caused by trial lenses that differ in power by 1.5D. Under these conditions, processing speed was equal in both eyes, and motion perception was veridical; targets specified by disparity to be oscillating in the frontal plane were correctly perceived as oscillating in the frontal plane (Figure 9.8B).

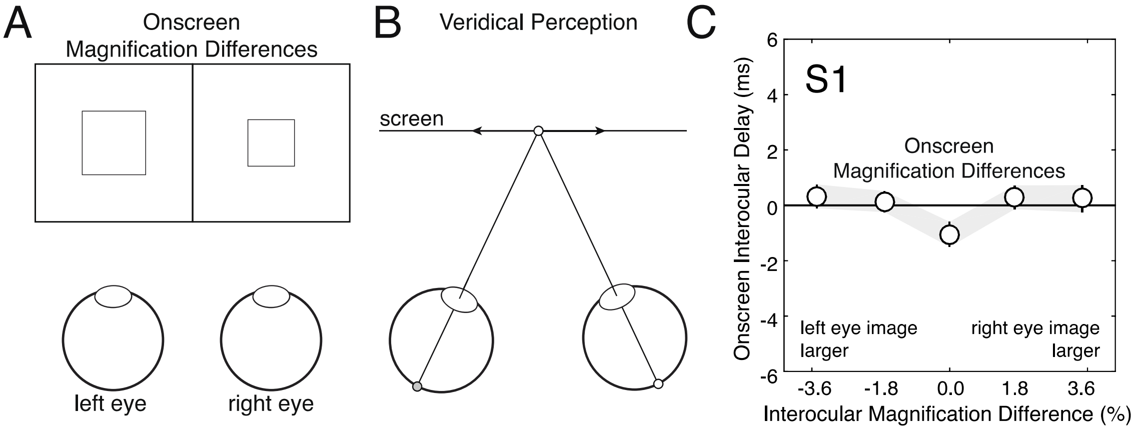

Figure 9.8. Magnification differences do not cause motion-in-depth misperceptions (Experiment 5). A. Stimulus conditions with interocular differences in magnification. The image in one eye was larger than the image in the other eye. Both images were equally sharp and equally bright. **B.** Magnification differences do not cause motion-in-depth misperceptions. Horizontally oscillating motion in the frontal plane is perceived veridically. **C.** Onscreen interocular delays equal zero for all interocular differences in magnification up to ±3.6%. Error bars indicate 68% confidence intervals from 1000 bootstrapped datasets. See Figure 9.10E for data from all human observers.

Data from the first human observer is shown in Figure 9.8C. The largest magnification differences caused negligible interocular mismatches in processing speed. Similar results were obtained for all human observers (Figure 9.10E). Across observers, the average interocular delay for a magnification difference of 3.6% was 0.0ms (SD=0.1ms). Magnification differences, therefore, do not cause the images in the two eyes to be processed at different speeds.

Summary of Experimental Results

The pattern of results across experiments is remarkably consistent for all human observers (Figure 9.9). In each observer, blur differences induced by contact lenses (Experiment 1) and trial lenses (Experiment 2) both cause the Reverse Pulfrich effect; the image in the blurrier (i.e., perturbed) eye is processed faster than the image in the sharper eye. In each observer, luminance differences cause the Classic Pulfrich effect (Experiment 3); the darker image is processed slower than the brighter image. In each human observer, anti-Pulfrich monovision corrections that are delivered with contact lenses eliminate the mismatches in processing speed that underlie the Reverse Pulfrich effect (Experiment 4). And in each human observer, magnification differences cause no differences in processing speed between the eyes (Experiment 5). The consistency of these results across the four human observers in this report, and the similarity of these results to previously published findings, should increase confidence that these findings are solid and will be replicable in new populations.

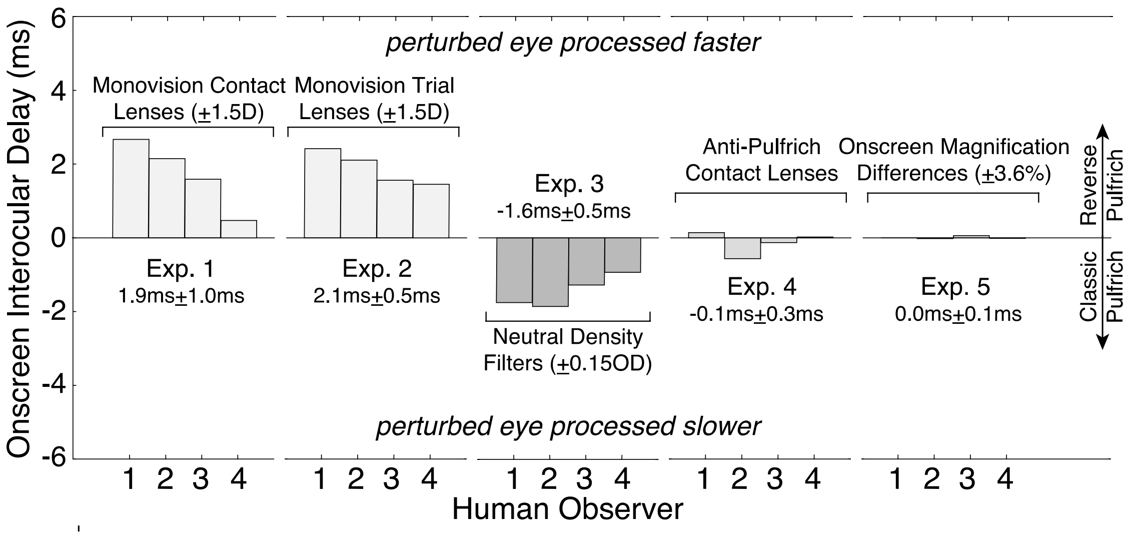

Figure 9.9. Summary of experimental data. Effect sizes across all experiments and human observers. Blurring one eye with contact lenses (Experiment 1) or blurring one eye with trial lenses (Experiment 2) causes the image in that same eye to be processed more quickly, leading to a Reverse Pulfrich effect. Darkening one eye causes the image in that eye to be processed more slowly (Experiment 3), leading to a Classic Pulfrich effect. Anti-Pulfrich corrections eliminate the increase in processing speed caused by blur alone by appropriately darkening the image in the blurry eye (Experiment 4), thereby eliminating the Reverse Pulfrich effect. Interocular differences in magnification (Experiment 5) up to ±3.6% do not impact interocular differences in processing speed.

Additionally, the results for all observers and all experiments are shown in Figure 9.10.

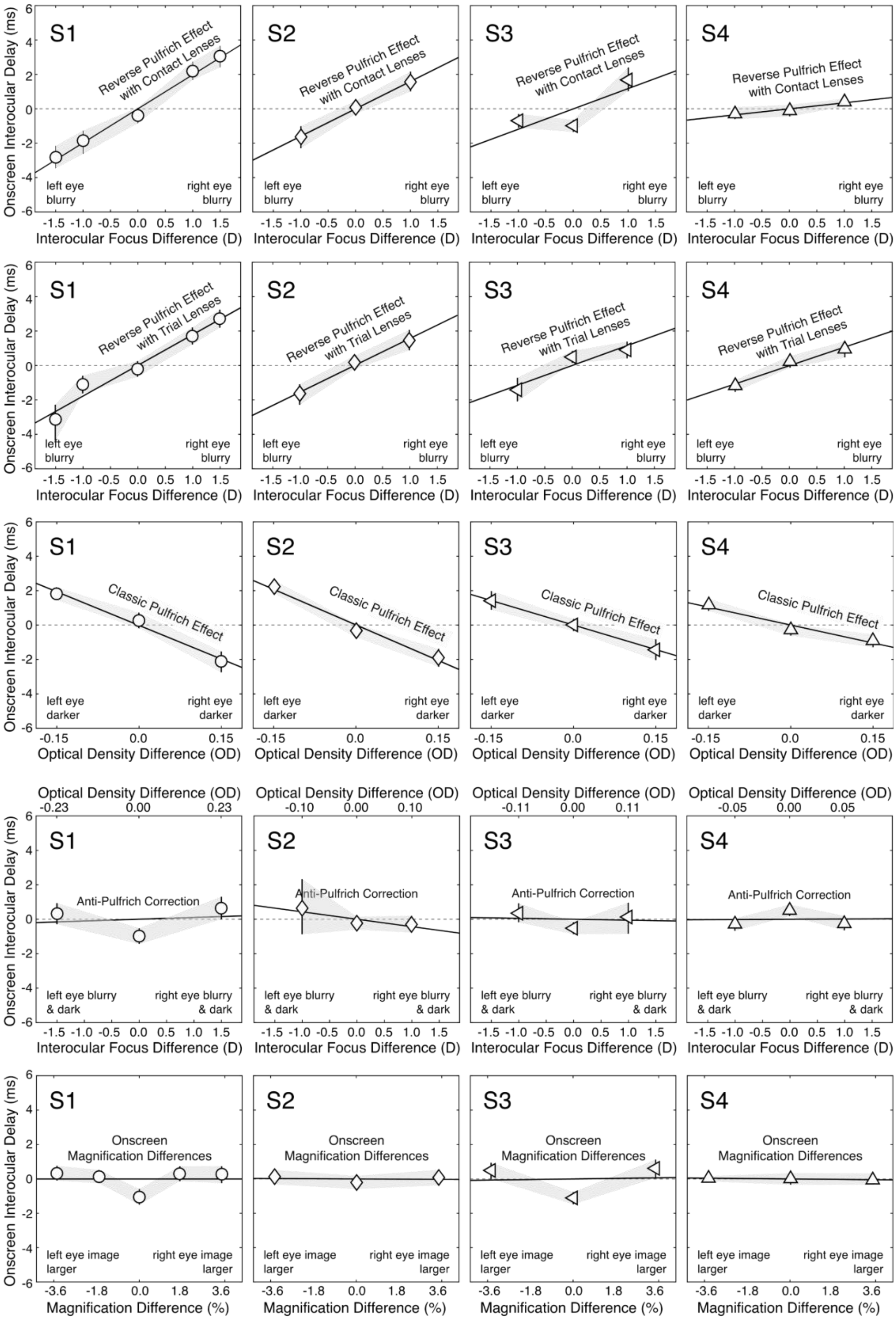

Figure 9.10. Data for all subjects and experiments. Error bars indicate 68% confidence intervals on each PSE (i.e., point of subjective equality) from 1000 bootstrapped datasets. **A.** Reverse Pulfrich effect with contact lenses for all four human observers (Exp. 1). Onscreen interocular delays required to null neural differences in processing speed that is induced by differences in optical power between the eyes. **B.** Reverse Pulfrich effect with trial lenses for all four human observers (Exp. 2). Onscreen interocular delays required to null neural differences in processing speed that is induced by differences in optical power between the eyes. **C.** Classic Pulfrich effect with luminance differences for all four human observers (Exp. 3). Onscreen interocular delays required to null neural delays induced by differences in luminance between the eyes.

Results are plotted as a function of the equivalent interocular difference in optical density. **D.** Anti-Pulfrich corrections with contact lenses eliminate the Reverse Pulfrich effect for all four human observers (Exp. 4). Appropriately tinting the blurring lens eliminates the neural differences in processing speed caused by blur alone. Onscreen interocular delays are no longer required to null misperceptions of motion in depth. The anti-Pulfrich Each observer required a different anti-Pulfrich correction (i.e., a different optical density difference for each focus error difference) because the ratio of the regression slopes in the reverse and Classic Pulfrich conditions (Exp. 1 & Exp. 3) differed for each observer (see Equation 9.11). **E.** Magnification differences do not cause motion-in-depth misperceptions, for all four human observers (Exp. 5). Onscreen interocular delays are equal to zero for all interocular differences in magnification.

9.4. Discussion

The Reverse Pulfrich effect can be caused by blur differences induced by soft contact lenses. For 1.5D differences in optical blur, a common monovision correction strength, the blurrier image is processed faster by approximately 2ms. Under certain conditions, these small differences in processing speed may provoke large misperceptions of depth (see Figure 9.1). Fortunately, anti-Pulfrich monovision corrections, which leverage the fact that increased blur and reduced retinal illuminance have opposite effects on processing speed, can eliminate the misperceptions in a large subset of viewing conditions (see below). These findings with soft contact lenses are quite likely to generalize to other approaches for delivering monovision corrections: semi-rigid contact lenses, surgically implanted intraocular lenses, or refractive surgery. We have also demonstrated that magnification differences of similar magnitude to those induced by trial lenses (±1.5D) do not cause or modify the Reverse Pulfrich effect. Together, these results place current explanations for the Reverse Pulfrich effect on firmer empirical grounds, invite a re-examination of monovision prescribing practices, and suggest potential directions for improving corrections for presbyopia.

Measuring the Reverse Pulfrich effect in the clinic

Many millions of people currently wear monovision corrections to compensate for presbyopia[103,301–303]. The prevalence of monovision corrections, the potential ramifications of the Reverse Pulfrich effect (see Figure 9.1), and the potential compensatory function of anti-Pulfrich corrections suggest a need for tests that can be deployed in the clinic.

There are two primary obstacles to developing tests for use in the clinic. The first obstacle is the development of cheap portable displays that can render stereo-3D content of sufficiently high spatial and temporal resolution so that useful measurements can be made. Ongoing work is attempting to address this issue[200]. The second obstacle is that the time available to gather data in the clinic (e.g., minutes) is severely limited compared to the time available to gather data in the lab (e.g., hours). Thus, it is of paramount importance to develop methods that enable the rapid collection of high-quality data that require little or no training, and that can be used with non-traditional populations including children. We are working to adapt target-tracking methods for continuous psychophysics for this purpose[326].

Blur suppression, eye dominance, and patient acceptance of monovision

The task in our experiments—reporting the perceived motion-in-depth trajectory of a stereoscopically specified target object—required that observers be capable of comparing inputs from both eyes. But patient acceptance of monovision is widely thought to depend, at least in part, on the ability to suppress one eye[280]. Does this mean that the observers in our experiment would be unsuccessful monovision wearers? We do not believe so. It is important to distinguish between the total suppression of information and the suppression of a feature like blur from the defocused eye. Although stereo vision is weakened by the optical conditions induced by monovision[98,99,325], most monovision wearers retain some degree of stereopsis[98,328]. Additionally, amongst successful monovision wearers, the ability to suppress blur varies widely across subjects and is poorly correlated with the quality of stereopsis[281,328]. Thus, the ability to perceive motion in depth in our experiments is not an indication that the observers would be unsuccessful monovision wearers.

Eye dominance is another factor that is widely thought to predict the likelihood of patient acceptance of monovision. Clinicians tend to prescribe the far-distance lens in the dominant eye and the near-distance lens in the non-dominant eye, in part because it is thought that the dominant eye will more successfully suppress blur. However, there is little support in the literature for this belief[162,280]. We did not measure eye dominance, but the approximate symmetry of the effect sizes regardless of which eye is blurred suggests that the role of eye dominance in both the Reverse and Classic Pulfrich effects is small in our observers, if it is present at all.

Anti-Pulfrich monovision corrections: Potential limitations and possible improvements
The results with anti-Pulfrich corrections suggest they have the potential for clinical practice. Thus, it is important to discuss their potential limitations and highlight the most important directions for future work. An effective anti-Pulfrich correction requires that a tint be applied to the lens forming the blurrier image. In natural viewing, however, the lens forming the blurrier image varies with the distance to the target. Appropriately tinting the near lens will eliminate the Reverse Pulfrich effect for far targets but aggravate it for near targets. Thus, anti-Pulfrich corrections can only work for a subset of target distances. Assuming that tinting the near lens is the preferred solution—which is plausible because the accurate perception of moving targets is probably more important for tasks at far than at near distances (e.g., driving vs. reading)—the range of distances for which motion misperceptions may be reduced or eliminated can be considerable: from the near point of the far lens to infinity. This range may be even larger for early presbyopes, who have some residual ability to accommodate because they tend to preferentially focus the eye with the far lens[331]. However, these issues need further study.

Understanding the effect of ambient illumination on both the Reverse and Classic Pulfrich effects is critical to determining how practical anti-Pulfrich corrections would be in a real-world setting. The size of the Classic Pulfrich effect is known to increase with decreases in ambient illumination and vice versa[203,208,319]. It is unknown how light level affects the size of the Reverse Pulfrich effect, but it is likely to behave similarly. For example, the size of the pupil—and thus the blur caused by a given focus error—increases with decreases in light level, and vice versa. This should cause larger Reverse Pulfrich effects in dim light and smaller Reverse Pulfrich effects in bright light. If changes in ambient illumination change the sizes of the Reverse and Classic Pulfrich effects by the same amounts, anti-Pulfrich monovision corrections will be straightforward to implement. However, if the two effects change differently with light level, prescribing anti-Pulfrich corrections may be more challenging. If so, a given difference in optical blur would have to be compensated for by transmittance differences that change with light level. Fortunately, photochromic contact lens technologies present a possible solution[342].

Photochromic lenses reduce transmittance with increases in ambient light levels[343]. A photochromic anti-Pulfrich correction could be applied with a photochromic contact lens in one eye and a standard contact lens in the other eye. The photochromic properties of the contact lens could be tuned to compensate because the effect sizes change with light level.

Another possibility to consider is an anti-Pulfrich photochromic correction that operates when the user is outdoors, and that reverts to Classic monovision when the user is indoors, where accurate perception of motion is likely to be less critical. Indoors, all the available light energy would be transmitted to the eye that is focused near, which would benefit near visual tasks like reading. Another, perhaps simpler, approach might be to combine a Classic monovision correction with sunglasses with custom transmittances in each eye that could provide an anti-Pulfrich correction when the patient is outdoors.

Finally, it would be important to determine whether the transmittance (e.g., tint) differences required for an anti-Pulfrich correction pose a cosmetic issue. In general, these differences in transmittance are small. For the observers of the current study, the required transmittance in the dark lens ranged from 59% to 89% of incoming light, assuming a 1.5D difference in optical power. A common pair of sunglasses transmits only 25% of the incoming light. It remains to be seen whether these transmittance differences would cause a cosmetic impediment for everyday wear. If so, we note that the issue is likely to occur only for anti-Pulfrich corrections prescribed with contact lenses, and not with surgically-implanted intraocular lenses[337,338]. Contact lenses cover the iris and are visible, and intraocular lenses are inserted into the capsular bag and are generally not visible. However, before ophthalmologists consider surgically implanting anti-Pulfrich monovision intraocular lenses, significant further study is required.

The impact of magnification differences on binocular processing

We have found no evidence that interocular differences in magnification cause interocular differences in processing speed. Contact lenses and trial lenses with equivalent power differences cause Reverse Pulfrich effects of nearly identical size (Experiment 1 and Experiment 2; see Figure 9.5D), and onscreen magnification differences without blur differences had no measurable impact on processing speed differences between the eyes. Magnification differences, however, do impact other aspects of binocular visual processing. As magnification differences increase, binocular contrast sensitivity worsens[344], binocular summation breaks down[344,345], fusion times increase, the largest disparity eliciting a depth percept decreases[346], and stereopsis functions less well[347–349]. Additionally, unilateral horizontal or unilateral vertical magnification differences (i.e., induced aniseikonia) can cause misperceptions of surface orientation known as the geometric and induced effects, respectively[350]. Horizontal magnification differences have previously been reported to cause Pulfrich-like effects[351], but these can be attributed to changes in the relative spatial positions of the target projections due to the prismatic properties of the magnifier, rather than to an induced interocular difference in processing speed[352]. In other words, instead of a time delay causing a neural disparity for moving objects, the magnifier causes an actual disparity in the retinal images. The results reported in this manuscript indicate strongly that magnification differences up to ±3.6% do not impact the relative speed of processing between the eyes. Blur differences, not magnification differences, drive the Reverse Pulfrich effect.

Applicability of current results to the presbyopic population

The human observers tested in the current experiments were between the ages of 25 and 30 and were thus all non-presbyopic. However, due to the experimental design, these observers were unable to clear induced optical blur with accommodation. In this respect, the non-presbyopic observers were like presbyopes in the current experiments. Still, it is unknown whether the current results will generalize to the population of presbyopes. Presbyopes' inability to accommodate increases the likelihood that blurry images will be formed on the retinas, which increases the likelihood that the presbyopes will be adapted to how blurry images appear[353,354]. Whether this increased exposure to blur decreases (or increases) presbyopes' susceptibility to the Reverse Pulfrich effect is unknown. Future research will have to evaluate the prevalence and range of effect sizes in the normal and presbyopic populations.

Stability of the Reverse Pulfrich effect over time
Do the processing speed differences associated with the Reverse Pulfrich effect decrease with extended exposure to differences in optical blur? The processing speed differences underlying the Classic Pulfrich effect are known to decrease over an extended period of time if the image in one eye is consistently darker than the image in the other eye[207,208,319]. With the Reverse Pulfrich effect, however, the eye with the blurrier image depends on the distance of the target being viewed, so one eye is unlikely to be consistently blurrier than the other. Presbyopes that habitually wear monovision corrections are more likely to be adapted to the appearance of optical blur differences between the eyes[332]. The same is likely to be true of non-presbyopes with mild anisometropia. But it is unknown whether adaptation to visual appearance is accompanied by an adaptation that decreases the processing speed differences underlying the Reverse Pulfrich effect. Future work will be required to determine whether the Reverse Pulfrich effect diminishes with extended exposure to moderate differences in optical power between the eyes.

The Reverse Pulfrich effect in the real world
To date, the Reverse Pulfrich effect has been measured only with simple laboratory stimuli. Ultimately, it will be important to understand how the effect manifests with real-world (i.e., natural) stimuli. One important facet of this understanding will be the ability to predict the interocular differences in processing speed from the image properties in the two eyes. This will be a difficult problem to solve. But recent developments in the ability to estimate the cues most relevant to the effect of natural images (i.e., defocus blur, binocular disparity, and motion) provide reasons for optimism[233,304,310,355]. Models that compute cue values directly from images ('image-computable models') have found recent success in predicting human performance in a range of visual tasks[356–362]. However, to our knowledge, there exists no theoretical or empirical work that tightly links the properties of natural images to processing speed. Methods for learning the most useful stimulus features for particular tasks may be helpful to these efforts[363–365]. Research with simple stimuli, which will be helpful to these goals, has shown that processing speed is directly impacted by the spatial and spatial frequency properties of images[103,366,367]. But a computational theory that relates the properties of natural images to processing speed is necessary for a full scientific understanding of Pulfrich-related phenomena. Such a theory would likely prove useful for understanding any vision system (biological or machine) that must combine complementary streams of information that are processed at different speeds.

9.5. Conclusions

This manuscript shows that interocular magnification differences up to ±3.6% do not cause or impact the Reverse Pulfrich effect, that the Reverse Pulfrich effect can be caused by contact lenses delivering monovision corrections, and that the Reverse Pulfrich effect can be eliminated with contact lenses delivering anti-Pulfrich monovision corrections. Although many questions must still be resolved before the suitability of anti-Pulfrich corrections can be determined for clinical practice, optometrists and ophthalmologists should consider making their patients aware of the Reverse Pulfrich effect when prescribing monovision. Because the Reverse Pulfrich effect is mediated by processing speed differences between the eyes, scientific and clinical progress will be facilitated by a computational theory that links the properties of individual images to neural processing speed.

Chapter 10. A unique case of spontaneous Reverse Pulfrich effect

In this chapter, we report a unique symptomatic case of spontaneous Reverse Pulfrich effect in a patient with monovision after a first cataract surgery. This 45-year-old patient had a pseudophakic eye (intraocular lens implanted) and an effective monovision correction by the non-compensation of the 2.5D of myopia in the right eye, correcting the left eye for far vision and the left eye for near vision. In this chapter, we report the re-adaptation timeline from the spontaneous Pulfrich effect and the parallel recovery from the symptoms.

This chapter is based on the article by Victor Rodriguez-Lopez et al. *"Monovision after cataract surgery: evidence of a spontaneous Reverse Pulfrich effect and neural adaptation",* submitted to *PLOS One (2022)*. The co-author of the study is Carlos Dorronsoro.

The contribution of the author of the thesis was the conceptualization and design of the study and the literature research, the design of the experiments, the collection and analysis of the data, the writing, and the editing of the chapter in collaboration with Carlos Dorronsoro.

10.1. Introduction

Binocular vision combines the input information from the two eyes to create an accurate 3D description of the world. Blur, scattering, or absorption are alterations often present in the optics of the eye that affect the retinal image quality and degrade the signal provided to the brain. Especially when different across eyes, even if they are subtle, these optical degradations can destabilize binocular vision more than monocular vision[368]. And when binocular vision is harmed, the daily activity of the patient can be affected.

Stereopsis, the 3D perception of the outer world, is known to decline with optical quality[97,369,370]. A more subtle binocular vision alteration, appearing with small amounts of interocular differences in the image of the eyes, is the Pulfrich effect[371]**.** This stereoscopic optical illusion introduces important distortions in the perception of depth of moving objects. In the classical description of the effect, when there is an imbalanced retinal illuminance between eyes, the signal of the dimmer eye is processed slower than the signal of the brighter eye. The higher neural delay in processing the image of one eye with respect to the other eye causes a neural disparity that explains the strong depth illusion perceived.

In Chapters 8 and 9 we reported that differences in retinal blur can also produce a misperception of depth of moving objects, the Reverse Pulfrich effect[339,372]. Those interocular blur differences can be naturally present in people with residual or uncorrected refractive errors that are different between eyes or can be a consequence of monovision-like ophthalmic corrections -solutions for presbyopia where one eye is corrected for near vision and the other eye for far vision-. The blurrier image present in one eye is processed faster than the sharper image present in the other eye, producing depth misperceptions of the opposite sign to the Classic Pulfrich effect.

The physical sources of the Pulfrich effect (i.e., interocular retinal blur or illuminance) can appear or change several times throughout life, both increasing and decreasing, as the eyes grow, change their refraction or prescriptions, age, or undergo surgeries. Neural adaptation and renormalization mechanisms constantly adjust the visual system to the new signal, in timeframes that expand from fractions of seconds to months[297,332,354,373,374].

Some diseases, such as optic neuritis, anisocoria, retinal diseases, and cataracts, provoke neural processing delays and are sources of spontaneous Classic Pulfrich effect[212–217]. Spontaneous Reverse Pulfrich effect has not been described so far, although the Reverse Pulfrich effect has been reported in the laboratory when monovision corrections are induced[103,372]. There might be clinical situations where both versions of the Pulfrich effect coexist. In this paper, we present a unique case of surgical monovision correction after unilateral cataract, where the visual system of the patient is forced to deal with Classic and Reverse Pulfrich effects at the same time.

Presbyopia (the loss of the ability to focus near objects, affecting 100% of the population over 45 years old) changes the refractive state of the eye and thus introduces important amounts of blur in near vision, in a process that takes many years to complete, forcing the visual system to a permanent recalibration to the increasing blur, and/or to the increasing addition in the ophthalmic correction.

The natural aging of the eye also produces a reduction in transmittance of the crystalline lens and therefore a reduction in the total amount of light reaching the retina compared to a young eye[375]. Along the same lines, cataract is a pathological condition also related to aging that produces a further reduction in transmittance due to the oxidation of the proteins of the tissue of the crystalline lens[376]. The prevalence of cataracts increases with age, from 3% at age 55 to 93% at age 80 and older[11]. Besides light absorption, it reduces the overall optical quality of the retinal image due to scattering of the light and blur produced by optical power alterations. The main symptoms of cataracts are glare and loss of visual acuity[377,378]. In fact, the reduction in visual acuity is strongly related to the reduction in the transmittance of the crystalline lens, and vice versa[12]. Thus, in some scenarios, cataracts can be approximated as a neutral density filter that blocks part of the incoming light.

Being a natural consequence of aging, cataract is often bilateral in the end, although in many cases it appears in one eye years before the other eye. Previous studies have reported symptoms of unilateral cataracts directly related to the Classic Pulfrich effect (differences in light between the eyes) such as difficulties during driving, walking, or in daily activities such as pouring out liquids or placing the key into the lock[214–216].

In cataract surgery, the crystalline lens is removed and replaced by a transparent intraocular lens (IOL). The IOL usually compensates for the refractive error and restores the transmittance (not only the one associated with the cataract, but with the natural aging process), all at once. Depending on the different characteristics of the cataract in each eye, the surgical strategy may vary[216]. Some clinicians do not operate both eyes within the same session due to potential problems that may affect both eyes at the same time. Usually, only one eye (often the most affected eye) is operated and the timing for the second eye surgery is not well established. This second approach likely produces interocular imbalances in scattering, transmittance (transparent intraocular lens vs aged -or even cataractous- crystalline lens), and optical power (corrected eye vs. natural refractive error, producing not only blur differences but also magnification differences).

A cataract is not a sudden effect. It grows progressively. The slow development of cataracts allows the visual system to adapt to the interocular differences in retinal illuminance and therefore reduces or eliminates the spontaneous Classic Pulfrich effect[379]. Furthermore, it has been demonstrated, using neutral density filters, that the visual system can adapt gradually to high differences in retinal illuminance between the eyes[48,333,380,381], and that the readaptation to the initial condition is remarkably quick, in terms of days[333]. If the cataract is considered as an optical element that mainly reduces transmittance, adaptation would potentially reduce the delay, slowing down the processing speed of the non-cataractous eye. But the clinical situation is not that simple. Cataract often entails a slow reduction of contrast (due to scattering) and, a progressive introduction of blur. While interocular contrast is known to provoke the Classic Pulfrich effect (scattering increases the effect of absorption), blur produces the Reverse Pulfrich effect, of the opposite sign.

If the difference in retinal illuminance, contrast, or blur suddenly disappeared (for example after bilateral surgery), the adaptation state would fail to compensate for the new delay, at least initially. Instead, the previous adaptation would induce an effective delay of the opposite sign, and strong symptoms might appear suddenly[215] until a new readaptation period, with similar time frames, compensates them again. The abrupt changes after cataract surgery are particularly important with surgically induced monovision, that besides removing scattering and absorption in at least one eye (unbalancing the adaptation to the Classic Pulfrich effect), induces interocular blur (provoking the Reverse Pulfrich effect). Evidence of neural adaptation to the Reverse Pulfrich effect after surgically inducing monovision, or readaptation after removing it, has not been previously reported.

In this study, we describe a unique case of a real patient corrected with surgical monovision of 2.50D after unilateral cataract surgery, who reports important symptoms related to spontaneous Pulfrich effect, and we analyze the conjunction between Classic and Reverse Pulfrich effects. The evolution of the patient in terms of spontaneous Pulfrich, Classic Pulfrich, Reverse Pulfrich effect sizes, and depth misperceptions, was monitored for several months. To understand the impact in the real world of the depth misperceptions produced by the evolving Pulfrich effects described here, we also provide an estimation of the illusion size after adaptation and readaptation, modeling the effects by combining basic geometry and optic flow algorithms in a walking environment with different types of terrains. In this representative case, the current methodology demonstrated to be useful in i) finding the origin of this spontaneous Pulfrich effect, ii) monitoring the progression of the spontaneous Pulfrich effect, iii) demonstrating the neural adaptation to the Reverse Pulfrich effect and estimating its time frame, and iv) showing the impact of spontaneous Pulfrich effect due to monovision in daily visual tasks.

10.2. Results

10.2.1. Case report

A 45-year-old male with mild myopia in both eyes attended the eyecare clinic (Fundacion Jimenez Diaz, Madrid, Spain) reporting blurry vision and glare in one eye. During that visit, he was diagnosed with a subcapsular cataract in the left eye (LE), which reduced Visual Acuity (VA) to 0.4 logMAR with his best correction. The right eye (RE) was considered transparent, with normal VA (0 logMAR).

One month later, the crystalline lens of the LE was surgically removed and substituted by a monofocal intraocular lens (IOL) which compensated for the refractive error of that eye, leaving a spherical equivalent of 0.00D. Combined with the refractive error of the RE (-2.50D spherical equivalent), this first surgical procedure resulted in effective monovision of 2.50D.

In the first revision visit, one month after surgery, the patient reported difficulties in binocular vision. Distances in depth were hard to estimate when walking downstairs (and, to a minor extent, upstairs). While walking in corridors, the observation of the floor and walls produced visual discomfort. The patient, an amateur mountain runner and cyclist, refrained from practicing these activities due to insecurities and lack of visual control of the action. Monocular VA was good (0 logMAR) in both eyes. The symptoms experienced by the patient in binocular vision could not be explained by conventional eye tests carried out in the clinic.

Symptoms did not disappear even 5 months after surgery, and the patient reported binocular vision problems and severe discomfort during this period. Six months after that first surgery in the LE, the patient underwent clear lens extraction surgery of the RE. An IOL was implanted to also correct the RE for far vision, reversing the previous monovision. After recovering from the second surgery, the patient reported that the discomfort had been alleviated and all the visual symptoms had disappeared.

In between surgeries, we started an independent non-interventional longitudinal monitoring of the patient, focused on binocular vision, at our research laboratory (Visual Optics and Biophotonics Lab, Institute of Optics, Madrid, Spain), where the patient, a scientist himself, had indirect research connections. From now on, we will refer to 'the patient' (of the clinic) as 'the subject' (of the study). Using conventional psychophysical techniques (described in section 10.4), we measured the spontaneous Pulfrich effect of the subject, the Classic Pulfrich effect size, and the Reverse Pulfrich effect size, 4 weeks before the second surgery and 3 times after the second surgery (in weeks 3, 11, and

26). Each measurement took about 1 hour to be performed. The results of the measurements were not shared with the patient/subject, nor with the clinic.

10.2.2. Measurements

Table 10.1 summarizes the longitudinal evolution of the patient across time (weeks -4 to 26, being week 0 the time point of the surgery in the second eye). Symptoms were very relevant before the second surgery (measurement A; with an IOL in the left eye but not in the right eye), but not later (measurements B, C, and D; with IOLs in both eyes). The table also shows, for each time point and each eye, the refractive error, and the visual acuity. The table also summarizes the main results of this longitudinal study: the quantitative estimation of the spontaneous, Classic, and Reverse Pulfrich effects, in terms of delays (interocular processing speed differences). To measure the spontaneous Pulfrich effect, the spontaneous delay (in milliseconds) was measured with no alteration in either eye. The Classic Pulfrich effect (in milliseconds/optical density (OD)) was measured with neutral density filters in one eye and then in the other eye. And the Reverse Pulfrich effect (in milliseconds/diopter (D)) was measured with optical defocus induced with trial lenses in one eye and then in the other eye.

Table 10.1. Temporal evolution of the symptoms, optical condition, refraction, visual acuity (VA), and delay from spontaneous Pulfrich, Classic Pulfrich effect size, and Reverse Pulfrich effect size. Between weeks -4 and 3, the subject suffered cataract surgery in the right eye (RE), reversing the monovision correction and matching interocular luminance differences. IOL means intraocular lens. Asterisk (*) in the refraction means that the subject did not have the refraction corrected (therefore inducing a monovision correction).

Measurement		A	B	C	D
Week		-4	3	11	26
Symptoms		Severe symptoms. Difficulty while walking and practicing sports (trekking, running, cycling) due to distortions in the ground, floor, stairs, and walls. Only visually comfortable while not moving.	No symptoms	No symptoms	No symptoms
Optical Condition	LE	IOL	IOL	IOL	IOL
	RE	50-yo crystalline lens	IOL	IOL	IOL
Refraction (D)	LE	0.00	0.00	0.00	0.00
	RE	-1.75-1.50x160º*	-1.50x150º	-1.50x150º	-1.50x150º
Spherical Equivalent (D)	LE	0	0	0	0
	RE	-2.50*	-0.75	-0.75	-0.75
VA (logMAR)	LE	0.0	0.0	0.0	0.0
	RE	0.0	0.0	0.0	0.0
Spontaneous Pulfrich (delay in ms)		-4.82	-1.90	-0.54	-0.78
Classic Pulfrich (ms/OD)		-24.39	-17.81	-16.96	-13.63
Reverse Pulfrich (ms/D)		-0.03	0.62	0.64	0.27

Figure 10.1 shows the temporal evolution of the spontaneous delay (spontaneous Pulfrich effect) for the subject of the study. The vertical dotted line indicates the time point of the second surgical procedure (clear lens extraction). The negative values of the

delay indicate that the processing speed of the right eye is lower (the right eye is delayed) compared to the left eye.

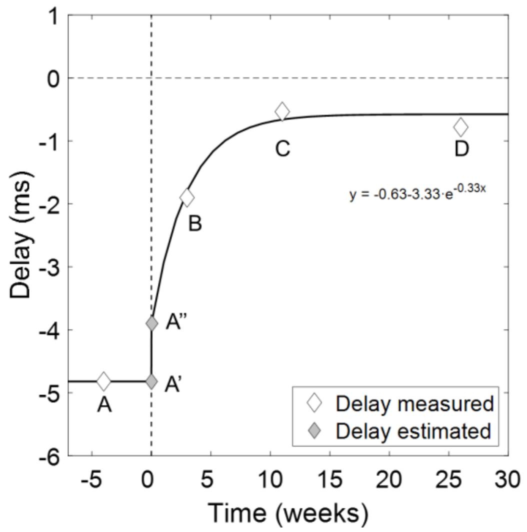

Figure 10.1. Changes in spontaneous Pulfrich effect across time. Change in neural delay, in milliseconds, across time, in weeks. Positive values indicate that the left-eye image processing speed is delayed with respect to the right-eye image, and negative values that the right-eye image processing speed is delayed with respect to the left-eye image. White diamonds indicate actual measurements (A, B, C, and D) and gray diamonds indicate estimations (A' and A''). The process of readaptation to the Pulfrich effect after the surgery (dashed vertical line) is very clear and is mathematically described by the equation, where x is the time in weeks and y is the delay in milliseconds.

Measurement A. The first measurement was performed five months after the first surgery (cataract surgery in the LE, see section 10.2.1) and 4 weeks before the second surgery (clear lens extraction in the RE). The main changes produced by the surgery are: 1) at far distances, RE was defocused and LE focused, due to monovision, potentially causing a Reverse Pulfrich effect (increment in the RE processing speed); 2) the transmission was different between the transparent intraocular lens in the LE and the aged crystalline lens in the RE, what can potentially cause a Classic Pulfrich effect (reduction in the RE processing speed). The measurements show a remarkable spontaneous Pulfrich effect of -4.82 ms, higher than any pathological Pulfrich effect previously reported[214,382], which could explain the severe binocular vision problems after the surgery reported in the clinical history.

Measurement B. One month after the first measurement, the patient underwent a second eye surgery (clear lens extraction in the RE; dashed vertical line at week 0 in Figure 10.1), which removed at once the monovision correction, the interocular illuminance difference, and the potential scattering. After this surgery, both eyes had the same ocular transmittance and were focused at far, and therefore no physical source for Classic nor Reverse Pulfrich effect was expected. But previous adaptation could be likely play a role. After the second surgery, the patient reported an immediate alleviation of the binocular vision problems. However, measurement B, performed 3 weeks after the second surgery still reported a significant spontaneous Pulfrich effect of -1.90 ms. This situation, where a non-symptomatologic patient showed a significant spontaneous Pulfrich effect, has already been described[215].

Measurement C. 11 weeks after the second surgery, the spontaneous Pulfrich effect was -0.54 ms, confirming the important reduction of the spontaneous delay with time.

Measurement D. The last measurement was performed 26 weeks after the second surgery. The value obtained (-0.78 ms) confirmed the low value of the spontaneous Pulfrich effect and the stabilization of the delay.

Fitting and estimations

Figure 10.1, summarizing all the measurements, suggests a progressive readaptation of the spontaneous Pulfrich effect after the second surgery, with timeframes of months. To estimate the time constant of the readaptation decay, we fitted the measurements to an exponential function, using mean least squares. The fitting was performed with the three measurements taken after week 0 (Measurements B, C, and D) when the optical conditions were similar between eyes and across measurements. An additional data point A'' was included in the fitting. A'' is not a measurement but an estimation of the postoperative delay, obtained from measurement A, as described next.

It can be considered that after 5 months of evolution from the first surgery, the neural delay was stable during the four last weeks before the second surgery. Thus, point A' in Figure 10.1 (week 0, but just before the second surgery) is obtained from a flat extrapolation of the measurement performed in week -4, and represents the preoperative delay. To estimate point A'', we assume two quick changes taking place during and right after the surgery: an immediate change in interocular transmittance during the surgery and a quick readaptation of the Classic Pulfrich effect. Artigas et al.[10] reported 96% transmittance for an intraocular lens in-eye, and 88% for a 50-year-old natural crystalline lens, the optical condition of the subject of this study. We estimated a preoperative interocular optical density difference of 0.04 OD. From that, we estimated a delay of -0.92ms for this subject (negative because the Classic Pulfrich effect produced a delay in the RE) considering the preoperative transmittance differences and the Classic Pulfrich effect size measured (i.e., the amount of neural delay induced by a reduction in retinal illuminance in one eye; see Table 10.1), -24.39 ms/OD. After the clear lens extraction, transmittances become essentially equal in both eyes and following measurements. It is known that readaptation to interocular differences in light level happens in only a few days[333]. Therefore, we can obtain the postoperative point A'' in Figure 10.1, as the difference between point A' (-4.82ms) and the estimated delay caused by the preoperative interocular transmittance differences (-0.92ms), resulting in -3.89ms. We assume two phases in the readaptation curve: i) the quick readaptation of the Classic Pulfrich effect from A' to A''; and ii) the long remaining readaptation period from A'' to D (Figure 10.1) corresponding to the Reverse Pulfrich effect alone. The exponential fitting to this second phase results in the following delay readaptation equation: $delay = -0.63 - 3.33 \cdot e^{-0.33t}$ where t is time, in weeks.

Evidence of readaptation and previous adaptation

Figure 10.1 shows a readaptation process after the second surgery because there is a very systematic evolution (reduction) of the delay once the interocular differences, both in luminance and blur, were eliminated. The mere existence of readaptation also implies a previous adaptation process, that in our subject took place after the first surgery (in between surgeries).

This adaptation/readaptation process could affect Classic Pulfrich, Reverse Pulfrich, or both. As already mentioned, the adaptation/readaptation to the Classic Pulfrich effect has been reported to occur in just a few days. In our case, it can only explain a minor part of the delay readaptation, and only in the first temporal step. The additional readaptation process found in our results, after eliminating the interocular blur and taking several weeks, points to a process of adaptation/readaptation to reverse the Pulfrich effect alone, not described before.

<u>Classic and Reverse Pulfrich effect sizes</u>
Figure 10.2 shows the temporal evolution of the Classic and Reverse Pulfrich effect sizes. Before the clear lens extraction (the second surgery), the visual system is sensitive to changes in interocular luminance, resulting (Measurement A; week -4) in a Classic Pulfrich effect size of -24.39 ms/OD, equivalent to a neutral density filter of 0.19OD in the right eye (or transmittance 63%), consistent with the range on values previously reported in the literature[103,372]. On the other side, the visual system, chronically exposed to 2.50 D of monovision at this time point, seems to be insensitive to interocular changes in blur, and the Reverse Pulfrich effect size measured was negligible, -0.03 ms/D.

After the clear lens extraction, in Measurement B, the Classic Pulfrich effect size was reduced (-17.81 ms/OD) and the Reverse Pulfrich effect size was increased (0.62 ms/D; comparable to other studies[372]). Classic and Reverse Pulfrich effect sizes remained quite constant with time afterward, with only a small reduction after the 23 weeks of evolution between Measurement B and D (from -17.81 to -13.63 in Classic; from 0.62 to 0.27 in Reverse). The Classic Pulfrich and the Reverse Pulfrich effect sizes measured have the expected sign, negative for the Classic Pulfrich (delaying the eye which less luminance) and positive for the Reverse Pulfrich (advancing the eye with more blur).

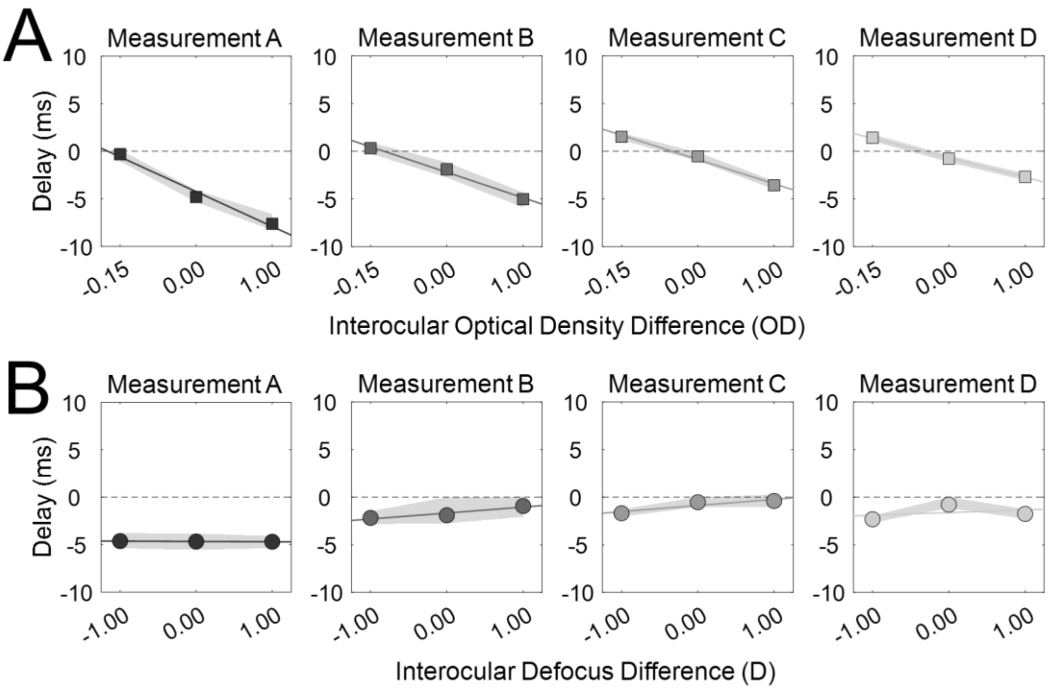

Figure 10.2. Changes in Classic and Reverse Pulfrich effects over time. **A**. Classic Pulfrich. Neural delay as a function of interocular optical density difference for each measurement (A to D). **B**. Reverse Pulfrich. Neural delay as a function of interocular defocus difference, in diopters, for each measurement.

10.2.3. Illusion size estimation

The illusion size in daily visual tasks was estimated for the spontaneous Pulfrich effect size measured when the patient suffered from symptoms (delay of 4.82ms in the RE). We used the mathematical description by Spiegler[202] to geometrically estimate the disparity caused by an interocular delay and the subsequent depth misperception (see section 10.4). In Figure 10.3, we show these estimations for two situations. Thin lines represent the actual position of the object and thick lines the illusory perception. Figure 10.3A shows a representative example of the relative movement of the observer in between two lines, like in a road lane while driving. We simulate a condition of a motorcyclist on the road, and how the lines of the road are distorted and curved due to the measured interocular delay. At 40km/h (a common speed limit in urban areas), the depth distortion of the line could be as high as 2 m, larger than the distance from the observer to the line (1.5 m). In Figure 10.3B, we simulated another condition in which the patient reported unbearable visual discomfort: walking downstairs. The simulation shows that each stair is perceived asymmetrically deformed, complicating the simple task of setting the foot on the ground. At walking speed (4km/h), the illusion size (distortion in step height) was as high as 0.2 m.

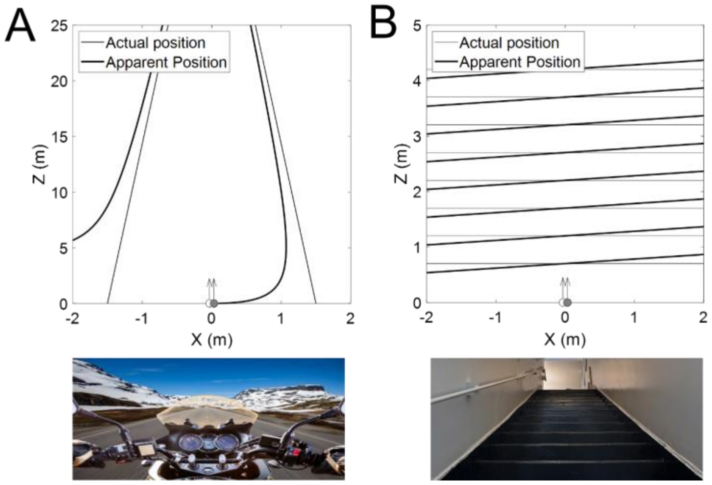

Figure 10.3. Depth misperceptions estimated for daily scenarios. Lower plots show scenes of representative situations with moving visual objects. Upper plots show the perceived trajectory of visual objects in the scenes. The observer's eyes are represented by two circles. In this case, the left eye (LE; white circles) is unperturbed, and the right eye (RE; gray circle) is delayed. The thin lines represent the actual trajectory/position of the object, and the thick lines represent the apparent trajectory/position of the object, estimated using Equation 10.3 and the magnitude of the spontaneous Pulfrich effect in Measurement A (before the second surgery) when the patient presented serious symptoms (4.82ms of delay in the RE). **A. Motorcyclist on the road.** Speed considered was 40 km/h. **B. Walking down the stairs**. Speed considered was 4 km/h.

These two synthetic examples illustrate the importance of the effect measured, in schematic visual scenarios. However, the free observation of the real world is much more complicated. Real visual scenes contain thousands of different visual objects moving at different speeds in any direction. Retinal optic flow measurements and algorithms can quantify these movements to provide a more reasonable description of depth misperceptions (described in section 10.4). Figure 10.4 shows the illusion size while walking in different terrains (flat and rough), estimated using Equation 10.3 and the retinal optic flow measured by Mattis et al.[383] (visual degrees per second, as the body, head, and eye move relative to the terrain). The illusion size was estimated for two of the interocular delays measured in the patient (-4.82 ms and -0.78 ms corresponding to Measurements A and D, in Figure 10.1) for an object in the ground located at 2m distance. Figure 10.4A shows the depth estimation with time for the delay measured in Measurement A, before the second surgery, when the patient had the strongest visual discomfort. The illusion size changes chaotically as a function of time, with an average of 0.20 m for flat terrain (0.16 m for rough terrain), larger than a conventional step, and standard deviations of 0.59 m (0.52 m for rough terrain). For the delay measured in the last visit (Measurement D), 0.78 ms in the RE, when the readaptation process is complete, the average depth illusions decrease to 0.03±0.28 m for flat terrain (and to 0.04±0.23m for rough terrain). The huge illusion size present in the first visit explains the difficulties reported by the patient while walking. Similarly, after monovision removal and delay readaptation, the illusion size recovers normal values, which can explain the vanishing of the visual symptoms in the same patient.

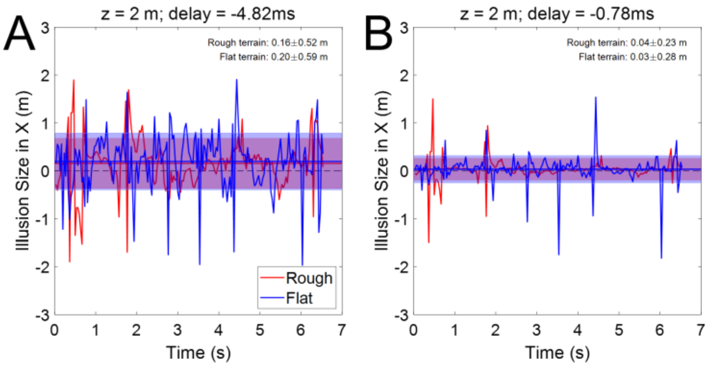

Figure 10.4. Depth misperception estimations using optic flow algorithms for different types of terrains. Illusion size in the horizontal direction in meters as a function of time for an object located at 2 m distance. The shaded regions display the standard deviation in illusion size, in meters, at both sides of the average illusion size (numerical values in the upper right corner of each graph). In red, rough terrain and blue, flat terrain. **A.** Estimation of the illusion size for a delay in the processing speed of the right eye (RE) of 4.82ms, when the patient suffered from symptoms. **B.** Estimation of the illusion size for a delay in the processing speed of the right eye (RE) of 0.78ms, when the patient did not suffer from symptoms.

10.3. Discussion

In this study we report a case of spontaneous Pulfrich effect after a cataract procedure, that is induced by the combination of a Classic Pulfrich effect (interocular light difference between the intraocular lens in one eye and the aged crystalline lens of the other eye) and a Reverse Pulfrich effect (interocular blur difference caused by the post-surgical monovision correction).

Spontaneous Pulfrich effect in cataract patients

The Pulfrich effect is a well-known phenomenon affecting the binocular vision of patients with interocular differences. Therefore, it is relevant in cataract patients, where the optics of the eye changes progressively as the cataract evolves, and abruptly during cataract surgery. Scotcher et al.[384] showed a spontaneous Pulfrich effect, needing a neutral density filter of 0.25 OD -on average- to neutralize the effect, in 12 patients after cataract surgery in one eye and before cataract surgery in the second eye. In the case of the patient of this study, the neutral density filter needed was 0.19 OD. Cetinkaya et al.[216] also reported a spontaneous Pulfrich effect in 36 patients in between cataract surgeries, needing a significantly higher filter to compensate for the spontaneous Pulfrich effect (1.2 OD on average). Diaper et al.[214] reported a spontaneous delay of 1.49 and 1.16 ms in two patients with unilateral cataract. However, the presence of a spontaneous Pulfrich effect does not always mean the presence of associated binocular vision problems[215,216]. But the spontaneous Pulfrich effect, and the associated symptoms, are always alleviated once the interocular differences are surgically removed, typically after cataract surgery in the second eye.

The Classic Pulfrich effect is well known and has been extensively studied. On the contrary, the Reverse Pulfrich effect is an unknown phenomenon only recently discovered in lab studies[103,372]. For that reason, the studies in the scientific literature assume that the Classic Pulfrich effect, due to interocular luminance differences and, to a lesser extent, scattering, is the reason behind the spontaneous Pulfrich effect in between surgeries. However, both cataracts and cataract surgery also induce blur changes, which are the source of the Reverse Pulfrich effect. Therefore, the spontaneous Pulfrich effect described in the literature -and also found in this study- could be due to a Classic Pulfrich effect, a Reverse Pulfrich effect, or a combination of both. But it is difficult to identify which of the changes taking place in the optics of the eye contribute to the delay found. This study sheds some light on the question by measuring the timeframe of readaptation to the spontaneous Pulfrich effect.

The Reverse Pulfrich effect as the cause of the spontaneous Pulfrich effect
The patient reported severe symptoms that conditioned his lifestyle and restricted his daily activities. The discomfort was harsh enough to explain the second surgery in the healthy eye -clear lens extraction- to remove the monovision correction. Remarkably, the patient was not significantly uncomfortable in static observation. Only the symptoms caused by movements in the visual scene were unbearable for him. There is a clear parallelism between the evolution of the symptoms and the important spontaneous Pulfrich effect measured in this study; in particular, between the reduction of the spontaneous delay with the surgery and the alleviation of the visual symptoms. The simulations and estimations of the illusion sizes from the measured delay (Figure 10.4), can explain the symptoms -or absence of symptoms- described by the patient at the different stages.

But, should the spontaneous Pulfrich effect be attributed to the Classic or to the Reverse Pulfrich effect? The key to answering this question is the timeline of readaptation of the patient, of several weeks, that cannot be explained by an adaptation to the Classic Pulfrich effect. Previous studies have measured the process of adaptation to interocular differences in luminance (i.e., Classic Pulfrich effect), induced on purpose with neutral density filters[333,380,381]. In those studies, the adaptation/readaptation to luminance differences take periods from hours to days, but far from 10 weeks, as Figure 10.1 may suggest. The long period of readaptation is not compatible with the shorter timelines of adaptation to luminance or to the Classic Pulfrich effect but is fully coherent with other studies of adaptation to blur, associated with much longer adaptation periods[297,332,354,374]. At least, in this case, the readaptation process after the surgery can be attributed to a previous adaptation to a Reverse Pulfrich effect. The important spontaneous Pulfrich effect measured in between surgeries is, for the most part, due to a Reverse Pulfrich effect caused to blur and induced by monovision.

Clinical relevance
Although recently discovered, the Reverse Pulfrich effect has already demonstrated potential implications in the clinic, due to its strong relationship with monovision, a common correction for presbyopia. This is the first study that evidences a pathological condition caused by the Reverse Pulfrich effect.

Aniseikonia, the interocular difference in retinal magnification, is often blamed as the origin of visual discomfort when there are interocular differences in refractive power. Monovision has the potential to produce aniseikonia and for that reason it is only prescribed with contact lenses, intraocular lenses, or refractive surgery, to avoid the more important magnification associated with the vertex distance of ophthalmic lenses. The patient of this study may have suffered also from some aniseikonia. But that source of visual discomfort would be permanent -as opposed to the Pulfrich effect that only appears with moving visual objects- and seems to be minor, as the patient reported comfortable vision of static scenes. Besides, previous studies have shown that interocular magnification differences do not induce any delay[372], and therefore do not play a role in the spontaneous Pulfrich effect.

The results of this study suggest that patients with interocular blur differences who report discomfort, particularly in dynamic visual environments, should be investigated in the search for a potential Reverse Pulfrich effect. In cases where there is a Reverse Pulfrich effect, there are other strategies to deal with the symptoms beyond reverting the interocular differences. For instance, placing a filter in one eye of a patient with spontaneous Pulfrich effect eliminate both the effect and the symptoms[214,215]. Similarly, Rodriguez-Lopez et al. proposed anti-Pulfrich monovision corrections, where the Reverse Pulfrich effect is compensated with a Classic Pulfrich effect of the same size and opposite sign[103,372]. The postoperative exploration of the Reverse Pulfrich effect could be particularly useful when monovision is surgically reversible, as in light adjustable lenses[385] or laser refractive surgery.

In this study, the measurements of the Pulfrich effect have been performed using a time-consuming psychophysical paradigm (1 hour per measurement). Clinical tools that provide fast, straightforward, and reliable measurements of the spontaneous Pulfrich effect may help to understand adaptation effects (of Reverse and Classic Pulfrich effects) and their relationship to no adaptation to monovision corrections. Future work needs to address massive measurements in a higher sample size to confirm the clinical relevance of the Reverse Pulfrich effect, establish normative values, and the prevalence of associated visual symptoms in patients with monovision corrections.

10.4. Methods

10.4.1. Setup

The setup and psychophysical paradigm were the same used in Chapters 8 and 9. The subject viewed the stimulus from 2 meters, through well-centered trial lenses, and with his head stabilized by a chin rest with forehead support. The stimulus in the Stereoscopic Monitor (SM, see section 2.2.2). In summary, the 3D monitor uses row-by-row spatial interlacing (i.e., the right eye sees pixels from odd rows and the left eye sees pixels from even rows) to present different images, coincident in time, to the left and the right eyes. The appropriate image for each eye was selected using passive circular polarization glasses. The spatial resolution of the display was 3840x2160 pixels. Only 3840x1080 pixels reached each eye after filtering by the polarization glasses.

As in previous studies of the Reverse Pulfrich effect[339,372], the stimulus was a white moving bar of 0.125x1º size on a gray background. A window of 1/f noise was used to aid fusion. The movement of the bar was horizontal in space with an amplitude of 2.5º, and sinusoidal in time, with 2.5º/s of peak speed in the center of the display and 0º/s in the lateral limits (at 2.5º to the left and the right). To induce disparity in the image, we introduced subtle manipulations of the horizontal position of the moving bar for one eye (OS), following a constant interocular temporal shift (Δt, also called delay or advance).

Positive values of Δt indicate that the RE is delayed relative to the LE, and negative values that the RE is advanced relative to the LE. When the temporal shift is zero, the bar moves on the plane of the screen. But delays and advances are translated into crossed disparities and uncrossed disparities, resulting in depth illusions that depend on the direction and speed of movement.

The task was a two-alternative forced choice (2AFC). The patient had to indicate the sign of the depth illusion (closer or further) when the bar was moving to the right or the left, obtaining a nine-level (i.e., nine temporal shifts) psychometric function. The 50% point of the psychometric means the Point of Subjective Equality (PSE) and indicated the interocular delay induced onscreen needed to null the neural delay caused by the interocular differences between the images. A more detailed explanation can be found in Burge et al.[339]. The performance of the subject of this study was similar to that of other subjects in other studies[103,372].

10.4.2. Experiments

The subject performed the measurements with his refractive error corrected, using his usual compensation. Besides, we added an extra +0.50D using trial lenses to focus the screen.

To induce the Classic Pulfrich effect, we introduced "virtual" differences in light by digitally reducing the luminance onscreen by a factor equivalent to a neutral density filter with a particular optical density (*OD*). We produced interocular optical density differences reducing the incoming light of one eye while keeping the other one unperturbed, and vice versa. We estimated the interocular luminance difference (ΔO) as the optical density difference between RE (O_R) and LE (O_L), as shown in Equation 10.1.

$$\Delta O = O_R - O_L \qquad 10.1$$

Similarly, to induce the Reverse Pulfrich effect, we produced interocular differences in defocus introducing defocus in one eye and keeping the other one unperturbed and vice versa. The defocus induced was always myopic defocus using concave (positive) trial lenses. The resultant retinal blur cannot be compensated by accommodation. We estimated the interocular defocus difference (ΔF) as the difference in optical power between the RE (F_R) and the LE (F_L)

$$\Delta F = F_R - F_L \qquad 10.2$$

negative values of ΔO and ΔF mean that the LE was perturbed and positive values that the RE was perturbed.

We measured the difference in processing speed for two conditions of ΔO, ±0.15 OD (Classic Pulfrich effect), and two conditions of ΔF, ±1.00 D (Reverse Pulfrich effect). Besides, the spontaneous Pulfrich effect was measured with both eyes equally illuminated and sharp.

The three measurements of delay for the Classic Pulfrich effect (negative optical density, no optical density, and positive optical density) were linearly fitted via a least-squares regression. The slope (delay vs optical density) indicates the Classic Pulfrich effect size. Similarly, the delays (or interocular differences in processing speed) for the Reverse Pulfrich effect (negative defocus difference, no defocus difference, and positive defocus difference) were linearly fitted to provide the size of the Reverse Pulfrich effect.

To evaluate the evolution with time before and after the second surgery, we considered those three metrics: 1) the spontaneous Pulfrich effect, i.e., the direct measurement of the neural delay without any induced disturbances in any eye; 2) the Classic Pulfrich effect size; and 3) the Reverse Pulfrich effect size.

10.4.3. Estimating depth misperceptions

The delays (or interocular differences in processing speed) caused by the different versions of the Pulfrich effect and measured according to the procedures described in the previous section, can produce misperceptions in depth. The magnitude of these misperceptions not only depends on the interocular differences in blur or luminance, but also on other factors such as distance of observation, the direction of motion, and speed of the target with respect to the observer, or interpupillary distance of the observer. Spiegler[202] derived from the problem geometry the equations to predict the misperceptions caused by a target moving at a constant speed (Figure 10.5A). A detailed derivation of the equations can be found in the original manuscript[202].

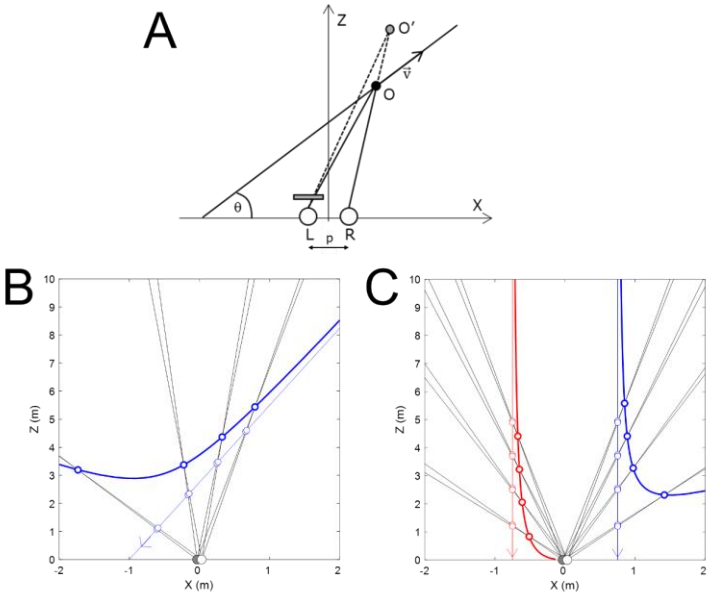

Figure 10.5. Estimating depth misperceptions caused by the Pulfrich effect using geometry. A. Schematic diagram on the depth misperception caused by the Pulfrich effect for a given point (O) of the trajectory of a moving object at a constant speed ($\vec{v}$). The trajectory subtends an angle θ with the horizontal axis. The two white circles represent the left (L) and the right (R) eyes, and p the distance between them (i.e., the interpupillary distance). A neutral density filter covering the left eye delays the processing speed of that eye with respect to the right eye, producing the object to be perceived further than its real position (O'). Adapted from Spiegler[202]. **B.** Full depth misperception trajectory for the moving object represented in A, with the same neutral density filter. The object is moving at a speed of 36 km/h and an angle θ of 70º, for an interpupillary distance of 65 mm. The left eye processing speed is delayed 5 ms with respect to the right eye. The thin blue line represents the actual trajectory of the object, and the bolded blue line is the apparent trajectory due to the Pulfrich effect. Black lines represent the gaze direction of both eyes. This figure also shows four representative points along the trajectory. The object is perceived further than its real position and the magnitude of the illusion changes with the movement of the object. **C.** Full depth misperception trajectory for two objects moving towards the observer in parallel trajectories separated 1.5m (0.75m at each side). The speed and delay are 36 km/h and 5 ms, respectively. The object to the left of the observer (thin red line) is perceived closer than its real position and finally collides with the observer (bold red line). The object to the right of the observer (thin blue line) is perceived further than its real position and moves away (bold blue line). This example can represent the lines of a lane in a road or the two walls of a corridor, each one suffering an illusion of different sign and magnitude.

A couple of representative examples can be found in Figures 10.5B and Figure 10.5C. In these examples, only the left eye was delayed ($t_R = 0$). The processing speed of the left eye image is delayed 5 ms with respect to the right eye image. In Figure 10.5B, the apparent trajectory (thick blue line) dramatically differs from the actual trajectory (thin blue line), with differences as high as 4 meters. Figure 10.5C shows an object approaching in a straight line 0.75 m separated to the left (red line) and the right (blue line) of the observer. For the object approaching from the left, the object appears to move towards the face of the observer. For the object approaching from the left, its illusory trajectory escapes from the observer at about 2 meters. As shown in these examples, a couple of milliseconds could represent a huge misperception in depth.

This mathematical description can estimate any misperception produced by objects moving in a predictable trajectory with respect to the eyes of the observer, assuming stable fixation without head movements: targets moving in front of the observer (e.g., a bicycle intersecting a road), targets that appear laterally from the field of view (e.g., a car in the other lane of a highway), targets moving towards the observer (e.g., a baseball ball), or static objects perceived as moving objects due to the relative motion of the observer (e.g., walls, steps, obstacles, lines, handrails, etc.). However, in the real visual world, with gaze changes and head movements, visual objects move across the visual field with unpredictable trajectories and at changing speeds, creating a complex and chaotic visual depth environment with considerable spatiotemporal variations which, in presence of a spontaneous interocular delay, are likely to produce a strong visual discomfort. The analytical description of Spiegler[202] may underestimate the potential implication of Pulfrich-caused misperceptions in real-world scenes. Retinal optic flow can provide a more realistic description of the motion of the objects in a scene, and therefore of the resultant depth misperceptions. Retinal optic flow refers to the apparent motion of objects in the retina caused by the relative motion of the observer (body, head, and eyes) and the visual scene.

In our study, we have used the dataset from Mattis et al.[383], describing the change in optical flow in visual degrees as a function of time for a subject walking through flat (easy to walk) and rough (rocky, more difficult to walk) terrains. For estimating the optic flow, they used eye-tracking, but they also monitored head and body movements. For the Pulfrich effect, only the horizontal component of the retinal optic flow is relevant (the vertical component will not create a meaningful Pulfrich effect). Thus, we estimated the speed of change of optical flow v for every time frame. The depth misperception caused for every frame was estimated using the following equation

$$\hat{d} = \frac{p}{p + v \cdot \Delta t} \cdot d \qquad 10.3$$

where $\hat{d}$ is the apparent position in depth, p the interpupillary distance, and d the actual position. We have computed the potential depth misperception for the first and the last measurement of the spontaneous Pulfrich effect of the patient, for an object located at 2 m.

10.4.4. Ethics

The research was in compliance with the tenets of the Declaration of Helsinki. Study protocols were approved by the CSIC Institutional Review Board. The subject signed a consent form after receiving an explanation of the nature of the measurements.

10.5. Conclusions

In this chapter, we present the case of a patient compensated with a monovision correction after unilateral cataract surgery, who showed an important spontaneous Pulfrich effect. By longitudinally monitoring the delay after removing the interocular differences between the eyes, we demonstrate for the first time a spontaneous Pulfrich effect produced by a combination of Classic and Reverse Pulfrich effects. This study shows for the first time the existence of readaptation to the Reverse Pulfrich effect, and the measurements establish a decay time of weeks, far from the timeline associated with the Classic Pulfrich effect, known to last only hours or days. Although strictly speaking we did not measure the adaptation process to the Reverse Pulfrich effect, its existence can be inferred from the measured readaptation occurring when the physical stimulus disappeared. The very different readaptation timelines for Classic and Pulfrich effects suggest very different neural adaptation mechanisms. The unique case shown in this study demonstrates the importance of the Pulfrich effect in medical interventions inducing interocular differences in retinal illuminance and blur. Measuring the spontaneous Pulfrich effect may help to understand and manage the symptoms of some patients with visual discomfort, even without differences in retinal illuminance.

Chapter 11. The effect of overall light level on the Classic and Reverse Pulfrich effects

In this chapter, we study the changes in the different versions of the Pulfrich effect as a function of luminance light level, aiming at understanding the potential consequences of the Reverse Pulfrich effect in daylight and nightlight.

This chapter, in collaboration with the University of Pennsylvania, is based on the article by Victor Rodriguez-Lopez et al. '*The effect of overall light level on the Classic and Reverse Pulfrich effects*" submitted to *Journal of Vision (2022)*. The co-authors of the article are Benjamin Chin, Carlos Dorronsoro, and Johannes Burge.

The contribution of the author of the thesis was the conceptualization and design of the study in collaboration with Carlos Dorronsoro and Johannes Burge, the literature research, the design of the experiments and the collection of the data in collaboration with Johannes Burge, the analysis of the data, the writing of the chapter and the editing of the chapter in collaboration with Johannes Burge and Carlos Dorronsoro.

This work was presented as a virtual poster contribution at the Vision Science Society (VSS) virtual meeting in 2022.

11.1. Introduction

Previous chapters (8 and 9) showed the potential impact of the Pulfrich effect on daily tasks and developed and demonstrated the anti-Pulfrich monovision corrections, i.e., dimming the blurry eye to compensate for the opposite effects of the Reverse and the Classic Pulfrich effect. However, overall light level changes during the day, and may affect the Classic Pulfrich effect, the Reverse Pulfrich effect, or both. This chapter evaluates the impact of overall light level in both versions of the Pulfrich effect.

Catching a ball at dusk is more difficult than catching a ball at high noon. Often, the ball arrives before one has had time to react. This phenomenon is explained, in part, by the fact that visual processing is slower when the overall light level is lower. Visual signals that are processed more slowly leave less time for action planning and behavioral response. The difficulties for vision further increase when the images in the two eyes differ from one another in certain ways. For example, when the image in one eye is brighter or blurrier than the image in the other, dramatic misperceptions of depth and the 3D direction of motion occur[103,203,367,371,372,386]. These effects are known, respectively, as the classic and Reverse Pulfrich effects. Signals from the brighter or blurrier eye are processed more quickly than those from the other eye. For moving objects, the differences in processing speed cause effective neural disparities, resulting in misperceptions. It has been reported that stereoacuity is affected by the luminance level[387,388]. But, how does overall light level impact the discrepancy in temporal processing caused by a given image difference between the eyes? The answer has implications for basic scientific understanding, and clinical ophthalmology practice.

Changes in overall light level are commonplace. Over a 24-hour period, light-level changes markedly, ranging from 10^9 cd/m^2 during the day to 10^{-4} cd/m^2 at night[389,390]. Do the images in the two eyes ever differ in retinal illuminance or blur? Substantial differences in retinal illumination between the left- and right-eye images occur when viewing specular objects, or when looking at a scene through a pair of sunglasses with one missing lens. Such viewing situations are relatively rare. Substantial blur differences (e.g., ±1.0D or more), on the other hand, are comparatively common[391,392]. Anisometropia, a condition characterized by interocular differences in optical power ±1.0D or more is thought to occur in up to 30% of some important demographic groups[393,394]. And, increasingly, monovision corrections, which intentionally induce blur differences between the eyes (e.g., 0.75-2.5D)[97], are being surgically implanted or delivered with contact lenses as alternatives to reading glasses, bifocals, and progressive lenses.

In this chapter, we investigate the influence of overall light level on the Classic Pulfrich effect and on the Reverse Pulfrich effect. By projecting diaphragms into the pupil with a custom 4f system, we gain control over the pupil size, thereby allowing us to isolate neural from optical influences on the effects. We find that the effect of light level on the Classic Pulfrich effect matches previous results in the literature[203,204]. Decreases in overall light level are associated with increases in processing speed differences caused by a given interocular difference in retinal illuminance. We also find that light level similarly impacts the Reverse Pulfrich Effect: decreases in overall light level are associated with increases in processing speed differences caused by a given interocular difference in retinal defocus blur. Our results implicate higher-order optical aberrations in modulating effect sizes because the effect sizes do not follow expectations that follow directly from geometric optics. We discuss the public safety implications of these findings for the prescription of monovision corrections.

11.2. Methods

11.2.1. Setup

In this chapter, we used the Haploscope system II (HII, see 2.2.1.2), a set of mirrors to show the image of one of two monitors (VPixx VIEWPixx LED displays) controlled by the same AMD Radion Pro5300M graphics card with 4GB GDDR6 memory. A 4f optical system projected optotunable lenses and precision-printed diaphragms of fixed sizes into the pupil planes of the eyes. This system provided a means to programmatically change the interocular focus difference on each trial, and to control the effective pupil size. One of the advantages of this setup is that allows changing only defocus without changes in magnification. In addition, the possibility of changing the optical power by software instead of manually, as performed in previous chapters, has positive implications in terms of measurement time. Through the entire optical system, the maximum luminance was 12.8cd/m^2. The optical distance from the eyes of the observer to the screen was 80 cm. Additionally, to avoid accommodation issues, we induced +1.25D using the optotunable lens system in both eyes and in all conditions to compensate for the distance of the eye to the screen.

11.2.2. Stimulus

The stimulus consisted of four strips textured with randomly positioned 1.00x0.25deg white bars moving horizontally at a constant speed of 4.0 degrees per second. Adjacent strips moved in opposite directions (Figure 11.1).

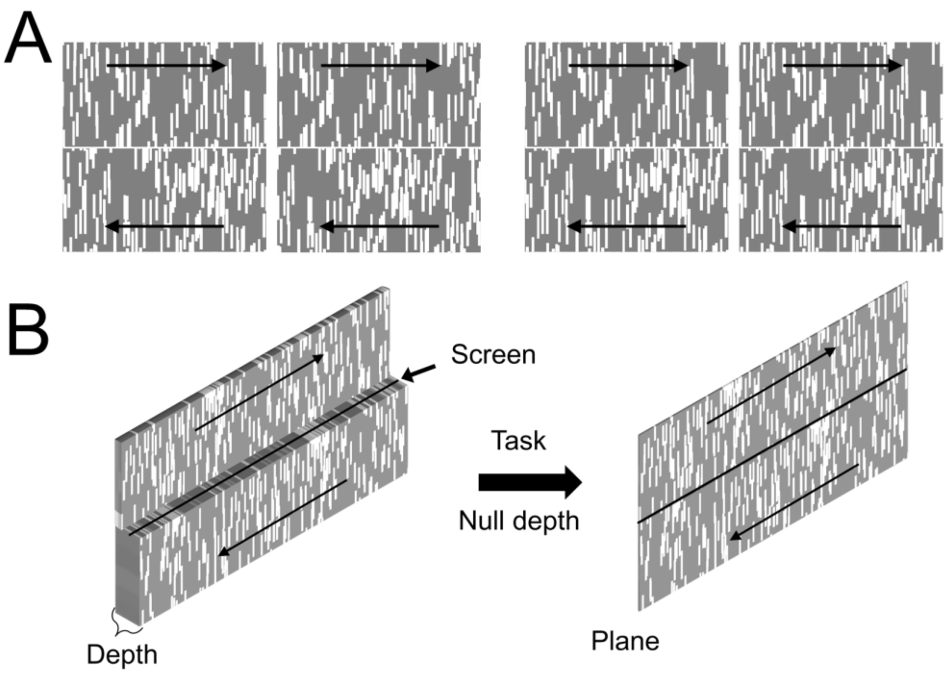

Figure 11.1. Stimulus used in this study (2 of 4 strips shown) and the task of nulling the perceived depth. Adjacent strips move in opposite directions. **A.** *S*timulus with non-zero onscreen disparities. Divergently fuse to see the right-moving plane of bars farther than the left-moving (bottom) plane of bars). Cross fuse to see the right-moving plane of bars closer than the left-moving (bottom) plane of bars. **B.** 3D view of experimental stimuli**.** Stimulus with onscreen disparities specifying non-planar depth structure (e.g., the upper plane of bars is specified by disparity to be behind the screen and the bottom plane of bars is specified to be in front of the screen). Stimulus with onscreen disparities specifying that both the upper and lower plane of bars is in the plane of the screen.

To induce an effective onscreen interocular temporal shift Δt (i.e., delay or advance), we first determine the equivalent onscreen spatial disparity in degrees of visual angle

$$\Delta x = v\Delta t \tag{11.1}$$

where v is the movement speed in degrees per second. The onscreen horizontal left- and right-eye positions of the strips in the two eyes evolve with time according to

$$\begin{aligned} x_L(t) &= vt + \Delta x/2 \\ x_R(t) &= vt - \Delta x/2 \end{aligned} \tag{11.2}$$

where x_L and x_R are the left- and right-eye x-positions in degrees of visual angle, and t is time.

When the onscreen interocular temporal shift equals zero, the strips are specified by onscreen spatial disparity to move in the plane of the screen. When the onscreen interocular temporal shift is non-zero, the strips are specified by onscreen spatial disparity to be in front or behind the screen. Negative interocular temporal shifts indicate that the left-eye onscreen image is delayed relative to the right-eye image. Positive interocular temporal shifts indicate that the left-eye onscreen image is advanced relative to the right-eye image. For negative temporal shifts, rightward and leftward moving strips are specified by disparity to be farther than and nearer than the screen plane, respectively. For positive temporal shifts, rightward and leftward moving strips are specified by disparity to be nearer than and farther than the screen plane, respectively.

Procedure
The task, represented in Figure 11.1, was to set the effective onscreen temporal shift (i.e., the onscreen spatial disparity) via an adjustment procedure until all strips appeared to move in the same depth plane (i.e., the plane of the screen). In each condition, six runs were conducted. On a given run, the initial onscreen interocular temporal shifts ranged from -15ms to +15ms. On a given trial within a run, the strips moved continuously with a fixed temporal shift until the observer made either a coarse adjustment ($\pm$1.0ms) or a fine adjustment ($\pm$0.2ms). Each adjustment initiated the next trial, with a new onscreen temporal shift. The observer continued running trials and adjusting the onscreen temporal shift until the observer signaled with a button press that the task had been completed. Throughout each trial, the observer fixated on the rightward-moving strip nearest the center of the screen. Sometimes, the rightward moving strip was just above the vertical midpoint of the screen; sometimes it was just below the vertical midpoint. The stimulus texture was updated with a new texture (different random configuration of the moving bars of the stimulus) in every run.

The point of subjective equality (PSE) for a given condition was estimated by averaging the final settings of the onscreen interocular temporal shift across the six runs. The PSE indicates the onscreen temporal shift required to null the neural delay caused by a particular interocular difference in retinal illuminance or defocus blur.

11.2.3. Overall luminance levels

Stimuli were presented at four overall luminance levels ranging from 12.8cd/m^2 (maximum luminance reaching the eye) to 0.2cd/m^2. To reduce the luminance from the maximum level, we positioned a neutral density filter into the light path for each eye. The neutral density filters were always matched between the eyes and had optical densities (OD) with one of four values (0.0, 0.6, 1.3, and 1.8). These optical densities correspond to transmittances of 100%, 25%, 5%, and 1.5%.

11.2.4. Pupil size

Pupil size was controlled by projecting a diaphragm of known size into the pupil plane of each observer using the custom 4f-optical system referenced above. Cycloplegic drops -2 drops of phenylephrine 2.5% and 2 drops of tropicamide in each eye- were administered to dilate the pupil and ensure that the entrance pupil diameter was determined by the projected diaphragm. Measurements were taken with fixed pupil diameters of 2mm, 4mm, and 6mm. Measurements were also taken with natural pupil diameter. For the natural pupil, no cycloplegic drops were administered and a diaphragm with a 10mm diameter was inserted into the 4f-optical system such that the entrance pupil of the optical system was the natural pupil of the observer's eye.

To obtain measurements of the natural pupil size, post-hoc measurements were taken under the exact same stimulus and lighting conditions as the main experiment. Observers wore Pupil Core 120Hz camera glasses (Pupil Labs, Berlin, Germany), a mobile eye tracking system that also provides pupillometry. Pupil diameter data were obtained for 1 sec (i.e., 120 frames) after 3 seconds of adaptation to the light level. We report the average across frames as the pupil size for a given stimulus condition. The results indicated that the natural pupil ranged in size from approximately 4mm to approximately 6mm, from the highest to the lowest overall light level.

11.2.5. Experiments

The conditions were grouped into two different experiments. The first measured the Classic Pulfrich effect. The second measured the Reverse Pulfrich effect.

The Classic Pulfrich effect was measured by reducing the luminance of one eye's image onscreen while leaving the other eye unperturbed. The interocular luminance difference, expressed in units of optical density (OD) is given by the difference between the effective optical density associated with the right-eye image minus the effective optical density on the left-eye image

$$\Delta O = OD_R - OD_L \qquad 11.3$$

For each overall light level, we measured two conditions. In one the left-eye image had lower luminance than the right (ΔO=-0.6 OD). In the other condition, the right eye image had lower luminance than the left (ΔO=+0.6 OD). These conditions correspond to the left eye receiving 25% of the light that the right eye received, and vice versa.

The Reverse Pulfrich effect was measured by inducing focus error in one eye, while leaving the other eye unperturbed. The interocular blur difference in diopters is given by the difference between the focus error induced in the right eye minus the focus error in the left eye

$$\Delta F = F_R - F_L \qquad 11.4$$

For each overall light level, we measured two conditions. In one, the left eye was defocus blurred and the right eye was sharp (ΔF=-3.0D). On the other, the right eye was defocus blurred and the left eye was sharp (ΔF=+3.0D). These defocus differences were induced by increasing the power of the optotunable lens in front of either the left eye or the right eye, thereby setting the optical distance of the corresponding monitor to beyond infinity and causing retinal defocus blur.

The effect sizes for the Classic and the Reverse Pulfrich effects were measured at all overall light levels and pupil sizes. Retinal illuminance level for each overall luminance level and pupil size was computed by multiplying the luminance by the pupil area

$$I = L \cdot \pi (A/2)^2 \qquad 11.5$$

where I is the retinal illuminance in trolands, L is the luminance level in cd/m^2 and A is the pupil size (diameter) in meters.

The delay and error for each retinal illuminance level were estimated as the mean and the standard deviation of the 68% confidence intervals from 1,000 bootstrapped datasets considering the absolute delay measured for each interocular condition (luminance ±0.60 for Classic Pulfrich effect and defocus ±3.00 for Reverse Pulfrich effect). The change of the delay as a function of retinal illuminance level was estimated as the log-log weighted regression. Each human observer ran in a total of 64 conditions (i.e., 4 overall light levels x 4 pupil sizes x 2 retinal illuminance differences x 2 defocus differences) for each experiment.

11.2.6. Data from the literature

For the Classic Pulfrich effect, there was data available from other experiments on how the Classic Pulfrich changes with overall light level. In both Lit[203] and Prestrude[204], they measured the delay for interocular differences in light levels up to 3.0 OD and for retinal illuminance levels ranging from 2.3 to 25000 trolands. Lit carried out measurements in two subjects and Prestrude in four subjects. For each luminance level, they measured several interocular luminance differences. However, for interocular differences in optical density higher than 1.0 OD, the change in the delay is not well-approximated by a linear function. Here, we measured luminance differences of 0.6 OD. For a fair comparison with the results of this study, we calculated the delay caused by a 0.6OD filter for each retinal illuminance level estimating the linear regression of the interocular delays measured up to 1.0 OD averaged across subjects in their studies. Figure 11.2 shows this estimation.

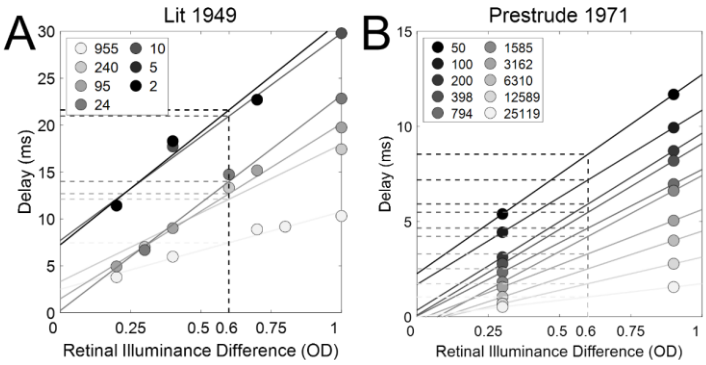

Figure 11.2 Changes in Classic Pulfrich effect as a function of the overall light level. Data from the literature. Each plot shows the delay as a function of interocular illuminance difference (in optical density) for different light levels, indicated with a different color (the whiter, the higher the light level). Auxiliar lines indicate the delay for 0.60 OD, used to compare with the results of this study. **A.** Lit 1949[203]. **B.** Prestrude 1971[204].

11.3. Results

In Figure 11.2 we show the pupil diameter measured for both subjects. The pupil measured will be used to estimate the retinal illuminance for each luminance level. For the highest luminance measured (12.8cd/m^2), pupil size is 4.56mm for S1 and 4.43 for

S2, and for the lowest luminance level measured (0.2 /m^2) pupil size is 6 and 6.25mm for S1 and S2, respectively. Measurements of the pupil size were used in the estimation for retinal illuminance in natural pupil condition.

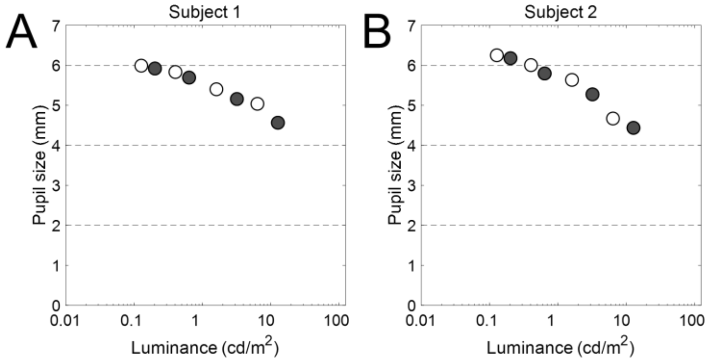

Figure 11.3. Pupil measurements. Pupil size in millimeters as a function of luminance level. Darker dots indicate pupil sizes for the overall light level conditions measured in this experiment. Horizontal dotted lines indicate fixed pupil sizes measured in this experiment (2, 4, and 6mm). **A.** Subject 1. **B.** Subject 2.

In Figure 11.4 we show the results for the Classic Pulfrich effect. In Figure 11.4A, we plot the onscreen delay required to null the perceptual illusion associated with interocular differences in retinal illuminance. Two conditions were measured for each overall luminance level two conditions measured, and – ΔO=0.6OD (left eye dimmer, dark gray in Figure 11.4A) and ΔO=+0.6OD (right eye dimmer, light gray in Figure 11.4A). Here results are shown for an overall luminance level of 3.2 cd/m^2. Negative delays indicate that the left eye was delayed onscreen and positive delays that the right eye is delayed onscreen. For each condition, the PSE and JND (average and standard deviation across the final settings from all runs for each condition) are -12.36±0.89ms and +12.6±1.01ms for +0.6OD and -0.6OD, respectively. In Figure 11.4B, the neural delay against the optical density difference is plotted. The slope of the linear regression is -20.80 ms/OD and the y-intercept 0.12ms, in agreement with previously reported results[103,203,372].

To quantify the effect of the overall light level, we estimated the absolute neural delay produced by a filter of 0.6 OD for each retinal luminance level. In this study, we measured 4 different luminance levels for different pupil diameters: natural pupil that changed with the overall light level and three fixed pupil sizes of 6, 4, and 2mm. In total, there were 16 retinal illuminance levels, estimated using Equation 11.5. As can be observed in Figure 11.4C, the relationship between the delay produced by the Classic Pulfrich effect and the illuminance level is linear on log-log axis. For S1 shown in Figure 11.4C, the slope of change is -0.14ms/troland and the y-intercept is 19.24ms.

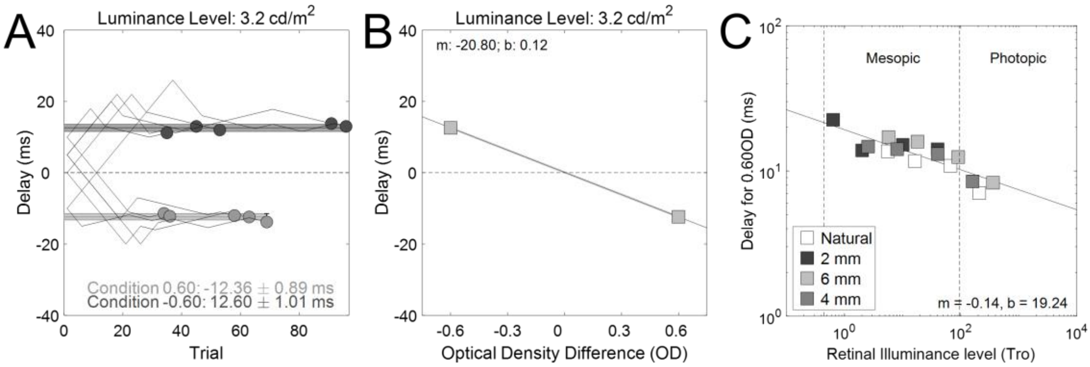

Figure 11.4. Classic Pulfrich effect changes for light level for one subject. A. It shows the change in onscreen delay in milliseconds across trials for each run. Dots represent the endpoint of the run, where the subject perceived the stimulus moving plane on the screen. Negative onscreen delay indicates that the right

eye image is processed slower than the left eye image, producing the stereo-depth illusion. Positive onscreen delay indicates that the left eye image is processed slower than the right eye image. Dark gray runs indicate the condition where the left eye image is perturbed (dimmer than the right eye placing an onscreen filter of 0.6 OD), and light gray runs where the right eye image is perturbed (dimmer than the left eye). Runs have different starting points (ranging from -15 to 15 ms). A shaded dark or light gray bar represents the average and its width the standard deviation across runs, indicating the Point of Subjective Equality (PSE) and the Just Noticeable Difference (JND) for both conditions. Particularly, this result is from S1 and the overall luminance level of 3.2 cd/m^2. **B.** It plots the PSE in milliseconds (estimated as the average across runs, see box A) versus the optical density difference. Also, the 95% confidence interval after bootstrapping with 1000 samples is displayed as a shaded error bar around data points. Negative optical density difference indicates that the left eye image is darker and positive that the right eye image is darker (Equation 11.3). The slope of the linear regression adjustment is an indicator of the effect size. For Classic Pulfrich effect is negative. **C.** It plots the absolute delay for a filter of 0.6 OD in ms for every retinal illuminance level measured. Different colors indicate different pupil sizes.

In Figure 11.5, we compare the results obtained from the subjects of this study versus the results of Lit[203] and Prestrude[204], which also measured the change in the Classic Pulfrich effect as a function of retinal illuminance. In our study, we measured more levels within the mesopic range. We found that the change in delay as a function of retinal illuminance is very similar among studies: for S1 and S2 in our study the change is -0.14ms/tro and -0.10ms/tro and for Lit's study was -0.17ms/tro to 0.23ms/tro and for Prestrude's was -0.24ms/tro. The difference in the slope may be attributed to the use of a different setup and a different stimulus and that both studies measured a different range of retinal illuminance levels.

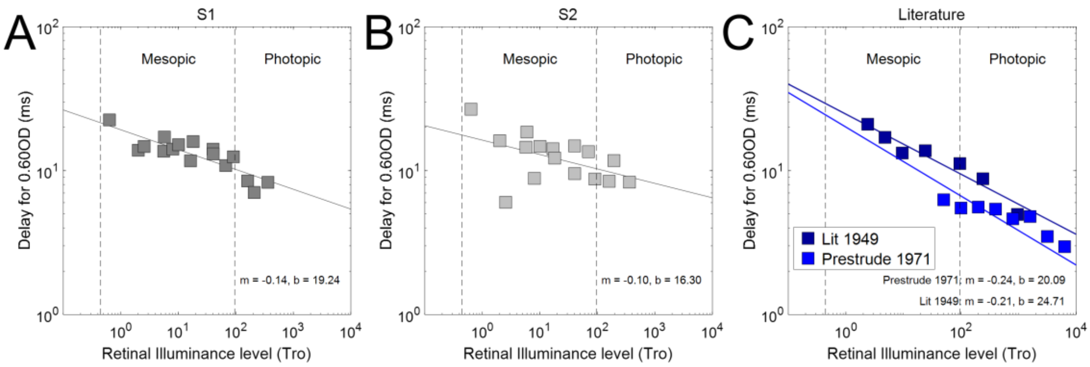

Figure 11.5. Classic Pulfrich effect results compared with the literature. Absolute neural delay for a condition of 0.6 OD in milliseconds as a function of retinal illuminance level in trolands. **A.** Results from the current study. **B.** Results obtained from Lit 1949[203] and Prestrude 1971[204].

In Figure 11.6 we show the results for the Reverse Pulfrich effect. In Figure 11.6A, we plot the neural delay measured in milliseconds along trials for each staircase and the two conditions measured, +3.0D (right eye blurrier, light gray) and -3.0D (left eye blurrier, dark gray), and an overall luminance level of 0.2 cd/m^2. For each condition, the PSE and the JND are 11.70±3.60ms and -11.40±4.91ms for +3.0D and -3.0D, respectively. In the Reverse Pulfrich effect, blurring the image of one eye produces a delay in the fellow eye, opposite to what is found in the Classic Pulfrich effect. In Figure 11.6B, the neural delay against the focus difference is plotted. The slope of the linear regression is 3.85ms/D and the y-intercept 0.15ms, in agreement with previously reported results[103,372]. To quantify the effect of the overall light level, we estimated the absolute neural delay produced by a lens of 3.0D for each retinal luminance level, plotted in Figure 6C. As can be observed, the relationship between the delay produced by the Classic Pulfrich effect and the retinal level is linear. For S1 shown in Figure 11.6C, the slope of change is 0.02 ms/troland and the y-intercept is 7.75ms.

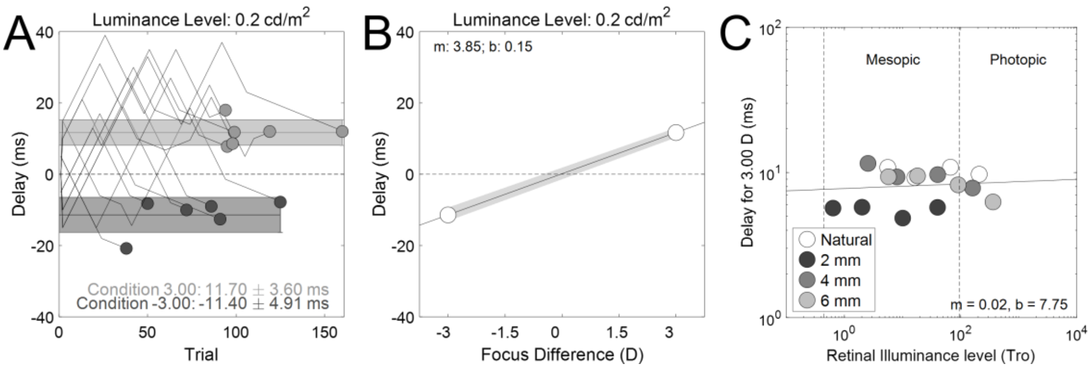

Figure 11.6. Reverse Pulfrich effect changes as luminance changes for one subject. **A.** This plot represents conditions of interocular differences in retinal blur (Reverse Pulfrich effect). Dark gray runs indicate the condition where the left eye image is perturbed (blurrier than the right eye inducing +3.00D of blur), and light gray runs where the right eye image is perturbed (blurrier than the left eye). Particularly, this example is from S1 and an overall luminance level of 0.2 cd/m^2. **B.** It plots the onscreen delay (estimated as the average across runs, see box A) versus the focus difference. Also, the 95% confidence interval after bootstrapping with 1000 samples is displayed as a shaded error bar around data points. Negative focus difference indicates that the left eye image is blurrier and positive focus difference that the right eye image is blurrier (Equation 11.4). For the Reverse Pulfrich effect, the slope of the linear regression adjustment is positive. **C.** It plots the absolute delay for a defocus of 3.0D in ms for every retinal illuminance level measured. Different colors indicate different pupil sizes.

As can be seen in Figure 11.6C, the Reverse Pulfrich effect changes across retinal illuminance levels similarly for all pupil sizes, except for 2mm in S1, which seems to follow a different trend. Figure 11.7 shows the slope changes for natural, 6mm, and 4mm pupil size together and for 2mm pupil size isolated, for both subjects. The slopes of change for natural, 6mm, and 4mm are -0.07ms/D and -0.06ms/D, and the y-intercept is 11.72ms and 17.71ms, respectively for S1 and S2. For 2mm pupil size, the slope and y-intercept are -0.01ms/D and 5.59ms for S1 and -0.05ms/D and 9.08ms for S2. The difference found in 2mm pupil size suggests that another factor different from the luminance level is influencing the neural delay, such as high order aberrations. It is known that reducing pupil size also reduces the aberrations of the eye and therefore the effective retinal blur. Thus, the similarity of interocular delays for 4 and 6 mm suggests that high order aberrations equate retinal blur in the Reverse Pulfrich effect.

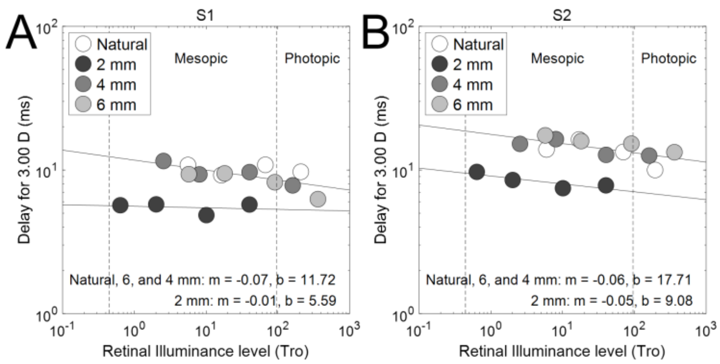

Figure 11.7. Reverse Pulfrich effect changes for 2 mm pupil size. Delays in milliseconds estimated for 3.0D of defocus for different retinal illuminance levels in trolands. Different colors indicate different pupil sizes. **A.** Subject 1. **B.** Subject 2.

11.4. Discussion

The Classic and the Reverse Pulfrich effects both increase in strength as overall light-level decreases. That is, as the overall light level decreases, the interocular delays increase, associated with both a given interocular (proportional) difference in luminance and a given interocular difference in focus error. The results reported for the Classic Pulfrich effect are in agreement with previously published data[203,204]. However, the results for the Reverse Pulfrich effect are novel. Besides. because our experiments had conditions in which pupil size was controlled, we also examined the impact of pupil size and its effects on the strengths of the classic and Reverse Pulfrich effects.

For the Classic Pulfrich effect, the influence of pupil size was negligible. However, for the Reverse Pulfrich effect, the 2mm pupil size is very different from the 4mm, 6mm, and natural pupil sizes. The reason behind these differences in the Reverse Pulfrich effect might be accounted for optical aberrations, which increase as the pupil size increases (especially high order aberrations)[17,395–397]. Therefore, the effective amount of blur for larger pupil sizes (4 and 6mm in our experiment) is higher than for small pupil sizes (2mm in our experiment), where mainly defocus is responsible for blur. The hypothesis for the Reverse Pulfrich effect is that blurring an image removes its high spatial frequency components, which are processed slower by the brain[94,96,317,318], and therefore the signal is processed faster. Reducing the pupil size reduces the effective retinal blur and the effective reduction of high-frequency components, which may explain the low Reverse Pulfrich effect when pupil size was small (2mm). Measurement of the optical aberrations may provide a more complete model for describing the Reverse Pulfrich effect.

Anti-Pulfrich monovision corrections take advantage of the opposite sign of the Classic and Reverse Pulfrich effects to eliminate the depth misperceptions by tinting the blurring lens by a certain amount of optical density, depending on the effect sizes measured and the amount of monovision[339,372]. However, both the Classic and Reverse Pulfrich effects change with overall light at different rates, needing to change hypothetical anti-Pulfrich monovision correction for each light level and therefore complicating the effectiveness of the possible solution. Recent solutions can change the transmittance of a contact lens in response to the ambient light level, photochromic contact lenses[343,398]. This type of solution may represent an appropriate delivery system for a complete anti-Pulfrich monovision correction. However, the efficacy of anti-Pulfrich correction itself must be validated.

11.5. Conclusions

In this study, we report that the Classic Pulfrich effect increases when the light level decreases (replicating findings reported in the literature) and that the Reverse Pulfrich effect also increases when the light level decreases (a novel result). The similarity of interocular delays for 4mm and 6mm pupils suggests that high order aberrations equate retinal blur in the Reverse Pulfrich effect.

Chapter 12. Prevalence of the Pulfrich effect

This chapter describes the development of a clinical tool to perform reliable measurements of the Reverse Pulfrich effect, based on a tablet with a sheet of lenticular lenses and a new stimulus designed to ease the visual task. Using these tools, we perfected the method to measure the Classic and the Reverse Pulfrich effects and performed measurements in 15 volunteers -so far- to get a first estimation of the prevalence of both effects in a young population, which will soon be completed in a higher sample.

This chapter, in collaboration with the University of Pennsylvania, is based on the article in preparation entitled '*Clinical tool to measure the Pulfrich effect in the clinic*" where Victor Rodriguez-Lopez is the first author. The co-authors of the article are Calista Dyer, Carlos Dorronsoro, and Johannes Burge.

The contribution of the author of the thesis was the conceptualization and design of the study in collaboration with Johannes Burge and Carlos Dorronsoro, the literature research, the design of the experiments, the collection of the data in collaboration with Calista Dyer and Johannes Burge, the analysis of the data, the writing of the chapter and the editing of the chapter in collaboration with Johannes Burge and Carlos Dorronsoro.

12.1. Introduction

Although only spontaneously present in some pathologies, it has been assumed that the Classic Pulfrich effect, when forced by inducing interocular luminance differences, occurs in all the population. The recent discovery of the Reverse Pulfrich effect (Chapter 8), caused by blur differences and affecting the optical quality differently for different people, poses the question of the prevalence and the size of the effect in the general population.

How prevalent are the different versions of the Pulfrich effect and how relevant is the effect size? We tackle this question in this chapter, by developing a new method of measurement of the Pulfrich effect, suitable for carrying out fast and reliable clinical measurements in a larger sample size. We present measurements of the Classic and Reverse Pulfrich effect (the latter induced with optical and onscreen blur) in an initial sample size of 15 young volunteers to provide a first estimation of the prevalence and the effect sizes of the different versions of the Pulfrich effect in the population. We developed measurement routines in an autostereoscopic electronic tablet to transfer the method from on-bench instruments to portable clinical devices.

12.2. Methods

12.2.1. Setup

The new stimulus (described below) was displayed on the Lenticular Lenses tablet (LLT) setup described in Chapter 2. In summary, the setup comprises an iPad Pro 3rd generation 12.9'' in combination with a MOPIC sheet of lenticular lenses to convert it into an autostereoscopic display (see section 2.6). The main limitation of the method is that only a specific application can be used to show 3D images and videos (MPlayer3D), and therefore the tablet cannot be driven directly from Psychtoolbox. In 3D mode, the effective refresh rate of the display, driven by an internal Apple A12X Bionic Graphic card, was 30 Hz. The row-by-row spatial interlacing (e.g., pixels in even rows to the left eye & pixels in odd rows to the right eye) was used to present different temporally coincident images to the left and right eyes, resulting in an effective spatial resolution of 960x1080.

The observer has their head stabilized with a chinrest and a forehead rest at 67cm from the display, which was viewed through trial lenses in custom-built mounts. The mounts were adjusted on the horizontal and vertical axes so that the optical element was centered along the line of sight of each eye. The display was held with a custom-3D printed mount.

12.2.2. Stimulus

In previous chapters, the stimulus was one moving bar that required concentration to perform the task and was difficult for some subjects. In this chapter, where the goal is to measure the prevalence of the Pulfrich effect, we developed a stimulus that covered a larger region of the visual field to produce a higher neural response and facilitate the task, similar to the stimulus designed in Chapter 11. The target was two centered stripes moving in opposite directions with random-positioned dynamic bars of 0.125x1º size. The size of each stripe was 5x2.25º, and the whole stimulus was 5x4.55º. Each stripe moved at 4 degrees/second, in opposite directions. Figure 12.1 shows the stimulus.

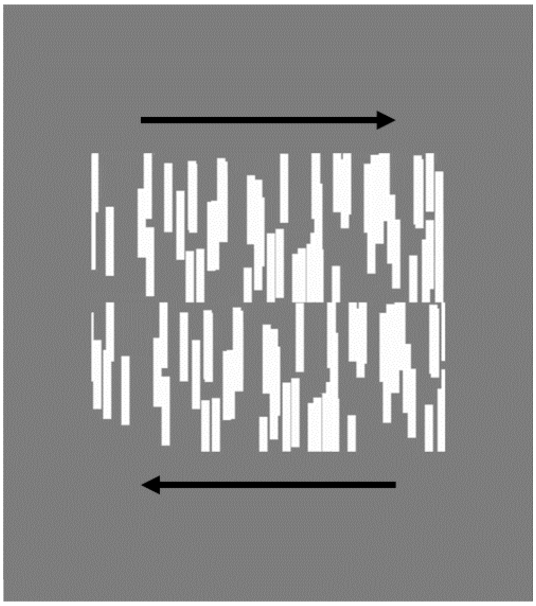

Figure 12.1. Stimulus used in this experiment. Upper stripe moves to the right and bottom stripe moves to the left.

12.2.3. Procedure

The stimulus was presented as part of a one-interval two-alternative forced-choice (2AFC) procedure, where the task was to report, using a keyboard, whether the upper or the bottom stripe appeared to be in front of the plane of the screen (crossed disparity). The upper stripe was always moving to the right and the bottom stripe to the left. The method of constant stimuli was used to present nine evenly spaced levels of onscreen interocular delay between -10 and 10 milliseconds. Sixteen trials per level were collected for a total of 144 trials per condition.

The proportion of 'front right' responses (the stripe moving to the right perceived in front of the screen) was collected as a function of onscreen interocular delay and the data was fitted to a cumulative Gaussian using maximum likelihood methods. The point of subjective equality (PSE) refers to the onscreen interocular delay required to perceive the target to move in the plane of the screen. The PSE indicated the neural differences in interocular processing speed equal in magnitude but opposite in sign. The just noticeable difference (JND) is derived from the psychometric curve as the difference in delay between the 70% and the 20% points in the curve. The PSE/JND is a metric used for estimating the relevance of the effect measured comparedto the sensitivity of the subject. A value of PSE/JND above 1 means that the effect measured is considerable. A value of PSE/JND below 1 means that the effect is not perceived by the subject.

Due to the limitations of the MPlayer3D application, the stimuli were presented as videos. Videos were conformed of 72 trials (8 repetitions of the same delay level) where the stimulus was shown for one second and then one second of response time. MATLAB was used to generate the videos that were later presented by MPlayer3D and Psychtoolbox[241] was used to independently collect responses to the videos. Figure 12.2 shows a diagram of the procedure.

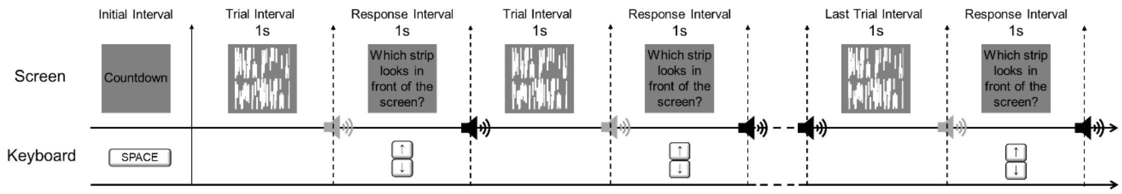

Figure 12.2. Trial sequence of the procedure. A representative trial of the test is shown. In each trial, the moving stimulus is presented during 1.0s followed by the response interval also during 1.0s. And an auditory tone is represented by a gray speaker.

12.2.4. Experiments

Each observer collected data in three experiments, each of them with multiple conditions (see below). In each experiment, data were collected across all conditions in blocks of 72 trials, each corresponding to one video. Each block (video) lasted 150 seconds. Experiment 1 measured the impact of interocular luminance differences induced onscreen. Experiment 2 measured the impact of interocular optical blur differences induced by trial lenses. Experiment 3 measured the impact of interocular blur differences induced by onscreen filtering of the image with a low-pass filter.

A calibration procedure to align the subject with the autostereoscopic display was followed before each procedure. Within MPlayer3D application, a static image conformed of 3 white rings surrounded by another larger ring was presented in 3D mode. To assure that the image of the left eye and the right were appropriately reaching each eye, the inner rings had to be sharply perceived in front of the plane of the screen (crossed disparity). If any ghosting was perceived, or the 3D perception was lost, the display was slightly moved in the horizontal axis until the subject perceived depth.

Depending on the experience of each observer on stereo psychophysical tasks, their sensitivity varied. To obtain sufficient data to construct a psychometric function, videos with different evenly spaced onscreen disparities were generated. Onscreen disparities varied from -10 to 10ms, -6 to 6ms, and -2 to 2ms. Before beginning each experiment, a testing video with onscreen disparities from -10 to 10ms in steps of 1ms was played to roughly estimate the threshold. According to that threshold, videos with different onscreen disparities were shown.

The Classic Pulfrich effect was measured by reducing the onscreen luminance of one eye by an amount of 0.15 optical density (OD) while keeping the other image unperturbed. The interocular optical density difference (ΔO) is estimated as the difference between the right eye optical density (OD_R) and the left eye optical density (OD_L, Equation 12.1). Two conditions were measured, dimming the left eye image (-0.15OD) and dimming the right eye (+0.15OD).

$$\Delta O = OD_R - OD_L \qquad 12.1$$

The Classic Pulfrich effect size was estimated as the ratio of delay as a function of interocular optical density difference (the slope of the linear regression adjustment) multiplied by 0.15OD.

The reverse Pulfrich effect was measured by increasing the blur of one eye and keeping the other eye sharp. The Reverse Pulfrich effect was tested optically increasing myopic defocus with a positive (convex) 1.00D. The interocular defocus difference (ΔF) is estimated as the difference between the right eye focus (F_R) and the left eye focus (F_L, Equation 12.2). Two conditions were measured, blurring the left eye image (-1.00D) and blurring the right eye (+1.0D).

$$\Delta F = F_R - F_L \tag{12.2}$$

The Reverse Pulfrich effect size with optical blur was estimated as the ratio of delay as a function of interocular focus difference (the slope of the linear regression adjustment) multiplied by 1.00D.

Besides, the Reverse Pulfrich effect was also measured by defocusing the image onscreen with a low pass gaussian filter of 4cpd cutoff frequency (half-height spatial frequency). The interocular blur difference (ΔB) is estimated as the difference between the right eye blur (B_R) and the left eye blur (B_L, Equation 12.3). Two conditions were measured, blurring the left eye image (-4.00cpd) and blurring the right eye (+4.00cpd).

$$\Delta B = B_R - B_L \tag{12.3}$$

The Reverse Pulfrich effect size with onscreen blur was estimated as the ratio of delay as a function of interocular focus difference (the slope of the linear regression adjustment) multiplied by 4.00cpd.

In each experiment, data were collected across all conditions in blocks of 72 trials, each corresponding to one video. Each block (video) lasted 150 seconds and each block was repeated twice. In total, 7 conditions were measured (no eyes perturbed, Classic Pulfrich effect in both eyes, Reverse Pulfrich effect with optical blur in both eyes, and Reverse Pulfrich effect with onscreen blur in both eyes). Therefore, each session took 45 minutes.

The experimental protocols were approved by the International Review Board of the University of Pennsylvania Ethics Committee and were in compliance with the Declaration of Helsinki. All participants provided written informed consent after explaining the nature of the measurements.

12.2.5. Statistical analysis

We used paired t-tests to analyze the statistical significance of different experiments (Classic Pulfrich, Reverse Pulfrich with optical blur, and Reverse Pulfrich with onscreen blur). We also analyzed differences in the PSEs, the JNDs, and the PSE/JND metric across subjects. The statistical level to achieve statistical significance was set to 5% (p=0.05).

12.3. Results

15 subjects participated in the study (25.1±6.3 years old). The average refractive error was -1.52±1.58D in spherical equivalent only 3 subjects reported astigmatism lower than 0.75D in the amount of astigmatism, estimated from the current prescription or with standard optometric techniques.

Figure 12.3 shows the psychometric function perturbing the left and perturbing the right eye for each experiment, the Classic Pulfrich effect, optical Reverse Pulfrich effect, and onscreen Reverse Pulfrich effect for one subject. Results are in agreement with previously reported studies (Chapters 8-11). Dimming the left eye image delays the left eye processing speed and the Point of Subjective Equality (PSE) is positive (0.88ms) and dimming the right eye image delays the right eye processing speed and the PSE is negative (-1.16ms), as shown in Figure 12.3A. The slope of the linear regression is negative (-6.8ms/OD). Figure 12.3B shows that blurring the left eye image with optical blur (defocus) advances the left eye processing speed and the PSE is negative (-1.73ms) and blurring with optical blur the right eye image advances the right eye processing speed and the PSE is positive (-1.34ms). The slope of the linear regression is positive (-1.5ms/D). Blurring the left eye image with onscreen blur advances the left eye processing speed and the PSE is negative (-1.73ms) and blurring with onscreen blur the right eye image advances the right eye processing speed and the PSE is positive (-1.34ms), shown in Figure 12.3C. The slope of the linear regression is positive (0.3ms/cpd).

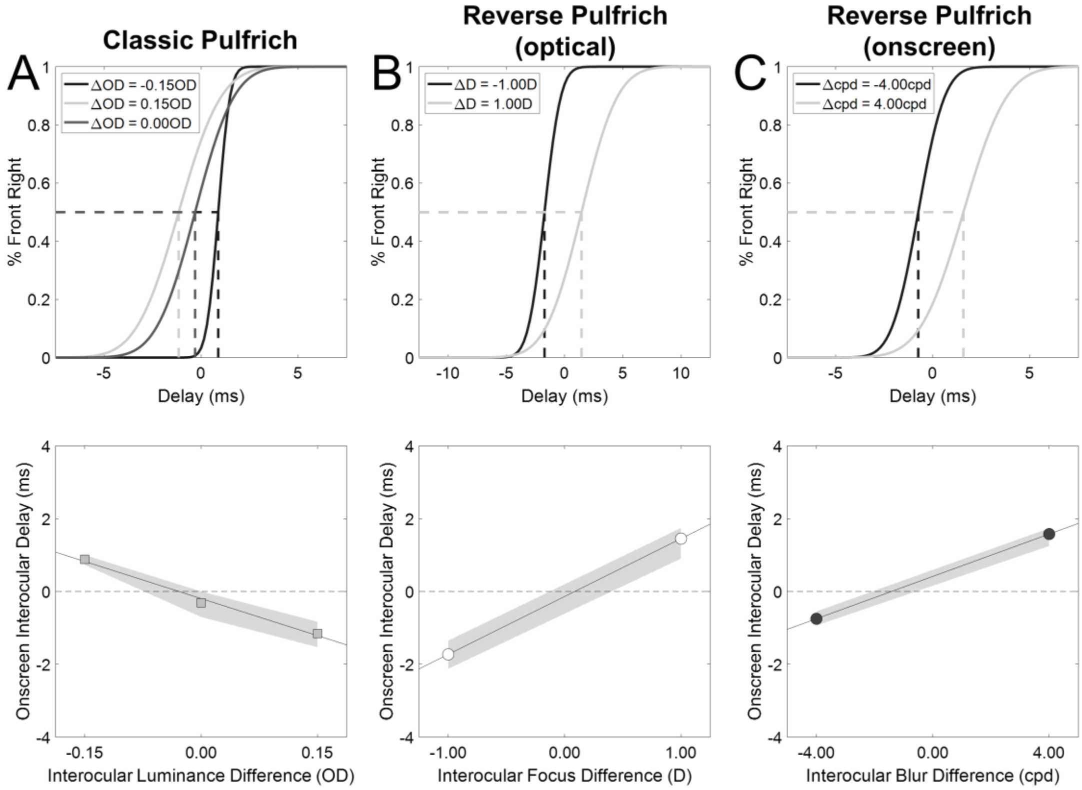

Figure 12.3. All experiments for one subject (S4). In upper plots of A, B, and C, dark gray indicated that the left eye was perturbed and light gray that the right eye was perturbed. Also, dotted lines indicate the Point of Subjective Equality (PSE), which represents the delay measured, the same magnitude but opposite in sign to the neural delay caused by the interocular difference. **A. Classic Pulfrich effect.** Upper plot shows the psychometric functions for left eye dimmer (-0.15OD, dark gray, PSE positive), for no eye perturbed (0.00OD, gray), and for right eye dimmer (0.15OD, light gray, PSE negative). Bottom plot shows the onscreen delay (PSE, in milliseconds) as a function of the interocular luminance difference (in OD). The slope of the linear regression is negative. **B. Reverse Pulfrich effect with optical defocus**. Upper plot shows the psychometric functions for the left eye defocused (-1.00D, dark gray, PSE negative) and for the right eye defocused (1.00D, light gray, PSE positive). Bottom plot shows the PSE as a function of the interocular focus difference (in D). The slope of the linear regression is positive. **C. Reverse Pulfrich effect with onscreen blur**. Upper plot shows the psychometric functions for the left eye blurrier (-4.00D, dark gray, PSE negative) and for the right eye blurrier (4.00D, light gray, PSE positive). Bottom plot shows the PSE as a function of the interocular blur difference (in cpd). The slope of the linear regression is positive.

In Figure 12.4A we show the Pulfrich effect size for each experiment and all subjects. For the Classic Pulfrich effect, 14/15 showed a negative effect size. For Reverse Pulfrich with optical blur 14/15 showed a positive effect size. For Reverse Pulfrich with onscreen blur, all subjects showed a positive effect size. The effect size averaged across subjects is -0.69±0.48ms, 1.41±0.91ms, and 1.17±0.67ms for the Classic Pulfrich, Reverse Pulfrich effect with optical blur, and Reverse Pulfrich effect with onscreen blur, respectively. There is a statistical difference between the Classic Pulfrich effect and the Reverse Pulfrich effect with optical and onscreen blur (paired t-test p<.05 in both comparisons) and there is no statistical difference comparing the Reverse Pulfrich effect with optical and onscreen blur (p>.05).

Figure 12.4B shows the Just Noticeable Difference (JND) for each experiment and all subjects. The average JND across subjects is 1.08±1.09ms, 2.08±2.03ms, and 1.85±1.88ms for the Classic Pulfrich effect, Reverse Pulfrich effect with optical blur, and Reverse Pulfrich effect with onscreen blur, respectively. Paired t-tests show statistically significant differences between Classic Pulfrich and both versions of the Reverse Pulfrich effect (p<.05 in both comparisons), but non-significant differences in JND between the Reverse Pulfrich with optical blur and with onscreen blur (p>.05).

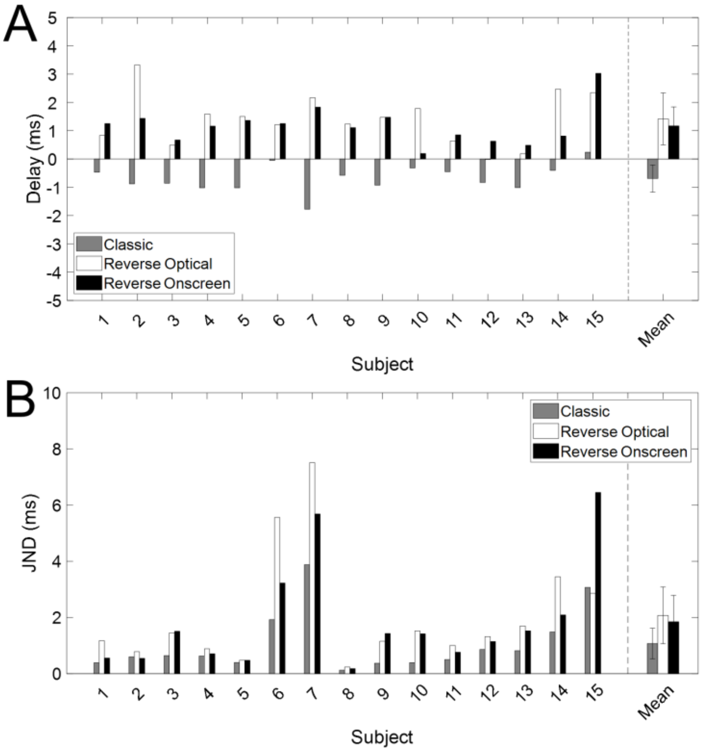

Figure 12.4. Pulfrich effect sizes for each subject. In gray, Classic Pulfrich effect, in white, Reverse Pulfrich effect with optical blur, and in black, Reverse Pulfrich effect with onscreen blur. The average across subjects is shown in a subplot at the right. **A.** Pulfrich effect sizes. **B.** Just Noticeable Difference (JND).

Correlation plots between Classic Pulfrich, Reverse Pulfrich with optical blur, and Reverse Pulfrich with onscreen blur are shown in Figure 12.5. The correlation coefficients are low and not significant, except for Figure 12.5C (r=.49 and p<.05).

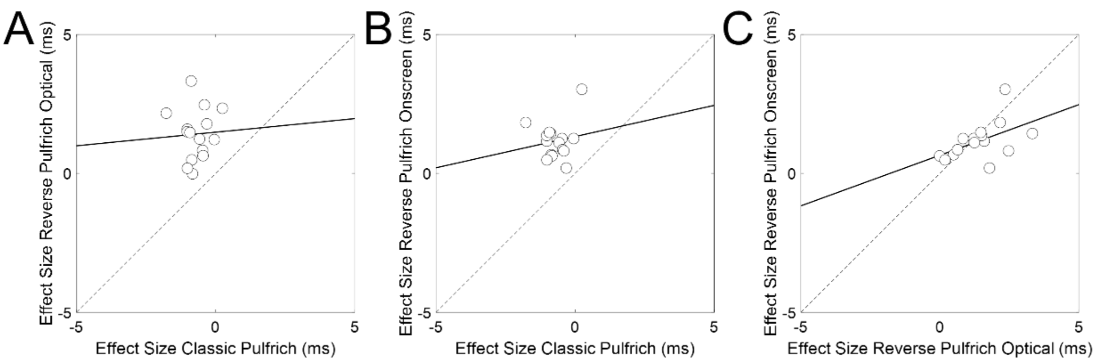

Figure 12.5. Correlation among experiments. **A.** Correlation between Reverse Pulfrich effect size with optical blur and Classic Pulfrich effect size. **B.** Correlation between Reverse Pulfrich effect size with onscreen blur and Classic Pulfrich effect size. **C.** Correlation between Reverse Pulfrich effect size with onscreen blur and Reverse Pulfrich effect size with optical blur.

Although the effect sizes are considerable for most of the subjects and experiments, the impact on perception is also affected by JND. Dividing the PSE by the Just Noticeable Difference (JND) is an accepted indicator of the actual impact of the illusion on the perception. If the PSE/JND metric is higher than one, the illusion caused by different versions of the Pulfrich effect is noticeable. Figure 12.6 shows this metric for all experiments and subjects. The PSE/JND averaged across subjects is 1.32±1.16, 1.37±1.57, and 1.37±1.58 for the Classic Pulfrich, Reverse Pulfrich effect with optical, Reverse Pulfrich effect with onscreen blur, respectively. For the three experiments, the average PSE/JND is above one. However, only 8/15 subjects reported results above one for the Classic Pulfrich effect, 6/15 for the Reverse Pulfrich effect with optical blur, and 7/15 for the Reverse Pulfrich effect with onscreen blur. Besides, only 5/15 subjects report results above one for the three experiments. Paired t-test showed no statistical difference between the PSE/JND metric (p>.05 in all comparisons).

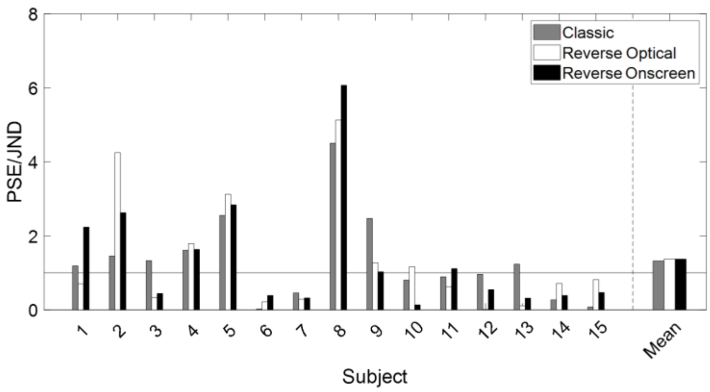

Figure 12.6. PSE vs. JND for all subjects and experiments. Also, the average across subjects is shown at the left of the plot. In gray, Classic Pulfrich effect, in white, Reverse Pulfrich effect with optical blur, and in black, Reverse Pulfrich effect with onscreen blur.

12.4. Discussion

Prevalence of the Pulfrich effect

This study provides for the first time an estimation of the prevalence of the Classic and Reverse Pulfrich effect in a young population. This study reveals that most of the subjects showed the Classic and Reverse Pulfrich effect (93% for Classic and Reverse with optical blur and 100% for Reverse with onscreen blur), all of them with the expected trend: dimming one eye delays the processing speed of one eye and blurring one eye advances the processing speed.

However, the just noticeable difference (JND) determines the perception of the optical illusion. The JND averaged across subjects is significantly lower for Classic Pulfrich than for Reverse Pulfrich (both optically and onscreen). This result suggests that dimming one eye does not affect binocular vision as much as blurring one eye does, in agreement with results already reported in the literature for blur [399] and luminance [388].

Furthermore, the PSE/JND metric reveals that only a few subjects were able to perceive a considerable optical illusion. Only 53% of the subjects, 40%, and 47% were above the limit to perceive a considerable optical illusion (PSE/JND>1) for Classic Pulfrich, Reverse Pulfrich with optical blur, and Reverse Pulfrich with onscreen blur. These results suggest that the optical illusion elicited by different versions of the Pulfrich effect might not have a strong impact on the perception of the population. However, the sample size is still relatively small and should be increased to yield conclusions about the prevalence of the different versions of the Pulfrich effect and its impact. Moreover, other age groups such as presbyopes -who can have a residual cataract or wear monovision and other presbyopia corrections- could be more affected and suffer more from the Reverse Pulfrich effect.

Clinical relevance
This study carried out an important technological advance in the study of Pulfrich effects. We have demonstrated the use of a portable autostereoscopic device (the combination of a tablet and a lenticular lens sheet) to measure different versions of the Reverse Pulfrich effect. Besides, the use of a new covering more retinal region and the use of a new paradigm with a moving stimulus with a constant speed movement instead of sinusoidal movement (like in Chapters 8,9, and 10) have facilitated the task, even for naïve subjects. Although full control of the screen would be needed to decrease measurement time and validation in a higher sample size, this technological advance shown in this study is promising for allowing fast and reliable measurements of the Pulfrich effect.

The Pulfrich effect is not very common in clinical practice, and it usually appears as a spontaneous Pulfrich effect. However, it has been reported to be relevant in some pathologies such as cataracts[214–216], laser surgery[214], optic neuritis[212,400,401], and multiple sclerosis[212,400], among others[217]. In Chapter 10, we also reported the presence of spontaneous Pulfrich effect due to monovision after a cataract procedure. The measurement of the Pulfrich effect in the clinic has not evolved much and clinicians carry out tests from the most traditional methods (based on positioning markers and using a pendulum)[402] to a digitally-generated pendulum on a computer[403]. None of them has been established as a gold standard[217]. In this chapter, we present a portable device that can potentially fill the gap and provide fast and accurate measurements of the spontaneous Pulfrich effect in clinic.

12.5. Conclusions

In this chapter, we have provided a first estimation of the prevalence of the Classic and Reverse Pulfrich effects in a young population. Most subjects showed both effects, and with the expected trend. Besides, we have described the development of a portable autostereoscopic tablet to allow measurements of the different versions of the Pulfrich effect, with the potential to approach standard clinical practice.

Chapter 13. Exploration of new technologies to improve binocular vision evaluation

This chapter describes the development of a fast stereoacuity test to be used in combination with Simvis Gekko in clinical sites, based on random dots and a four alternatives forced-choice task. The stereoacuity test was evaluated at different distances (far at 4m and near at 0.4m) and using different methods to create depth (anaglyph, polarizers, parallax barrier -only in near distance-).

Once a sufficient sample of subjects will be measured, this chapter will be the base for an article entitled '*Evaluation of stereoacuity for different distances using SimVis Gekko*" where Victor Rodriguez-Lopez is the first author. The co-authors of the study are Xoana Barcala, Irene Sisó, Alberto de Castro, Nora El Harchaoui, and Carlos Dorronsoro.

The contribution of the author of the thesis was the design of the stimuli in collaboration with Alberto de Castro and Carlos Dorronsoro, the conceptualization and design of the study in collaboration with Xoana Barcala and Irene Siso, the literature research, the design and programming of the experiments, the collection of the data in collaboration with Nora El Harchaoui, the analysis of the data, the writing of the chapter, and the editing of the chapter in collaboration with Carlos Dorronsoro.

13.1. Introduction

Some presbyopia corrections such as multifocal or monovision can potentially harm binocular vision, as previous chapters have shown with the Reverse Pulfrich effect. Besides, it has been reported that monovision and other presbyopia corrections increase stereoacuity thresholds[98,99].

The main use of SimVis Gekko is letting the patient test presbyopia corrections before prescribing them, something especially important in surgery-related corrections (intraocular lenses and monovision). The accuracy of the simulation provided by SimVis Gekko in terms of optical quality has been validated using through-focus visual acuity, perceptual scoring methods, or questionnaires[229,269,295]. However, to fully predict the behavior of different presbyopia corrections, binocular vision and stereoacuity should be part of that visual evaluation.

SimVis Gekko is binocular and see-through, and therefore stereoacuity measurements can be performed straightforwardly. However, those measurements had not been validated, until this study. The validation is important since SimVis Gekko projects optotunable lenses onto the eye using a different optical projection system for each eye. The superimposition of visual fields is different for each distance, potentially affecting binocular vision in far vision, near vision, or both.

During this thesis, important know-how has been gathered on designing binocular vision tests and using and programming SimVis Gekko for research purposes. This know-how has allowed us to tackle the validation of binocular measurements and stereoacuity through SimVis Gekko.

Stereoacuity measures the discrimination threshold of depth. Different methods have been developed to measure stereoacuity, for example using physical depth, or creating disparity using filters (anaglyph, polarizer). For physical depth, the Frisby test is the most used. Some tests that use polarizer filters are the Titmus or Randot tests, which are the most extended in clinical practice. The most common commercial test that uses anaglyph filters is the TNO test, which uses red/green filters. Interestingly, a poor agreement has been reported across the different methods[48].

Some novel technologies aimed at eliminating the use of filters to create stereoacuity are the so-called autostereoscopic technologies. These technologies present a different image to each eye (alternating pixel rows) mainly by using lenticular lenses or parallax barriers. The working principle of these methods is described in section 1.4.2.2. Their main advantage is that they don’t need glasses to create 3D perception. Oriented to clinical measurements, new methodologies to estimate stereoacuity have arisen from autostereoscopic technologies. ASTEROID is a gamified application to estimate stereoacuity using a parallax barrier tablet[200,404]. Lang stereo test[196] and BEST[198] test use lenticular lenses approach to estimate stereoacuity.

This chapter shows the development and validation of a new method for estimating stereoacuity using an adaptive procedure and compares one of the clinical gold standards, the Titmus test, with different methods to create 3D perception (anaglyph, polarizers, and parallax barrier), for different distances (far and near vision), and using different devices (Trial Frame and SimVis Gekko). Additionally, we also evaluated, using SimVis Gekko, the impact of monovision corrections on stereoacuity.

13.2. Methods

13.2.1. Subjects

Five subjects (26±2.3 years old on average) participated in the study. All of them had normal color vision and no history of eye surgery or eye disease. The spherical equivalent component of the refractive error was tested with standard optometric techniques and ranged between -7.50 and +1.75D (-3.05±3.21D on average), and the cylindrical component between 0 and 1.75D (-0.72±0.56D). The study followed the tenets of the Declaration of Helsinki. Study protocols were approved by the CSIC Institutional Review Board. Subjects signed a consent form after receiving an explanation of the nature and possible consequences of the study.

13.2.2. Stimulus

Figure 13.1 shows the stimulus designed for this study. The stimulus was a large square subtending 5.5x5.5º, divided into 4 medium squares 2.5x2.5º each, made of randomly distributed white square dots of 0.075x0.075º over a gray background. The center of each medium square was displaced 1.5x1.5º from the center of the large square, which was centered with the screen.

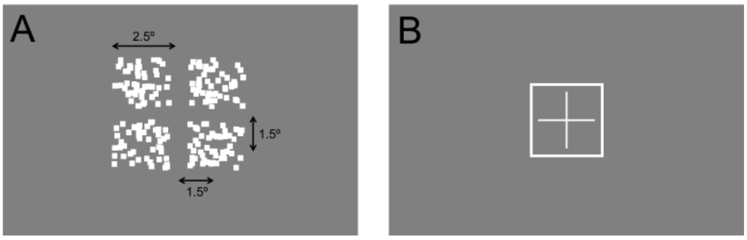

Figure 13.1. Stimulus used in the experiment. A. Stimulus. Disparity is randomly assigned to one of the squares. **B.** Fixation cross for alignment purposes. The central cross has 300'' of crossed disparity and the white square is plane on the screen and serves as a reference.

13.2.3. Apparatus

Two different systems were used and directly compared, to induce different corrections (far vision, near vision, and, monovision; described in the next section) while measuring stereoacuity: the traditional trial frame and SimVis Gekko. Already described in section 2.1.1 of this thesis, SimVis Gekko is a binocular device able to induce programmable optical power variations with an optotunable lens (Optotune Inc, Dietikon, Switzerland) in each eye channel. The refractive error of the subject was corrected with trial lenses in both systems.

Custom software was written in MATLAB (Math-works Inc., Natick, MA, USA) to control the optical power induced independently in the right and left SimVis Gekko channels. The Psychophysical Toolbox for MATLAB[241] was used for stimuli creation and presentation, and response collection.

Stimuli for far and near vision were displayed on the Stereoscopic Monitor (SM, see section 2.2.2, of the General Methodology), a stereo-3D UK UHD 49" monitor (LG49UH850V, LG, Seoul, South Korea), driven by an NVIDIA® Quadro® P4000 dual Graphic card. In the anaglyph experiment (described later), all the resolution of the monitor was used. In the polarizers experiment, after filtering with the glasses, only 3840x1080 interlaced pixels reached each eye. For the experiments at far vision, the subject viewed the display at 2 meters, and, for near, vision at 40 cm.

Another setup based on parallax barrier technology (PBII setup, see section 2.2.3.3) was also used to evaluate stereoacuity at near distance: a prototype tablet display by See3D 10.1'' (See3D Tablet Corporation, Toronto, Canada), driven by the same graphic card. A custom setup for holding the tablet in front of the subject was designed and 3D-printed. Pilot experiments were performed with the setup PBI (Commander 3D) before obtaining the updated parallax barrier tablet (See 3D).

13.2.4. Experiments

To obtain the stereoacuity, we used a QUEST Bayesian adaptive procedure[228] implemented in a four-alternative forced-choice (4AFC) task over 30 trials. In each trial, only one of the medium squares of the stimulus had crossed disparity, that was randomly assigned. The task of the observer was to indicate which of the 4 squares is perceived in front of the screen. To create disparity and depth perception, the stimulus for the right eye was displaced some pixels in the horizontal axis. Antialiasing sub-pixel technique based on Serrano-Pedraza et al. description[199] allows displaying disparities as low as 3 arc seconds for far distance and 7 arc seconds for near distance.

In this study, we measured 24 different conditions, illustrated in the diagrams of Figure 13.2, each condition taken from the combinations of two possible distances (far and near vision, 2 and 0.4 m, respectively), two devices (Trial Frame and SimVis Gekko), four 3D methods (Titmus test, anaglyph filters, polarizer filters, and parallax barrier), and three optical corrections (both eyes focusing the screen, monovision in one eye, monovision in the other eye).

Of the four methods of creating 3D that were tested in this study, anaglyph filters (using red/green filters) and polarizer filters were used for both far and near vision, and conventional Titmus and parallax barrier were used only for near vision.

Four different corrections were tested. Each correction was named with the value of the optical power difference between the right eye and the left eye. For far vision, far correction (FF, both eyes focused on far vision, correction 0.00D) was evaluated using Trial Frame and using SimVis Gekko. With SimVis Gekko, monovision of 1.50D in the left eye (ML, left eye focused on near and right eye focused on far vision, correction -1.50D) and monovision of 1.50D in the right eye (MR, left eye focused on far and right eye focused on near vision, correction 1.50D) were also tested. For near vision, near correction (NN, both eyes focused on far vision, correction 0.00D, equivalent to FF but in near vision) was evaluated using trial lenses in the Trial Frame and using SimVis Gekko. SimVis Gekko was also used in near vision to test monovision of 1.50D in the left eye and the right eye (corrections -1.50D and 1.50D, respectively). To avoid accommodation issues and to compensate for the optical distance to the monitor, an extra 0.50D was added to the optical correction in both eyes for far vision, and an extra 2.50D to the optical correction in near vision. With SimVis Gekko, the extra power was added using the tunable lenses, and Trial Frame using trial lenses.

The head of the subject was stabilized with a chin rest, that aligned the eyes with the center of the monitor. Before beginning each measurement, the experimenter made sure that the Trial Frame or the SimVis Gekko were perfectly aligned with the visual axis of the subject. Before beginning each condition, a white cross with 300'' arc sec of crossed disparity inside a white frame without disparity (served as a reference, Figure 13.1B) was displayed to check that the optical axis of the eyes and both optical systems (Trial Frame and SimVis Gekko) were properly aligned. If the subject did not or barely perceived depth in the cross, the experiment was interrupted, and the alignment procedure was performed again.

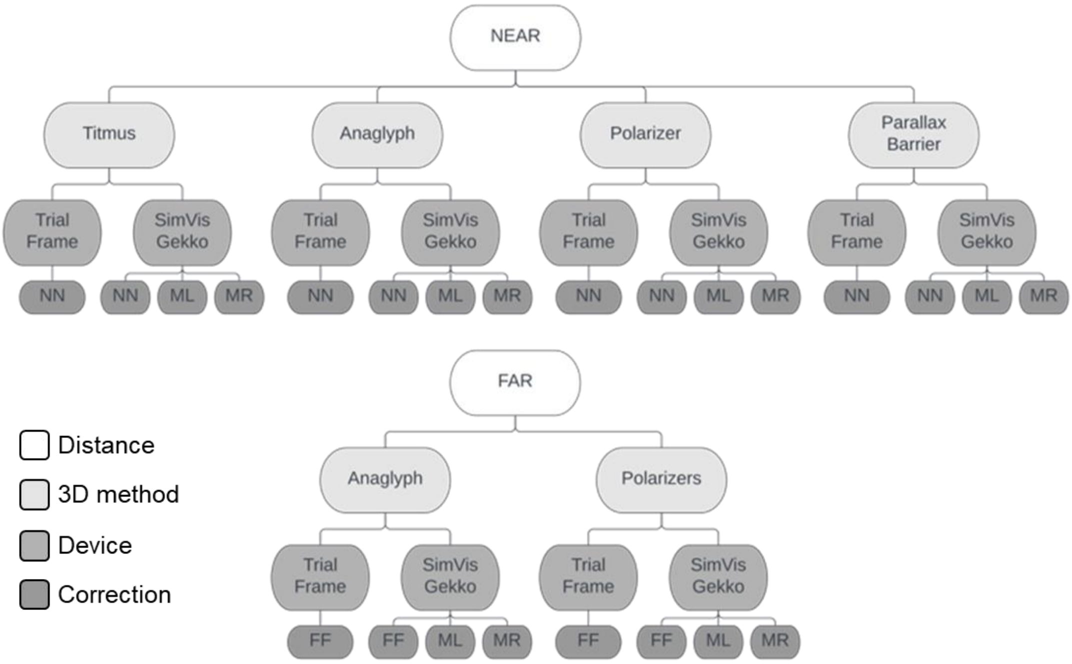

Figure 13.2. Conditions measured in the study. FF means far correction (both eyes focused on far vision), NN means near correction (both eyes focused on near vision), ML means monovision in the left eye (left eye focused on near vision and right eye focused on far vision), and MR monovision in the right eye (left eye focused on near vision and right eye focused on far vision).

13.2.5. Statistical analysis

Kruskal-Wallis test for non-parametric variables was performed to analyze differences between conditions (distances, 3D method, device, and corrections). Wilcoxon signed-rank test was used to compare the results for each condition individually. The difference is considered significant if $p<.05$.

13.3. Results

As an example of a particular measurement for the adaptive psychophysical method, Figure 13.3 shows the result for subject S1 for anaglyph filters using SimVis Gekko for far vision, for three corrections: far correction (FF, black), monovision in the left eye (ML, blue), and monovision in the right eye (MR, red). Figure 13.3A displays the evolution of each QUEST staircase for each condition. Each staircase results in a threshold (i.e., the stereoacuity of the subject for the particular condition), illustrated in Figure 13.3A as the final point of each QUEST curve. Figure 13.3B gathers the final stereoacuity estimations across the conditions shown in Figure 13.3A. For this subject, the stereoacuity for FF is 7.2'', ML is 11.2'', and MR is 17.0''. Stereoacuity slightly increases with monovision, although the change is negligible.

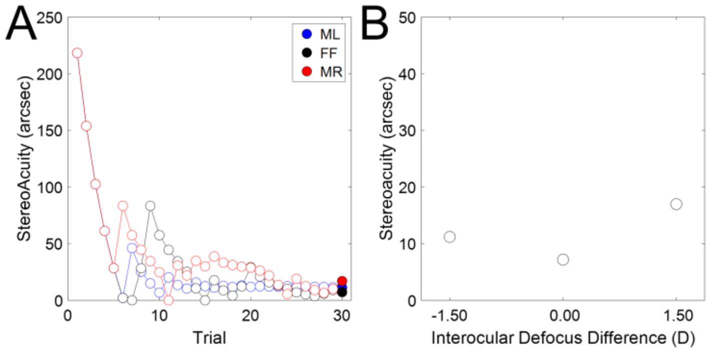

Figure 13.3. Result for one subject (S1) for anaglyph filters using SimVis Gekko in far vision. Black data represents the FF condition, blue data ML condition, and red data MR condition. **A.** Progress along trials of the QUEST procedure for each condition. Endpoints represent the threshold (i.e., stereoacuity). **B.** Stereoacuity (in arc seconds) as a function of interocular defocus difference (in D).

Figure 13.4 shows the result obtained with the Titmus test for all subjects. Figure 13.4A shows the result for Trial Frame and Figure 13.4B for SimVis. On average across subjects, stereoacuity for NN (black bars in Figure 13.4) is 25±8.7'' and 27.4±8.6'' for Trial Frame and SimVis, respectively, for ML (blue bars in Figure 13.4) and MR (red bars in Figure 13.4) with SimVis is 29.8±7.6'' and 34.4±8.8'', respectively.

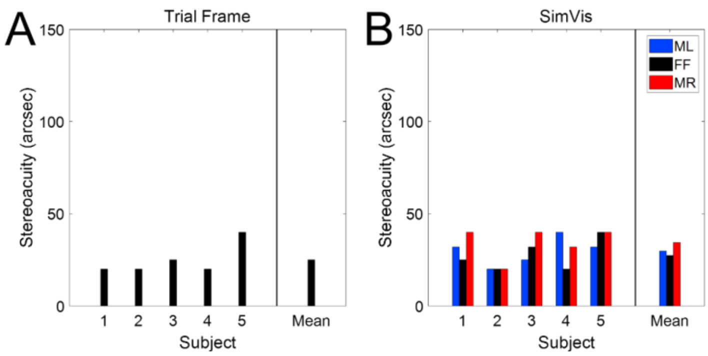

Figure 13.4. Stereoacuity measured with the Titmus test in far vision for all subjects. A subplot to the right shows the average across subjects. Black bars represent NN condition, blue bars ML condition, and red bar MR condition. **A.** Using Trial Frame. **B.** Using SimVis Gekko.

Figure 13.5 shows the result obtained with anaglyph filters in near vision for all subjects. Figure 13.5A shows the result for Trial Frame and Figure 13.5B for SimVis. On average across subjects, stereoacuity for NN is 55.3±25.3'' and 69.1±39.6'' for Trial Frame and SimVis, respectively, for ML and MR with SimVis is 47±9.8'' and 65.3±37.7'', respectively.

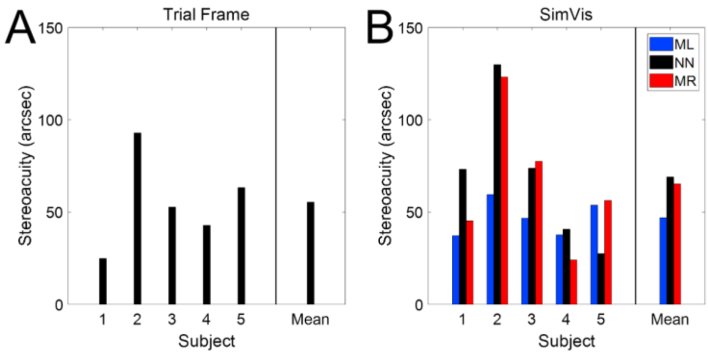

Figure 13.5. Stereoacuity measured with anaglyph filters in near vision for all subjects. A subplot to the right shows the average across subjects. Black bars represent NN condition, blue bars ML condition, and red bar MR condition. **A.** Using Trial Frame. **B.** Using SimVis Gekko.

Figure 13.6 shows the result obtained with polarizer filters in near vision for all subjects. Figure 13.6A shows the result for Trial Frame and Figure 13.6B for SimVis. On average across subjects, stereoacuity for NN is 24.2±14.1'' and 22.4±5.7'' for Trial Frame and SimVis, respectively, for ML and MR with SimVis is 19.8±7.1'' and 22.7±12'', respectively.

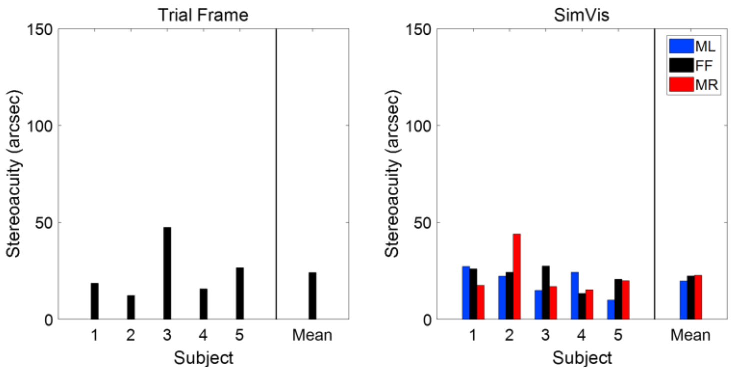

Figure 13.6. Stereoacuity measured with polarizer filters in near vision for all subjects. A subplot to the right shows the average across subjects. Black bars represent NN condition, blue bars ML condition, and red bar MR condition. **A.** Using Trial Frame. **B.** Using SimVis Gekko.

Figure 13.7 shows the result obtained with parallax barrier in near vision for all subjects. Figure 13.7A shows the result for Trial Frame and Figure 13.7B for SimVis. On average across subjects, stereoacuity for NN is 20.8±12.6'' and 12.9±4.5'' for Trial Frame and SimVis, respectively, for ML and MR with SimVis is 30.0±24.3'' and 44.6±38.5'', respectively.

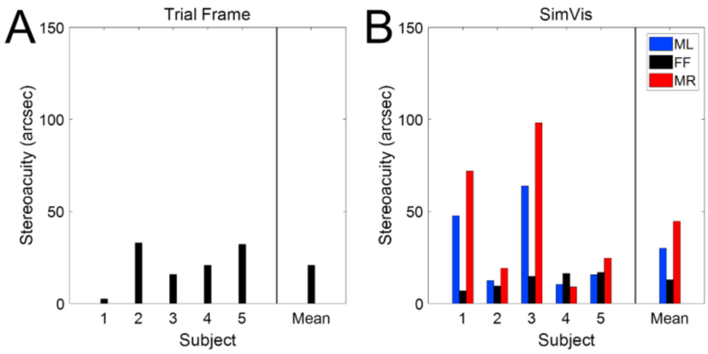

Figure 13.7. Stereoacuity measured with parallax barrier in near vision for all subjects. A subplot to the right shows the average across subjects. Black bars represent NN condition, blue bars ML condition, and red bar MR condition. **A.** Using Trial Frame. **B.** Using SimVis Gekko.

Figure 13.8 shows the result obtained with anaglyph filters in far vision for all subjects. Figure 13.8A shows the result for Trial Frame and Figure 13.8B for SimVis. On average across subjects, stereoacuity for FF (black bars in Figure 13.8) is 36.1±19.8'' and 26.3±9.2'' for Trial Frame and SimVis, respectively, for ML and MR with SimVis is 35.5±15.5'' and 41.7±14.4'', respectively.

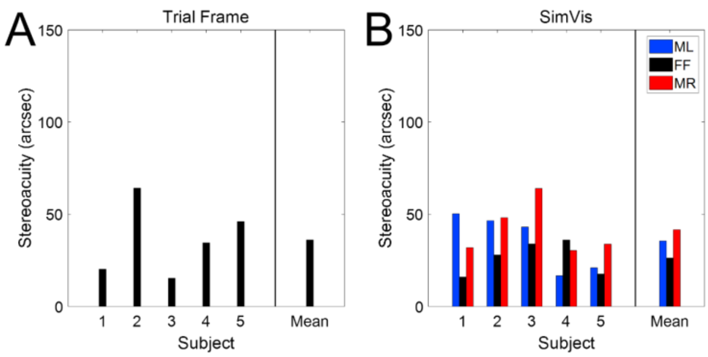

Figure 13.8. Stereoacuity measured with anaglyph filters in far vision for all subjects. A subplot to the right shows the average across subjects. Black bars represent FF condition, blue bars ML condition, and red bar MR condition. **A.** Using trial frame. **B.** Using SimVis Gekko.

Figure 13.9 shows the result obtained with polarizer filters in far vision for all subjects. Figure 13.9A shows the result for Trial Frame and Figure 13.9B for SimVis. On average across subjects, stereoacuity for FF is 16.0±6.5'' and 17.5±8.2'' for Trial Frame and SimVis, respectively, for ML and MR with SimVis is 11.8±4.9'' and 25.8±16.3'', respectively.

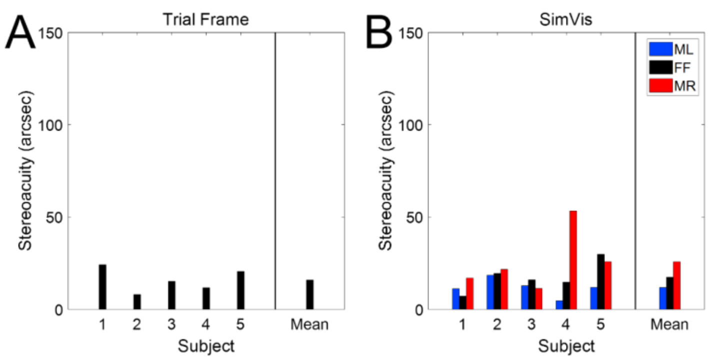

Figure 13.9. Stereoacuity measured with polarizer filters in far vision for all subjects. A subplot to the right shows the average across subjects. Black bars represent FF condition, blue bars ML condition, and red bar MR condition. **A.** Using trial frame. **B.** Using SimVis Gekko.

Summary of the results

Figure 13.10 shows the average stereoacuity across subjects for all corrections, 3D methods, devices, and distances. Figure 13.10A shows the results for Trial frame (FF and NN conditions in black) and Figure 13.10B for SimVis (FF and NN, ML, and MR conditions in black, blue, and red, respectively).

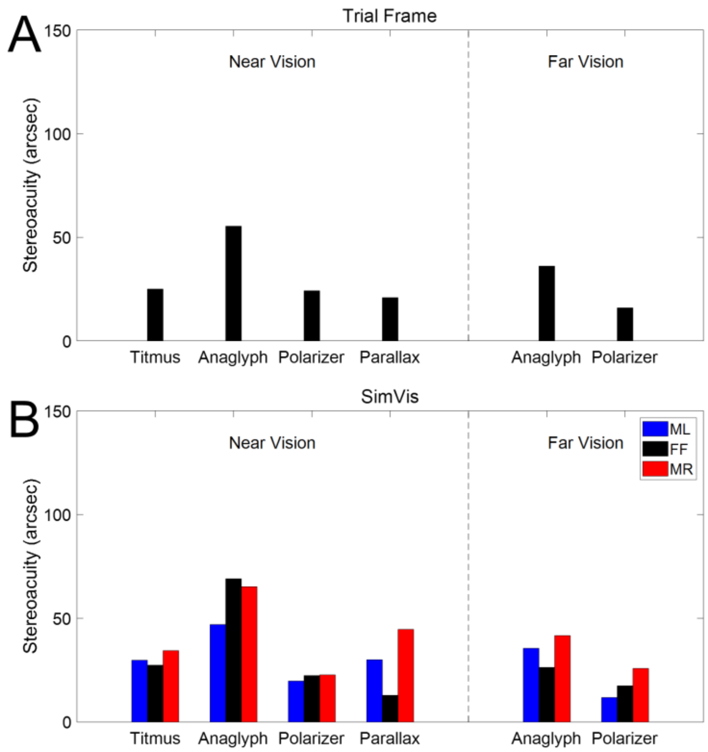

Figure 13.10. Summary of the experimental data. Stereoacuity averaged across subjects for all conditions. Black bars represent FF correction (in far vision) and NN correction (in near vision), blue bars ML correction, and red bars MR correction. **A.** Trial Frame results. **B.** SimVis Gekko results.

In this study, all 4 variables are categorical: distance (far vs. near), device (trial frame vs. SimVis Gekko), 3D method (anaglyph filters, polarizer filters, parallax barrier, and Titmus test), and correction (FF, ML, and MR). A Kruskal-Wallis test reports non-significant differences (p>0.05) for the device (Trial Frame vs. SimVis), in 3D methods for parallax barrier compared both with Titmus and polarizer filters and in corrections for FF compared with ML. For the rest of the conditions, there are statistical differences (p<0.05).

Figure 13.11 shows Bland-Altman plots comparing distance, device, and Titmus vs the other 3D methods. The mean difference in stereopsis obtained when comparing near vs far vision (Figure 13.11A) was -14.39±24.04'' (Limits of Agreement (LOAs): [-61.51 to 32.74]''), indicating a better stereoacuity (lower magnitude) in far vision than in near vision, that is statistically significant (Wilcoxon signed-rank test *p*<.05). The mean difference in stereopsis obtained when comparing Trial Frame vs. SimVis Gekko (Figure 13.11B) was 0.31±18.54'' (LOAs: [-36.03 to 36.65]''), indicating essentially the same stereopsis with both devices (Wilcoxon signed-rank test *p*>.05). The mean difference in stereopsis obtained comparing Titmus with anaglyph filters, polarizer filters, and parallax barrier (Figure 13.11C) are -30.01±33.13'' (LOAs: [-94.94 to 34.92]''), 6.88±13.43'' (LOAs: [-19.44 to 33.20]''), and -2.05±22.88'' (LOAs: [-42.80 to 46.90]''), respectively, reporting significant differences for Titmus vs anaglyph filters and polarizer filters (Wilcoxon signed-rank test *p*<.05), but non-significant for Titmus vs parallax barrier (Wilcoxon signed-rank test *p*>.05).

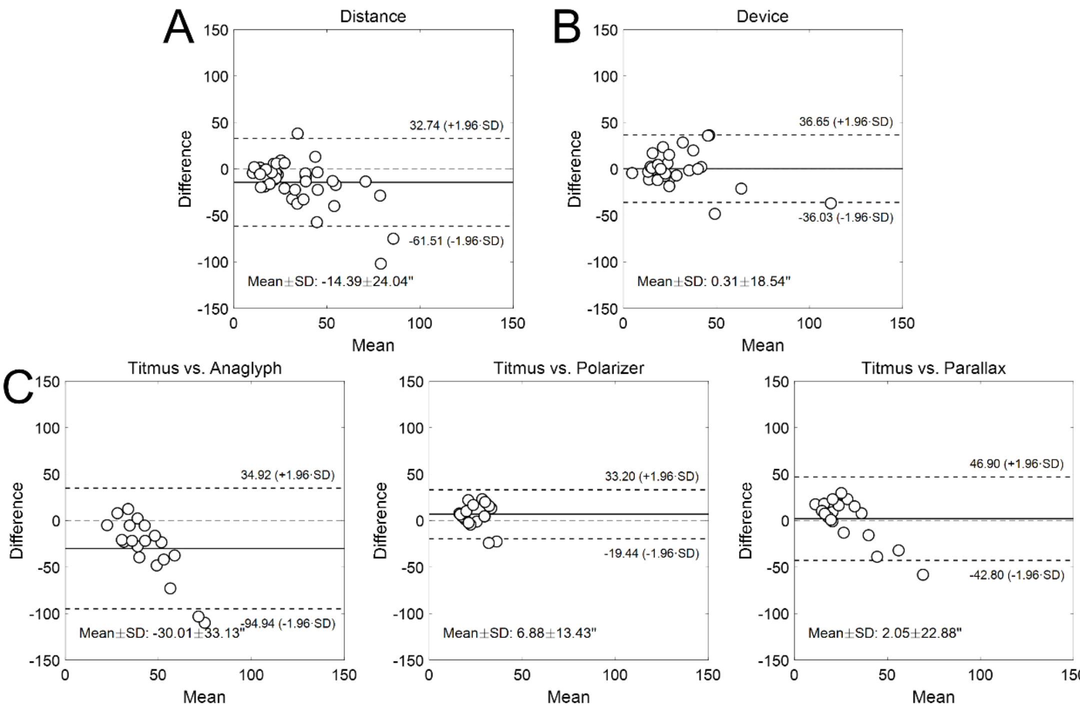

Figure 13.11. Bland-Altman analysis for different conditions. Each panel shows a Bland-Altman plot, indicating the Limits of Agreement (LOAs, 95% Confidence Interval), mean, and standard deviation of the sample. **A.** Plot comparing near and far distances for all corrections, devices, and 3D methods. **B.** Plot comparing Trial Frame and SimVis Gekko for all distances and 3D methods. **C.** Plot comparing Titmus test vs. other 3D methods in near distance for all devices and corrections. Titmus and anaglyph filters in the left plot, Titmus and polarizer filters in the middle plot, and Titmus and parallax barrier in the right plot.

13.4. Discussion

SimVis Gekko for measuring stereopsis

In clinical practice, stereoacuity with conventional tests (considering Titmus test the gold standard in this study) is routinely measured using trial lenses in a trial frame. The results of this study report non-significant differences between measuring the Titmus test using Trial Frame or SimVis Gekko. Moreover, not only for the conventional Titmus test but also across all conditions (different 3D methods and distances) there were no statistical differences. These results demonstrate that the projection of the pupils of the eyes and the convergence of both eye channels taking place in SimVis Gekko do not influence the measurement of stereoacuity and therefore measurements through this device are possible and accurate. However, higher sample size must be evaluated before drawing further conclusions.

Adaptive method and 3D tablet

In this study, we have developed a test to measured stereoacuity using an adaptive psychophysical method, which allowed us to find the threshold with high precision by adapting the disparity displayed at each step, based on the previous responses of the subject. Instead, conventional clinical tests use the psychophysical method of limits to find the threshold by testing every fixed step of disparity of the test. The main limitation of conventional tests is the use of fixed steps, that may not precisely capture the actual threshold and can induce a learning effect[177,405]. Moreover, if testing many corrections, the fixed steps of the Titmus can induce a learning effect that might falsify the stereoacuity measurement. The random nature of the adaptive method eliminates any learning effect. We have demonstrated the possibility to measure stereoacuity using adaptive methods, as other studies have carried out [200,406].

Additionally, we have measured stereoacuity using a novel 3D autostereoscopic display based on parallax barrier technology, providing similar results to the gold standard of this study, the Titmus test, which uses polarizer filters. Parallax barrier technologies have previously been used to measure stereoacuity. ASTEROID stereoacuity test uses moving stimuli instead of static stimuli. It has already been tested in the clinic with promising results in adult[200,230,404] and pediatric[201] populations.

The combination of the adaptive procedure, the new parallax barrier tablet, and SimVis Gekko has the potential to provide fast and reliable measurements of stereoacuity for different optical corrections in a clinical environment. However, further validation and development of this synergic combination need to be addressed.

Influence of the 3D method

At least for the sample size measured in this study, stereoacuity depends on the method for producing 3D. The stereoacuity found with anaglyph filters is worse than for the other methods and reports statistical differences among them. Other studies found similar results comparing the most extended anaglyph-based test (TNO) with other commercial tests, reporting worse values of stereopsis with the TNO but non-significant differences[407–410]. The fact that we found statistical differences might be due to the small sample size. Although most of the subjects subjectively found it more difficult to carry out the anaglyph test, which might account for the worse stereoacuity measured, this result should be confirmed in a higher sample size.

Influence of the distance

The distance was another variable in this study. We measured stereoacuity using anaglyph and polarizer filters at far distance (optical infinity) and near distance (40 cm). We report non-significant differences between the results at far and at near distances, suggesting that distance does not influence stereoacuity. Other studies have also reported non-significant differences in testing in near and far vision[181,182,184], in agreement with the results of this study, for both Trial Frame and SimVis.

Influence of the optical correction

Additionally, we measured stereoacuity for different optical corrections: both eyes focused (FF correction and NN correction, at far and near distance, respectively), monovision in the left eye (more optical power in the right eye, ML), and monovision in the right eye (more optical power in the right eye, MR). We did not find statistical differences across corrections. In contrast, it has been reported in the literature that monovision corrections harm stereovision and therefore stereoacuity[98,99]. We did not find in our study this reduction with monovision, and the reason might be in the age of the sample size. Our observers were still young (26 years old on average) and with intact accommodation capacity. Further studies must include a presbyopic population.

13.5. Conclusions

There are many different corrections for presbyopia in the market, and the selection of the optimal correction is difficult for the patients. SimVis Gekko has already been used to help in this selection, replicating the through-focus optical quality of existing lens models. In this chapter of the thesis, we have expanded the use of SimVis Gekko to the measurement of stereoacuity, the most important feature of binocular vision, with different methods, and we have validated their accuracy against a standard clinical test. Besides, we have developed a new stereoacuity test using an adaptive psychophysical method in a parallax barrier tablet. Their combination can potentially help clinicians to also perform fast and reliable measurements of stereoacuity, providing a more complete description of the visual function of their patients with different optical corrections.

Chapter 14. Ongoing research

During this thesis, we have developed the proof of concept for new methods and new research lines, that are in all cases complementary to the research activities described in previous chapters and continue the research results obtained. The most promising preliminary results are described here. Although still incipient and non-conclusive, these results are relevant because have the potential to open future research lines and anticipate several future experiments.

14.1. Chromatic temporal defocus sensitivity function

In Chapter 3 we have described the use of tunable lenses to measure for the first time the temporal defocus sensitivity function (TDSF), using grayscale stimuli (Gabor patches and natural images). Chapter 4 describes the Direct Subjective Refraction, a method that takes advantage of the maximum temporal frequency of sensitivity to defocus to create flicker chromatic cues in a blue and red stimulus that can provide the refractive error of an eye. Furthermore, Chapter 6 describes the evolution of the stimulus of the DSR method to a custom display made of pure monochromatic LEDs. That chapter also shows that the DSR task is not easy for many of the subjects, which is probably the most important limitation of the DSR method, and the issue requires more research effort. Considering all those results of this thesis altogether, it seems evident that studying the temporal defocus sensitivity function for chromatic stimuli could provide key knowledge to advance the DSR method and maximize the performance of the patients while performing the task.

Pilot measurements of the chromatic TDSF were carried out using a display of Red LEDs (peak wavelength at 627nm) and a display of Blue LEDs (peak wavelength at 470 nm). The stimulus used was a dot stimulus subtending 1 degree. One experimented subject performed the task with free accommodation. The task was not easier, not more difficult, than with the grayscale stimuli. Figure 14.1 shows the TDSF for the red stimulus (red line) and the TDSF for the blue stimulus (blue line). The influence of the wavelength does not seem to be critical at the medium temporal frequencies of interest, although the graph suggests some deviations at low and high temporal frequencies. Those results should be confirmed and quantified in a higher number of subjects.

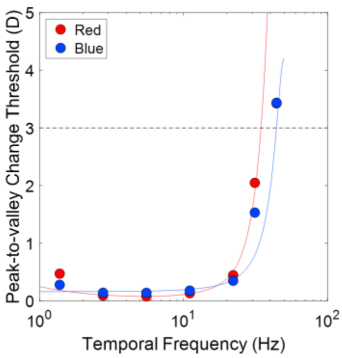

Figure 14.1. Chromatic Temporal Defocus Threshold Function. It shows the peak-to-valley defocus change threshold as a function of the temporal frequency. Dots represent temporal frequencies measured and line the fitting. In red, for a red stimulus, and in blue for a blue stimulus.

14.2. Reverse Pulfrich effect and multifocal contact lenses

The Reverse Pulfrich effect, discovered with monovision, a popular correction for presbyopia, might have a potential impact on the daily life of the patients. The main hypothesis to explain the effect suggests that the high-spatial frequency filtering, producing a reduction in high spatial frequencies in the blurrier image, is responsible for the depth illusion, as described in Chapters 8 to 12. However, monovision is not the only correction for presbyopia. The use of multifocal approaches is increasing, particularly mix and match, modified monovision, or blended vision, all of them placing different corrections in the two eyes, and at least one multifocal correction in one of the eyes. As in pure monovision, combining monovision with multifocality introduces interocular differences in blur. We performed a pilot experiment to evaluate if the Reverse Pulfrich effect also occurs with multifocal lenses of different additions. We measured in one subject the delay produced by placing a multifocal contact lens in one eye while keeping the other eye unperturbed (sharp image). The procedure was the same as used in Chapters 8, 9, and 10. We measured three types of multifocal contact lenses with additions of 1.25D, 1.75D, and 2.50D. After measuring with the multifocal contact lens in one eye, the lens was removed, and we measured with an identical multifocal contact lens in the other eye. Figure 14.2 describes the results. Figure 14.2A shows the psychometric functions and the PSE for each condition indicated in the upper-left corner (negative conditions mean that the multifocal lens was induced in the left eye and positive in the right eye). Positive PSEs mean that the right eye processing speed was advanced with respect to the left eye, and negative PSEs that the left eye processing speed was advanced. In Figure 14.2B, we plotted the PSEs as a function of the condition, distinguishing between the three multifocal designs using different levels of gray. The ratio of delay per diopter of multifocal addition is much higher for 2.50D of addition (0.90ms/D) than for 1.25 and 1.75D (0.22ms/D and 0.16ms/D, respectively), which are essentially the same. This result suggests that the multifocal designs of 1.25D and 1.75D, which induce much less blur than the design of 2.50D, are not inducing relevant depth distortions. However, the design 2.50D is certainly inducing a Reverse Pulfrich effect, of a comparable magnitude that the one obtained with pure monovision in the same subject (see Figure 8.1 in Chapter 8). These pilot results encourage the study of the Reverse Pulfrich effect also in multifocal corrections due to its potential impact on vision and therefore its clinical relevance.

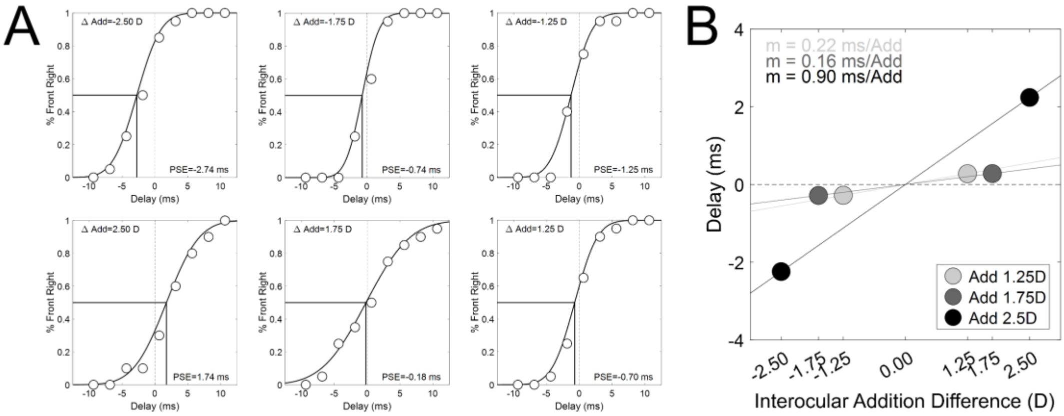

Figure 14.2. Multifocal blur and Reverse Pulfrich effect. **A**. Psychometric function for each condition (from -2.50 to 2.50D interocular addition differences). Left eye perturbed conditions are plotted in the upper row and right eye conditions in the bottom row. **B**. Delay as a function of the interocular addition difference. Data for 1.25, 1.75, and 2.50D of addition is displayed in light gray, dark gray, and black, respectively.

14.3. Reverse Pulfrich effect and pupil dilation

Increasing pupil size also increases the amount of light entering the eye and magnifies the degrading effect of optical aberrations. Regarding the Pulfrich effect, the two components (amount of light and retinal blur) interact in the same direction when the pupil of only one eye dilates. On the one hand, the increased retinal blur also increases the processing speed of the dilated eye. On the other hand, the increased retinal illuminance reduces the processing speed of the dimmer eye (in this case, the non-dilated eye) and effectively increases the processing speed of the dilated eye. Therefore, dilating the pupil should increase the processing for two different reasons. In our pilot experiment, two subjects measured the interocular delay dilating only one eye (the right eye) using cycloplegic drugs. We also dimmed the dilated eye to find the filter needed to compensate for the increase of light produced by the higher pupil size. Figure 14.3 shows the results. For subject S1 (Figure 14.3A), the difference in delay between dilated pupil and normal pupil was 4.82ms, and the filter needed to null the extra delay induced by the dilation was 0.13OD. For subject S2 (Figure 14.3B), the difference in delay was 3.35ms, and the filter needed for nulling the extra delay induced by the dilation was 0.32OD. The extra neural delay caused by pupil dilation cannot be attributed to the additional luminance or the additional retinal blur alone. This condition, easy to induce, provides a framework to investigate the influence of each factor, as each factor can be independently removed, and therefore the other factor isolated. The effect of luminance can be isolated by equalizing the interocular retinal blur (with lenses or even with adaptive optics) and the effect of blur by equalizing the interocular retinal luminance with neutral density filters or with on-screen virtual filters. The use of artificial pupils (in contact lenses or projected onto the eye with SimVis Gekko or with a similar device) provides even more versatility. This line of research can help us understand the role of the different mechanisms involved in the Reverse Pulfrich effect.

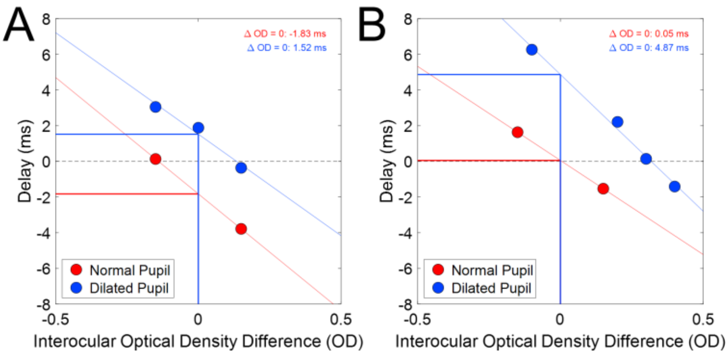

Figure 14.3. Pupil dilation and the Pulfrich effect. Blue data represents the condition with no dilation. Red data represents the condition with the right eye dilated. **A**. Subject 1. **B**. Subject 2.

14.4. Reverse Pulfrich effect and an aberration model

Along the same lines as the previous paragraph, the Reverse Pulfrich effect has been hypothesized to be caused by the filtering of high-spatial frequencies in the image, when the image is degraded by blur. According to that hypothesis, the blurred image is processed faster because the visual system does not need to process all the information contained in those frequencies. The effect of defocus in the image can be predicted from the aberration wavefront with several metrics, described in section 1.2.2. For example, the MTF describes the contrast passing through the optical system. It has been described that metrics such as the Strehl Ratio (SR) or the Visual Strehl Ratio (VSOTF) provide a high correlation with perceptual visual quality. The goal of this study is to develop a model based on aberrations that can predict the Reverse Pulfrich effect of a given interocular condition. This model is based on computing the interocular difference of a given aberration-based metrics (such as SR, VSOTF, or others), for different defocus differences. For example

$$difVSOTF = VSOTF_L(D_L) - VSOTF_R(D_R) \quad 14.1$$

where $difVSOTF$ is interocular difference in Visual Strehl Ration, and $VSOTF_L$ and $VSOTF_R$ are the Visual Strehl Ratios of the right and left eye, and D_L and D_R is the defocus for the right and left eye, respectively. To simulate the Reverse Pulfrich effect, like in monovision corrections, when one eye is defocused (for example, $D_L > 0$), the other eye is focused ($D_R = 0$). Therefore, positive values of $difVSOTF$ mean defocus in the right eye and negative values mean defocus in the left eye. Figure 14.4A shows the process to obtain this metric for VSOTF (Equation 14.1). A similar calculation can be performed for the Strehl Ratio

$$difSR = SR_L(D_L) - SR_R(D_R) \qquad 14.2$$

$difSR$ is the interocular SR difference, and SR_L and SR_R are the SR of the right and left eye, respectively.

The first predictions of the model are shown in Figure 14.4B for the two metrics (VSOTF and SR) and the same subject. Black circles represent the Reverse Pulfrich effect measured, and red circles the prediction with each metric. All the metrics follow a similar trend to predict the Reverse Pulfrich effect and provide similar ratios of 5:1 of the delay in milliseconds to the difSR or difVSOTF, at least for this subject (correlations *r*=.97 and *p*<.05 for both metrics). Both metrics correlate well with the Reverse Pulfrich effect data. This result is not surprising, as VSOTF and SR are the metrics that better predict the perceptual response to blur and degraded optical quality. There are dozens of metrics in the literature that can be tested in future studies, and certainly, a much higher number of patients should be used. Nevertheless, the model proposed could already be used as a first approximation to predict the Reverse Pulfrich effect from the wavefront map.

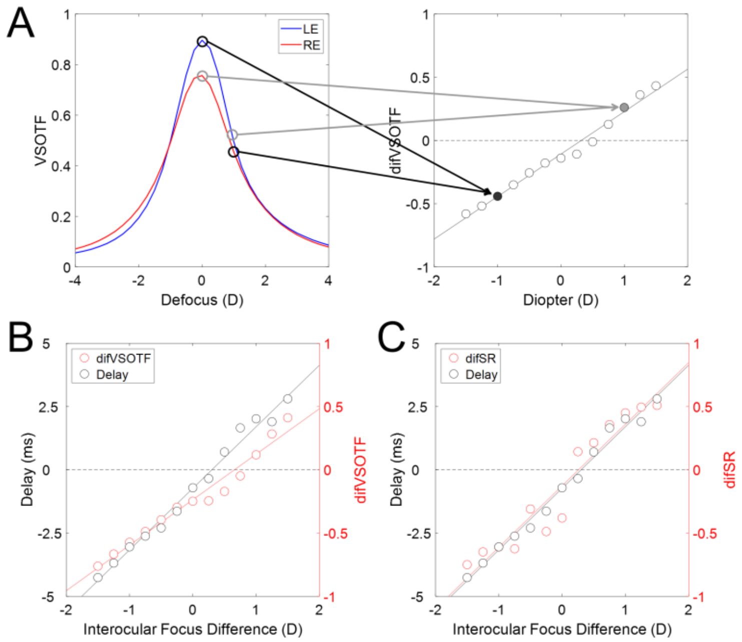

Figure 14.4. Pulfrich effect and aberration model. **A**. Explanation of the obtention of aberration metrics (in this case, difVSOTF metric). **B**. Reverse Pulfrich effect results and aberration metrics (difVSOTF in the left plot, and difSR in the right plot) as a function of the interocular function difference.

14.5. The Pulfrich effect measured in the periphery of the visual field

Within the retina, different types of photoreceptors populate each region. In the central retina, the fovea, cones are much more prevalent than rods. However, when eccentricity increases, the amount of rods increases, and the number of cones decreases (see Figure 1.2). This implies that the visual paths that send to the brain the information reaching the retina differ. In fact, the information collected by rods is faster processed than the information collected by cones (see section 1.2.1). In this experiment, we measured the Classic and Reverse Pulfrich effects by changing the interocular luminance onscreen and by changing the optical blur, respectively, in two different regions of the retina, in the central (fovea, 0º) and the periphery (at 5º of eccentricity).

One subject participated. The procedure followed was the same as the one described in Chapters 8, 9, and 10. For the Classic Pulfrich effect (Figure 14.5A), there is barely any difference in the measurement performed in the fovea or the periphery (slope of linear regression is -13.1 and -11.0 ms/OD for the fovea and the periphery, respectively). However, for the Reverse Pulfrich effect (Figure 14.5B), there is no effect when the blur differences occur in the periphery, compared with the fovea (slope of linear regression is 0.2 and 1.98ms/D, respectively). These results might be explained by the different sampling rates of the two photoreceptors (cones and rods) in the different peripheral regions, and by the different wiring of the ganglion cells in different retinal regions, leading to a very different performance in the processing of highly detailed images with or without blur. Again, addressing measurements in higher sample sizes can provide more insights into the role of the visual pathway in the Pulfrich effect optical illusion.

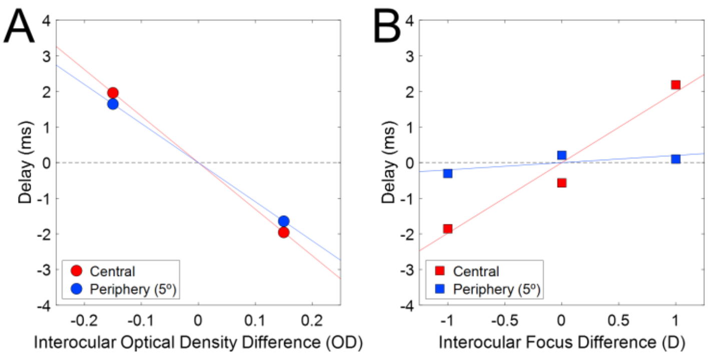

Figure 14.5.Pulfrich effect in the periphery. Red data represents the results in the central retina (fovea) and blue data represents the results in the peripheral retina (5º of eccentricity). **A**. Classic Pulfrich effect. **B**. Reverse Pulfrich effect.

14.6. Chromatic Pulfrich effect

One common and cheap method to generate 3D images is anaglyph 3D, in which a red/green stimulus is filtered with green/red filters. Cyan or blue are often used instead of green. Using anaglyph filters to generate the stereoscopic image seems to be a natural alternative to the measurement of the Pulfrich effect. However, placing one filter in one eye and another filter in the other eye, produces two different effects. On one hand, and according to the human spectral sensitivity function, the visual system is more sensitive to green wavelengths than to red wavelengths. The difference in perceived brightness may produce a Classic Pulfrich effect. On the other hand, due to the longitudinal chromatic aberration of the eye, there is a dioptric difference between green and red wavelengths. This defocus difference between the eyes may produce a Reverse Pulfrich effect. Therefore, the eye with the red filter may suffer theoretically, at the same time, a delay in the processing speed due to less brightness (Classic Pulfrich) and an advance in the processing speed due to more defocus (Reverse Pulfrich). In a pilot study, we measured one subject the Pulfrich effect when placing a green filter in the left eye and a red filter in the right eye and compared it with a grayscale stimulus with polarizer filters. The task was possible. The results displayed in Figure 14.6 show a negative delay (-1.88ms, meaning right eye delayed) in the anaglyph condition compared to the polarizer filters (-0.28ms, negligible delay). This result suggests that the only presence of anaglyph filters produces a meaningful Pulfrich effect. However, we cannot confidently attribute the difference measured to Classic Pulfrich or Reverse Pulfrich. More research is needed to understand the effect of the anaglyph on the Pulfrich effect, and the possibility of compensating for it.

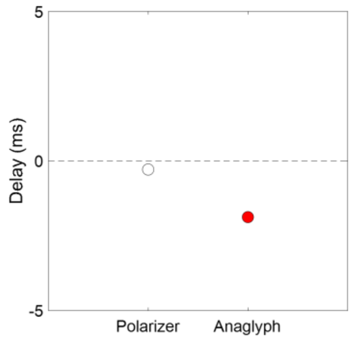

Figure 14.6. Chromatic Pulfrich effect. Delay measured using polarizer filters (white dot) vs. anaglyph filters (red dot).

14.7. Measurement of the Pulfrich effect using portable glasses-free displays

The results of this thesis have shown the influence of monovision corrections or cataracts on the depth perception of moving objects. Therefore, the potential impact of the Pulfrich effect on public safety increases the interest in measuring it in the clinical environment. More measurements of the prevalence of the Pulfrich effect are needed. This entails the measurement of a high number of patients in a clinical environment. Developing an easy and portable tool for measuring the Pulfrich effect may enable it. Years ago, at the beginning of this thesis, we tried to perform these measurements using the Commander 3D autostereoscopic tablet, based on parallax barrier technology (see section 2.2.3.2). However, we found that the temporal resolution of the tablet was not enough for showing fast-moving stimuli, like the ones we used in Chapter 8. We then began a scientific collaboration with the Commander 3D development team, where new requirements and possibilities for the tablet were established. In 2022, the development came to an end the company provided us with a See 3D tablet display prototype, a proof of concept with the specifications needed to tackle Reverse Pulfrich measurements in the clinical environment. New experiments have been programmed for the new display. Preliminary measurements, some of them reported in Chapter 13 (stereoacuity), have demonstrated the enormous potential of this new display for clinical use. The full scientific and clinical potential will be demonstrated in future studies.

In Chapter 12 we have shown the use of an autostereoscopic display based on lenticular lenses to measure the Pulfrich effect. However, both the hardware and the software (an iPad 12.9'' tablet with MPlayer3D application) imposed serious restrictions (especially regarding the temporal rate and the control of the display), limiting the implementation of psychophysical methods and ultimately the scope of the experiments. However, the See3D tablet can be used in the future as a secondary screen of a computer, therefore providing unlimited control in the experiment design. Thus, the paradigm used in the experiment of Chapter 12, which has already provided fast and repeatable measurements of the Pulfrich effect, could be directly applied to an autostereoscopic tablet with very little effort. In a pilot experiment, one subject measured the Pulfrich effect using the See 3D tablet (PBII setup), using the same stimulus, procedure, and task as in Chapter 11. This subject also participated in the experiments of Chapter 11 (using Haploscope system II (HII) and the same psychophysical paradigm -nulling task in a staircase) and in the experiments of Chapter 12 (Lenticular Lens Tablet (LLT) display and a constant stimuli procedure). The results of this subject in terms of the Pulfrich effect and JND measured are essentially the same in the three setups, but the time in each setup is very different (1.5 minutes using the PBII setup and the HII setup vs. 5 minutes of the LLT setup).

Chapter 15. Conclusions

The **main goal** of the thesis, to study blur perception and its potential application to the development of clinical instrumentation for eye care in clinical practice, have been fulfilled, as well as all of the specific goals (section 1.7). Particularly, four main clinical applications have been developed in the field of optometry and ophthalmology by manipulating the perception of the subjects with blur, both in static and dynamic conditions, using regular lenses and optotunable lenses: 1) the Direct Subjective Refraction method using temporal defocus changes, 2) the Eye Dominance Strength (EDS) metric for monovision corrections, 3) the Reverse Pulfrich effect, an optical illusion induced by interocular differences in blur, and 4) the development of the anti-Pulfrich monovision corrections. Besides, two portable devices, based on autostereoscopic techniques, have been developed to measure different features of binocular vision.

The main **accomplishments** of this thesis are:

1. Development of seven setups for measuring different aspects of vision related to blur, from basic features of blur perception to refractive error, eye dominance, and binocular vision.

2. Measurement of the spatiotemporal sensitivity to defocus, providing basic scientific knowledge about human perception (goals 1 and 2).

3. Development of a new method to measure the refractive error of an eye, the Direct Subjective Refraction. Additionally, an evolution from an on-bench setup to a portable device to perform the first measurements in real patients in a clinical environment (goals 3 and 4).

4. Development of a new metric for measuring the strength of eye dominance (goal 5).

5. Discovery of the Reverse Pulfrich effect, a new version of a 100-year-old optical illusion of moving objects in depth, with implications in monovision corrections for presbyopia.

6. Development of an anti-Pulfrich monovision correction, that eliminates the undesirable effect caused by the Reverse Pulfrich effect.

7. Progress on the knowledge of the Pulfrich effect illusion, particularly in the physical sources that elicit the illusion, the presentation of the first clinical case of spontaneous Reverse Pulfrich effect, the influence of overall light level, and the prevalence of the Classic and Reverse Pulfrich effects on a young population.

8. Development of a portable device for measuring stereoacuity using an adaptive psychophysical procedure.

The **main results of the specific conclusions** of the different studies of this thesis are:

1. The use of tunable lenses allows for the description of the spatiotemporal defocus sensitivity function (STDSF), determining the perceptual limits to defocus perception. The STDSF provides a framework for emerging technologies that take advantage of changes in defocus. This result demonstrates hypotheses 1 and 2.

2. The Direct Subjective Refraction (DSR) method to measure the refractive error of an eye was conceived and developed. The DSR method uses a tunable lens to create fast changes in defocus and a bichromatic stimulus to create flicker and chromatic distortions cues, and the task is to minimize said cues. For the spherical equivalent, it has been demonstrated in 25 young volunteers that the DSR method is more repeatable (average standard deviation across subjects: ±0.17D) and faster (average time per repetition: 39 seconds) than the gold standard, the traditional subjective refraction method (SD: 0.28D, time: more than 6 minutes). Besides, the method barely requires any supervision by the clinician and minimizes the impact of the accommodation on the outcome.

3. The DSR method was also demonstrated to be fast and precise in measuring the astigmatism amount of an eye. Pilot measurements in 4 experienced observers showed the suitability of the method for capturing the amount of astigmatism in high agreement with the results of the gold standard.

4. The setup for performing the DSR method evolved into a clinical device that allowed measurements in clinical environments. In fact, the DSR technology was tested in real patients. Although the validation of the technology needs to be addressed in higher sample size and some improvements to the methodology have to be carried out, the initial results show the potential of this technology to evaluate the refractive error fast and accurately. Hypothesis 3 has been demonstrated, although more validation is needed.

5. A metric for estimating the Eye Dominance Strength (EDS) for determining the laterality in monovision corrections was developed and validated in 20 subjects. The use of this new metric can be useful for prescribing more accurate presbyopia corrections. Hypothesis 4 has been validated.

6. The Reverse Pulfrich effect, a motion-in-depth optical illusion elicited by interocular differences in blur, was discovered in this thesis, with potential implications for public safety. A blurry image is processed faster than a sharp image. Moreover, the hypothesis that the Reverse Pulfrich effect is driven due to the high-frequency spatial filtering caused by blur was also confirmed. Hypothesis 5 has been demonstrated.

7. The development of anti-Pulfrich monovision corrections for compensating the potential illusion caused by the Reverse Pulfrich effect was confirmed with contact lenses, the most common delivery system for monovision corrections. Besides, in this thesis, we demonstrated that interocular magnification differences do not elicit any type of Pulfrich effect. Hypotheses 6 and 7 have been demonstrated.

8. A spontaneous Pulfrich effect caused by the Reverse Pulfrich effect was found for the first time in a patient after monocular cataract surgery and a subsequent surgical monovision correction. A process of adaptation to the Reverse Pulfrich effect and the timeframe of the readaptation was also reported. Hypothesis 8 has been demonstrated.

9. The influence of overall light level in the different versions of the Classic and Reverse Pulfrich effect was described in this thesis, finding that reducing the overall light level increases both versions of the Pulfrich effect and therefore their associated optical illusions. This result has implications for the development of anti-Pulfrich monovision corrections. Hypothesis 9 has been demonstrated.

10. The prevalence of the Classic and Reverse Pulfrich effect was reported in a small young population thanks to the development of a portable device that allowed fast and reliable measurements. Although most of the subjects reported the Classic and Reverse Pulfrich effects, only half of them were able to perceive the optical illusions.

11. A new method for estimating stereoacuity fast and accurately was developed using an adaptive psychophysical method. Besides, an autostereoscopic display based on parallax barrier technology was used to perform the measurements, reporting similar results to clinical tests of reference (Titmus). The suitability of SimVis Gekko to perform stereoacuity measurements was validated. The combination of the new method, display, and SimVis Gekko allow fast and reliable measurements of stereoacuity for different presbyopia corrections.

Chapter 16. Bibliography

1. Atchison, D. A. & Smith, G. Chapter 2 - Refracting components: cornea and lens. in *Optics of the Human Eye* 11–20 (2000). doi:https://doi.org/10.1016/B978-0-7506-3775-6.50006-7.
2. Barbero, S. Refractive power of a multilayer rotationally symmetric model of the human cornea and tear film. *J. Opt. Soc. Am.* **23**, 1578–1585 (2006).
3. Hartridge, H. Helmholtz's theory of accommodation. *Br. J. Ophthalmol.* **9**, 521–523 (1925).
4. Myers, G. A. & Stark, L. Topology of the near response triad. *Ophthalmic Physiol. Opt. J. Br. Coll. Ophthalmic Opt.* **10**, 175–181 (1990).
5. Duane, A. Studies in monocular and binocular accommodation, with their clinical application. *Trans. Am. Ophthalmol. Soc.* **20**, 132–157 (1922).
6. Coates, W. R. Amplitudes of accommodation in South Africa. *Br. J. Physiol. Opt.* **12**, 76–81; passim (1955).
7. Turner, M. J. Observations on the normal subjective amplitude of accommodation. *Br. J. Physiol. Opt.* **15**, 70–100 (1958).
8. Cobb, S. R. An investigation into accommodation by Ayrshire Study Circle. *Br. J. Physiol. Opt.* **21**, 31–35 (1964).
9. Charman, W. N. The eye in focus: Accommodation and presbyopia. *Clin. Exp. Optom.* **91**, 207–225 (2008).
10. Artigas, J. M., Felipe, A., Navea, A., Fandiño, A. & Artigas, C. Spectral transmission of the human crystalline lens in adult and elderly persons: Color and total transmission of visible light. *Investig. Ophthalmol. Vis. Sci.* **53**, 4076–4084 (2012).
11. Liu, Y. C., Wilkins, M., Kim, T., Malyugin, B. & Mehta, J. S. Cataracts. *Lancet* **390**, 600–612 (2017).
12. Sadun, A. A. & Libondi, T. Transmission of light through cataracts. *Am. J. Ophthalmol.* **110**, 710–712 (1990).
13. Dartnall, H. J. A., Bowmaker, J. K. & Mollon, J. D. Human visual pigments: microspectrophotometric results from the eyes of seven persons. *Proc. R. Soc. London. Ser. B, Biol. Sci.* **220**, 115–130 (1983).
14. Stockman, A. & Sharpe, L. T. The spectral sensitivities of the middle- and long-wavelength-sensitive cones derived from measurements in observers of known genotype. *Vision Res.* **40**, 1711–1737 (2000).
15. Osterberg, G. Topography of the layer of rods and cones in the human retina. *Acta Ophthalmol.* **13**, 6–97 (1935).
16. Charman, W. N. Wavefront aberration of the eye: a review. *Optom. Vis. Sci.* **68**, 574–583 (1991).
17. Liang, J., Grimm, B., Goelz, S. & Bille, J. F. Objective measurement of wave aberrations of the human eye with the use of a Hartmann–Shack wave-front sensor. *J. Opt. Soc. Am. A* **11**, 1949–1957 (1994).
18. Barbero, S., Marcos, S., Merayo-Lloves, J. & Moreno-Barriuso, E. Validation of the estimation of corneal aberrations From videokeratography in keratoconus. *J. Refract. Surg.* **18**, 263–270 (2002).
19. Airy, G. B. On the diffraction of an object-glass with circular aperture. *Trans. Cambridge Philos. Soc.* **5**, 283 (1835).
20. Thibos, L. N., Applegate, R. A., Schwiegerling, J. T. & Webb, R. Standards for

reporting the optical aberrations of eyes. in *Vision Science and its Applications* SuC1 (Optica Publishing Group, 2000). doi:10.1364/VSIA.2000.SuC1.
21. Porter, J., Guirao, A., Cox, I. G. & Williams, D. R. Monochromatic aberrations of the human eye in a large population. *J. Opt. Soc. Am. A* **18**, 1793–1803 (2001).
22. Francisco Castejón-Mochón, J., López-Gil, N., Benito, A. & Artal, P. Ocular wave-front aberration statistics in a normal young population. *Vision Res.* **42**, 1611–1617 (2002).
23. Thibos, L. N., Hong, X., Bradley, A. & Cheng, X. Statistical variation of aberration structure and image quality in a normal population of healthy eyes. *J. Opt. Soc. Am. A* **19**, 2329–2348 (2002).
24. Thibos, L. N., Wheeler, W. & Horner, D. Power vectors: an application of Fourier analysis to the description and statistical analysis of refractive error. *Optom. Vsion Sci.* **74**, 367–375 (1997).
25. Thibos, L. N., Xin, H., Bradley, A. & Applegate, R. A. Accuracy and precision of objective refraction from wavefront aberrations. *J. Vis.* **4**, 329–351 (2004).
26. Hartwig, A. & Atchison, D. A. Analysis of higher-order aberrations in a large clinical population. *Invest. Ophthalmol. Vis. Sci.* **53**, 7862–7870 (2012).
27. Yazar, S. *et al.* Comparison of monochromatic aberrations in young adults with different visual acuity and refractive errors. *J. Cataract Refract. Surg.* **40**, (2014).
28. Cheng, X. U., Bradley, A., Hong, X. I. N. & Thibos, and L. N. Relationship between Refractive Error and Monochromatic Aberrations of the Eye. *Optom. Vis. Sci.* **80**, (2003).
29. Marcos, S., Barbero, S., Llorente, L. & Merayo-Lloves, J. Optical response to LASIK surgery for myopia from total and corneal aberration measurements. *Invest. Ophthalmol. Vis. Sci.* **42**, 3349–3356 (2001).
30. McLellan, J. S., Marcos, S. & Burns, S. A. Age-related changes in monochromatic wave aberrations of the human eye. *Invest. Ophthalmol. Vis. Sci.* **42**, 1390–1395 (2001).
31. Artal, P., Berrio, E., Guirao, A. & Piers, P. Contribution of the cornea and internal surfaces to the change of ocular aberrations with age. *J. Opt. Soc. Am. A. Opt. Image Sci. Vis.* **19**, 137–143 (2002).
32. He, J. C., Burns, S. A. & Marcos, S. Monochromatic aberrations in the accommodated human eye. *Vision Res.* **40**, 41–48 (2000).
33. Howarth, P. A. The lateral chromatic aberration of the eye. *Ophthalmic Physiol. Opt.* **4**, 223–226 (1984).
34. Ogboso, Y. U. & Bedell, H. E. Magnitude of lateral chromatic aberration across the retina of the human eye. *J. Opt. Soc. Am. A* **4**, 1666–1672 (1987).
35. Marcos, S., Burns, S. A., Prieto, P. M., Navarro, R. & Baraibar, B. Investigating sources of variability of monochromatic and transverse chromatic aberrations across eyes. *Vision Res.* **41**, 3861–3871 (2001).
36. Walsh, G. The effect of mydriasis on the pupillary centration of the human eye. *Ophthalmic Physiol. Opt.* **8**, 178–182 (1988).
37. Simonet, P. & Campbell, M. C. W. The optical transverse chromatic aberration on the fovea of the human eye. *Vision Res.* **30**, 187–206 (1990).
38. Aissati, S., Vinas, M., Benedi-Garcia, C., Dorronsoro, C. & Marcos, S. Testing the effect of ocular aberrations in the perceived transverse chromatic aberration. *Biomed. Opt. Express* **11**, 4052–4068 (2020).
39. Marcos, S., Burns, S. A., Moreno-Barriusop, E. & Navarro, R. A new approach to the study of ocular chromatic aberrations. *Vision Res.* **39**, 4309–4323 (1999).
40. Wald, G. & Griffin, D. R. The change in refractive power of the human eye in dim and bright light. *J. Opt. Soc. Am.* **37**, 321–336 (1947).
41. Rynders, M. C., Navarro, R. & Losada, M. A. Objective measurement of the off-axis longitudinal chromatic aberration in the human eye. *Vision Res.* **38**, 513–522 (1998).
42. Vinas, M., Dorronsoro, C., Cortes, D., Pascual, D. & Marcos, S. Longitudinal

chromatic aberration of the human eye in the visible and near infrared from wavefront sensing , double-pass and psychophysics. *Biomed. Opt. Express* **23**, 513–522 (2015).
43. Charman, W. N. & Jennings, J. A. M. Objective measurements of the longitudinal chromatic aberration of the human eye. *Vision Res.* **16**, 999–1005 (1976).
44. Llorente, L., Diaz-Santana, L., Lara-Saucedo, D. & Marcos, S. Aberrations of the human eye in visible and near infrared illumination. *Optom. Vis. Sci.* **80**, (2003).
45. Thibos, L. N., Ye, M., Zhang, X. & Bradley, A. The chromatic eye: a new reduced-eye model of ocular chromatic aberration in humans. *Appl. Opt.* **31**, 3594–3600 (1992).
46. Callaway, E. M. Structure and function of parallel pathways in the primate early visual system. *J. Physiol.* **566**, 13–19 (2005).
47. Grill-Spector, K. & Malach, R. The human visual cortex. *Annu. Rev. Neurosci.* **27**, 649–677 (2004).
48. Howard, I. P. & Rogers, B. J. *Seeing in depth, Vol. 2: Depth perception.* (University of Toronto Press, 2002).
49. Cheng, X., Bradley, A. & Thibos, L. N. Predicting subjective judgment of best focus with objective image quality metrics. *J. Vis.* **4**, 7 (2004).
50. Marsack, J. D., Thibos, L. N. & Applegate, R. A. Metrics of optical quality derived from wave aberrations predict visual performance. *J. Vis.* **4**, 322–328 (2004).
51. Campbell, F. W. & Green, D. G. Optical and retinal factors affecting visual resolution. *J. Physiol.* **181**, 576–593 (1965).
52. Pelli, D. G. & Bex, P. Measuring contrast sensitivity. *Vision Res.* **90**, 10–14 (2013).
53. van der Schaaf, A. & van Hateren, J. H. Modelling the power spectra of natural images: statistics and information. *Vision Res.* **36**, 2759–2770 (1996).
54. Owsley, C. Contrast sensitivity. *Ophthalmol. Clin. North Am.* **16**, 171–177 (2003).
55. Hess, R. & Woo, G. Vision through cataracts. *Invest. Ophthalmol. Vis. Sci.* **17**, 428–435 (1978).
56. Rubin, G. S., Adamsons, I. A. & Stark, W. J. Comparison of acuity, contrast sensitivity, and disability glare before and after cataract surgery. *Arch. Ophthalmol.* **111**, 56–61 (1993).
57. Regan, D., Raymond, J., Ginsburg, A. P. & Murray, T. J. Contrast sensitivity, visual acuity and the discrimination of Snellen letters in multiple sclerosis. *Brain* **104**, 333–350 (1981).
58. Kaiserman, I., Hazarbassanov, R., Varssano, D. & Grinbaum, A. Contrast sensitivity after wave front-guided LASIK. *Ophthalmology* **111**, 454–457 (2004).
59. Hoffmann, L., Rossouw, P., Guichard, M.-M. & Hatz, K. Strongest correlation between contrast sensitivity and morphological characteristics in bilateral nAMD. *Frontiers in Medicine* vol. 7 (2021).
60. Michael, R., Guevara, O., de la Paz, M., Alvarez de Toledo, J. & Barraquer, R. I. Neural contrast sensitivity calculated from measured total contrast sensitivity and modulation transfer function. *Acta Ophthalmol.* **89**, 278–283 (2011).
61. Lange, D, H. Research into the dynamic nature of the human fovea-cortex systems with intermittent and modulated light. I. Attenuation characteristics with white and colored light. *J. Opt. Soc. Am.* **48**, 777–784 (1958).
62. Watson, A. B. Temporal Sensitivity. *Handbook of Perception and Human Performance* 6:1-6:43 (1986) doi:10.1016/0003-6870(87)90144-X.
63. Mayer, M. J., Kim, C. B. Y., Svingos, A. & Glucs, A. Foveal flicker sensitivity in healthy aging eyes. I. Compensating for pupil variation. *J. Opt. Soc. Am. A* **5**, 2201–2209 (1988).
64. Tyler, C. W. Two processes control variations in flicker sensitivity over the life span. *J. Opt. Soc. Am. A* **6**, 481–490 (1989).
65. Wright, C. E. & Drasdo, N. The influence of age on the spatial and temporal contrast sensitivity function. *Doc. Ophthalmol.* **59**, 385–395 (1985).
66. Seiple, W., Greenstein, V. & Carr, R. Losses of temporal modulation sensitivity in

retinal degenerations. *Br. J. Ophthalmol.* **73**, 440–447 (1989).
67. Mayer, M. J., Spiegler, S. J., Ward, B., Glucs, A. & Kim, C. B. Foveal flicker sensitivity discriminates ARM-risk from healthy eyes. *Invest. Ophthalmol. Vis. Sci.* **33**, 3143–3149 (1992).
68. Mayer, M. J., Spiegler, S. J., Ward, B., Glucs, A. & Kim, C. B. Preliminary evaluation of flicker sensitivity as a predictive test for exudative age-related maculopathy. *Invest. Ophthalmol. Vis. Sci.* **33**, 3150–3155 (1992).
69. Li, R., Ge, J. & Wang, Z.-Q. The study on neural contrast sensitivity function at temporal frequencies. *Optik (Stuttg).* **123**, 343–347 (2012).
70. Robson, J. G. Spatial and temporal contrast-sensitivity functions of the visual system. *J. Opt. Soc. Am.* **56**, 1141 (1966).
71. Watson, A. B., Ahumada, A. & Farrell, J. E. Window of Visibility: a psychophysical theory of fidelity in time-sampled visual motion displays. *NASA Tech. Pap.* **3**, 300–307 (1983).
72. Burbeck, C. A. & Kelly, D. H. Spatiotemporal characteristics of visual mechanisms: excitatory-inhibitory model. *J. Opt. Soc. Am.* **70**, 1121–1126 (1980).
73. Van Den Branden Lambrecht, C. J. & Kunt, M. Characterization of human visual sensitivity for video imaging applications. *Signal Processing* **67**, 255–269 (1998).
74. Lesmes, L. A., Lu, Z.-L., Baek, J. & Albright, T. D. Bayesian adaptive estimation of the contrast sensitivity function: the quick CSF method. *J. Vis.* **10**, 17.1-21 (2010).
75. Wooten, B. R., Renzi, L. M., Moore, R. & Hammond, B. R. A practical method of measuring the human temporal contrast sensitivity function. *Biomed. Opt. Express* **1**, 47–58 (2010).
76. Watson, A. B. & Ahumada, A. J. Blur clarified : A review and synthesis of blur discrimination. *J. Vis.* **11**, 1–23 (2011).
77. Hamerly, J. R. & Dvorak, C. A. Detection and discrimination of blur in edges and lines. *J. Opt. Soc. Am.* **71**, 448–452 (1981).
78. Watt, R. J. & Morgan, M. J. The recognition and representation of edge blur: Evidence for spatial primitives in human vision. *Vision Res.* **23**, 1465–1477 (1983).
79. Hess, R. F., Pointer, J. S. & Watt, R. J. How are spatial filters used in fovea and parafovea? *J. Opt. Soc. Am. A* **6**, 329–339 (1989).
80. Wuerger, S. M., Owens, H. & Westland, S. Blur tolerance for luminance and chromatic stimuli. *J. Opt. Soc. Am. A* **18**, 1231–1239 (2001).
81. Campbell, F. W. & Westheimer, G. Sensitivity of the eye to differences in focus. *J. Physiol.* **143**, 18P (1958).
82. Legras, R., Chateau, N. & Charman, W. N. Assessment of just-noticeable differences for refractive errors and spherical aberration using visual simulation. *Optom. Vis. Sci.* **81**, (2004).
83. Wang, B. & Ciuffreda, K. J. Foveal blur discrimination of the human eye. *Ophthalmic Physiol. Opt.* **25**, 45–51 (2005).
84. Ciuffreda, K. J., Wang, B. & Vasudevan, B. Conceptual model of human blur perception. *Vision Res.* **47**, 1245–1252 (2007).
85. Mather, G. The use of image blur as a depth cue. *Perception* **26**, 1147–1158 (1997).
86. Mather, G. & Smith, D. R. R. Blur discrimination and its relation to blur-mediated depth perception. *Perception* **31**, 1211–1219 (2002).
87. Held, R. T., Cooper, E. A., O'Brien, J. F. & Banks, M. S. Using blur to affect perceived distance and size. *ACM Trans. Graph.* **29**, (2010).
88. Kruger, P. B. & Pola, J. Stimuli for accommodation: Blur, chromatic aberration and size. *Vision Res.* **26**, 957–971 (1986).
89. World Health Organization. *World report on vision*. *World health Organization* vol. 214 (2019).
90. Wallace, D. K. *et al.* Pediatric eye evaluations preferred practice pattern: I. Vision screening in the primary care and community setting; II. Comprehensive

ophthalmic examination. *Ophthalmology* **125**, P184–P227 (2018).
91. Elliott, D. B. *Clinical procedures in primary eye care*. (2014).
92. Thibos, L. N. & Horner, D. Power vector analysis of the optical outcome of refractive surgery. *J. Cataract Refract. Surg.* **27**, 80–85 (2001).
93. Alvarez, T. L. *et al.* Adaptation to progressive lenses by presbyopes. in *2009 4th International IEEE/EMBS Conference on Neural Engineering* 143–146 (2009). doi:10.1109/NER.2009.5109255.
94. Nachmias, J. Effect of exposure duration on visual contrast sensitivity with square-wave gratings. *J. Opt. Soc. Am.* **57**, 421–427 (1967).
95. Shapley, R. M. & Victor, J. D. The effect of contrast on the transfer properties of cat retinal ganglion cells. *J. Physiol.* **285**, 275–298 (1978).
96. Levi, D. M., Harweth, R. S. & Manny, R. E. Suprathreshold spatial frequency detection and binocular interaction in strabismic and anisometropic amblyopia. *Investig. Ophthalmol. Vis. Sci.* **18**, 714–725 (1979).
97. Evans, B. J. W. Monovision: A review. *Ophthalmic Physiol. Opt.* **27**, 417–439 (2007).
98. McGill, E. & Erickson, P. Stereopsis in presbyopes wearing monovision and simultaneous vision bifocal contact lenses. *Optom. Vis. Sci.* **65**, 619–626 (1988).
99. Schor, C. & Heckmann, T. Interocular differences in contrast and spatial frequency: Effects on stereopsis and fusion. *Vision Res.* **29**, 837–847 (1989).
100. Heron, G., McQuaid, M. & Morrice, E. The pulfrich effect in optometric practice. *Ophthalmic Physiol. Opt.* **15**, 425–429 (1995).
101. Nakagawara, V. B. & Véronneau, S. J. Monovision contact lens use in the aviation environment: a report of a contact lens-related aircraft accident. *Optometry* **71**, 390–395 (2000).
102. Bennett, E. S. Contact lens correction of presbyopia. *Clin. Exp. Optom.* **91**, 265–278 (2008).
103. Burge, J., Rodriguez-Lopez, V. & Dorronsoro, C. Monovision and the Misperception of Motion. *Curr. Biol.* **29**, 2586-2592.e4 (2019).
104. Galindo-Ferreiro, A., Galindo-Alonso, J. & Sánchez-Tocino, H. Un nuevo método de diagnóstico y cuantificación de la aniseiconia subjetiva. *Arch. Soc. Esp. Oftalmol.* **82**, 81–88 (2007).
105. Mantry, S. & Shah, S. Surgical management of presbyopia. *Contact Lens Anterior Eye* **27**, 171–175 (2004).
106. Reinstein, D. Z., Archer, T. J. & Gobbe, M. E. Aspheric ablation profile for presbyopic corneal treatment using the MEL80 and CRS Master Laser Blended Vision module. in (2011).
107. MacRae, S. *et al.* Special report: American Academy of Ophthalmology task force consensus statement for extended depth of focus intraocular lenses. *Ophthalmology* **124**, 139–141 (2017).
108. Rampat, R. & Gatinel, D. Multifocal and Extended depth-of-focus intraocular lenses in 2020. *Ophthalmology* **128**, e164–e185 (2021).
109. Pepin, S. M. Neuroadaptation of presbyopia-correcting intraocular lenses. *Curr. Opin. Ophthalmol.* **19**, (2008).
110. Fernandes, P. R. B., Neves, H. I. F., Lopes-Ferreira, D. P., Jorge, J. M. M. & González-Meijome, J. M. Adaptation to multifocal and monovision contact lens correction. *Optom. Vis. Sci.* **90**, 228–235 (2013).
111. Kim, E., Bakaraju, R. C. & Ehrmann, K. Power profiles of commercial multifocal soft contact lenses. *Optom. Vis. Sci.* **94**, 183–196 (2017).
112. Chang, D. F. Disruptive innovation and refractive IOLs: How the game will change with adjustable IOLs. *Asia-Pacific J. Ophthalmol.* **8**, 432–435 (2019).
113. Dorronsoro, C. *et al.* Portable simultaneous vision device to simulate multifocal corrections. *Optica* **3**, (2016).
114. Brar, S., Ganesh, S., Arra, R. R. & Sute, S. S. Visual and refractive outcomes and patient satisfaction following implantation of monofocal IOL in one wye and ERV

IOL in the contralateral eye with mini-monovision. *Clin. Ophthalmol.* **15**, 1839–1849 (2021).
115. Labiris, G., Giarmoukakis, A., Patsiamanidi, M., Papadopoulos, Z. & Kozobolis, V. P. Mini-monovision versus multifocal intraocular lens implantation. *J. Cataract Refract. Surg.* **41**, 53–57 (2015).
116. de Medeiros, A. L. *et al.* Comparison of visual outcomes after bilateral implantation of a diffractive trifocal intraocular lens and blended implantation of an extended depth of focus intraocular lens with a diffractive bifocal intraocular lens. *Clin. Ophthalmol.* **11**, 1911–1916 (2017).
117. Goldberg, D. G., Goldberg, M. H., Shah, R., Meagher, J. N. & Ailani, H. Pseudophakic mini-monovision: high patient satisfaction, reduced spectacle dependence, and low cost. *BMC Ophthalmol.* **18**, 293 (2018).
118. Hayashi, K., Sato, T., Igarashi, C. & Yoshida, M. Comparison of visual outcomes between bilateral trifocal intraocular lenses and combined bifocal intraocular lenses with different near addition. *Jpn. J. Ophthalmol.* **63**, 429–436 (2019).
119. Ouchi, M. & Shiba, T. Blended vision achieved by combining high and low addition power diffractive intraocular lenses with micromonovision: A clinical outcome. *J. Ophthalmol.* **2020**, 6143832 (2020).
120. Tabernero, J., Chirre, E., Hervella, L., Prieto, P. & Artal, P. The accommodative ciliary muscle function is preserved in older humans. *Sci. Rep.* **6**, 25551 (2016).
121. Marcos, S., Alejandre, N., Lamela, J., Dorronsoro, C. & Kochevar, I. E. Toward new engagement paradigms for Intraocular Lenses: Light-Initiated bonding of capsular bag to lens materials. *Invest. Ophthalmol. Vis. Sci.* **56**, 4249–4256 (2015).
122. Alio, J. L., Plaza-Puche, A. B., Férnandez-Buenaga, R., Pikkel, J. & Maldonado, M. Multifocal intraocular lenses: An overview. *Surv. Ophthalmol.* **62**, 611–634 (2017).
123. Kabat, A. G., Lievens, C. W., Newman, C. M. & Weber, J. Accuracy, speed and repeatability of the voice assisted subjective refractor (VASR). *Clin. Ophthalmol.* **13**, 1807–1813 (2019).
124. Zadnik, K., Mutti, D. O. & Adams, A. J. The repeatability of measurement of the ocular components. *Investig. Ophthalmol. Vis. Sci.* **33**, 2325–2333 (1992).
125. Pesudovs, K., Parker, K. E., Cheng, H. A. N. & Applegate, R. A. The precision of wavefront refraction compared to subjective refraction and autorefraction. *Optom. Vis. Sci.* **84**, 387–392 (2007).
126. Mallen, E. A. H., Gilmartin, B., Wolffsohn, J. S. & Tsujimura, S. I. Clinical evaluation of the Shin-Nippon SRW-5000 autorefractor in adults: An update. *Ophthalmic Physiol. Opt.* **35**, 622–627 (2015).
127. Sheedy, J., Schanz, P. & Bullimore, M. Evaluation of an automated subjective refractor. *Optom. Vis. Sci.* **81**, 334–340 (2004).
128. Hervella, L., Villegas, E. A., Prieto, P. M. & Artal, P. Assessment of subjective refraction with a clinical adaptive optics visual simulator. *J. Cataract Refract. Surg.* **45**, 87–93 (2019).
129. Wosik, J., Patrzykont, M. & Pniewski, J. Comparison of refractive error measurements by three different models of autorefractors and subjective refraction in young adults. *J. Opt. Soc. Am. A* **36**, B1 (2019).
130. Hament, W. J., Nabar, V. A. & Nuijts, R. M. M. A. Repeatability and validity of Zywave aberrometer measurements. *J. Cataract Refract. Surg.* **28**, 2135–2141 (2002).
131. Lebow, K. A. & Campbell, C. E. A comparison of a traditional and wavefront autorefraction. *Optom. Vis. Sci.* **91**, 1191–1198 (2014).
132. Bennett, J. R., Stalboerger, G. M., Hodge, D. O. & Schornack, M. M. Comparison of refractive assessment by wavefront aberrometry, autorefraction, and subjective refraction. *J. Optom.* **8**, 109–115 (2015).
133. Bamdad, S., Momeni-Moghaddam, H., Abdolahian, M. & Piñero, D. P. Agreement

of wavefront-based refraction, dry and cycloplegic autorefraction with subjective refraction. *J. Optom.* (2020).
134. Stoor, K., Karvonen, E., Liinamaa, J. & Saarela, V. Evaluating refraction and visual acuity with the Nidek autorefractometer AR-360A in a randomized population-based screening study. *Acta Ophthalmol.* **96**, 384–389 (2018).
135. Samanta, A., Shetty, A. & Nelson, P. C. Better one or two? A systematic review of portable automated refractors. *J. Telemed. Telecare* **95**, 1135–1141 (2020).
136. Agarwal, A. *et al.* Comparing low-cost handheld autorefractors: A practical approach to measuring refraction in low-resource settings. *PLoS One* **14**, 1–8 (2019).
137. Varadarajan, A. V. *et al.* Deep learning for predicting refractive error from retinal fundus images. *Investig. Ophthalmol. Vis. Sci.* **59**, 2861–2868 (2018).
138. Joseph, S. *et al.* Investigation of the Accuracy of a low-cost, portable sutorefractor to provide well-tolerated eyeglass prescriptions: a randomized crossover trial. *Ophthalmology* **128**, 1672–1680 (2021).
139. Ohlendorf, A., Leube, A. & Wahl, S. Steps towards amarter solutions in optometry and ophthalmology—Inter-device agreement of subjective methods to assess the refractive errors of the eye. *Healthcare* **4**, 41 (2016).
140. Carracedo, G., Carpena-Torres, C., Serramito, M., Batres-Valderas, L. & Gonzalez-Bergaz, A. Comparison between aberrometry-based binocular refraction and subjective refraction. *Transl. Vis. Sci. Technol.* **7**, 11 (2018).
141. Otero, C., Aldaba, M. & Pujol, J. Clinical evaluation of an automated subjective refraction method implemented in a computer-controlled motorized phoropter. *J. Optom.* **12**, 74–83 (2018).
142. Venkataraman, A. P., Sirak, D., Brautaset, R. & Dominguez-Vicent, A. Evaluation of the performance of algorithm-based methods for subjective refraction. *J. Clin. Med.* **9**, 1–8 (2020).
143. Pujol, J. *et al.* Spherical subjective refraction with a novel 3D virtual reality based system. *J. Optom.* **10**, 43–51 (2017).
144. Taneri, S., Arba-Mosquera, S., Rost, A., Kießler, S. & Dick, H. B. Repeatability and reproducibility of manifest refraction. *J. Cataract Refract. Surg.* **46**, 1659–1666 (2020).
145. Ruiss, M., Findl, O., Draschl, P., Harrer-Seely, A. & Hirnschall, N. Agreement and variability of subjective refraction, autorefraction, and wavefront aberrometry in pseudophakic patients. *J. Cataract Refract. Surg.* **47**, 1056–1063 (2021).
146. MacKenzie, G. E. Reproducibility of sphero-cylindrical prescriptions. *Ophthalmic Physiol. Opt.* **28**, 143–150 (2008).
147. Atchison, D. A., Schmid, K. L., Edwards, K. P., Muller, S. M. & Robotham, J. The effect of under and over refractive correction on visual performance and spectacle lens acceptance. *Ophthalmic Physiol. Opt.* **21**, 255–261 (2001).
148. Freeman, C. E. & Evans, B. J. W. Investigation of the causes of non-tolerance to optometric prescriptions for spectacles. *Ophthalmic Physiol. Opt.* **30**, 1–11 (2010).
149. Bist, J., Kaphle, D., Marasini, S. & Kandel, H. Spectacle non-tolerance in clinical practice – a systematic review with meta-analysis. *Ophthalmic Physiol. Opt.* **41**, 610–622 (2021).
150. Ravikumar, A., Applegate, R. A., Shi, Y. & Bedell, H. E. Six just-noticeable differences in retinal image quality in 1 line of visual acuity: Toward quantification of happy versus unhappy patients with 20/20 acuity. *J. Cataract Refract. Surg.* **37**, 1523–1529 (2011).
151. Curtis, R. *et al.* Validation of a portable, remotely delivered refraction approach compared to standard in-clinic refraction in a low-vision population. *J. Telemed. Telecare* (2020) doi:10.1177/1357633X20960628.
152. Leube, A., Kraft, C., Ohlendorf, A. & Wahl, S. Self-assessment of refractive errors using a simple optical approach. *Clin. Exp. Optom.* **101**, 386–391 (2018).
153. Tousignant, B., Garceau, M. C., Bouffard-Saint-Pierre, N., Bellemare, M. M. &

Hanssens, J. M. Comparing the Netra smartphone refractor to subjective refraction. *Clin. Exp. Optom.* **103**, 501–506 (2020).
154. Wisse, R. P. L. *et al.* Validation of an independent web-based tool for measuring visual acuity and refractive error via the MORE (Manifest Versus Online Refractive Evaluation) trial: Prospective open-label noninferiority clinical trial. *J. Med. Internet Res.* **21**, 1–13 (2019).
155. Dave, T. & Fukuma, Y. Clinical evaluation of the Topcon BV-1000 automated subjective refraction system. *Optom. Vis. Sci.* **81**, 323–333 (2004).
156. Putnam, N. M. *et al.* Comparing habitual and i. Scription refractions. *BMC Ophthalmol.* **19**, 1–7 (2019).
157. Ingelstam, E. & Ragnarsson, S. I. Eye refraction examined by aid of speckle pattern produced by coherent light. *Vision Res.* **12**, 411–420 (1972).
158. Doustkouhi, S. M., Turnbull, P. R. K. & Dakin, S. C. The effect of refractive error on optokinetic nystagmus. *Sci. Rep.* **10**, 1–14 (2020).
159. Rodriguez-Lopez, V., Hernandez-Poyatos, A. & Dorronsoro, C. The Direct Subjective Refraction: Unsupervised measurements of the subjective refraction using defocus waves. *bioRxiv* 2021.12.04.471123 (2021) doi:10.1101/2021.12.04.471123.
160. Rodríguez-Lopez, V., Esteban-Ibañez, E. & Dorronsoro, C. Fast subjective estimation of astigmatism with the Direct Subjective Refraction. *Invest. Ophthalmol. Vis. Sci.* **62**, 2913 (2021).
161. Rodriguez-Lopez, V. & Dorronsoro, C. Beyond traditional subjective refraction. *Curr. Opin. Ophthalmol.* **Publish Ah**, 228–234 (2022).
162. Wolffsohn, J. S. & Davies, L. N. Presbyopia: Effectiveness of correction strategies. *Prog. Retin. Eye Res.* (2018) doi:10.1016/j.preteyeres.2018.09.004.
163. Bailey, I. L. & Lovie, J. E. The design and use of a new near-vision chart. *Am. J. Optom. Physiol. Opt.* **57**, 378–387 (1980).
164. Chaikitmongkol, V., Nanegrungsunk, O., Patikulsila, D., Ruamviboonsuk, P. & Bressler, N. M. Repeatability and agreement of visual acuity using the ETDRS number chart, landolt C chart, or ETDRS alphabet chart in eyes with or without sight-threatening diseases. *JAMA Ophthalmol.* **136**, 286–290 (2018).
165. Harris, P. A. & Keim, E. Validation of the Dyop^{TM} Visual Acuity Test. *Invest. Ophthalmol. Vis. Sci.* **56**, 3888 (2015).
166. Barnett-Itzhaki, G., Barnett-Itzhaki, Z. & Ela-Dalman, N. The dynamic optotype (Dyop): a novel visual acuity test for use in children. *J. AAPOS* **25**, 285.e1-285.e5 (2021).
167. Harris, M. G. & Classé, J. G. Clinicolegal considerations of monovision. *J. Am. Optom. Assoc.* **59**, 491–495 (1988).
168. Jain, S., Arora, I. & Azar, D. T. Success of monovision in presbyopes: Review of the literature and potential applications to refractive surgery. *Surv. Ophthalmol.* **40**, 491–499 (1996).
169. Raju, D. The monovision approach to presbyopia. *Retrieved from https//www. Opt.* 0–3 (2016).
170. Mapp, A. P., Ono, H. & Barbeito, R. What does the dominant eye dominate? A brief and somewhat contentious review. *Percept. Psychophys.* **65**, 310–317 (2003).
171. Barbeito, R. Sighting dominance: An explanation based on the processing of visual direction in tests of sighting dominance. *Vision Res.* **21**, 855–860 (1981).
172. Coren, S. & Kaplan, C. P. Patterns of ocular dominance. *Am. J. Optom. Arch. Am. Acad. Optom.* **50**, 283–292 (1973).
173. Seijas, O. *et al.* Ocular dominance diagnosis and its influence in monovision. *Am. J. Ophthalmol.* **144**, (2007).
174. Ross, N. C., Bowers, A. R. & Peli, E. Peripheral prism glasses. *Optom. Vis. Sci.* **89**, 1343–1352 (2012).
175. García-Pérez, M. A. & Peli, E. Psychophysical tests do not identify ocular

dominance consistently. *Iperception.* **10**, (2019).
176. Rutstein, R. P. & Daum, K. M. *Anomalies of binocular vision: diagnosis and management*. (Mosby, St. Louis, MO, 1998).
177. O'connor, A. R. & Tidbury, L. P. Stereopsis: are we assessing it in enough depth? *Clin. Exp. Optom.* **101**, 485–494 (2018).
178. Fender, D. & Julesz, B. Extension of Panum's fusional area in binocularly stabilized vision. *J. Opt. Soc. Am.* **57**, 819–830 (1967).
179. Otero-Millan, J., Macknik, S. L. & Martinez-Conde, S. Fixational eye movements and binocular vision. *Frontiers in Integrative Neuroscience* vol. 8 (2014).
180. Mather, G. & Smith, D. R. R. Depth cue integration: Stereopsis and image blur. *Vision Res.* **40**, 3501–3506 (2000).
181. Bohr, I. & Read, J. C. A. Stereoacuity with Frisby and revised FD2 stereo tests. *PLoS One* **8**, e82999 (2013).
182. Wong, B. P. H., Woods, R. L. & Peli, E. Stereoacuity at distance and near. *Optom. Vis. Sci.* **79**, (2002).
183. Iwata, Y., Fujimura, F., Handa, T., Shoji, N. & Ishikawa, H. Effects of target size and test distance on stereoacuity. *J. Ophthalmol.* **2016**, 7950690 (2016).
184. Rodríguez-Vallejo, M., Ferrando, V., Montagud, D., Monsoriu, J. A. & Furlan, W. D. Stereopsis assessment at multiple distances with an iPad application. *Displays* **50**, 35–40 (2017).
185. Leske, D. A., Birch, E. E. & Holmes, J. M. Real depth vs randot stereotests. *Am. J. Ophthalmol.* **142**, 699–701 (2006).
186. Matsuo, T., Negayama, R., Sakata, H. & Hasebe, K. Correlation between depth perception by three-rods test and stereoacuity by distance Randot Stereotest. *Strabismus* **22**, 133–137 (2014).
187. Walraven, J. Amblyopia screening with random-dot stereograms. *Am. J. Ophthalmol.* **80**, 893–900 (1975).
188. Heron, G., Dholakia, S., Collins, D. E. & McLaughan, H. Stereoscopic threshold in children and adults. *Optom. Vis. Sci.* **62**, (1985).
189. Simons, K. & Elhatton, K. Artifacts in fusion and stereopsis testing based on red/green dichoptic image separation. *J. Pediatr. Ophthalmol. Strabismus* **31 5**, 290–297 (1994).
190. Bogdanovich, G., Roth, N. & Kohl, P. Properties of anaglyphic materials that affect the testing and training of binocular vision. *J. Am. Optom. Assoc.* **57**, **899–903** (1986).
191. van Doorn, L. L. A., Evans, B. J. W., Edgar, D. F. & Fortuin, M. F. Manufacturer changes lead to clinically important differences between two editions of the TNO stereotest. *Ophthalmic Physiol. Opt.* **34**, 243–249 (2014).
192. Jorke, H. & Fritz, M. Infitec-A new stereoscopic visualization tool by wavelength multiplex imaging. *J. Three Dimens. Images* **19**, 31–42 (2005).
193. Birch, E. & Salomão, S. Infant Random Dot stereoacuity cards. *J. Pediatr. Ophthalmol. & Strabismus* **35**, 86–90 (1998).
194. Dodgson, N. A. Autostereoscopic 3D displays. *Computer (Long. Beach. Calif).* **38**, 31–36 (2005).
195. Holliman, N. S., Dodgson, N. A., Favalora, G. E. & Pockett, L. Three-Dimensional displays: a review and applications analysis. *IEEE Trans. Broadcast.* **57**, 362–371 (2011).
196. Lang, J. A new stereotest. *J. Pediatr. Ophthalmol. Strabismus* **20**, 72–74 (1983).
197. Huynh, S. C., Ojaimi, E., Robaei, D., Rose, K. & Mitchell, P. Accuracy of the Lang II stereotest in screening for binocular disorders in 6-year-old children. *Am. J. Ophthalmol.* **140**, 1130–1132 (2005).
198. Lagstein, O., Hecht, I. & Anteby, I. Comparison of a new, filter-free stereopsis test (BEST) with the Randot stereotest in a pediatric cohort. *J. Pediatr. Ophthalmol. Strabismus* **57**, 129–135 (2020).
199. Serrano-Pedraza, I., Vancleef, K. & Read, J. C. A. Avoiding monocular artifacts in

clinical stereotests presented on column-interleaved digital stereoscopic displays. *J. Vis.* **16**, 13 (2016).
200. Vancleef, K. *et al.* ASTEROID: A new clinical stereotest on an autostereo 3D tablet. *Transl. Vis. Sci. Technol.* **8**, 25 (2019).
201. Casanova, T. *et al.* The impact of active research involvement of young children in the design of a new stereotest. *Res. Involv. Engagem.* **6**, 29 (2020).
202. Spiegler, J. B. Apparent path of a Pulfrich target as a function of the slope of its plane of motion: a theoretical note. *Am. J. Optom. Physiol. Opt.* **63**, 209–216 (1986).
203. Lit, A. The magnitude of the Pulfrich stereophenomenon as a function of binocular differences of intensity at various levels of illumination. *Am. J. Psychol.* **62**, 159–181 (1949).
204. Prestrude, A. M. Visual latencies at photopic levels of retinal illuminance. *Vision Res.* **11**, 351–361 (1971).
205. Lit, A. The magnitude of the Pulfrich stereophenomenon as a function of target velocity. *J. Exp. Psychol.* **59**, 165–175 (1960).
206. Rock & Fox. Two Aspect of the Pulfrich Phenomenon. *Am. J. Psychol.* **62**, 279–284 (1949).
207. Standing, L. G., Dodwell, P. C. & Lang, D. Dark adaptation and the Pulfrich effect. *Percept. Psychophys.* **4**, 2–4 (1968).
208. Rogers, B. J. & Anstis, S. M. Intensity versus adaptation and the Pulfrich stereophenomenon. *Vision Res.* **12**, 909–928 (1972).
209. Rogers, B. J., Steinbach, M. J. & Ono, H. Eye movements and the Pulfrich phenomenon. *Vision Res.* **14**, 181–185 (1974).
210. Wallach, H. & Goldberg, J. An exploration of the Pulfrich effect. *Scand. J. Psychol.* **18**, 231–236 (1977).
211. Ono, H. & Steinbach, M. J. The Pulfrich phenomenon with eye movement. *Vision Res.* **23**, 1735–1737 (1983).
212. Rushton, D. Use of the pulfrich pendulum for detecting abnormal delay in the visual pathway in multiple sclerosis. *Brain* **98**, 283–296 (1975).
213. Kirkham, T. H. & Coupland, S. G. Multiple regression analysis of diagnostic predictors in optic nerve disease. *Can. J. Neurol. Sci. Can. des Sci. Neurol.* **8**, 67–72 (1981).
214. Diaper, C. J. M., Heron, G. & MacMillan, E. S. Correction of the Pulfrich phenomenon by surgery and laser. *J. Cataract Refract. Surg.* **28**, 369–372 (2002).
215. Scotcher, S. M., Laidlaw, D. A. H., Canning, C. R., Weal, M. J. & Harrad, R. A. Pulfrich's phenomenon in unilateral cataract. *Br. J. Ophthalmol.* **81**, 1050–1055 (1997).
216. Cetinkaya, A., Oto, S. & Akova, Y. A. Decision-making in second-eye cataract surgery: Can presence of Pulfrich phenomenon help? *Eye* **21**, 52–57 (2007).
217. Heng, S. & Dutton, G. N. The Pulfrich effect in the clinic. *Graefe's Arch. Clin. Exp. Ophthalmol.* **249**, 801–808 (2011).
218. Reynaud, A. & Hess, R. F. Interocular contrast difference drives illusory 3D percept. *Sci. Rep.* **7**, 1–6 (2017).
219. Marcos, S., Sawides, L., Gambra, E. & Dorronsoro, C. Influence of adaptive-optics ocular aberration correction on visual acuity at different luminances and contrast polarities. *J. Vis.* **8**, 1 (2008).
220. Sawides, L. *et al.* Adaptation to astigmatic blur. *J. Vis.* **10**, 22 (2010).
221. Sawides, L., Gambra, E., Pascual, D., Dorronsoro, C. & Marcos, S. Visual performance with real-life tasks under adaptive-optics ocular aberration correction. *J. Vis.* **10**, 19 (2010).
222. Vinas, M., Dorronsoro, C., Garzón, N., Poyales, F. & Marcos, S. In vivo subjective and objective longitudinal chromatic aberration after bilateral implantation of the same design of hydrophobic and hydrophilic intraocular lenses. *J. Cataract Refract. Surg.* **41**, 2115–2124 (2015).

223. Vinas, M. *et al.* Testing vision with angular and radial multifocal designs using Adaptive Optics. *Vision Res.* **132**, 85–96 (2017).
224. Lu, Z.-L. & Dosher, B. Visual psychophysics: From laboratory to theory. (2013) doi:10.7551/mitpress/9780262019453.001.0001.
225. Wichmann, F. A. & Hill, N. J. The psychometric function: I. Fitting, sampling, and goodness of fit. *Percept. Psychophys.* **63**, 1293–1313 (2001).
226. Blackwell, H. R. Studies of psychophysical methods for measuring visual thresholds. *J. Opt. Soc. Am.* **42**, 606–616 (1952).
227. Treutwein, B. Adaptive psychophysical procedures. *Vision Res.* **35**, 2503–2522 (1995).
228. Watson, A. B. & Pelli, D. G. Quest: A Bayesian adaptive psychometric method. *Percept. Psychophys.* **33**, 113–120 (1983).
229. Barcala, X. *et al.* Multifocal acceptance score to evaluate vision: MAS - 2EV. *Sci. Rep.* **11**, 1–15 (2021).
230. McCaslin, A. G., Vancleef, K., Hubert, L., Read, J. C. A. & Port, N. Stereotest comparison: efficacy, reliability, and variability of a new glasses-free stereotest. *Transl. Vis. Sci. Technol.* **9**, 29 (2020).
231. Mannos, J. L. & Sakrison, D. J. The effects of a visual fidelity criterion on the encoding of images. *IEEE Trans. Inf. Theory* **20**, 525–536 (1974).
232. van Nes, F. L., Koenderink, J. J., Nas, H. & Bouman, M. A. Spatiotemporal modulation transfer in the human eye. *J. Opt. Soc. Am.* **57**, 1082–1088 (1967).
233. Burge, J. & Geisler, W. S. Optimal defocus estimation in individual natural images. *Proc. Natl. Acad. Sci. U. S. A.* **108**, 16849–16854 (2011).
234. Walsh, G. & Charman, W. N. Visual sensitivity to temporal change in focus and its relevance to the accommodation response. *Vision Res.* **28**, 1207–1221 (1988).
235. Mathews, S. & Kruger, P. B. Spatiotemporal transfer function of human accommodation. *Vision Res.* **34**, 1965–1980 (1994).
236. Bilson, A. C., Mizokami, Y. & Webster, M. A. Visual adjustments to temporal blur. *J. Opt. Soc. Am. A* **22**, 2281 (2005).
237. Dorronsoro, C. *et al.* Tunable lenses: Dynamic characterization and fine-tuned control for high-speed applications. *Opt. Express* **27**, (2019).
238. Dorronsoro, C. *et al.* Portable simultaneous vision device to simulate multifocal corrections. *Optica* **3**, 918–924 (2016).
239. Dorronsoro, C. *et al.* Tunable lenses: dynamic characterization and fine-tuned control for high-speed applications. *Opt. Express* **27**, 2085 (2019).
240. Vazquez, J., Párraga, C. A., Baldrich, R. & Maria, V. Color constancy algorithms: Psychophysical evaluation on a new dataset. *J. Imaging Sci. Technol.* **53**, 1–9 (2009).
241. Brainard, D. H. The Psychophysics Toolbox. *Spat. Vis.* **10**, 433–436 (1997).
242. Sharmin, N. & Vohnsen, B. Monocular accommodation response to random defocus changes induced by a tuneable lens. *Vision Res.* **165**, 45–53 (2019).
243. Heron, G., Charman, W. N. & Schor, C. Dynamics of the accommodation response to abrupt changes in target vergence as a function of age. *Vision Res.* **41**, 507–519 (2001).
244. Elliott, D. B. What is the appropriate gold standard test for refractive error? *Ophthalmic Physiol. Opt.* **37**, 115–117 (2017).
245. Bullimore, M. A. *et al.* Patient acceptance of auto-refractor and clinician prescriptions: A randomized clinical trial. *Vis. Sci. its Appl. Tech. Dig. Ser.* **37**, S704 (1996).
246. Rosenfield, M. & Chiu, N. N. Repeatability of subjective and objective refraction. *Optom. Vis. Sci.* **72**, 577–579 (1995).
247. Strang, N. C., Gray, L. S., Winn, B. & Pugh, J. R. Clinical evaluation of patient tolerance to autorefractor prescriptions. *Clin. Exp. Optom.* **81**, 112–118 (1998).
248. Sun, J. K. *et al.* Evaluation of visual acuity measurements after autorefraction vs manual refraction in eyes with and without diabetic macular edema. *Arch.*

Ophthalmol. **130**, 470–479 (2012).
249. Segura, F., Sanchez-Cano, A., Lopez de la Fuente, C., Fuentes-Broto, L. & Pinilla, I. Evaluation of patient visual comfort and repeatability of refractive values in non-presbyopic healthy eyes. *Int. J. Ophthalmol.* **8**, 1031–1036 (2015).
250. McAlinden, C., Pesudovs, K. & Moore, J. E. The development of an instrument to measure quality of vision: The quality of vision (QoV) questionnaire. *Investig. Ophthalmol. Vis. Sci.* **51**, 5537–5545 (2010).
251. Choong, Y. F., Chen, A. H. & Goh, P. P. A comparison of autorefraction and subjective refraction with and without cycloplegia in primary school children. *Am. J. Ophthalmol.* **142**, 68–74 (2006).
252. Rauscher, F. G. *et al.* Agreement and repeatability of noncycloplegic and cycloplegic wavefront-based autorefraction in children. *Optom. Vis. Sci.* **96**, 879–889 (2019).
253. Kotegawa, Y., Hara, N., Ono, K., Arimoto, A. & Mukuno, K. Influence of accommodative response and visual symptoms on visual display terminal adult operators with asthenopia through adequately corrected refractive errors. *Nihon. Ganka Gakkai Zasshi* **112**, 376–381 (2008).
254. Dorronsoro, C. & Rodriguez-Lopez, V. Device and system to conduct optometric measurements and method to adjust the optical power of a tunable lens. OEPM Patent Application Number: 201930198.
255. Radhakrishnan, A., Pascual, D., Marcos, S. & Dorronsoro, C. Vision with different presbyopia corrections simulated with a portable binocular visual simulator. *PLoS One* **14**, 1–13 (2019).
256. Dorronsoro, C. *et al.* Perceptual and physical limits to temporal multiplexing simulation of multifocal corrections. *Invest. Ophthalmol. Vis. Sci.* **60**, 6465 (2019).
257. Neary, C. The effect of high frequency flicker on accommodation. *Ophthalmic Physiol. Opt.* **9**, 440–446 (1989).
258. Flitcroft, D. I. Accommodation and flicker: evidence of a role for temporal cues in accommodation control? *Ophthalmic Physiol. Opt.* **11**, 81–90 (1991).
259. Chauhan & Charman. Accommodation responses to flickering stimuli. *Ophthalmic Physiol. Opt.* **16**, 391–408 (1996).
260. Zhang, L. *et al.* The effects of colour and temporal frequency of flickering light on variability of the accommodation response in emmetropes and myopes. *BMC Ophthalmol.* **21**, 88 (2021).
261. Otero, J. M. Influence of the State of Accommodation on the Visual Performance of the Human Eye. **41**, 942–948 (1951).
262. Artal, P., Schwarz, C. & Ca, C. Night Myopia Studied with an Adaptive Optics Visual Analyzer. *PLoS One* **7**, 1–6 (2012).
263. Bedford, R. E. & Wyszecki, G. Axial Chromatic aberration of the human eye. *J. Opt. Soc. Am.* **47**, 564_1-565 (1957).
264. Coe, C., Bradley, A. & Thibos, L. Polychromatic refractive error from monochromatic wavefront aberrometry. *Optom. Vis. Sci.* **91**, 1167–1174 (2014).
265. Thibos, L. N. Unresolved Issues in the Prediction of Subjective Refraction From Wavefront Aberration Maps. *J. Refract. Surg.* **20**, 533–536 (2004).
266. Leube, A. *et al.* Individual neural transfer function affects the prediction of subjective depth of focus. *Sci. Rep.* **8**, 1–8 (2018).
267. Rodriguez-Lopez, V. & Dorronsoro, C. Direct subjective refraction with temporal defocus waves. *Investig. Ophthalmol. Vis. Sci.* **60**, 4265 (2019).
268. Rubio, M. *et al.* Validation of an affordable handheld wavefront autorefractor. *Optom. Vis. Sci.* **96**, 726–732 (2019).
269. Vinas, M. *et al.* Pre-operative simulation of post-operative multifocal vision. *Biomed. Opt. Express* **10**, 5801 (2019).
270. Visnjić, M. B. *et al.* Astigmatism and diagnostic procedures. *Acta Clin. Croat.* **51**, 285–288 (2012).
271. Padhy, D., Bharadwaj, S. R., Nayak, S., Rath, S. & Das, T. Does the accuracy

and repeatability of refractive error estimates depend on the measurement principle of autorefractors? *Transl. Vis. Sci. Technol.* **10**, 1–11 (2021).
272. Walline, J. J., Kinney, K. A., Zadnik, K. & Mutti, D. O. Repeatability and validity of astigmatism measurements. *J. Refract. Surg.* **15**, 23–31 (1999).
273. Durr, N. J. *et al.* Design and clinical evaluation of a handheld wavefront autorefractor. *Optom. Vis. Sci.* **92**, (2015).
274. Sharpe, L. T., Stockman, A., Jagla, W. & Jägle, H. A luminous efficiency function, V*(λ), for daylight adaptation. *J. Vis.* **5**, 3 (2005).
275. Stockman, A. & Sharpe, L. T. Spectral Sensitivity. in *The senses: A comprehensive reference* (eds. Masland, R. H. et al.) 87–100 (2008). doi:https://doi.org/10.1016/B978-012370880-9.00300-5.
276. Athaide, H. V. Z., Campos, M. & Costa, C. Study of ocular aberrations with age. *Arq. Bras. Oftalmol.* **72**, 617–621 (2009).
277. Zhang, F.-J. *et al.* Comparison of age-related changes between corneal and ocular aberration in young and mid-age myopic patients. *Int. J. Ophthalmol.* **4**, 286–292 (2011).
278. Sun, Y., Wu, H., Qiu, Y. & Yue, Z. Stereoacuity of black-white and red-green patterns in individuals with and without color deficiency. *J. Ophthalmol.* **2018**, 1926736 (2018).
279. Ozates, S., Sekeroglu, M. A., Ilhan, C., Doguizi, S. & Yilmazbas, P. Depth perception in patients with congenital color vision deficiency. *Eye (Lond).* **33**, 674–678 (2019).
280. Schor, C., Landsman, L. & Erickson, P. Ocular dominance and the interocular suppression of blur in monovision. *Am. J. Optom. Physiol. Opt.* **64**, 723–730 (1987).
281. Collins, M. J. & Goode, A. Interocular blur suppression and monovision. *Acta Ophthalmol.* **72**, 376–380 (1994).
282. Yang, E., Blake, R. & McDonald, J. E. A new interocular suppression technique for measuring sensory eye dominance. *Investig. Ophthalmol. Vis. Sci.* **51**, 588–593 (2010).
283. Liu, L., Tyler, C. W. & Schor, C. M. Failure of rivalry at low contrast: Evidence of a suprathreshold binocular summation process. *Vision Res.* **32**, 1471–1479 (1992).
284. Dieter, K. C., Sy, J. L. & Blake, R. Individual differences in sensory eye dominance reflected in the dynamics of binocular rivalry. *Vision Res.* **141**, 40–50 (2017).
285. Squier, K. Ocular sensory dominance and viewing distance. *Master's thesis. Nov. Southeast. Univ. Retrieved from NSUWorks, Coll. Optom. https//nsuworks.nova.edu/hpd_opt_stuetd/12.* (2017).
286. Jiang, F. *et al.* Association between ocular sensory dominance and refractive error asymmetry. *PLoS One* **10**, 1–12 (2015).
287. Han, C., He, Z. J. & Ooi, T. L. On sensory eye dominance revealed by binocular integrative and binocular competitive stimuli. *Investig. Ophthalmol. Vis. Sci.* **59**, 5140–5148 (2018).
288. Dieter, K. C., Sy, J. L. & Blake, R. Individual differences in sensory eye dominance reflected in the dynamics of binocular rivalry. *Vision Res.* **141**, 40–50 (2017).
289. Malott, L. E., Clare, D. P. & Lowther, G. E. Ocular dominance testing. *Int. Contact Lens Clin.* **23**, 50–54 (1996).
290. Schor, C. & Erickson, P. Ocular dominance, accommodation, and the interocular suppression of blur in monovision. *Presbyopia Res.* **64**, 273–288 (1991).
291. Xiong, S. *et al.* Comparison of refractive measures of three autorefractors in children and adolescents. *Optom. Vis. Sci.* **94**, 894–902 (2017).
292. Zhang, F., Sugar, A., Arbisser, L., Jacobsen, G. & Artico, J. Crossed versus conventional pseudophakic monovision: Patient satisfaction, visual function, and spectacle independence. *J. Cataract Refract. Surg.* **41**, 1845–1854 (2015).
293. Nabie, R., Andalib, D., Amir-Aslanzadeh, S. & Khojasteh, H. Effect of artificial

anisometropia in dominant and nondominant eyes on stereoacuity. *Can. J. Ophthalmol.* **52**, 240–242 (2017).
294. Zheleznyak, L., Alarcon, A., Dieter, K. C., Tadin, D. & Yoon, G. The role of sensory ocular dominance on through-focus visual performance in monovision presbyopia corrections. *J. Vis.* **15**, 1–12 (2015).
295. Barcala, X. *et al.* Multifocal contact lens vision simulated with a clinical binocular simulator. *Contact Lens Anterior Eye* 101716 (2022) doi:10.1016/j.clae.2022.101716.
296. Veerle Van, S., Sven Van, L. & Marcel Ten, T. Not dominance but the loss of binocularity determines the success of monovision. *J. Clin. Res. Ophthalmol.* **8**, 018–022 (2021).
297. Kompaniez, E. J., Sawides, L., Marcos, S. & Webster, M. A. Adaptation to interocular differences in blur. *J. Vis.* **13**, 1–14 (2013).
298. Fricke, T. R. *et al.* Global prevalence of presbyopia and vision impairment from uncorrected presbyopia: systematic review, meta-analysis, and modelling. *Ophthalmology* **125**, 1492–1499 (2018).
299. Westendorf, D. H., Blake, R., Sloane, M. & Chambers, D. Binocular summation occurs during interocular suppression. *Journal of Experimental Psychology: Human Perception and Performance* vol. 8 81–90 (1982).
300. Zheleznyak, L., Sabesan, R., Oh, J.-S., MacRae, S. & Yoon, G. Modified monovision with spherical aberration to improve presbyopic through-focus visual performance. *Invest. Ophthalmol. Vis. Sci.* **54**, 3157–3165 (2013).
301. Cope, J. R. *et al.* Contact lens wearer demographics and risk behaviors for contact eye infections–United States, 2014. *MMWR Morb. Mortal. Wkly. Rep.* **64**, 865–870 (2014).
302. Morgan, P. *et al.* International contact lens prescribing in 2018. *Contact Lens Spectr.* **34**, 26–32 (2019).
303. Ingenito, K. Premium cataract options gain ground. *Ophthalmol. Manag.* **19**, 42–43 (2015).
304. Burge, J. & Geisler, W. S. Optimal speed estimation in natural image movies predicts human performance. *Nat. Commun.* **6**, 7900 (2015).
305. Pulfrich, C. Die stereoskopie im dienste der isochromen und heterochromen photometrie. *Naturwissenschaften* **10**, 751–761 (1922).
306. Julesz, B. & White, B. Short term visual memory and the Pulfrich phenomenon. *Nature* **222**, 639–641 (1969).
307. Morgan, M. J. & Thompson, P. Apparent motion and the Pulfrich effect. *Perception* **4**, 3–18 (1975).
308. Carney, T., Paradiso, M. A. & Freeman, R. D. A physiological correlate of the pulfrich effect in cortical neurons of the cat. *Vision Res.* **29**, 155–165 (1989).
309. Wheatstone, C. On some remarkable, and hitherto unobserved, phenomena of binocular vision. *Philos. Trans. R. Soc. London* **128**, 371–394 (1838).
310. Burge, Johannes; Geisler, W. Optimal disparity estimation in natural stereo images Johannes. *J. Vis.* **14**, 1–18 (2014).
311. Dean, A. F. & Tolhurst, D. J. Factors influencing the temporal phase of response to bar and grating stimuli for simple cells in the cat striate cortex. *Exp. Brain Res.* 143–151 (1986).
312. Albrecht, D. G. Visual cortex neurons in monkey and cat: Effect of contrast on the spatial and temporal phase transfer functions. *Vis. Neurosci.* **12**, 1191–1210 (1995).
313. Bair, W. & Movshon, J. A. Adaptive temporal integration of motion in direction-selective neurons in macaque visual cortex. *J. Neurosci.* **24**, 7305 LP – 7323 (2004).
314. Navarro, R., Artal, P. & Williams, D. R. Modulation transfer of the human eye as a function of retinal eccentricity. *J. Opt. Soc. Am.* **10**, 201–212 (1993).
315. Atchison, D. A., Woods, R. L. & Bradley, A. Predicting the effects of optical

defocus on human contrast sensitivity. *J. Opt. Soc. Am.* **15**, 2536–2544 (1998).
316. Burge, J. & Geisler, W. S. Optimal imaged-based defocus estimates from individual natural images. *Proc. Natl. Acad. Sci. U. S. A.* **2011**, 2–4 (2011).
317. Vassilev, A., Mihaylova, M. & Bonnet, C. On the delay in processing high spatial frequency visual information: reaction time and VEP latency study of the effect of local intensity of stimulation. **42**, 851–864 (2002).
318. Westheimer, G. Clinical evaluation of stereopsis. *Vision Res.* **90**, 38–42 (2013).
319. Wilson, J. A. & Anstis, S. M. Visual delay as a function of luminance. *Am. J. Psychol.* **82**, 350–358 (1969).
320. Qian, N. & Andersen, R. A. A physiological model for motion-stereo integration and a unified explanation of Pulfrich-like phenomena. *Vision Res.* **37**, 1683–1698 (1997).
321. Anzai, A., Ohzawa, I. & Freeman, R. D. Joint-encoding of motion and depth by visual cortical neurons: Neural basis of the Pulfrich effect. *Nat. Neurosci.* **4**, 513–518 (2001).
322. Read, J. C. a & Cumming, B. G. The stroboscopic Pulfrich effect is not evidence for the joint encoding of motion and depth. *J. Vis.* **5**, 417–34 (2005).
323. Read, J. C. a & Cumming, B. G. All Pulfrich-like illusions can be explained without joint encoding of motion and disparity. *J. Vis.* **5**, 901–927 (2005).
324. Qian, N. & Freeman, R. D. Pulfrich phenomena are coded effectively by a joint motion- disparity process. **1**, 233–245 (2012).
325. Westheimer, G. & McKee, S. P. Stereoscopic acuity with defocused and spatially filtered retinal images. *J. Opt. Soc. Am.* **70**, 772–778 (1980).
326. Bonnen, K., Burge, J., Yates, J., Pillow, J. & Cormack, L. K. Continuous psychophysics: Target-tracking to measure visual sensitivity. *J. Vis.* **15**, 14 (2015).
327. Stockman, A. & Sharpe, L. T. Into the twilight zone: The complexities of mesopic vision and luminous efficiency. *Ophthalmic Physiol. Opt.* **26**, 225–239 (2006).
328. Schor, C. M., Carson, M., Peterson, G., Suzuki, J. & Erickson, P. Effects of interocular blur suppression ability on monovision task performance. *Journal of the American Optometric Association* vol. 60 188–192 (1989).
329. Landy, M. S., Maloney, L. T., Johnston, E. B. & Young, M. Measurement and modeling of depth cue combination: in defense of weak fusion. *Vision Res.* **35**, 389–412 (1995).
330. Ernst, M. O. & Banks, M. S. Humans integrate visual and haptic information in a statistically optimal fashion. *Nature* **415**, 429–433 (2002).
331. Almutairi, M. S., Altoaimi, B. H. & Bradley, A. Accommodation in early presbyopes fit with bilateral or unilateral near add. *Optom. Vis. Sci.* **95**, 43–52 (2018).
332. Radhakrishnan, A., Dorronsoro, C., Sawides, L., Webster, M. A. & Marcos, S. A cyclopean neural mechanism compensating for optical differences between the eyes. *Curr. Biol.* **25**, R188–R189 (2015).
333. Wolpert, D. M., Miall, R. C., Cumming, B. & Boniface, S. J. Retinal adaptation of visual processing time delays. *Vision Res.* **33**, 1421–1430 (1993).
334. Flitcroft, D. I., Judge, S. J. & Morley, J. W. Binocular interactions in accommodation control: effects of anisometropic stimuli. *J. Neurosci.* **12**, 188 LP – 203 (1992).
335. Marran, L. & Schor, C. M. The effect of target proximity on the aniso-accommodative response. *Ophthalmic Physiol. Opt.* **19**, 376–392 (1999).
336. Breitmeyer, B. G. & Ganz, L. Temporal studies with flashed gratings: Inferences about human transient and sustained channels. *Vision Res.* **17**, 861–865 (1977).
337. Zhang, M., Xiao, J. & Jiang, C. Pseudophakic monovision is an important surgical approach to being spectacle-free. *Indian J. Ophthalmol.* **59**, 481 (2011).
338. Davidson, R. S. *et al.* Surgical correction of presbyopia. *J. Cataract Refract. Surg.* **42**, 920–930 (2016).
339. Burge, J., Rodriguez-Lopez, V. & Dorronsoro, C. Monovision and the Misperception of Motion. *Curr. Biol.* **29**, (2019).

340. Bannon, R. E., Neumueller, J., Boeder, P. & Burian, H. M. Aniseikonia and space perception-after 50 years. *Am. J. Optom. Arch. Am. Acad. Optom.* **47**, 423–441 (1970).
341. Erickson, P. & Schor, C. Visual function with presbyopic contact lens correction. *Optom. Vis. Sci.* **67**, 22–28 (1990).
342. Molock, F., Cullerton, G., Spaulding, T. L. & Shivkumar, M. Photochromic contact lenses and methods for their production. (2005).
343. Hammond, B. R. *et al.* The effects of light scatter when using a photochromic vs. non-photochromic contact lens. *J. Optom.* **13**, 227–234 (2020).
344. Jiménez, J. R., Ponce, A. & Anera, R. G. Induced aniseikonia diminishes binocular contrast sensitivity and binocular summation. *Optom. Vis. Sci.* **81**, 559–562 (2004).
345. Katsumi, O., Tanino, T. & Hirose, T. Effect of aniseikonia on binocular function. *Invest. Ophthalmol. Vis. Sci.* **27**, 601–604 (1986).
346. Jiménez, J. R., Ponce, A., del Barco, L. J., Díaz, J. A. & Pérez-Ocón, F. Impact of induced aniseikonia on stereopsis with random-dot stereogram. *Optom. Vis. Sci.* **79**, 121–125 (2002).
347. Highman, V. N. Stereopsis and aniseikonia in uniocular aphakia. *Br. J. Ophthalmol.* **61**, 30–33 (1977).
348. Lovasik, J. V & Szymkiw, M. Effects of aniseikonia, anisometropia, accommodation, retinal illuminance, and pupil size on stereopsis. *Invest. Ophthalmol. Vis. Sci.* **26**, 741–750 (1985).
349. Vlaskamp, B. N. S., Filippini, H. R. & Banks, M. S. Image-size differences worsen stereopsis independent of eye position. *Journal of Vision* vol. 9 1–13 (2009).
350. Ogle, K. N. *Researches in binocular vision*. *Researches in binocular vision.* (W. B. Saunders, 1950).
351. Ames Jr., A. Binocular vision as affected by relations between uniocular stimulus-patterns in commonplace environments. *The American Journal of Psychology* vol. 59 333–357 (1946).
352. Miles, P. W. The pulfrich stereo-effect produced by monocular magnification without reducing illumination. *Am. J. Ophthalmol.* **36**, 240–243 (1953).
353. Artal, P. *et al.* Neural compensation for the eye's optical aberrations. *J. Vis.* **4**, 4 (2004).
354. Sawides, L., de Gracia, P., Dorronsoro, C., Webster, M. A. & Marcos, S. Vision is adapted to the natural level of blur present in the retinal image. *PLoS One* **6**, e27031 (2011).
355. Burge, J. & Geisler, W. S. Optimal defocus estimates from individual images for autofocusing a digital camera. in *Proc.SPIE* vol. 8299 (2012).
356. Kane, D., Bex, P. & Dakin, S. Quantifying "the aperture problem" for judgments of motion direction in natural scenes. *J. Vis.* **11**, 25 (2011).
357. Sebastian, S., Burge, J. & Geisler, W. S. Defocus blur discrimination in natural images with natural optics. *J. Vis.* **15**, 16 (2015).
358. Sebastian, S., Abrams, J. & Geisler, W. S. Constrained sampling experiments reveal principles of detection in natural scenes. *Proc. Natl. Acad. Sci.* **114**, E5731–E5740 (2017).
359. Kim, S. & Burge, J. The lawful imprecision of human surface tilt estimation in natural scenes. *Elife* **7**, e31448 (2018).
360. Chin, B. M. & Burge, J. Predicting the partition of behavioral variability in speed perception with naturalistic stimuli. *The Journal of Neuroscience* vol. 40 864–879 (2020).
361. Kim, S. & Burge, J. Natural scene statistics predict how humans pool information across space in surface tilt estimation. *PLOS Comput. Biol.* **16**, e1007947 (2020).
362. Morgenstern, Y. *et al.* An image-computable model of human visual shape similarity. *PLOS Comput. Biol.* **17**, e1008981 (2021).
363. Geisler, W. S., Najemnik, J. & Ing, A. D. Optimal stimulus encoders for natural

tasks. *Journal of Vision* vol. 9 (2009).
364. Jaini, P. & Burge, J. Linking normative models of natural tasks to descriptive models of neural response. *J. Vis.* **17**, 16 (2017).
365. Burge, J. & Jaini, P. Accuracy maximization analysis for sensory-perceptual tasks: computational improvements, filter robustness, and coding advantages for scaled additive noise. *PLOS Comput. Biol.* **13**, e1005281 (2017).
366. Lages, M., Mamassian, P. & Graf, E. W. Spatial and temporal tuning of motion in depth. *Vision Res.* **43**, 2861–2873 (2003).
367. Min, S. H., Reynaud, A. & Hess, R. F. Interocular differences in spatial frequency influence the pulfrich effect. *Vis. (Basel, Switzerland)* **4**, (2020).
368. Pardhan, S. & Gilchristt, J. The effect of monocular defocus on binocular contrast sensitivity. *Ophthalmic Physiol. Opt.* **10**, 33–36 (1990).
369. Jiménez, J. R., Castro, J. J., Jiménez, R. & Hita, E. Interocular differences in higher-order aberrations on binocular visual performance. *Optom. Vis. Sci.* **85**, 174–179 (2008).
370. Costa, M. F., Moreira, S. M. C. F., Hamer, R. D. & Ventura, D. F. Effects of age and optical blur on real depth stereoacuity. *Ophthalmic Physiol. Opt.* **30**, 660–666 (2010).
371. Pulfrich, C. Die Stereoskopie im Dienste der isochromen und heterochromen Photometrie. *Naturwissenschaften* (1921).
372. Rodriguez-Lopez, V., Dorronsoro, C. & Burge, J. Contact lenses, the reverse Pulfrich effect, and anti-Pulfrich monovision corrections. *Sci. Rep.* **10**, 1–16 (2020).
373. Clifford, C. W. G. *et al.* Visual adaptation: Neural, psychological and computational aspects. *Vision Res.* **47**, 3125–3131 (2007).
374. Vinas, M., Sawides, L., de Gracia, P. & Marcos, S. Perceptual adaptation to the correction of natural astigmatism. *PLoS One* **7**, e46361 (2012).
375. Felipe, A., Buades, M. J. & Artigas, J. M. Influence of the contrast sensitivity function on the reaction time. *Vision Res.* **33**, 2461–2466 (1993).
376. Allen, D. & Vasavada, A. Cataract and surgery for cataract. *Br. Med. J.* **333**, 128–132 (2006).
377. Elliott, D. B. Evaluating visual function in cataract. *Optom. Vis. Sci.* **70**, (1993).
378. Van Den Berg, T. J. T. P. *et al.* Straylight effects with aging and lens extraction. *Am. J. Ophthalmol.* **144**, 358-363.e1 (2007).
379. Sadun, A. A., Bassi, C. J. & Lessell, S. Why cataracts do not produce afferent pupillary defects. *Am. J. Ophthalmol.* **110**, 712–714 (1990).
380. Macmillan, E. S., Gray, L. S. & Heron, G. Visual adaptation to interocular brightness differences induced by neutral-density filters. *Investig. Ophthalmol. Vis. Sci.* **48**, 935–942 (2007).
381. Landrigan, D. T. Measurements of the Pulfrich effect over days of exposure. *J. Psychol.* **117**, 125–133 (1984).
382. Mojon, D. S., Rösler, K. M. & Oetliker, H. A bedside test to determine motion stereopsis using the Pulfrich phenomenon. *Ophthalmology* **105**, 1337–1344 (1998).
383. Matthis, J. S., Muller, K. S., Bonnen, K. L. & Hayhoe, M. M. *Retinal optic flow during natural locomotion*. *PLoS Computational Biology* vol. 18 (2022).
384. Scotcher, S. M., Laidlaw, D. A. H., Canning, C. R., Weal, M. J. & Harrad, R. A. Pulfrich's phenomenon in unilateral cataract. *Br. J. Ophthalmol.* **81**, 1050–1055 (1997).
385. Schwartz, D. M., Sandstedt, C. A., Chang, S. H., Kornfield, J. A. & Grubbs, R. H. Light-adjustable lens: development of in vitro nomograms. *Trans. Am. Ophthalmol. Soc.* **102**, 64–67 (2004).
386. Chin, B. M. & Burge, J. Perceptual consequences of interocular imbalances in the duration of temporal integration. *bioRxiv* 2022.02.16.480712 (2022) doi:10.1101/2022.02.16.480712.

387. Livingstone, M. S. & Hubel, D. H. Stereopsis and positional acuity under dark adaptation. *Vision Res.* **34**, 799–802 (1994).
388. Reynaud, A., Zhou, J. & Hess, R. F. Stereopsis and mean luminance. *J. Vis.* **13**, 1 (2013).
389. Halsted, C. Brightness, luminance, and confusion. *Inf. Disp. (1975).* **9**, 21–24 (1993).
390. Kunkel, T., Daly, S., Miller, S. & Froehlich, J. Chapter 15 - Perceptual Design for High Dynamic Range Systems. in *High Dynamic Range Video* 391–430 (2016). doi:https://doi.org/10.1016/B978-0-08-100412-8.00015-2.
391. Linke, S. J., Richard, G. & Katz, T. Prevalence and associations of anisometropia with spherical ametropia, cylindrical power, age, and sex in refractive surgery candidates. *Invest. Ophthalmol. Vis. Sci.* **52**, 7538–7547 (2011).
392. Lee, C.-W. *et al.* Prevalence and association of refractive anisometropia with near work habits among young schoolchildren: The evidence from a population-based study. *PLoS One* **12**, e0173519 (2017).
393. Weale, R. A. On the Age-Related Prevalence of Anisometropia. *Ophthalmic Res.* **34**, 389–392 (2002).
394. Abrahamsson, M. & Sjöstrand, J. Natural history of infantile anisometropia. *Br. J. Ophthalmol.* **80**, 860–863 (1996).
395. Oshika, T., Klyce, S. D., Applegate, R. A. & Howland, H. C. Changes in corneal wavefront aberrations with aging. *Invest. Ophthalmol. Vis. Sci.* **40**, 1351–1355 (1999).
396. Oshika, T., Klyce, S. D., Applegate, R. A., Howland, H. C. & El Danasoury, M. A. Comparison of corneal wavefront aberrations after photorefractive keratectomy and laser in situ keratomileusis. *Am. J. Ophthalmol.* **127**, 1–7 (1999).
397. Yan, W., Kanxing, Z., Ying, J., Yafei, N. & Tong, Z. Changes of higher order aberration with various pupil sizes in the myopic eye. *J. Refract. Surg.* **19**, S270–S274 (2003).
398. Renzi-Hammond, L. *et al.* A contra-lateral comparison of the visual effects of a photochromic vs. non-photochromic contact lens. *Contact Lens Anterior Eye* **43**, 250–255 (2020).
399. Li, R. W. *et al.* Monocular blur alters the tuning characteristics of stereopsis for spatial frequency and size. *R. Soc. Open Sci.* **3**, 160273 (2022).
400. Wist, E. R., Brandt, T., Diener, H. C. & Dichgans, J. Spatial frequency effect on the pulfrich stereophenomenon. *Vision Res.* **17**, 391–397 (1977).
401. Heron, G., Thompson, K. J. & Dutton, G. N. The symptomatic Pulfrich phenomenon can be successfully managed with a coloured lens in front of the good eye - A long-term follow-up study. *Eye* **21**, 1469–1472 (2007).
402. Thompson, P. & Wood, V. The Pulfrich pendulum phenomenon in stereoblind subjects. *Perception* **22**, 7–14 (1993).
403. Feinsod, M., Bentin, S. & Hoyt, W. F. Pseudostereoscopic illusion caused by interhemispheric temporal disparity: clinical and experimental observations. *Arch. Neurol.* **36**, 666–668 (1979).
404. Read, J. C. A. *et al.* ASTEROID stereotest v1.0: lower stereo thresholds using smaller, denser and faster dots. *Ophthalmic Physiol. Opt.* **40**, 815–827 (2020).
405. Piano, M. E. F., Tidbury, L. P. & O'Connor, A. R. Normative values for near and distance clinical tests of stereoacuity. *Strabismus* **24**, 169–172 (2016).
406. Hess, R. F. *et al.* A robust and reliable test to measure stereopsis in the clinic. *Invest. Ophthalmol. Vis. Sci.* **57**, 798–804 (2016).
407. Marsh, W. R., Rawlings, S. C. & Mumma, J. V. Evaluation of clinical stereoacuity tests. *Ophthalmology* **87**, 1265–1272 (1980).
408. Simons, K. A comparison of the Frisby, Random-Dot E, TNO, and Randot Circles stereotests in screening and office use. *Arch. Ophthalmol.* **99**, 446–452 (1981).
409. Hall, C. The relatioship between clinical stereotests. *Ophthalmic Physiol. Opt.* **2**, 135–143 (1982).

410. Broadbent, H. & Westall, C. An evaluation of techniques for measuring stereopsis in infants and young children. *Ophthalmic Physiol. Opt.* **10**, 3–7 (1990).

Blur is somewhat assumed and happens naturally due to the imperfect optics of the visual system such as in refractive errors (myopia, hyperopia, astigmatism, presbyopia), during the accommodation process (changing the observation object from near to far), or even as a cue for the perception of depth (focused objects are perceived closer to defocused objects, when they are in the same scene). In this thesis, optotunable lenses, electronically driven lenses that allow the programmatic control of the optical power very quickly, in the order of milliseconds, have been used to study blur in different static and dynamic scenarios.

This thesis has covered different aspects of vision related to blur perception, from their theoretical description to their direct clinical application. First, a new subjective refraction method for measuring the refractive error of an eye based on quick blur changes and a stimulus made of blue and red components was developed and validated, providing fast and accurate measurements with high potential for clinical implementation. Second, a new metric for selecting the best eye for monovision corrections was designed and tested providing a measurement of the strength of eye dominance. Third, a new optical illusion caused by differential ocular blur, with important clinical implications, was discovered. Fourth, a new optical correction to compensate for the optical illusion previously discovered, the anti-Pulfrich monovision correction, was developed and demonstrated using contact lenses. Finally, two new portable devices based on autostereoscopic techniques were developed with the potential to measure different aspects of binocular vision, stereoacuity and the Pulfrich effect, in clinical environments.

In summary, the outcomes of this thesis have advanced the understanding of blur perception and the application of that knowledge to the development of clinical instrumentation in optometry and ophthalmology.

CSIC
Consejo Superior de Investigaciones Científicas

uc3m | Universidad Carlos III de Madrid